January 2011

Dynamic Measurement Of Soluble Human Aβ In A Combined Microdialysis-Experimental Traumatic Brain Injury Mouse Model

Katherine Schwetye
Washington University in St. Louis

WASHINGTON UNIVERSITY IN ST. LOUIS

Division of Biology and Biomedical Sciences

Neurosciences

Dissertation Examination Committee:
David L. Brody, Chair
John R. Cirrito
Jeffrey M. Gidday
David M. Holtzman
Timothy M. Miller
Robert E. Schmidt
C. Conrad Weihl

DYNAMIC MEASUREMENT OF SOLUBLE HUMAN Aβ IN A COMBINED MICRODIALYSIS-EXPERIMENTAL TRAUMATIC BRAIN INJURY MOUSE MODEL

by

Katherine E. Schwetye

A dissertation presented to the
Graduate School of Arts and Sciences
of Washington University in
partial fulfillment of the
requirements for the degree
of Doctor of Philosophy

May 2011

St. Louis, Missouri

ABSTRACT OF THE DISSERTATION

Dynamic Measurement of Soluble Human Aβ in a Combined Microdialysis-Experimental Traumatic Brain Injury Mouse Model

by

Katherine E. Schwetye

Doctor of Philosophy in Biology and Biomedical Sciences

Neurosciences

Washington University in St. Louis, 2011

Professor David L. Brody, Chairperson

The amyloid-β peptide (Aβ) plays a central pathophysiological role in Alzheimer's disease, but little is known about its dynamics in the brain's extracellular space. A recent microdialysis-based study in human patients with severe brain injuries found that extracellular Aβ dynamics correlate with changes in neurological status. Because neurological status is generally diminished following injury, this correlation suggests that extracellular Aβ is reduced relative to baseline. However, human studies cannot assess pre-injury Aβ levels, very early post-injury Aβ levels, nor the relationship between extracellular Aβ and total tissue levels. Therefore, we developed a mouse model that combines experimental TBI with microdialysis to address these gaps. In this model, Aβ levels were stable at baseline and after sham-injury. Following controlled cortical impact TBI, we found that Aβ levels were immediately and persistently decreased in the ipsilateral hippocampus. These results were found in both wild-type mice and young pre-plaque PDAPP mice that produce human-sequence Aβ. Similar decreases were observed

in PBS-soluble hippocampal extracts, but no changes were found in carbonate or guanidine extracts. Reductions in Aβ were not due to changes in microdialysis probe function, APP levels nor Aβ deposition. Hippocampal depth electrode recordings demonstrated that electroencephalographic activity was decreased over 24 hours following TBI. Thus, we propose that in mice and likely injured human patients, post-injury extracellular Aβ levels are acutely decreased relative to baseline. Reduced neuronal activity may contribute, though the underlying mechanisms have not been definitively determined.

One hypothesized mechanism for reduced extracellular levels is that Aβ is retained at the synapse following injury. To test this, we prepared synaptosomes in sham and injured PDAPP mice and measured levels of Aβ and APP by ELISA. No significant differences between sham and 2.0 mm-injured mice were detected. Future experiments will determine whether enhanced clearance accounts for decreased extracellular Aβ.

In summary, we have designed a mouse model to address questions that cannot be answered in patients. Using this model, we measured Aβ dynamics and their relationship to tissue levels and a possible relationship with neuronal activity. Studies of other peptides and treatment strategies might benefit from use of this model.

ACKNOWLEDGEMENTS

First and foremost, I would like to thank my mentor, Dr. David Brody, for his tireless guidance and support over the past four years. As a physician-scientist, his knowledge, experience, enthusiasm, and conscientiousness has inspired me in this research. Dr. Brody takes his role as a mentor very seriously and goes beyond what is expected of a PhD adviser. He trusted in my abilities, and actively encouraged the development of independent, scientific thought. It was a privilege and a gift to have been his student.

I would also like to thank Dr. David Holtzman and all the members of his lab, past and present. His generous support has fostered our growth in many respects.

I would like to thank Dr. John Cirrito. Our project is largely based on his original studies of ISF Aβ physiology. Over the years, his thoughtful discussions, technical assistance, and offers of resources, reagents and time made these investigations possible.

I would like to thank the members of my Committee: the chairman, Dr. Jeffrey Gidday, Dr. Robert Schmidt, Dr. Timothy Miller and Dr. Chris Weihl, for their advice and guidance in this project and for their support of my education. Their various areas of expertise informed and enhanced different aspects of the work. It was an honor to have the consideration of these accomplished, independent researchers.

The members of the Brody lab are colleagues and friends, and I am grateful to have been part of such a hard-working and cooperative group. Dr. Christine Mac Donald, post-doctoral fellow in the Brody lab, has been an extraordinary example for me. TJ Esparza, our senior technician, is an insightful and careful scientist who keeps the lab running smoothly. Hien Tran, my fellow student, has an incredible work ethic and generously offered her assistance in immunohistochemical techniques. Dr. Jon Willie, our neurosurgeon researcher, has taken the combined CCI-MDA model to another level in his investigations of orexin dynamics, and I am grateful for his discussions and insight. Dr. Yoshi Shitaka, a senior researcher, has added much to the lab with his creativity and approach to problem solving. I would like to thank past members of the Brody lab: Michael Spinner, Dan Refai, Dana Cooper, Nick Peters, Kurt Wall, and others.

I would like to acknowledge our two collaborators in the clinical microdialysis project, Dr. Gregory Zipfel at Washington University and Dr. Sandra Magnoni at the Ospedale Maggiore Policlinico in Milan.

The Neuroscience community at Washington University exemplifies an ideal of scientific collegiality, and this is the result of great leadership and individual efforts. I would also like to acknowledge the Medical Scientist Training Program and the Neurosciences program at Washington University.

This work has been supported by the MSTP training grant, the NIH, the Burroughs-Wellcome Career Award in Biomedical Sciences, the Thrasher Research Fund, and the Cure Alzheimer's Fund.

Lastly, I would like to thank my parents, Thom and Ann Schwetye; my sisters, Ellie and Kris; the Genovese family; and friends, Sarah and Jeanne Trulaske, Si Kincaid, and Alexandra Kalwerisky, for your love, support, and patience.

TABLE OF CONTENTS

List of Figures .....

List of Tables .....

Chapter 1.

Introduction

Traumatic brain injury is thought to be an important acquired risk factor for dementia and Alzheimer's disease (Jellinger, 2004, Lye and Shores, 2000, Van Den Heuvel, et al., 2007). However, the mechanisms responsible for the development of TBI-associated dementia are poorly understood. The amyloid-β peptide (Aβ) is believed to play a central role in both familial and late-onset Alzheimer's disease (AD), and may also be involved in TBI-related dementia. Before we consider its specific role, let us review the literature for the evidence of a link between TBI and dementia.

Evidence for increased risk of dementia after TBI: scope and definition

There is much evidence to support a link between TBI occuring in early or middle adulthood with the development of dementia later in life. However, not all studies conclude that TBI is a risk factor. Still others find that increased risk may depend on injury severity, gender, or genetic predisposition. These seemingly variable results are likely due to differences in study populations, inclusion criteria for brain injury, and the definition and diagnosis of dementia. To review the more recent literature, we will use the following 3 questions to summarize the main findings of individual studies:

1. Does TBI increase risk for development of AD or other dementias?
2. Does TBI hasten the onset of AD or other dementias?
3. What genetic factors may interact with TBI to increase risk of dementia?

First, let us narrow the scope of the review to studies that consider only single or several instances of TBI, in contrast to the repeated injuries suffered by professional boxers or football players on a regular basis. Second, we will include only studies that consider long-term outcome, years after the initial injury, as opposed to the short-term cognitive sequelae that are common in the weeks to months following TBI. Third, "dementia" will be broadly defined, since many studies differ in their diagnostic criteria.

How should dementia be defined? Many studies used common rating scales for diagnosis of AD patients such as the DSM-III or NINCDS-ADRDA criteria. Some of these scales are "snapshots" of cognitive functioning, while others (CAMDEX, for example) account for decline in function. However, Leon-Carrion is careful to note that an acquired dementia syndrome in TBI patients is often distinct from other progressive dementias in elderly patients (Leon-Carrion, 2002).

The DSM-IV syndrome of Dementia Due to Head Trauma offers an alternative to the scales developed for diagnosis of Alzheimer's disease. According to these criteria, there must some degree of memory impairment, either the ability to form new memories or to recall formerly learned information; at least one of the following: aphasia, apraxia, agnosia, or impaired executive function; and a significant decrease from previous functioning and impaired social functioning. In contrast to other types of dementia, progression is not required to fulfill these criteria.

Not all patients who suffer TBI go on to develop a clinical dementia, however. The concept of cognitive reserve might explain how TBI increases this risk. Cognitive reserve is the cumulative effect of genetic endowment, education, health status, and other

aspects of social and intellectual functioning early in life that protects or delays neurodegenerative processes (Stern, 2009). Likewise, insults acquired early in life, such as TBI, chronic stress, and lower educational attainment, challenge cognitive reserve, possibly lowering the threshold for development of a clinical dementia later in life. In this scheme, a testable model would have to account for such early-life contributors in the evaluation of risk of dementia following TBI (Kesler, et al., 2003). Few studies to date have done this on a broad scale. For now, the protective role of cognitive reserve against TBI-related dementia remains a hypothesis to be tested, ideally in a large prospective study. Further research in the epidemiology of TBI-related dementia is necessary as our "baby boomer" population continues to age, and the obligation of society to care for those patients grows ever larger.

Epidemiology of TBI-related dementias: early investigations

Over the past decades, many studies have considered the role of traumatic brain injury in the development of an Alzheimer's-type dementia. A well-documented example of dementia after TBI is that of professional as well as amateur boxers (Clausen, et al., 2005, Loosemore, et al., 2007). Those studies will not be addressed here due to the uniquely repetitive, chronic nature of the trauma. Here, we will consider only the effects of one or several, remote TBI on the later development of dementia.

As early as the 1940s, case reports described insidious intellectual deterioration following a single TBI. For example, one paper details the course of a 50-year-old male patient who suffered a brain injury in a car accident (Corsellis and Brierley, 1959). There

was a documented loss of consciousness immediately following the accident, with post-traumatic amnesia. Over the next four years, this patient visited his physician frequently, complained of concentration and memory problems, and became unable to run his business. Over the next few years, this patient experienced emotional disturbances and a progressive deterioration in intellectual function until he became severely demented. Approximately five years after the injury, the patient died and the brain was autopsied for the presence of Alzheimer's-like pathology. It was found that this 55-year-old man possessed plaques and tangles as revealed by silver staining techniques. These features were especially prominent in more superficial layers of cortex, as was later demonstrated in a large case series of TBI patients (Jellinger, et al., 2001). Other case reports have described similar findings in young patients not otherwise expected to have such pathology (Clinton, et al., 1991, Ikonomovic, et al., 2004, Roberts, et al., 1994).

Beginning in 1960s and 1970s, researchers began to consider the issue of TBI-related dementia more systematically. For example, a study published in 1979 looked at the outcomes in a consecutive series of 291 head-injured patients from among 7000 admittances to a single hospital (Lewin, et al., 1979). The criterion for inclusion was amnesia greater than 1 week. All injuries had occurred between 10 and 24 years before the outcome assessment. Of the 291 patients contacted for follow-up, 31 or 11% had progressive intellectual deterioration, which was twice the prevalence in the local population over 65 years old.

Many studies involving tens to thousands of patients have since been published. The following discussion will be organized by 3 questions to summarize the main findings of individual studies.

1. Does TBI increase risk for development of AD or other dementias?
2. Does TBI hasten the onset of AD or other dementias?
3. What genetic factors may interact with TBI to increase risk of dementia?

Does TBI increase risk for development of AD or other dementias?

The types of studies that have attempted to answer this question include retrospective (historical) and prospective cohort, matched and unmatched case controls, and meta-analyses of case-controls. Most of these considered a population of patients with probable or definite dementia, including Alzheimer's disease, and asked whether they had suffered a TBI at any point prior to the onset of their dementia.

Graves et al. conducted a case-control study of 130 matched pairs in geriatric psychiatry clinics to ask whether a head injury severe enough to have warranted a visit to a physician or a hospital, or to have experienced any loss of consciousness, increased the risk for development of dementia or Alzheimer's disease (Graves, et al., 1990). Two cohorts of cases and controls were enrolled. Between 1980 and 1982, dementia was diagnosed by the DSM-III criteria for primary degenerative dementia. Between 1983 and 1985, both the DSM-III and NINCDS-ADRDA criteria were used. Patients were considered not to be demented if the MMSE > 26. Overall, irrespective of loss of

consciousness, incidence of TBI increased the odds ratio for dementia to 3.5 (95% C.I., 1.6-7.7). One weakness of this study was the low statistical power.

In a retrospective cohort study drawn from the resources of the Rochester Epidemiology Project, Williams et al. reviewed the medical records of Olmsted County residents kept between 1935 and 1974 for a diagnosis of dementia (Williams, et al., 1991). Records were limited to residents at least 40 years old at last visit. Dementia was qualitatively described as a decline in intellect, memory, or social function of duration longer than 6 months. This diagnosis was made by the patient's own physician. There were 821 records that met these criteria that were then screened for documented head injury. Among these, 23 men and 13 women were identified as having had both a head injury and dementia. When compared to the expected incidence rates of dementia in Olmsted County by a standardized morbidity ratio (SMR), the authors concluded there was no increased risk for dementia conferred by TBI. For males, the SMR = 1.22 (95% C.I. 0.77-1.83), and for females, the SMR = 0.87 (0.46-1.49). One weakness of this study was the lack of standardized, published criteria to evaluate dementia or AD.

In an earlier case-control study, French and Mortimer described a population of 78 male patients in the V.A. system with a diagnosis of dementia of the Alzheimer's type (French, et al., 1985, Mortimer, et al., 1985). The 40 control subjects were drawn from both hospital and neighborhood populations. Diagnosis of head injury was made from a structured interview with an informant along with evaluation for other putative risk factors (toxic, metabolic, infectious, etc.). The criteria for dementia were insidious onset, gradual progression, intact consciousness and no focal neurological signs. In 30 cases

that subsequently died during the course of the study, 16 brains came to autopsy. Histopathological confirmation of Alzheimer's disease was found in 14 of these 16 brains. The odds ratio for having dementia after a TBI was 4.50 (95% C.I., 1.44-15.69). However, this series was limited by a low statistical power, and was later reconsidered in the context of a meta-analysis (Mortimer, et al., 1991).

In another case-control study of patients with dementia, Rasmusson et al. queried patients enrolled at an Alzheimer's Disease Research Center (ADRC) for prior history of traumatic brain injury (Rasmusson, et al., 1995). They compared the incidence of TBI in familial AD to TBI in sporadic AD, and to TBI in cognitively normal age-matched controls. The TBI was ascertained by a structured telephone interview with a spousal informant, and AD was evaluated by NINCDS-ADRDA criteria. It was found that TBI was significantly more common in AD cases (n=68) than in controls (n=34) (OR = 13.75, 95% C.I. 1.76-107.52). Although TBI was more common in true sporadic AD (10 of 23) than in familial AD (6 of 30), the odds ratio was not statistically significant. One potential criticism of this study is that severe head injury warranted exclusion from initial enrollment in the ADRC. The enrolled patients in the AD group, then, were thus likely to have suffered milder injuries. These researchers concluded that even mild injuries confer risk for AD.

In an unmatched case-control study of patients referred to a psychogeriatric hospital, Salib and Hillier asked whether TBI increased the risk of Alzheimer's disease or of dementias in general (Salib and Hillier, 1997). The AD population consisted of 198 patients with AD by NINCDS-ADRDA criteria, compatible with DSM-III and ICD-9

standards. The “other dementias” population was comprised of 164 patients who scored less than 17 on the MMSE and either a Hachiniski score > 7, or another known etiology (alcohol abuse, metabolic disorder). History of TBI was ascertained by interview with an informant, where open-ended questions were asked to determine age at the time of TBI, severity, circumstances surrounding the injury, and aspects of the medical treatment. The control (non-demented) group consisted of 176 patients with an MMSE score > 23. This study found that TBI increased the risk of “dementia” when defined as all dementias (OR = 2.4, 95% C.I. 1.4-4.1), any dementias other than AD (OR = 2.36, 95% C.I. 1.4-4.0), and AD alone (OR = 2.4, 95% C.I. 1.3-4.1). A clear weakness of this study is the potential disparities between cases and controls due to the lack of matching.

In a very large set of cases and controls culled from 13 centers in the U.S., Germany, and Canada as part of the MIRAGE study, Guo et al. measured the incidence of head injury in NINCDS-ADRDA-diagnosed AD patients (n=2233) and compared their rates to both first-degree family members (parents or siblings, n=7694) and to spouses (n=2509) (Guo, et al., 2000). Either the subject or the spouse reported TBI based on the question, “Has your relative ever had a head injury which required medical care or caused a loss of consciousness?” Medical care included visiting a physician or a hospital, either inpatient or outpatient. They were also queried as to the age at TBI and the duration of loss of consciousness (LOC), if any. When compared with spouses, the presence of TBI with LOC increased the relative risk to 9.9. This effect was seen in both men (RR = 5.6) and women (RR = 3.2). Without LOC, there was still an increased risk (RR = 3.1). When compared with parents and siblings, TBI with LOC increased RR =

4.0 (95% C.I., 2.9-5.5); without LOC, TBI still increased the risk (RR = 2.0, 95% C.I., 1.5-2.7).

A prospective study looked at the presence or absence of TBI in new-onset dementia in non-demented, older patients (Mehta, et al., 1999). As part of the Rotterdam Study, Mehta et al. began with a population of 6645 volunteer adults aged 55 years or older, and followed them for an average of 2.1 years from enrollment to test for new-onset dementia (Mehta, et al., 1999). The occurrence of TBI was ascertained by self-report of head injury with loss of consciousness to an examining physician. A three-stage assessment was conducted, consisting of the MMSE and GMS-A in the screening step. Then, if the MMSE < 26 or the GMS-A > 0, the CAMDEX was administered. Finally, a neurological exam, MRI, and previous medical records were reviewed and diagnosis was made by DSM-III criteria, with subtyping by NINCDS-ADRDA criteria. The logistic regression model for total dementia risk, after adjusting for age, gender and education, revealed no increased risk due to TBI (RR = 1.0, 95% C.I. 0.5-2.0). Neither was there an effect on risk for AD, specifically (RR = 0.8, 95% C.I. 0.4-1.9). In addition, there was neither an effect of ApoE4 status, nor the number of years since the injury, nor the duration of LOC on risk of dementia. One weakness of this study was the short follow-up time. Initial assessments were conducted between 1990 and 1993, and reassessments between 1993 and 1994. Another criticism of this study is that participants were all volunteers from the community and may have represented a bias towards better-educated, healthier individuals who were therefore less likely to become demented.

A prospective cohort study was conducted by Plassman and colleagues on 548 World War II Navy and Marine veterans whose military records documented a closed head injury (Plassman, et al., 2000). The TBI was rated as mild, moderate or severe based on loss of consciousness, post-traumatic amnesia, and skull fracture. The control population consisted of 1228 similar veterans who did not suffer head injury, but who were hospitalized for either pneumonia or laceration-type wounds. This study made a standardized diagnosis of dementia and Alzheimer's disease by a three-step process. First, participants were screened with the Telephone Interview for Cognitive Status, based closely on the MMSE. A spouse or child verified the participant's cognitive status. Further testing was then conducted using the Dementia Questionnaire. Finally, a clinical evaluation including neuropsychological testing was used to make a definitive diagnosis of dementia by the DSM-III criteria, and AD by the NINCDS-ADRDA. This study found a hazard ratio for dementia conferred by even a single, moderate TBI compared to no TBI (HR = 2.32, 95% C.I., 1.04-5.17). For severe TBI, the hazard ratio was 4.51 (95% C.I., 1.77-11.47). The risk for dementia in general was similar to that for AD in particular.

Another, smaller prospective cohort study by Schofield et al. assessed the risk conferred by TBI for incident dementia in 271 community-dwelling participants. All participants were at least 60 years old in a longitudinal aging study in north Manhattan (Schofield, et al., 1997). At the time of enrollment, participants had no cognitive impairment. Cognitive status was assessed by a neuropsychological evaluation, including tests of memory, orientation, abstract reasoning, language, and construction. A CDR

rating was determined for each participant during a consensus conference among examining physicians. The occurrence of TBI was assessed during the risk factor interview and by the examining physician. During the risk factor interview, patients were asked about loss of consciousness and amnesia. The examining physician asked only about loss of consciousness. An informant in the home verified the occurrence of TBI. These participants were then followed each year for a total of 5 years and reassessed for cognitive status. By the criterion of TBI as assessed by the examining physician, TBI conferred a risk for early-onset dementia (RR = 1.4, 95% C.I. 1.3-12.7). However, by the stricter criteria of the risk factor interviewer, the risk did not reach significance (RR = 2.0, 95% C.I. = 0.7-6.2). If loss of consciousness was greater than 5 minutes, the risk increased (RR = 11.2, 95% C.I. 2.3–59.8). If the TBI had occurred within 30 years of dementia onset, risk was also increased (RR = 5.4, 95% C.I. 1.5-19.5).

Finally, two meta-analyses were performed using data from previous case-control studies. The first, published in 1991 by Mortimer and colleagues, pooled data from 7 case-control studies conducted in the U.S., Italy, the Netherlands, and Australia. Individually, each of these studies found a significant increase in the relative risk for dementia conferred by TBI. However, the statistical power was less than 0.2 in all 7 studies. When these data were pooled, however, the statistical power increased to 0.97 to yield an RR = 1.82 (95% C.I. 1.26-2.67) (Mortimer, et al., 1991). When stratified by gender, the meta-analysis found an increased risk for dementia among males (RR = 2.67, 95% C.I. 1.64-4.41) but not females (0.85, 95% C.I. 0.43-1.70). Following the publication of this initial meta-analysis, a replication study was done by Fleminger and

colleagues (Fleminger, et al., 2003). Using 8 case-control studies included in various analyses in the original Mortimer study as well as 7 case-control studies published since, this meta-analysis examined whether TBI with loss of consciousness conferred a risk for dementia. Their inclusion criteria were as follows: they specified that a requirement for a collateral source in both cases and controls, and that the TBI had occurred some number of years prior to the onset of dementia. Finally, all studies had to have used NINCDS-ADRDA criteria for possible or probable AD, and DSM criteria for dementia of the Alzheimer's type. Overall, this study found that the odds ratio conferred by TBI for dementia was 1.58 (95% C.I. 1.21-2.06). When stratified by gender, males had an increased risk (OR = 2.29, 95% C.I. 1.47-3.58) while females did not (OR = 0.91, 95% C.I. 0.56-1.47). The authors concluded that this technique of meta-analysis of case-control studies is replicable given the strict inclusion criteria imposed on the individual studies analyzed.

In summary, it appears that even a single incident of TBI with loss of consciousness or post-traumatic amnesia increases the risk for dementia later in life, particularly in men.

Does TBI hasten the onset of AD or other dementias?

In both studies that did and did not find an increased *incidence* of dementia or Alzheimer's disease, a separate question can be asked regarding the age of onset in patients with and without a history of TBI. For this question, we will reconsider some of the studies in the previous section as well as others.

A preliminary study published in 1989 examined a retrospective cohort to evaluate the specific effects of TBI on age of onset of dementia (Gedye, et al., 1989). Information was gathered from a pool of 148 patients with probable AD, excluding known familial cases, and 33 others with dementias unlikely to be AD. All cases were selected from a consecutive series of 400 patients referred to an Alzheimer's disease clinic. Each received a thorough physical exam, cognitive assessment, genetics interview, social work interview and neurological exam. Collateral sources were asked about the patient's history of TBI and specifically about the duration of loss of consciousness, a feeling of being "stunned," dizziness, confusion, and behavioral changes. TBI was rated on a 7-point scale. Cases with possible confounding factors, such as alcohol or medication abuse, were excluded. Diagnosis of definite or probable AD was made according to the NINCDS-ADRDA criteria. For patients who suffered a severe TBI before age 65, the median age of onset for AD was 8 years earlier (mean, 6.8 years earlier) than those without a history of TBI. A similar trend occurred in the group of patients with dementia unlikely to be Alzheimer's, but the sample size was too small to perform statistical analysis. A correlation was found between the severity of the trauma and the age of onset of probable AD (Spearman rank-order correlation $r = -0.60$ for 35 patients whose TBI rated 2-7; $r = -0.3$ for 24 patients rated 3-7). This study concluded that the mere incidence of TBI was not sufficient to *cause* AD or another dementia, but it may hasten the onset.

Nemetz et al. examined an historical cohort from the medical records compiled as part of the Rochester Epidemiology Project (Nemetz, et al., 1999). The TBI was included

in the study if there were documented loss of consciousness, post-traumatic amnesia, or focal neurologic signs. Head trauma with skull fracture was not included. Of 1283 patients with recorded incidents of TBI from 1935-1984, aged 40 or older in 1988, 31 later developed dementia. The diagnosis was made by the patient's own physician and confirmed in the medical record by a study neurologist who took the first mention of cognitive or behavioral difficulties that were later attributed to Alzheimer's disease as "time of onset." This study did not find an increased incidence of dementia among TBI patients compared to patients without a history of TBI. However, the authors constructed survival curves of Alzheimer's-free status at every age, and compared the groups of Alzheimer's patients with (n=31) and without (n=689) TBI. For patients who suffered a TBI before age 65, there was a twofold increase in the risk of early-onset dementia as compared to the expected incidence, defined as onset before the age of 75 (standardized incidence ratio = 2.2, 95% C.I. 1.1-4.0).

Luukinen and colleagues asked whether fall-related TBI can hasten the onset of dementia in a longitudinal study from an elderly, population-based cohort (Luukinen, et al., 2005). They examined 325 non-demented individuals aged at least 70 years old between 1991 and 1992. Researchers then contacted participants every three months by telephone to inquire whether a fall had occurred, the nature of the injury and subsequent medical treatment. TBI with brain involvement was specified by nausea, dizziness, headache, seizures, focal neurological deficits, and/or skull fracture. The severity of the TBI was rated according to duration of loss of consciousness, post-traumatic amnesia, and initial GCS score. A full follow-up examination was conducted eight to nine years

after the initial assessment in 150 of the original patients. Participants' cognitive status was assessed by the MMSE, DSM-IV, imaging and lab tests, a clinical and neurological exam, and a brief battery of neuropsychological exams. A clinical diagnosis was determined by consensus conference between two examining neurologists. Of the 150 patients in the follow-up group, 8 had sustained a TBI at a mean interval of 1438 and 1642 days from the initial and final exams, respectively. Five patients suffered a mild TBI, of which three developed dementia. Three patients suffered a moderate TBI, of which two became demented. It was found that fall-related TBI in this older population conferred an age-specific hazard ratio of dementia (HR = 2.78, 95% C.I. 1.32–5.86). After adjustment for baseline low educational status and sex, TBI was still a significant hazard (HR = 2.80, 95% C.I., 1.35–5.81).

Recently, McMurtray et al. published a study of patients in the V.A. system presenting with a memory or cognitive complaint (McMurtray, et al., 2006). Patients were assessed for dementia using the criteria of deficits in two or more domains of cognition: a significant impairment in social or occupational functioning, and a significant decline from a previous level of functioning as quantified by the DSM-IV. Previous medical records were reviewed for a primary etiology of the complaint. Etiologies included TBI, alcohol abuse, HIV status, and neurological disorders: Alzheimer's disease, vascular dementia, Parkinson's disease, FTLD, or MS. Finally, patients were stratified by the onset of dementia: early-onset dementia (EOD) if onset occurred prior to age 65 (n=268; mean age of onset, 51 ± 11) or late-onset dementia (LOD) if onset occurred after age 65 (n=670, mean age of 75 ± 5). It was found that

among the primary etiologies, TBI, alcohol abuse, HIV status, and FTLD were significantly associated with an increase in frequency among the EOD group than LOD by a χ^2 analysis. Specifically, the X^2 statistic for TBI was 71.6 with a p-value of less than 0.0001. By contrast, AD as an independent primary etiology was associated with an increased frequency in the LOD group. This study suggests that when TBI is a primary etiology for dementia other than that of the Alzheimer's type, it more frequently occurs as an EOD rather than an LOD.

In summary, most studies support the hypothesis that TBI is associated with an earlier onset or detection of dementia as compared to a non-injured population.

What genetic factors may interact with TBI to increase risk of dementia?

A final query of the literature might consider whether TBI interacts with certain other risk variables to increase the risk of dementia. One commonly assessed risk factor is gender. In several studies that demonstrated a significant increase in risk due to TBI, the study population was comprised of current or former military personnel and consisted almost entirely of males (French, et al., 1985, McMurtray, et al., 2006, Mortimer, et al., 1985, Plassman, et al., 2000). In studies that assessed approximately equal numbers of males and females, several found an increased risk in males, but not in females (Fleminger, et al., 2003, Himanen, et al., 2006, Launer, et al., 1999, Mortimer, et al., 1991, Salib and Hillier, 1997). By contrast, a large-scale study across 13 centers in North America and Europe found increased risk in both males and females, although risk was still greater in males (Guo, et al., 2000). However, the increased rates of TBI and

increased severity of TBI among males as compared to females might contribute to these apparent disparities.

Another putative risk factor is apolipoprotein E4 (ApoE4) status. Possession of one or two ApoE4 alleles has been shown to be an important genetic risk factor for late-onset Alzheimer's disease (Strittmatter, et al., 1993). Several studies have assessed its role in TBI-associated dementia. Mayeux and colleagues published a case-control study that compared community-dwelling individuals with AD to a cognitively normal group aged 65 or older to measure the effects of TBI and ApoE4 on the incidence of dementia (Mayeux, et al., 1995). A diagnosis of probable AD was made according to NINCDS criteria. Head injury with loss of consciousness was ascertained by a semi-structured interview as previously described (Mayeux, et al., 1993). Cases and controls were matched by age and gender, cases having 74.5% women aged 74 ± 10.5 years, and controls having 69.1% women aged 72 ± 9.1 years. Ethnicity was also matched. However, the cases had significantly fewer years of education than controls. As expected, the ApoE4 allele was significantly more frequent among cases (0.29) than controls (0.16; $X^2 = 13.4$, $p < 0.001$), but did not differ by age, gender, or years of education within either group. For ApoE4 homozygosity, the OR for AD risk was 3.9 (95% CI, 1.2-13.2) and that associated with heterozygosity was 2.0 (95% CI, 1.2-3.6, $p < 0.01$). Of the cases, 13 or 11.5% reported a TBI with loss of consciousness occurring at least two years before the onset of dementia. Of the controls, 10 or 8.1% had a history of TBI with loss of consciousness. Irrespective of ApoE4 status, TBI did not confer a significant risk for AD (OR = 1.5, 95% CI, 0.5-3.5). However, using the non-injured,

non-ApoE4+ individuals as a reference group, TBI and at least one ApoE4 allele together conferred a risk for AD (OR = 10.5; 95% CI, 1.3-87.8). This study suggested that TBI and ApoE4 status may act synergistically to increase the risk of AD. However, this study was too small to detect a significant interaction between these variables. Additionally, the TBI was only required to have occurred as soon as two years prior to onset of dementia. This length of time may not be sensitive enough to determine a true "onset" based solely on medical records.

The synergistic effects of TBI and ApoE4 status on the development of AD among older individuals are supported by the findings of Luukinen et al. (Luukinen, et al., 2005). In a group of individuals aged 70 or older who were cognitively normal at enrollment, ApoE4 status acted synergistically with fall-related TBI to confer risk for new-onset dementia by an age-specific hazard ratio of 7.68 (95% C.I., 2.32–25.3).

By contrast, two large studies that examined the effect of TBI occurring at younger ages have found no such synergism with ApoE4 status (Mehta, et al., 1999, Plassman, et al., 2000). Similar to Mayeux et al., the analysis of head injury as a risk factor for incident dementia in the large, community-based Rotterdam Study by Mehta and colleagues did not report that TBI was an independent risk factor (Mehta, et al., 1999). However, they did not find a synergistic effect ApoE4 genotype with TBI. The prospective cohort study by Plassman et al. was also powered to detect such an interaction (Plassman, et al., 2000). They reported a non-significant trend towards a stronger association between ApoE4 status and risk for dementia among men with a remote history of moderate or severe TBI. This study maintains that moderate-to-severe

TBI is an independent risk factor for later development of dementia, and that one or two ApoE4 alleles might confer additional risk.

In summary, it appears that male gender and ApoE4 status might further increase the risk for dementia in individuals with a history of TBI.

Alzheimer's pathology in remote TBI

Given the evidence that TBI likely increases the risk of dementia, possibly by increasing the likelihood of early-onset disease or acting in synergy with genetic factors, what might be the histopathological basis for this increased risk? One possibility is that TBI is associated with Alzheimer's pathology; specifically, the hallmark extracellular Aβ plaques and intracellular neurofibrillary tangles. One study has addressed the question of Alzheimer's pathology in the setting of TBI by comparing two cohorts of autopsied brains (Jellinger, et al., 2001). In the first, brains from 58 individuals aged at least 60 years known to have residual, closed TBI were examined for coincident Alzheimer's pathology. In the second cohort, 57 age-matched samples known to have Alzheimer's pathology were examined for TBI residuals. A number of markers were examined, including routine stains, Bielschowsky silver stain, and immunohistochemistry for $A\beta_{1-42}$, hyperphosphorylated tau, ubiquitin, and α-synuclein. Within the first cohort, 7 of 57 brains were classified as having definite, severe neuritic AD pathology, with 6 more diagnosed as "probable AD." The AD+ brains included 4 males and 3 females, ranging in age at death from 69-83 years old, with occurrence of TBI ranging from 10 to 30 years prior to death (if known). The duration of dementia was 4-7 years. Among the 6 brains

with probable AD pathology, TBI had occurred between 8 and 39 years prior to death, with duration of cognitive impairment ranging from 3 to 7 years. The prevalence of AD pathology in this cohort was 22%, higher than expected in the general population aged at least 65 years old. Within the second cohort, individuals ranged in age from 71-91 years old at the time of death. Four of these 57 brains showed signs of residual TBI. Although 30% of all cases possessed at least one ApoE4 allele, none of the TBI brains were ApoE4+. A single TBI had occurred in each of these four cases, ranging between 7-54 years before the onset of dementia.

In summary, no large-scale studies have examined the true coincidence of Alzheimer's pathology in documented cases of remote TBI when there is no obvious evidence of residual brain injury. For example, diffuse axonal injury can be quite a severe TBI, but lacks the focal lesions that are grossly evident such as the contusions described in the Jellinger study. Future studies are warranted to address this gap in the literature.

Alzheimer's pathology in acute TBI

If TBI increases the risk of dementia through the mechanisms of classic Alzheimer's pathology, it could be asked: when does this process occur? Is it immediate or delayed? Several studies have examined the incidence of acute pathology and have found that Aβ deposits are present as early as 2 hours after injury in a subset of young TBI patients coming to autopsy or requiring decompressive surgery (Fig. 1) (Ikonomovic, et al., 2004, Roberts, et al., 1994, Smith, et al., 2003). This suggests that TBI might

accelerate the pathophysiological processes resulting in dementia. However, Aβ staining patterns following TBI differ from those associated with clinical AD, and only 1/3 of patients demonstrate any pathology (Ikonomovic, et al., 2004, Johnson, et al., 2009, Roberts, et al., 1994, Smith, et al., 2003). These immunohistochemical studies were limited to single-timepoint analysis of Aβ deposits in only the most severe injuries. It is unknown whether these patterns persist or evolve over longer periods of time.

Figure 1. Aβ staining of patterns of deposition after acute TBI. A, Compact, irregular Aβ deposits detected as early as 2h after injury. **B,** plaques present at 16h after injury. **C,** large, dispersed neuropil accumulates. **D,** intracellular Aβ deposits in the cytoplasm of cortical pyramidal neurons. **E,** intracellular Aβ deposits in axons of a plaque-negative case. **F,** sporadic, Aβ-positive glial cells in a plaque-negative case. Scale bar 200μ (A–C); 100μ (D–F). **G,** age group distribution of cases with cortical Aβ-immunoreactivity. Cases were severely head-injured patients who came to autopsy 4 hours to 2.5 years after TBI. **A-F**, From Ikonomovic et al., 2004. **G**, Adapted from Roberts et al., 1994.

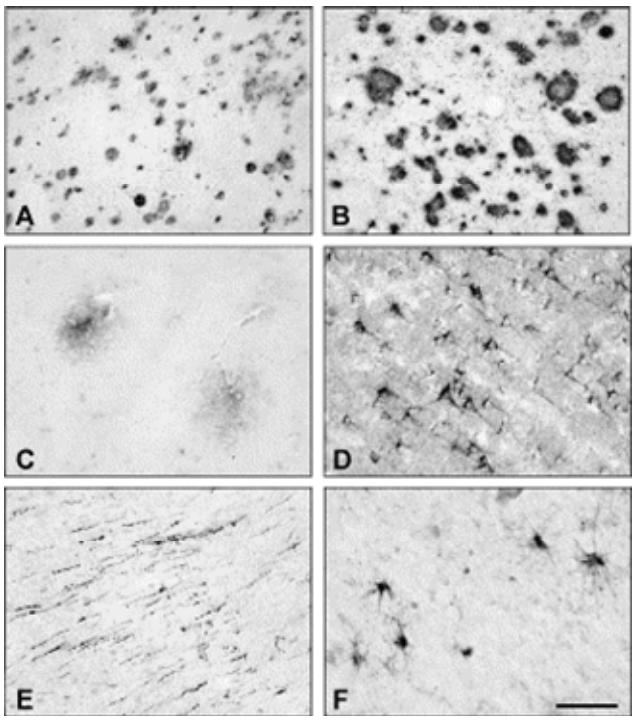

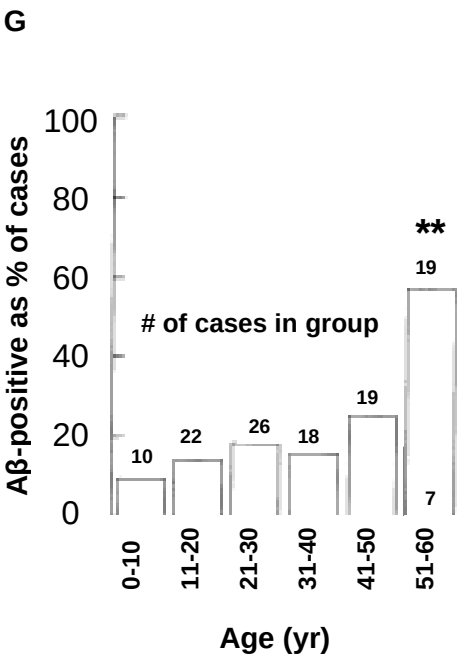

Microdialysis measures ISF Aβ dynamics in living subjects

Immunohistochemistry can reveal deposition and accumulation of Aβ, but is possible only in the subset of patients who require tissue resection or who come to autopsy. We wanted to understand what was happening to soluble forms of the peptide in the extracellular space, presumably before deposition occurs. Essentially, we wanted to measure intracerebral Aβ dynamics. For this purpose, we considered microdialysis.

Brain microdialysis is a minimally-invasive technique that permits longitudinal sampling of small molecules in the extracellular space of living, awake subjects. Previous experimental studies from the Holtzman laboratory have demonstrated that it is possible to assess the dynamics of Aβ in the brain interstitial fluid (ISF) using intracerebral microdialysis in the brains of awake, behaving mice (Cirrito, et al., 2003). Additional studies uncovered a clear relationship between neuronal activity and ISF Aβ concentrations (Cirrito, et al., 2005, Kamenetz, et al., 2003). In subsequent work, it was shown that ISF Aβ levels depend in large part on synaptically-coupled endocytosis (Cirrito, et al., 2008).

Physiological manipulations of neuronal activity also affect Aβ levels. Both acute and chronic stress can result in elevations of ISF Aβ levels (Kang, et al., 2007). Furthermore, ISF Aβ levels were found to correlate with cortical EEG measures of wakefulness (Kang, et al., 2009).

Clinical microdialysis (Hillered, et al., 2005) has been used to measure interstitial fluid (ISF) Aβ in the brain extracellular space of human patients at multiple timepoints. Recently, our group published a study in which we measured the concentration of

amyloid-β peptide (Aβ) recovered by intracerebral microdialysis every 2 hours for at least 72 hours after catheter implantation in human patients who had suffered either an aneurysmal subarachoid hemorrhage or a traumatic brain injury (Fig. 2) (Brody, Magnoni et al., 2008). We found a significant correlation between changes in microdialysis levels of ISF Aβ and changes in neurological status, as assessed by one or two-step changes in the GCS. Aβ levels rose as neurological status improved, and fell as neurological status declined (Fig. 3). Measures of impaired cerebral metabolism and physiological factors associated with depressed functional status were significantly correlated with reduced Aβ levels. Marklund et al. presented results consistent with these findings; ISF Aβ levels were relatively high in a patient who did well and undetectable in a patient who died with severely abnormal brain metabolic parameters (Marklund, et al., 2009).

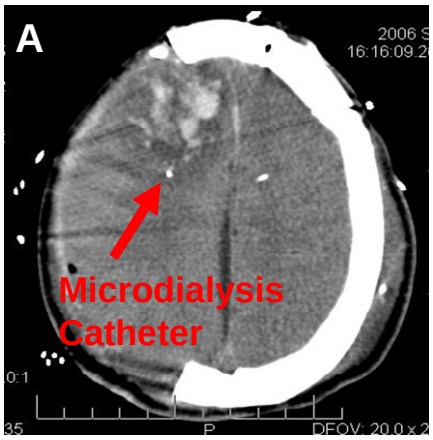

Figure 2. Microdialysis in a severely brain-injured patient. A, CT scan of study patient with microdialysis catheter tip at pericontusional location (red arrow). Courtesy of Sandra Magnoni, Ospedale Maggiore Policlinico, Milan, Italy. **B,** Aβ levels collected as 2-hour microdialysis samples and measured by ELISA. Hours shown from implantation at t=0. Analysis by Michael Spinner, lab of D. L. Brody.

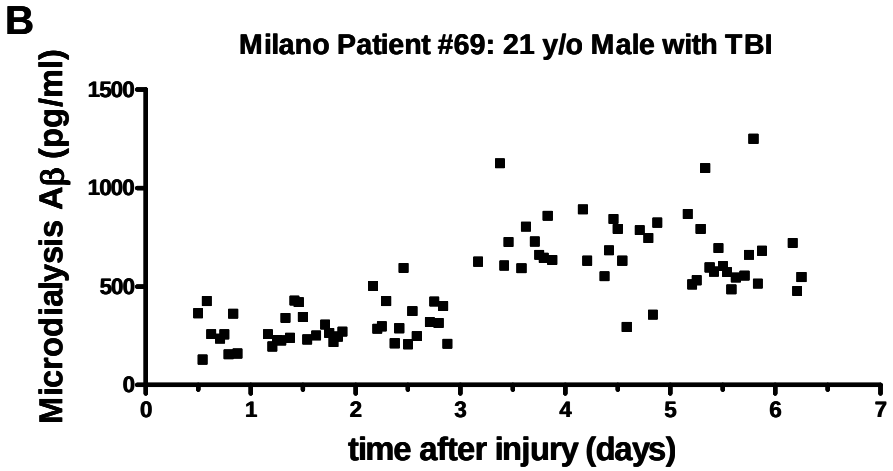

Figure 3. Non-parametric correlation of fold change in Aβ levels from baseline with change in Glasgow Coma Score (GCS). From Brody, Magnoni et al. 2008.

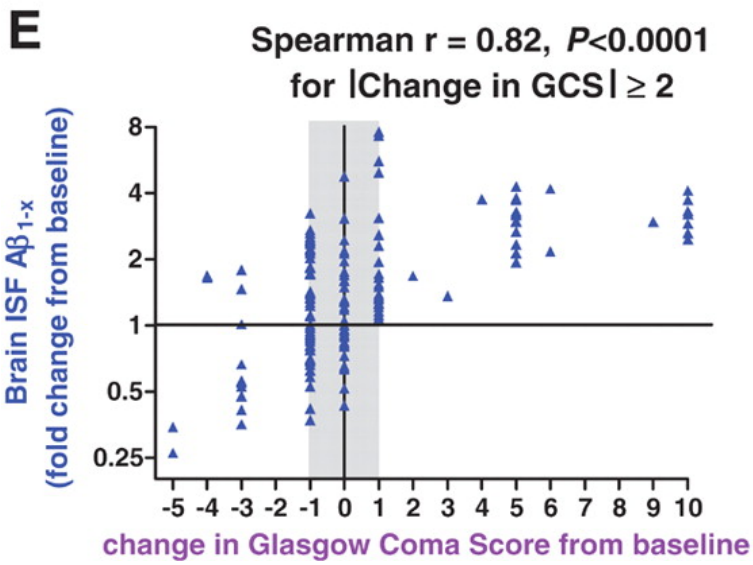

Outstanding questions raised by clinical microdialysis studies

There were several key questions generated by the results of our study. Firstly, the relationship of post-injury measurements to pre-injury levels was unclear. Intracerebral microdialysis is indicated only for severely injured patients under close supervision in a hospital ICU setting. With the exception of monitoring during an elective neurosurgical procedure in an otherwise healthy patient, it is impossible to directly measure baseline, or pre-injury, levels (Brody, Magnoni et al., 2008). Since the dynamics and deposition of the Aβ is of great interest to both the Alzheimer's and the TBI communities, it was critical to understand whether the post-injury levels were significantly increased, equal, or decreased relative to baseline levels. Secondly, we were interested in the relationship of Aβ concentrations in the ISF to levels in other tissue compartments. Finally, most human patients did not begin monitoring until approximately 12 hours or more after an insult had occurred. We were interested to understand the immediate dynamics of ISF Aβ following an injury.

The correlation between fold change in Aβ levels from baseline and change in Glasgow Coma Score (GCS) (Fig. 3) was an important result from this human study. The GCS is considered by clinicians to be a measure of neurological status. Recent animal studies by our group and others have demonstrated the dependence of ISF Aβ levels on neuronal activity (Cirrito, et al., 2008, Cirrito, et al., 2005, Kamenetz, et al., 2003). Taken together, the experimental and human data strongly suggest that injury-related changes in neuronal activity might affect ISF Aβ dynamics. Therefore, we hypothesized that measurement of a surrogate of neuronal activity, such as local EEG

recording, would provide insight into a potential mechanism of post-injury regulation of ISF Aβ.

Need for an animal model: combined CCI-MDA in wild-type animals

For these reasons, we turned to an animal model of a standardized brain injury and microdialysis probe placement. Our group has previously published a well-characterized model of controlled cortical impact (CCI) using a precise electromagnetically driven device (Brody, et al., 2007). We combined the CCI technique with intracerebral microdialysis using a hippocampal probe placement. This combination of techniques permitted us to measure Aβ before and after an injury and in sham-injured animals. We used a wild-type mouse in which murine Aβ is cleaved from full-length amyloid precursor protein (APP) under endogenous promoter control. These experiments demonstrated a trend towards decreased endogenous Aβ in the injured brain. A set of complete results and analysis of these experiments are described in the body of a submitted manuscript included in Chapter 5 of this thesis.

Use of transgenics to measure human sequence Aβ in CCI-microdialysis model

Because this combined CCI-microdialysis model was optimized to address specific questions that arose from the human study, we wanted a more direct comparison of the dynamics of a *human-sequence* Aβ in the interstitial fluid and better time resolution, at least every two hours as was done in the human study. For these reasons, we employed two transgenic mouse models, Tg2576 and PDAPP mice. We hypothesized

the feasibility of this approach based on previous literature. Firstly, the histological and functional sequelae of CCI in PDAPP mice have been extensively characterized (Brody and Holtzman, 2006, Nakagawa, et al., 1999, Nakagawa, et al., 2000, Smith, et al., 1998). Although direct cortical impacts were not yet described in the Tg2576 mice, they had been studied using a model of repetitive-concussive closed-skull injury (Uryu, et al., 2002, Yoshiyama, et al., 2005). Secondly, intracerebral microdialysis of human-sequence Aβ has been described in both PDAPP and Tg2576 (Cirrito, et al., 2008, Cirrito, et al., 2003, Cirrito, et al., 2005, Kang, et al., 2007, Kang, et al., 2009). This allowed us better time resolution as well as the measurement of human-sequence peptide, whose dynamics may significantly differ than the non-aggregating mouse homologue. As in the wild-type mice, ISF levels of human-sequence Aβ in PDAPP mice were significantly decreased compared to baseline. Complete results of experiments with all transgenic mice are described in the submitted manuscript (Ch. 5) and elsewhere as appropriate.

Addition of local EEG to test the potential correlation with ISF Aβ dynamics

Given the correlation between changes in Aβ with changes in neurological status as demonstrated by the human study, we decided to incorporate measurement of local neuronal activity in our animal model. Others in the group had used a simple two-electrode recording system to measure potential differences in the vicinity of a microdialysis probe (Cirrito, et al., 2008, Cirrito, et al., 2005, Kang, et al., 2007, Kang, et al., 2009). We determined that this system would provide a suitable way to test the

hypothesis that TBI-induced changes in local neuronal activity might be related to post-injury Aβ dynamics.

Final considerations of mechanism

What other factors are associated with the acute decrease in interstitial levels of Aβ? Previous studies from the group have shown that ISF Aβ levels are dependent in large part on synaptically-coupled endocytic activity (Cirrito, et al., 2008). Might the changes we observed in our initial experiments be due to changes in neuronal or synaptic activity following TBI? We designed and tested several of these potential mechanisms, which will be described in later chapters of this thesis. The next chapter will present the model of injury, electromagnetic-controlled cortical impact, previously characterized in the lab.

Chapter 2.

Experimental TBI and functional evaluation

Types of experimental TBI

There are a number of well-characterized animal models of experimental traumatic brain injury (Morales, et al., 2005). Experimental TBI can be subdivided into focal, diffuse, and mixed types of injury. Focal models include weight-drop, controlled cortical impact, midline fluid percussion, and optic nerve stretch. Diffuse models include impact acceleration and inertial acceleration injuries. Mixed injury is modeled by the lateral fluid percussion technique. A novel type of injury, commonly termed "blast," results from exposure to the explosive devices employed in military conflict and terrorist activity (Cernak and Noble-Haeusslein, 2009). Blast injury has profoundly devastating systemic effects, acting simultaneously on the brain and body. Efforts are ongoing to fully characterize this injury in the clinical realm and to develop appropriate animal models.

Controlled cortical impact (CCI) is achieved by a metal impounder "tip" driven by a column of compressed air (pneumatic CCI) or electromagnetic discharge (EM-CCI). As the name implies, the cortex is directly contacted by the impounder tip. To do this, the skull is removed by trephinning (craniotomy) prior to impact. Injury severity is graded primarily by varying the depth, but also velocity and dwell time of the impact. The resultant injury is a focal contusion. In humans, this type of injury is also usually described as a contusion.

As an experimental model, CCI recapitulates salient features of clinical contusions, including acute hemorrhage, axonal injury, contusion, blood–brain barrier dysfunction and, in some species, coma. Early spontaneous seizures within 24 hours

after CCI have been observed in rats (Nilsson, et al., 1994). A very recent report suggests the occurrence of post-traumatic epilepsy 6-10 weeks after injury in CD-1 mice (Hunt, et al., 2009). The histological and functional effects of CCI have been described in wild-type mice (Saatman, et al., 2006, Smith, et al., 1995) and in PDAPP mice (Brody and Holtzman, 2006, Nakagawa, et al., 1999, Nakagawa, et al., 2000, Smith, et al., 1998).

Controlled cortical impact: details of the technique

CCI is conducted only on deeply anesthetized animals. The cortex is first exposed by removing the bone above the area that will be impacted. The bone may be drilled by a hand trephine or microdrill. Dura mater is left intact. The diameter of the craniotomy usually depends on the size of the impactor tip. For example, a widely used combination is a 5.0 mm craniotomy for a flat-tip 3.0 mm impactor tip. Stereotaxic coordinates are used to precisely orient the drill and tip relative to fiduciary landmarks on the skull, such as bregma, sagittal, and lambdoid sutures. Then, the impactor tip is centered over the region of interest and a reference depth is established. In our lab, we use a low-voltage touch sensor that produces both light and sound when the impactor tip just touches the dura. The tip is then withdrawn into a cocked position, lowered to the desired depth of impact, and discharged to full extension to impact the cortex. Impactor velocities typically range from 2-7 m/s with a dwell time on the order of 100s of milliseconds. Our impactor discharges at 5 m/s, with a dwell time of 100 ms.

Figure 4. Electromagnetic impactor mounted on stereotactic frame with microdrill and 5.0 mm trephine. Inset, 3.0 mm impactor tip. From Brody et al., 2007.

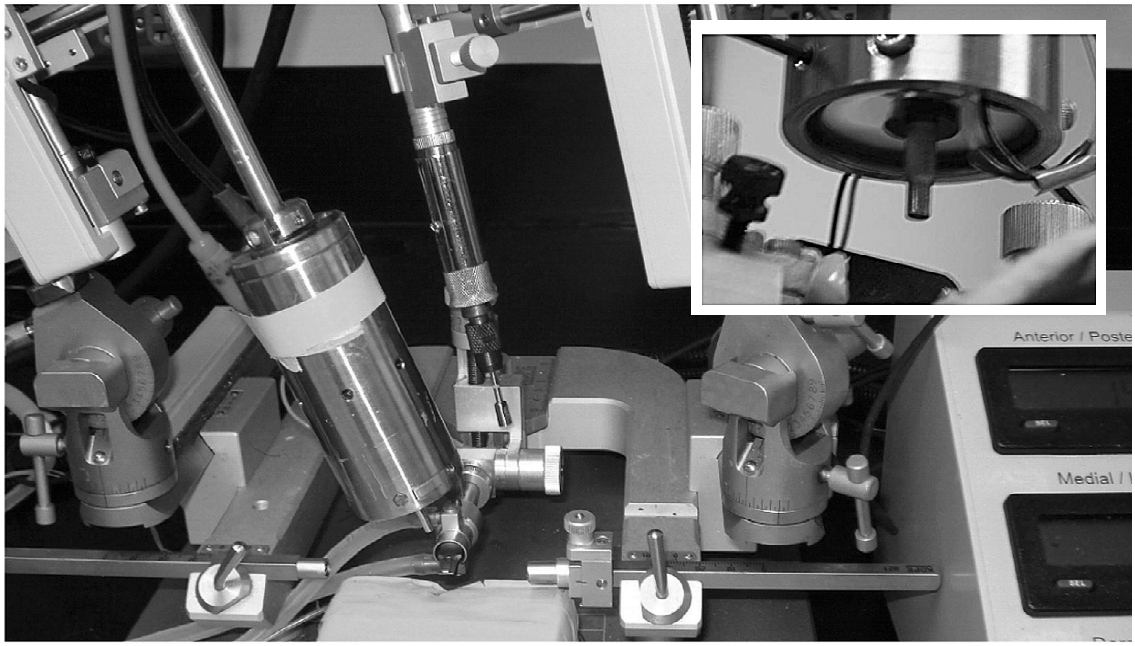

Advantages of the electromagnetic controlled cortical impact (EM-CCI)

Because we use transgenic mice, it was important to have a system that was reliable and precise in order to reduce the variability, thereby reducing the number of mice needed to detect significant differences. Original versions of this model employed a pneumatic system, whereby the flat-tip metal impounder was driven by a column of compressed air. In conjunction with a professor of mechanical engineering, Philip Bayly, the lab designed an electromagnetic coil-based system operated by a custom MATLAB program (Fig. 4; hereafter referred to as "EM-CCI"). A chief advantage of EM-CCI device over pneumatic impactors is the relative absence of overshoot (Brody, et al., 2007). A range of injury severities were characterized by gross histology, stereological cell counting, Morris water maze testing, and rotarod testing. These results were

compared to those described for injuries produced by a pneumatic impactor. It was determined that the increased control in the impactor's trajectory yielded more precise, reproducible injuries. As a consequence, a lesser number of mice per group was required to detect significant differences (Brody, et al., 2007).

Usefulness of the hippocampus as an experimental test structure

Because we wanted to recreate important aspects of clinical TBI in the CCI model, an appropriate behavioral evaluation was necessary. Sensitive functional tests for CCI-injured mice include composite neuroscore, wire grip, beam balance, beam walk, rotarod, grid walk, forelimb use, Barnes maze, and Morris water maze tasks (Fujimoto, et al., 2004). These tests assess a range of functions, including sensorimotor and memory functions. Due to our overarching interest in TBI-related dementia, we chose to model memory impairments. Many brain-injured patients suffer debilitating deficits in implicit and explicit memory (Vakil, 2005). Functional MRI and PET studies suggest that different types of memory functions depend on different networks of structures and tracts (Gabrieli, 1998, Mizumori, et al., 2004). Likewise, human TBI is typically of a diffuse nature, affecting multiple structures. How do we isolate a testable memory function in our animal model?

In rodents, spatial learning and memory were first believed to localize to the hippocampus based on *in vivo* recording of "place cells" of the CA1 and CA3 regions (O'Keefe and Dostrovsky, 1971). Based on these initial observations and an extensive literature, it is well documented that selective damage to the hippocampus results in

impaired spatial learning and memory in rodent models. Such impairments are evaluated by various maze assessments (Paul, et al., 2009).

CCI is an appropriate injury model to create hippocampal damage and deficits in spatial learning and memory. The epicenter of impact can be stereotactically positioned over the hippocampus. There are a range of depths that will damage the hippocampus in a graded manner as quantified by cell loss, IgG extravasation, reactive gliosis, and MAP2 immunoreactivity within 15 minutes to 7 days post-injury (Saatman, et al., 2006) and atrophy at 30-45 days post-injury (Brody, et al., 2007). It has previously been shown that CCI-induced damage affects spatial learning and memory as assessed by the Morris water maze in various strains of wild-type and transgenic mice (Fox, et al., 1999, Nakamura, et al., 1999, Scherbel, et al., 1999, Sinz, et al., 1999). The Morris water maze can also reveal deficits in executive functions such as search strategy, particularly in mice that express various forms of human APP (Brody and Holtzman, 2006, Janus, 2004).

The Morris water maze: set-up and brief procedural details

The Morris water maze is a well-characterized, widely used model of spatial learning and memory in rodents (Crawley, 2000, Morris, et al., 1982). It has been employed in various areas of neuroscience research, including experimental TBI (Fujimoto, et al., 2004). The task is predicated on the observation that mice can swim, but are motivated to escape water. The apparatus consists of a pool (diameter, 118 cm) filled to within 10 cm of the upper edge with water made opaque by white nontoxic tempera paint (Fig 5). The pool contains a round platform (diameter, 11 cm) that the

mice can climb on to escape the water. The pool is located in a well-lit room that contains different visual "cues" in fixed locations. For example, we use colorful posters and worklights. Mice are first trained in the escape task with a marked, visible platform during 60 s-trials. Then, during similar timed trials, mice are required to learn and remember the location of a platform hidden just below the surface of the opacified water. To track and record the mouse's trajectory, an overhead video camera records the animals' swim paths (Fig 5; San Diego Instruments, San Diego, CA).

Figure 5. Morris water maze. Pool filled with opacified water during the HIDDEN task. Trajectories recorded by the software are superimposed on a photograph. From http://www.iop.kcl.ac.uk/iopweb/blob/downloads/locator/l_622_watermaze.jpg.

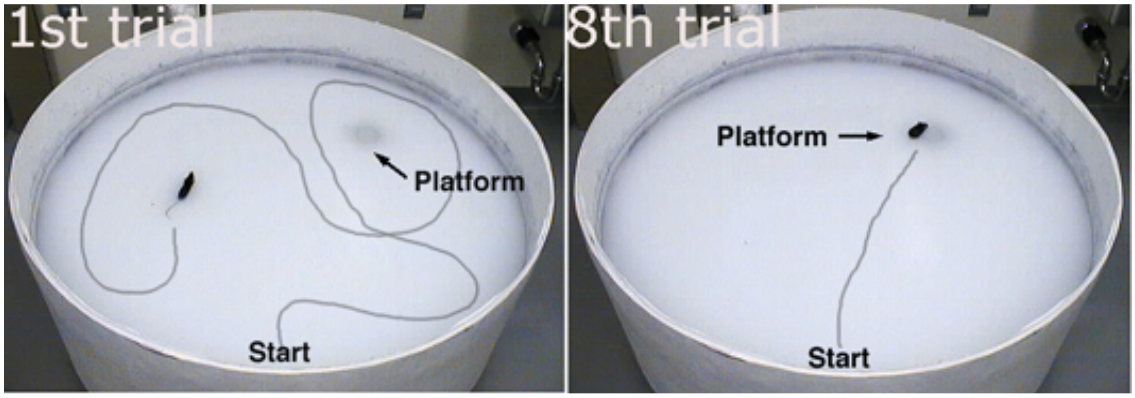

Specific tasks in the MWM assess learning and memory

For the training period, also called CUED or VISIBLE task, the platform is visibly marked by a bright orange, 1-foot tall stick. The platform surface is also slightly above the water level. Mice are placed into the pool by hand at one of four release points. The mouse can then see the platform and learns to swim to the platform and climb on it to escape the water. Importantly, the mice are released from each of 4 different quadrants in each trial. The novelty of the start location requires the mouse to

rely on multiple cues, including the orange stick and cues around in the room, to construct a complex spatial configuration. For most experiments, 4 trials per day, 1 quadrant per trial, for each of 3 days of CUED training are sufficient for the mice to learn to quickly and directly swim to the platform. The mice are then allowed two days of rest and consolidation. Next comes the testing period, which often consists of two main tasks: the HIDDEN or SPATIAL task, and the PROBE trial. In the HIDDEN task, the orange stick is removed and the platform surface is submerged 0.5 cm below the surface of the water such that it is not directly visible to a swimming mouse. The HIDDEN task is often conducted at a rate of 4 trials per day for each of 5 days. Mice must again learn and remember the location of the platform using only the visual cues in the room (the colorful posters and worklights). At the end of the 5^{th} day, the PROBE trial is conducted. In this test, the platform is removed entirely from the pool and the mice will swim around in the vicinity of the platform. Mice are allowed only 30 s and are then removed from the pool. Mice that have learned the location of the platform will spend a greater proportion of the time in the quadrant that formerly held the platform.

Training for the MWM: Hartman study

To better learn the execution and analysis of Morris water maze testing, I was recruited to conduct an experiment to complete a study by a previous postdoctoral candidate in the Holtzman laboratory, Richard Hartman. He assessed the effects of long-term administration of pomegranate juice with respect to amyloid plaque burden, Aβ tissue levels, and assessment of spatial memory (Hartman, et al., 2006). In this study,

mice expressing a prion-promoter controlled transgene for the Swedish mutant human amyloid precursor protein (referred to in the paper as APPSw; also called Tg2576 mice) were given pomegranate juice (PJ) at a concentration equivalent to that of an adult human consuming 1 or 2 8-oz glasses of juice per day. The treatment regimen began at 6 months of age and continued until 11.5 months, when behavioral testing was initiated. Treatment was continued throughout testing. The control group received sugar water in an identical composition and concentration of that found in PJ. APPSw mice fed PJ demonstrated superior learning in the Morris water maze, finding the platform more quickly in the CUED task and spending more time in the vicinity of the platform in contrast to APPSw mice fed sugar water. To determine whether or not the effects of PJ were specific to the tissue levels of human Aβ and amyloid plaque formation, the same experiment was conducted on wild-type (littermate) mice. I was assigned to conduct all treatment and MWM testing in the wildtypes. There were no differences between groups given either PJ or sugar water, neither in distance traveled nor in swim speed (Fig. 6). This result means that the mice learned and remembered platform location equally, and their physical abilities and motivation to escape the water were also equal. This suggested that the effects of PJ on MWM learning were specifically mediated through effects on Aβ and amyloid plaque burden.

Figure 6. MWM testing. Wildtype controls were fed either pomegranate juice (PJ, dark circles) or sugar water (vehicle, open circles) for six weeks and tested in the MWM using CUED and SPATIAL tasks. **A**, total distance recorded in the CUED and SPATIAL tasks. **B,** swim speed calculated in the CUED and SPATIAL tasks. Neither total distance nor swim speed differed between groups. From Hartman et al., 2006.

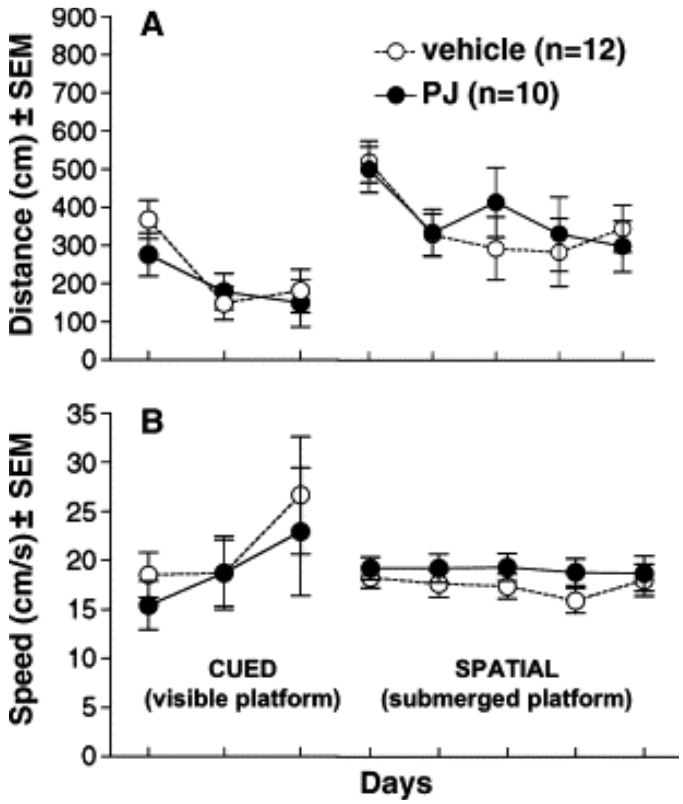

Learning assessment of CCI-injured mice in the MWM: Brody study

Secondly, in response to a manuscript review for the lab's paper describing the characterization of the EM-CCI device, we were asked to evaluate an additional, milder injury severity in terms of MWM (Brody, et al., 2007). I was recruited to perform injuries and assess mice in the MWM. Three groups of B6SJL mice (wild-type) were pseudo-randomly assigned to a sham, 1.5 mm, or 2.5 mm injury. These mice were allowed to recover for 12 days, and tested in the MWM by myself and a senior

technician, Michael Spinner. A similar experimental design as in the previous study was used: 3 days of visible testing, 2 days of rest, and 5 days of hidden testing with a probe trial at the end of the 5th day. Shown below is a figure describing the lack of an effect in the MWM of 1.5 mm depth (Fig. 7). Not shown are data for the 2.5 mm injury; deficits in MWM tasks were similar to the previous two investigators' groups, also presented in this paper.

Figure 7. B6SJL (wildtype) mice injured at 1.5 mm depth show no significant differences from sham-injured animals in the visible and hidden tasks in MWM. From Brody et al., 2007.

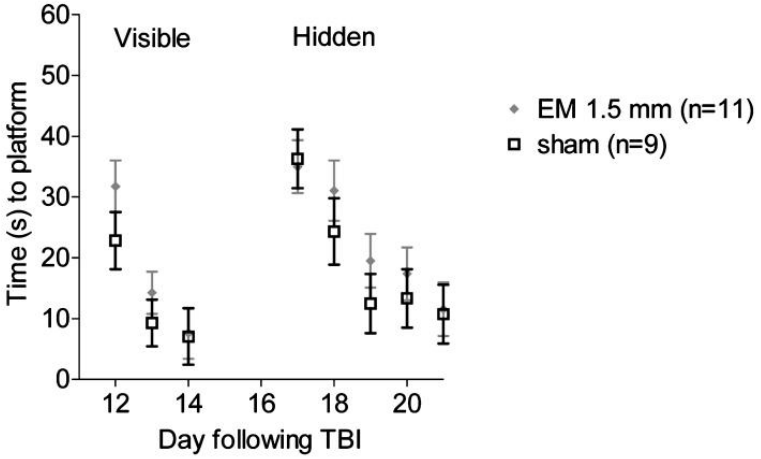

The concordance of the results of these behavioral experiments in wild-type mice with others in the lab suggested that we were prepared to combine CCI with microdialysis, first in wild-type and then in APP-transgenic mice, towards our ultimate goal of measuring hippocampal Aβ dynamics before and after brain injury. The next chapter will provide some background on brain microdialysis in research and clinical applications.

Chapter 3.

Brain microdialysis in research and clinical studies

Microdialysis: origins in the push-pull canula

The origins of microdialysis were first described in the early 1960s, when push-pull canulas were inserted into animal tissues to sample from the extracellular space (Myers, 1986). Before *in vivo* sampling was possible, it was difficult if not impossible to measure specific neurotransmitters in discrete anatomical regions. Most techniques relied on biochemical extraction and analysis of post-mortem tissue. To improve the specificity for region-specific physiological activity, push-pull canulas were developed for use in the brain. Two canulas, usually metal but sometimes glass or plastic, are placed side by side into tissue. Early designs employed large-bore syringe needles, for example. A syringe or peristaltic pump pushes fluid through one canula, and a separate pump pulls fluid from the second canula at the same rate. Using an adaptation of a design originally to measure bradykinin in the skin of human volunteers (Fox and Hilton, 1958), Delgado and colleagues measured acetylcholine (ACh) release in the caudate nucleus and motor cortex in unanesthetized monkeys (Delgado and Rubinstein, 1964). In addition, they placed an electrode next to the canulas and were able to measure the effects of local electrical stimulation on neurotransmitter levels (Fig. 8).

Figure 8. Push-pull canulation in the awake monkey. Two #27 stainless steel tubes (1), soldered together with electric recording probes (5). Figure from J.M.R. Delgado, 1966. Intracerebral perfusion in awake moneys. Arch. Int. Pharmacodyn. Ther. 161: 442-462.

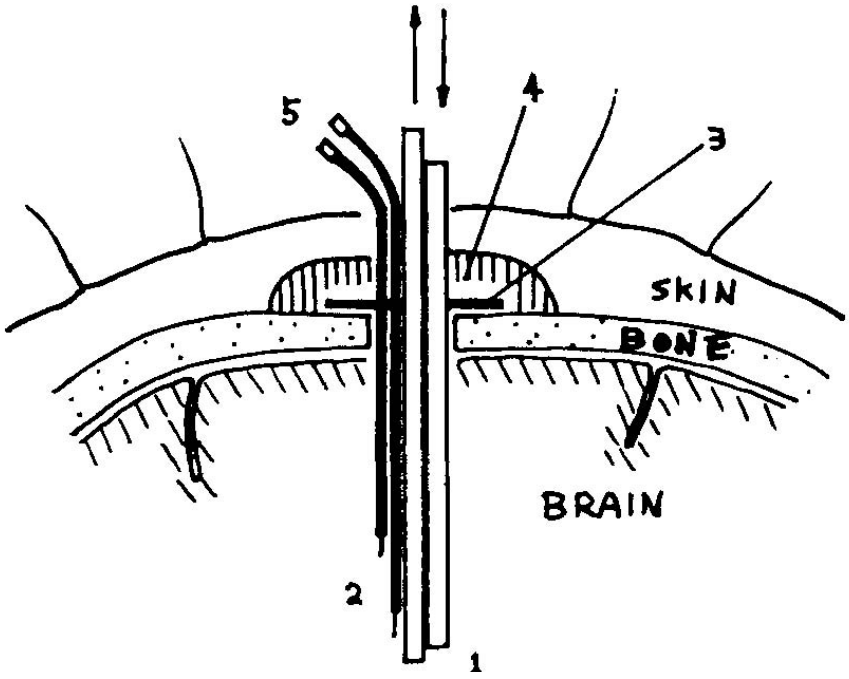

In the same year, a colleague reported measurements of ACh and dopamine in the caudate nucleus of anesthetized cats, and enhanced ACh release upon thalamic stimulation (McLennan, 1964). Perfusion became a critical technique to study discrete brain regions in living animals. Not only could cerebral metabolites, neurotransmitters, and hormones be measured under physiological conditions, the response to homeostatic challenges such as temperature and appetite could be documented. For example, cross-perfusion experiments revealed the solubility and sites of production and action of hypnogenic, appetitive, and satiety factors (Drucker-Colin, 1973, Yaksh and Myers,

1972). Further, the effect of drugs and electrical stimulation on endogenous species could be investigated. These initial studies established push-pull perfusion as an invaluable experimental tool.

Limitations of push-pull canulas

However, push-pull canulas were limited by their tendency to cause tissue damage and the lack of controls for effects of technical design details. Firstly, even in the absence of perfusion, simple insertion of the rigid canula into soft tissues such as brain parenchyma was enough to cause a measureable lesion along the tract (Yaksh and Yamamura, 1974). Secondly, at perfusion rates 50-100 times faster than are typically used in modern probes, fluid pressure could damage tissue as reflected in dialysate protein concentration (Yaksh and Yamamura, 1974). A lesion could also result from pressure differences due to a mismatch in push and pull flow rates. In this case, dislodged tissue fragments could occlude the canula lumen (Myers, 1986). Finally, there were very few controlled experiments to determine the effects of repeated insertions of the canula, the size of the device, the perfusion rate, separation between the tips of the push and pull tubes, and the longevity of perfusion (Myers, et al., 1998).

Evolution of the modern microdialysis probe

In contrast to an open push-pull canula system in which neural tissue is bathed directly in perfusate, other configurations consisted of a "dialysis bag." This was a permeable membrane attached to the end of the canulae, filled with perfusion fluid and

left to equilibrate with the surrounding medium (Bito, et al., 1966, Delgado, et al., 1972). This is equivalent to the "zero flow method" for which complete equilibration across the membrane is allowed to occur over a theoretically unrestricted period of time. However, for longitudinal measurements in the same subject, samples need to be collected after a finite period of time. Furthermore, the exchange surface needs to be constantly refreshed with new perfusion fluid. A flow of perfusate would thus permit partial equilibration of solutes across the membrane, but also allow samples to be collected in discrete time intervals. These ideas were realized by the "hollow-fiber" configuration (Delgado, et al., 1984). In 1974, Ungerstedt and Pycock reported on the use of hollow fibers in their study of dopamine transmission in the rodent brain (Ungerstedt and Pycock, 1974). The fibers were composed of semi-permeable material. A perfusion fluid was flowed through the hollow fibers. Only molecules that could diffuse across the material, the membrane, were collected in the dialysate. The method had many advantages over the push-pull canulation systems. While sampling was selective for small, easily diffusible species, tissue damage using a soft, flexible membrane probe was minimal and measurements were more reliable than push-pull canulation (Myers, et al., 1998). These prototypes evolved into modern versions of the microdialysis probe. An example of a rodent research probe is shown in Figure 9.

Figure 9. Bioanalytical Systems BR-2 38 kD cutoff microdialysis probe and guide canula for rodents. Left, microdialysis probe has inlet (yellow) and outlet (green) ports. The 2.0 mm-long, 0.320 mm diameter exchangeable membrane is seen at the tip of the probe. Right, corresponding guide canula with plastic shaft. The probe fits by tongue-and-groove through guide canula, shown with dummy stylet. When inserted into guide canula, only the 2.0 mm probe membrane protrudes.

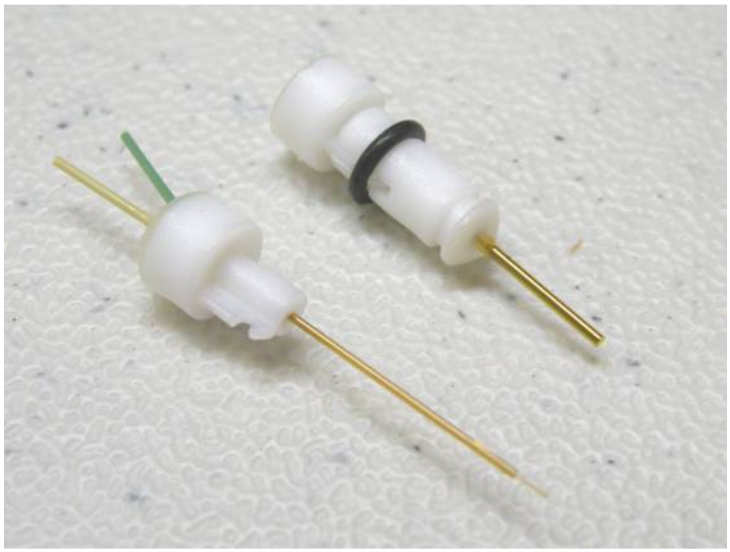

Theory of microdiaylsis sampling

Microdialysis sampling primarily depends on several factors: concentration gradient of the molecule of interest, flow rate of the perfusate, and the area and diffusion characteristics of the membrane (Benveniste and Huttemeier, 1990). Another consideration is the configuration of the inlet and outlet ports with the exchange membrane. A number of arrangements have been described, including side by side tubing, loop dialysis probes and linear or "transverse" configurations (Fig. 10) (Benveniste and Huttemeier, 1990, de Lange, et al., 1997).

Figure 10. Different probe geometries used for intracerebral microdialysis. A, loop or vertical, U-shaped membrane. **B**, side-by-side or vertical, L-shaped membrane. **C**, linear or horizontal/transverse membrane. From de Lange et al.,1997.

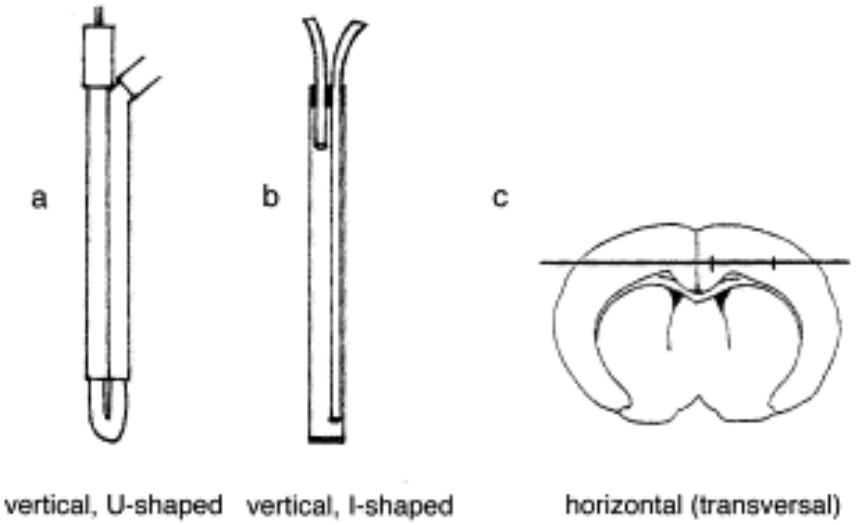

Most commercially-available probes use a concentric configuration (Fig. 11).

Figure 11. A concentric configuration of inlet and outlet tubings in a probe designed for intracerebral sampling. Adapted from Beraldi Ribeiro, 2009.

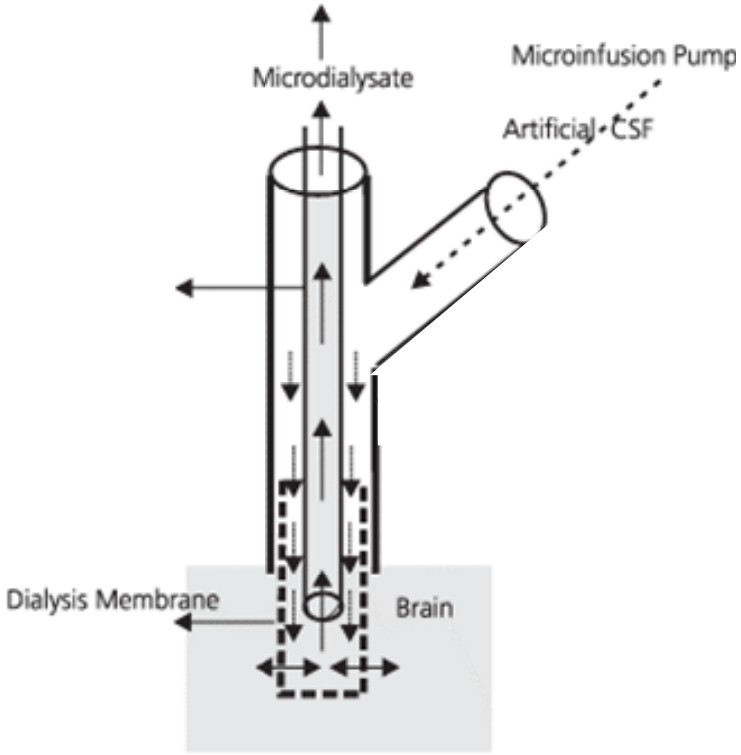

The choice of probe configuration depends on the specific application. For example, long-term experiments to measure circadian fluctuations of melatonin in the pineal gland have been facilitated by a linear or transverse probe (Borjigin and Liu, 2008).

The first principle is that molecules move according to their concentration gradient, from areas of higher to lower concentration (Fig. 12). For example, if a molecule is to be infused into tissue, there should be a much higher concentration in the perfusate than in the surrounding tissue. Likewise, if an endogenous molecule is to be sampled from the tissue, its concentration in the perfusate should be much lower than the region of interest.

Figure 12. Schematic of a research microdiaysis probe schematic demonstrating inflow and outflow pathways, and exchange of small molecules across the membrane. The perfusate contains an infused molecule (black circles) that can exchange across the membrane into the tissue. Simultaneously, an endogenous molecule (white circles) exchanges across the membrane into the outflow dialysate. Adapted from Chaurasia et al. AAPS-FDA Workshop White Paper: Microdialysis Principles, Application, and Regulatory Perspectives Report From the Joint AAPS-FDA Workshop, November 4-5, 2005, Nashville, TN. *AAPS Journal*. 2007; 9(1): E48-E59.

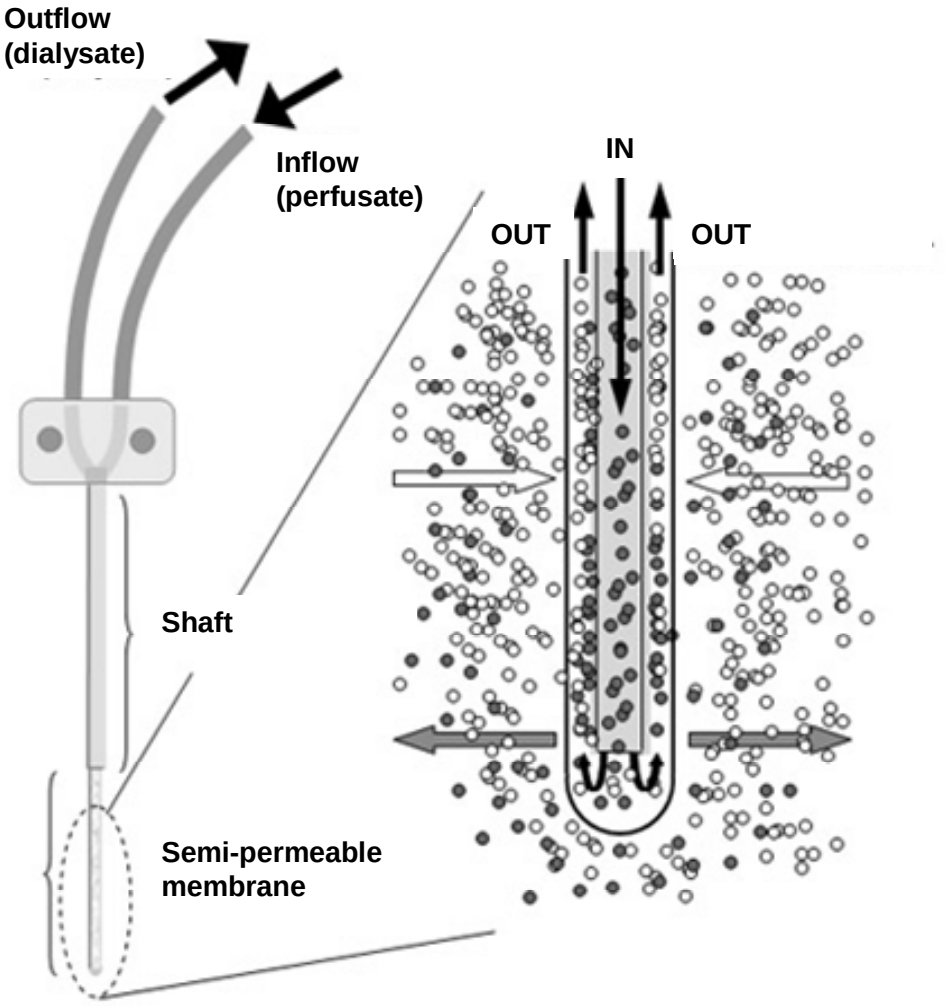

The second principle is that recovery is inversely related to perfusion rate. Based on theoretical models of diffusion and informed by empirical data, a mathematical function can be used to predict recoveries based on flow rate (Jacobson, et al., 1985,

Johnson and Justice, 1983, Menacherry, et al., 1992). Often, this function takes the form of a first-order exponential decay, although empirical data should always be used to determine the best-fit function.

Thirdly, the choice of membrane material will influence the types and quantity of sampled species. Materials are described as "semi-permeable" or "porous." Beyond that, materials vary considerably in their electrostatic nature. Some are more hydrophilic (cellulose acetate, polycarbonate, polyacrylonitrile), whereas others are more hydrophobic (polysulfone-based materials). While the recovery of some small molecules, such as urea, does not appear to differ meaningfully among membranes, material composition can have a dramatic effect of recovery of large species, such as β2 microglobulin (Ouseph, et al., 2008). Proteins pose a particular challenge. Not only can they adsorb to the synthetic polymer materials, they can accumulate in pores. Pores resemble tunnels relative to the size of most relevant proteins when examined at the resolution of a scanning electron micrograph (Fig. 13, from Rosenbloom et al., 2005).

Figure 13. Scanning electron micrograph of CMA 20 (PES) microdialysis membrane. Left, close *en face* view of material porosity. Scale bar, 2 μm. Right, cross-sectional view at lesser magnification. Scale bar, 50 μm. From Rosenbloom et al., 2005.

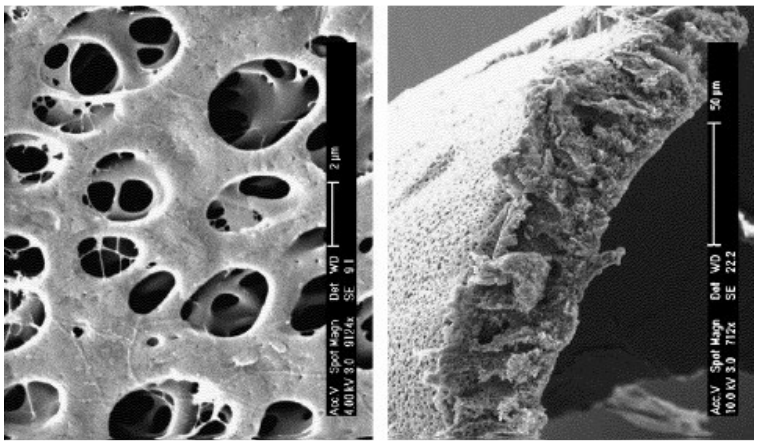

Hydrophobic materials are especially adsorptive for proteins. One solution is to create an intermediate composition by the addition of a polymer such as polyvinylpyrrolidone (PVP) to impart hydrophilicity. Such a material then has hydrophilic-hydrophobic "microdomains," such as polyarylethersulfone (PAES).

Related to material composition is the molecular weight cutoff (MWCO). The MWCO is a boundary beyond which approximately 80% of dextrans of that size are non-exchangeable (CMA literature). Because the MWCO rating is empirically determined using the exchange characteristics of dextrans, it is nominal with respect to biological macromolecules. The MWCO rating often fails to accurately describe the recovery of proteins. For example, a recent study concluded that proteins larger than 43 kD were mostly irrecoverable using a CMA 20 probe of nominal cutoff 100 kD (Rosenbloom, et al., 2005). This study recommended the CMA 20 be rated at 29 kD for most proteins.

Membrane pore sizes in high MWCO membranes are often orders of magnitude larger than the expected radius of individual proteins. The discrepancy between apparently favorable pore-to-protein size ratios and the low recovery of higher molecular weight species may seem paradoxical. However, the path through a network of pores to reach the inside of probe is tortuous, and may be 10,000 times longer than the protein's diameter. The relationship of each protein to each membrane material must be individually characterized.

A related factor in the recovery of large molecular weight species in a high MWCO probe is that of volume recovery. Volumes of the dialysate can either be increased due to ultrafiltration (fluid flow into the probe from tissue) or decreased due to

loss of perfusate into the tissue. In a low MWCO probe, given the isotonicity and ionic balance between perfusate and tissue, net fluid exchange does not usually occur. However, in higher MWCO probes with pore sizes on the order of microns, net fluid exchange can be problematic. The balance between hydrostatic pressure of the fluid column through the membrane and oncotic pressure on the dialysate from the tissue will dictate the net gain or loss of water from the microdialysis probe. Because of the relatively large pore size in the high MWCO membranes, and the back-pressure imposed by the perfusion rate, fluid will escape from the system into the lower pressure tissue without any colloidal forces to maintain net zero pressure.

Finally, many proteins tend to bind synthetic surfaces, including membranes, tubing and at junctions. For example, despite a molecular weight of approximately 4 kD for monomeric Aβ, this species is irrecoverable without the addition of albumin to the perfusate. It is thought that albumin coats or carries this highly "sticky" peptide across the membrane and through the tubing, preventing its binding to synthetic surfaces.

Clinical applications of microdialysis

Since the first publications from Ungerstadt and colleagues in the mid-1980s, the clinical cerebral microdialysis literature has amassed hundreds of studies describing measurement of metabolic molecules such as lactate, pyruvate, glucose, and urea; the neurotransmitters, glutamate, GABA, glycine, acetylcholine, dopamine, serotonin, and histamine; and other molecules. The full range of clinical applications has not been fully explored and is under active investigation. Although cerebral microdialysis is used

routinely in some centers in Europe to monitor surrogates of cerebral metabolism, it is not commonly used in the U.S. The delayed adaptation of new monitoring technology is not uncommon in intensive care, as is demonstrated by the case of invasive intracranial pressure monitoring (Hillered, et al., 2005). In the case of microdialysis, there are a few well-studied markers of clinical events that would merit widespread adaptation of this technique. Most notably, microdialysis measurement is very sensitive to disturbed glucose metabolism as detected by glucose, lactate, pyruvate, the lactate/pyruvate ratio, the lactate/glucose ratio, and pH (Hillered, et al., 2005). These studies have provided otherwise inaccessible information about metabolic disturbances in the extracellular space in a variety of neurological insults (Hillered, et al., 2005).

Not only can microdialysis aid in the characterization of physiological events, it can help to monitor the effectiveness of interventions. For a drug treatment, these methods are pharmacokinetics (the measurement of drug metabolism) and pharmacodynamics (the measurement of a drug's effect on a particular target). The targets in published pharmacodynamic studies are often the same molecules and neurotransmitters first described in studies of basic physiology (Hillered, et al., 2005).

However, many drugs target larger peptides and proteins. In 2005, our lab was actively testing anti-Aβ strategies such as passive immunotherapy and γ-secretase inhibitors. Therefore, we conceived the microdialysis experiments as a novel technique for pharmacodynamic studies of such anti-Aβ strategies. At this time, we were also developing an interest in proteins thought to be increased in the CSF after TBI and subarachnoid hemorrhage, such as tau and neurofilament, and began to explore the

technology available to measure the ISF levels of these species by microdialysis. As these proteins are approximately 50 and 68 kD, respectively, their detection would be unlikely using the standard clinical catheters. Fortunately, a high MWCO human catheter had recently been introduced (Fig. 14).

Figure 14. CMA-71 100 kD cutoff patient microdialysis catheter.

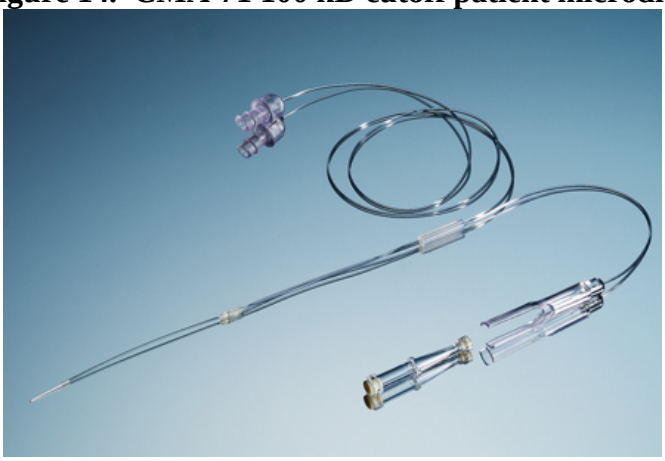

Measurement of higher-molecular weight species using human catheters

The only catheters that are FDA-approved for use in human patients are manufactured by CMA Microdialysis of Sweden. Measurement of small molecules in the brain has been extensively studied using the CMA70 model, which has a 20 kD MWCO rating (Hillered et al., 2005). The exchange membrane of a CMA70 consists of a polyamide material. More recently, the introduction of the CMA71 catheter with a 100 kD MWCO rating has permitted detection of larger species such as cytokines, as well as peptides and proteins implicated in neurodegenerative disease (Brody, et al., 2008, Marklund, et al., 2009). The exchange membrane is composed of the synthetic material, polyarylethersulphone (PAES), and is approximately 10.0 mm long with a diameter of 0.50 mm. Using a standard flow rate of 0.3 μL/min, the lab was able to measure tau and

neurofilament light-chain in some patient microdialysis samples (Magnoni, 2009). The recovery of small molecules is similar to the CMA 70 (Hillman, et al., 2005). However, very few studies have been able to measure detectable levels of such large proteins, and none have conducted controlled experiments to quantify relative recovery.

The challenges of microdialysis with high molecular weight membranes have been described in the literature (Clough, 2005, Rosenbloom, et al., 2005). Recently, a study used scanning electron microscopy to compare a CMA 71 probe used in only an *in vitro* solution (the *in vitro* probe) with another CMA 71 probe that had been placed in a human patient for 48 h (the *ex vivo* probe). These images demonstrate the invasion of pores by biological debris in the *ex vivo* probe (Helmy, et al., 2009). In contrast to an *in vitro* probe (Fig. 15), the *ex vivo* probe appears to be clogged or "biofouled" (Fig. 16).

Figure 15. Scanning electron micrograph at various magnifications of CMA 71, after 48h *in vitro* experiment bathed in CNS perfusion fluid + recombinant IL-1. A, PAES outer membrane showing large pores and occasional merged pores. **B**, inner shaft of non-porous material polyurethane. **C**, higher magnification view of porous material. **D**, on-end view of pores within outer PAES membrane. From Helmy et al., 2009.

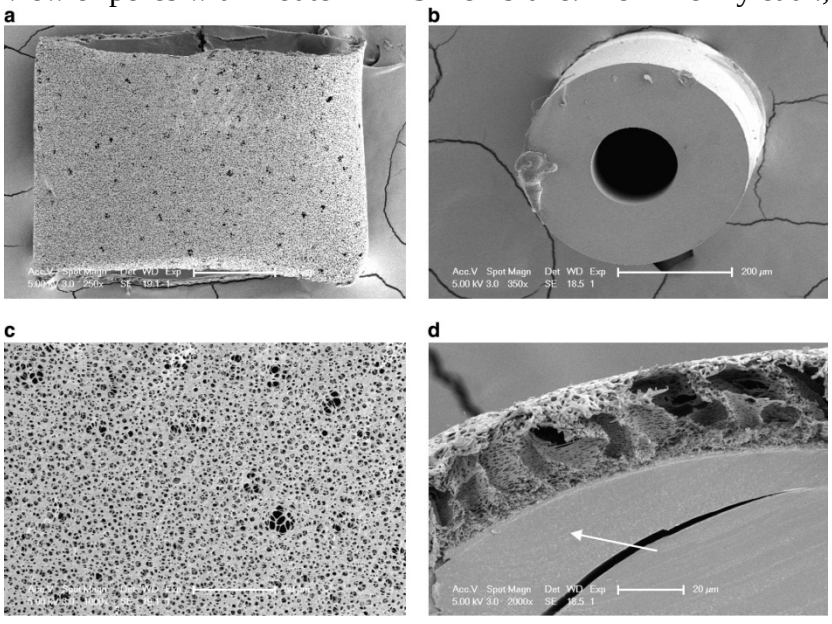

After 48 hours *in vivo*, it appears there may be some invasion of the pores by large biological debris, such as cells (Fig. 16).

Figure 16. Scanning electron micrograph of CMA 71 after 48h *in vivo*. **A**, on-end view of isolated membrane. The inner tube has fallen out. Note larger pore size on the outer surface, compared to the inner surface. **B**, higher magnification view of outer membrane showing pores of diameter several microns with occasional particulates, possibly cells. **C, D, E,** highest magnification view of outer surface membrane demonstrating material in pores. **F**, pores on the inner surface of the membrane appear to have a much smaller diameter than on the outer surface. From Helmy et al., 2009.

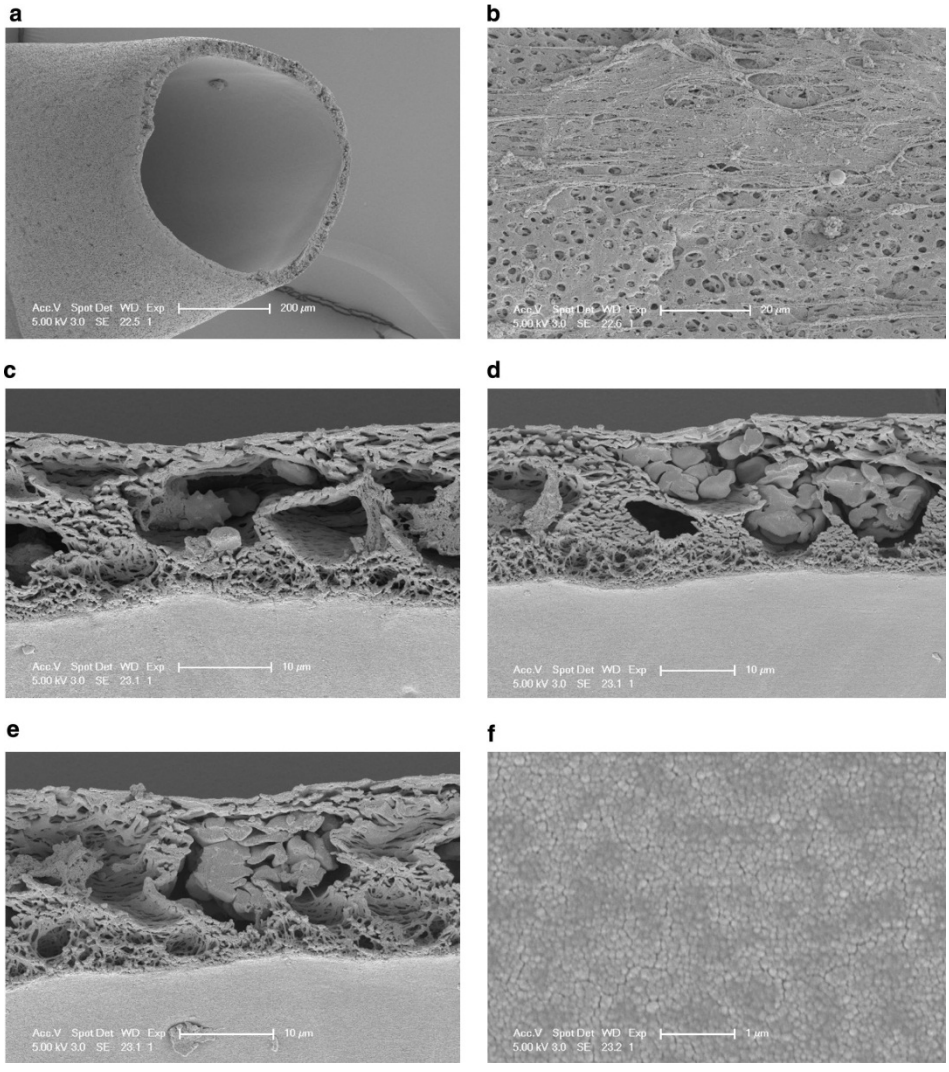

Cytokines: example of recovery of higher molecular weight species

One example of recovery of higher molecular weight species in cerebral applications is that of inflammatory cytokines. Since 2005, several groups have reported the recovery of cytokines using the CMA 71 100 kD catheter (Hillman, et al., 2005, Hillman, et al., 2007, Hutchinson, et al., 2007, Mellergard, et al., 2008). Using a standard pump rate of 0.3 μL/min, perfusion solutions contained either 3.5% human albumin or Ringer-dextran 60 (RD60) to avoid net volume loss. In particular, levels of IL-6 tracked with changes in the L/P ratio and glycerol levels in patients with severe TBI or subarachnoid hemorrhage (Hillman, et al., 2005). IL-6 has a molecular weight of ~24 kD. A follow-up study validated these initial results using 3.5% human albumin exclusively in the perfusate as an oncotic agent. It was determined that interstitial levels of IL-6 corresponded better than IL-1β to ischemic events and general brain "stress" (Hillman, et al., 2007). Additionally, this paper described the measurement of vascular endothelial growth factor (VEGF) and cathepsin-D in one or two patients, indicating that recovery of these proteins is also possible. VEGF exists as a homodimer of molecular weight 45 kD, and as a monomer of approximately 23-26 kD. Cathepsin-D has multiple mature isoforms, with molecular weights detected at 15 kD (light chain) and 28-35 kD (heavy chain). Further studies looked at the roles of other cytokines: IL-1α, IL-1β, and IL-1ra, and again compared their dynamics to the L/P ratio as a marker of anaerobic stress (Hutchinson, et al., 2007). The molecular weights of IL-1α, IL-1β and IL-1ra are approximately 17 kD. Finally, another group looked at concentrations of a number of other cytokines as well as VEGF and basic fibroblast growth factor (bFGF, molecular

weight ~17 kD) (Mellergard, et al., 2008). They compared two probe locations, one in macroscopically normal tissue and one in pericontusional tissue. All probes were perfused with Ringer dextran 60 (RD60). As expected, ISF levels of cytokines were at a detectable level throughout the monitoring periods. In contrast, VEGF was undetectable in the sickest patients. FGF was detectable in the first 6-12 hours immediately after microdialysis catheter was implanted, but rapidly dropped off to a plateau and remained close to the limit of detection over the course of 36 hours.

Experimental probes have been custom-built to study other, larger proteins in human patients. Recently, one group reports that use of a 3000 kD MWCO probe (Metalant, Sweden) with peristaltic push-pull perfusion permits the *in vivo* measurement of the inflammatory cytokines, IL-1β and IL-6, and nerve growth factor (NGF) from patients with severe TBI (Winter, et al., 2002, Winter, et al., 2004). NGF is secreted into the extracellular space and exists *in vivo* as a 26-29 kD dimer. As endogenous controls, total protein and albumin levels measured in dialysate remained relatively constant over periods of up to 5 days.

Importance of pumping method: push-pull vs standard pumping

Despite these promising results, measurement of larger proteins has been challenging in the CMA 71 probes using the standard, constant-flow clinical pump. Studies have been done in other tissues, such as skin, with the CMA 60 catheter (Sjogren, et al., 2002). Like the CMA 71 designed for cerebral monitoring, the CMA 60 has a 100 kD MWCO rating. This study compared push-pull pumping with standard pumping at

the same flow rates. Recovery of the cytokine IL-6 was undetectable until ~120 minutes after implantation of the probe in the standard conditions, whereas it was detected by 100 minutes under push-pull conditions. Levels of IL-6 remained elevated throughout the rest of the experiment (~210-270 minutes) in both conditions, but were higher in push-pull conditions. Notably, this study did not correct for volume loss through the probe with an oncotic agent, such as albumin or dextrans.

Motivation and rationale for higher molecular weight species in TBI

In the search for "biomarkers" of traumatic brain injury, there are several compartments that can be sampled. Two are accessible by routine methods: plasma, by simple arterial or venous blood sampling, and CSF, by ventricular drain or lumbar puncture if increased ICP is not a concern. Proteomic studies in these compartments have revealed significant changes in many species, including higher molecular weight species (Hanrieder, et al., 2009, Ottens, et al., 2007, Prieto, et al., 2008).

While it was clear that measurement of pre- and post-injury dynamics of Aβ was possible, we were also interested in known protein markers of traumatic axonal injury described in studies of post-injury CSF samples. For example, ventricular CSF measurements show that the microtubule-stabilizing protein, tau (50 kD), is increased in the setting of acute injuries and correlates with 1-year outcome (Ost, et al., 2006). Similarly, various isoforms of neurofilament-heavy chain are acutely increased in the CSF after injury (Siman, et al., 2009).

Although CSF profiles from injured patients can be significantly different than healthy controls, the meaning of these changes with respect to the injured brain is less straightforward. The passage of proteins such as tau and neurofilament from the ISF into the CSF is complex. CSF levels may not accurately reflect changes in brain parenchyma. Direct measurement of tau and neurofilament in the ISF would be preferable. Such proteins posed a significant challenge to our mouse model, however. Until this point, we had been using the BAS BR-2 probe designed for mice, which had a molecular weight cutoff rating of 38 kD. To begin, we turned to the rodent research version of the CMA 71, the CMA12, to attempt dynamic measurement of tau.

Initial studies with CMA 12 probes

We first characterized the CMA 12 probe's recovery characteristics *in vitro*. The CMA 12 was chosen because its probe membrane material was made of polyethersulfone (PES) and is currently made from PAES, identical to the CMA 71 probes used in our initial human studies. This basic research version of the CMA 71 is 2 mm long and 0.5 mm diameter (Fig. 17).

Figure 17. CMA-12 100 kD cutoff research probe.

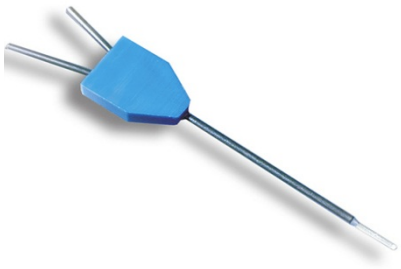

First, the issue of perfusate fluid loss was addressed. Addition of a bulk solute to the perfusate is a common strategy to correct for an imbalance between hydrostatic and oncotic pressures, thereby preventing the loss of fluid into the surrounding tissue through the pores. The CMA product literature recommended using 3% dextran solution. Since we were already using 1.5% human albumin (hAlb) in the human studies, we decided to substitute hAlb for dextran. A range of hAlb concentrations was compared at a single flow rate, 0.5 μL/min: 0.15%, 1.5%, 3%, and 4%. This flow rate was chosen based on the recommendations from the CMA product literature, that an acceptable flow rate range was 0.5 – 2.0 μL/min. We used our standard syringe pump. Volumes were estimated by a mass measurement of the returned volume. Of these flow rates, 0.15% and 1.5% returned ~50-67% of the expected volume across at least 6 hours of testing. The higher concentrations of albumin returned 90-100%, with 4% hAlb giving 100% return. The results of this experiment suggested that 4% hAlb was the optimal amount of solution to avoid fluid loss.

Then, we wanted to repeat Aβ microdialysis using the CMA 12 probe in mice that we had already characterized using the BR-2 38 kD cutoff probe: PDAPP and Tg2576 transgenics. Later, we planned to use the 3X Tg mouse model because it overexpresses a human (mutant) form of tau prone to deposition (Oddo, et al., 2003). Ultimately, we wanted to know if we could measure tau dynamics after TBI in these mice.

Using the CMA 12 probe with 4% hAlb at a flow rate of 0.5 μL/min, the Aβ measurements in PDAPP and Tg2576 mice were not as consistent both in terms of absolute levels and dynamics during baseline as well as post-injury periods. We

attempted Aβ microdialysis in young Tg2576 (#90), with baseline levels of 500, 200, and 380 pg/mL and post-TBI levels at 100, then nearly zero over 120 h. In a second experiment again using a young Tg2576 mouse, only one baseline measurement of 800 pg/mL was measureable on the ELISA standard curve, suggesting a major probe malfunction. After injury, levels ranged between 400-500 pg/mL for approximately 48 h, then began to rise to overshoot the baseline (from 800 to a peak of 1600 pg/mL between 48 and 108 hrs. These dynamics were abnormal and suggested that the CMA 12 probe was not behaving in a predictable way.

Below are results of the experiments with older PDAPP, young Tg2576, and older Tg2576 mice (Fig. 18). The general conclusion from these initial studies is that the concentrations and dynamics measured using the CMA 12 probe with 4% hAlb at a flow rate of 0.5 μL/min were less reliable than our standard protocol, using the BR-2 probe with 0.15% hAlb at a flow rate of 1.5 μL/min, as described in Chapter 5.

Figure 18. **% baseline Aβ in transgenic mice implanted with CMA 12 probes, before and after 1.5 mm TBI.** All experiments conducted at 0.5 µL/min. 4% human albumin was added to perfusion fluid except in (A). **A**, 3% hAlb in an older PDAPP mouse. **B**, an older PDAPP mouse. **C-D**, young Tg2576 littermates. **E**, a 20-month-old Tg2576 mouse. **F**, a young Tg2576 mouse.

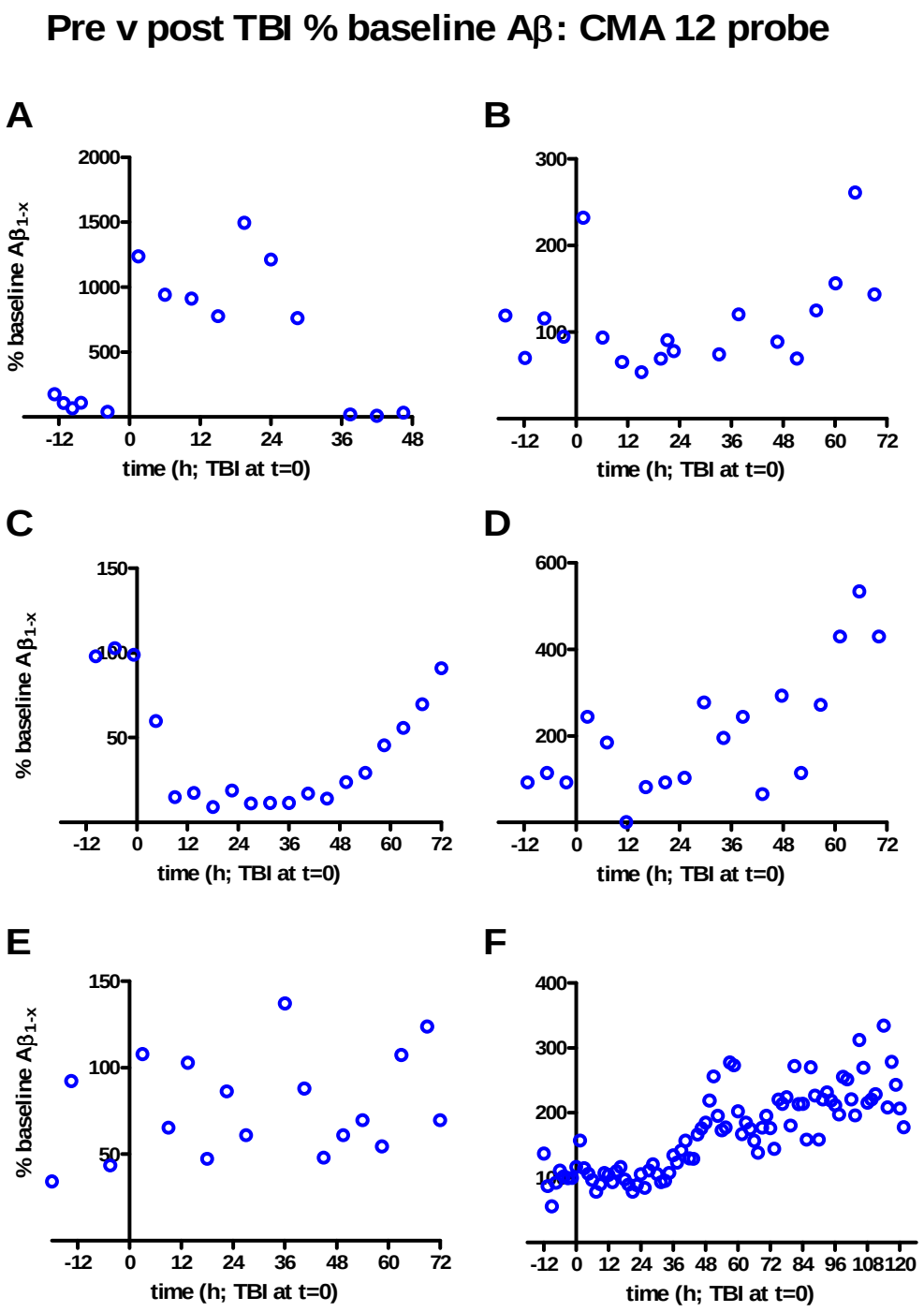

After these unsuccessful *in vivo* experiments in the summer of 2007, we returned to using the BR-2 probe with 0.15% hAlb.

The following spring, we reattempted *in vivo* microdialysis with the CMA 12 probe. On the hypothesis that some of our issues may have resulted from the high percentage of hAlb in the solution, and the possibility that hAlb was clogging the membrane, we decided to substitute high-concentration (hyperosmolar) saline solution. We determined that 455 μM NaCl was equivalent to 3% human albumin in terms of molarity. Below is a plot of the recovered volumes. From the time of implantation over the course of the next 18-21 hours, volume recovery reached only 40% of expected. As it is plainly evident, hyperosmolar saline solutions do not resolve the fluid loss issues with the CMA 12 probe (Fig. 19).

Figure 19. % volume recovery using hyperosmolar NaCl at an equivalent molarity to 3% hAlb (455 μM) . Volume recovery is initially low at 10% of expected. Volume rises over time, but plateaus by 18 h at 40%.

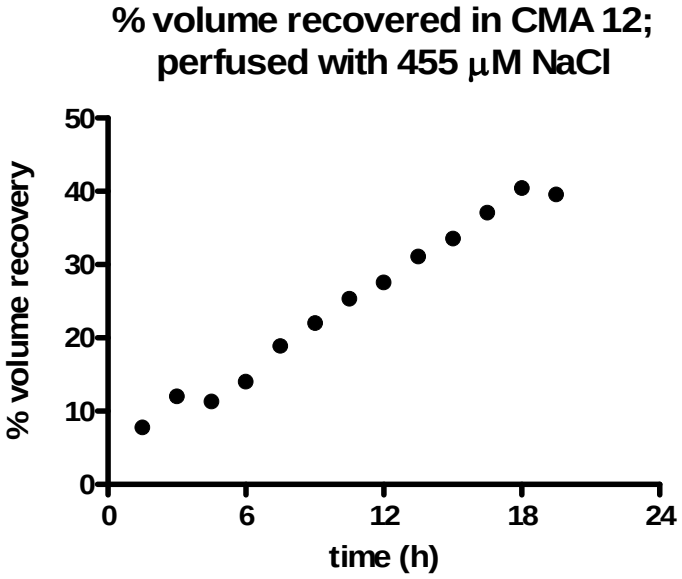

We returned to using 3% hAlb as was done in the original tests in PDAPP and Tg2576 mice. We then thought perhaps the volume recovery might be dependent on the flow rate. Since the back-pressure from the syringe pump might vary according to flow rate, we compared 0.3 and 1.5 μL/min in the same animal, before and after TBI. Similarly to the BR-2 probe, recovery of Aβ varied with flow rate. According to our zero-flow extrapolation experiments using the BR-2 probe, it was determined that a flow rate of 1.5 μL/min yields approximately 6-7% recovery, while 0.3 μL/min yields approximately 30% recovery. Theoretically, the dialysate concentrations collected at 0.3 μL/min should be approximately 5 times greater than that measured at 1.5 μL/min. Using the CMA12 probe, the average Aβ concentration over 24 hours at 1.5 μL/min was 19.4 (standard deviation, ± 9.5 pg/mL), while Aβ concentration over 24 hours at 0.3 μL/min was 108.9 (standard deviation, ± 42.1 pg/mL). The relative recovery at 0.3 μL/min as compared with 1.5 μL/min is 5.6, which is similar to the BR-2 probe (Fig. 20).

Figure 20. Effect of flow rate on Aβ concentration and dynamics using the CMA12 probe perfused with 3% hAlb in a 3X Tg mouse. Levels were low and at times undetectable at 1.5 μL/min, but increased at 0.3 μL/min. Levels did not appear to reach steady state at 0.3 μL/min over 20 hours. Taken as a 24-hour average, recovery was approximately 5.6 times higher at 0.3 μL/min than at 1.5 μL/min.

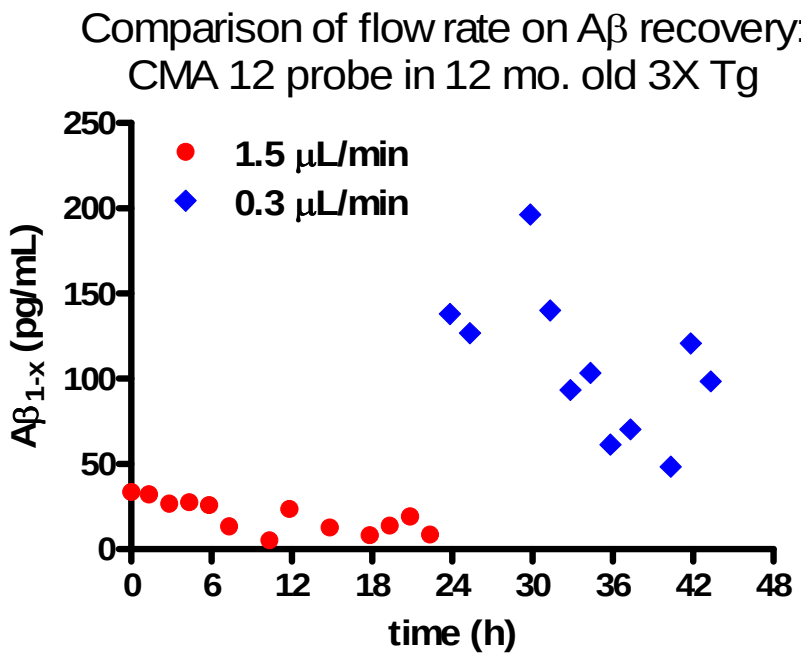

Next, we wanted to determine whether we could measure tau using the CMA 12 probe. Using the standard syringe pump at a flow rate of 0.5 μL/min, we performed *in vitro* experiments using a variety of tau-containing solutions. Additionally, due to concern that the hAlb (molecular weight, ~50-70 kD) might be clogging this probe, we decided to use a higher molecular weight species than the MWCO rating for our oncotic agent. We chose 150 kD dextran at a concentration of 3%. For the tau-containing *in vitro* solution, we chose a PBS-extracted brain homogenate from an aged 3X Tg mouse. This mouse produces a human form of tau, which could be compared with other experiments using human microdialysis and ventricular CSF samples. Below are the

results of that experiment (Fig. 21). Briefly, there were significant fluid losses in the initial samples, which eventually normalized over 18 hours.

Figure 21. % volume recovery using the CMA12 probe perfused at 0.5 µL/min with 3% 150 kD dextrans. Probe was immersed in a 3X Tg mouse brain homogenate.

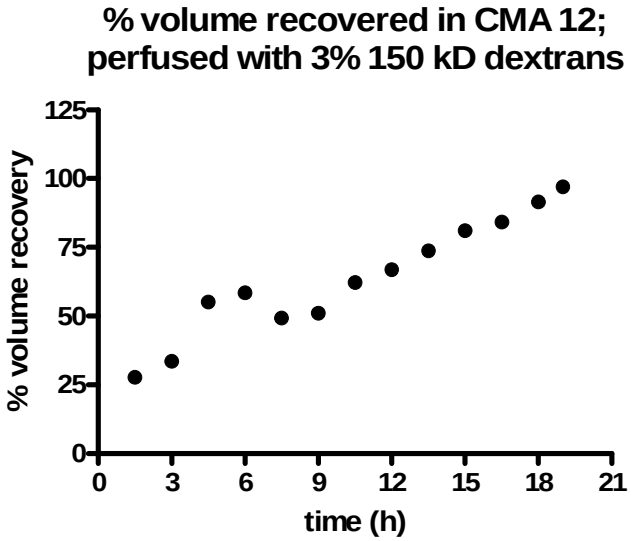

The concentration of Tau in microdialysate samples was quite high in the first two samples, but quickly dropped off to near limits of detection by 4.5 h (Fig. 22).

Figure 22. Tau recovery *in vitro* using the CMA12 probe perfused at 0.5 µL/min with 3% 150 kD dextrans. Probe was immersed in a 3X Tg mouse brain homogenate.

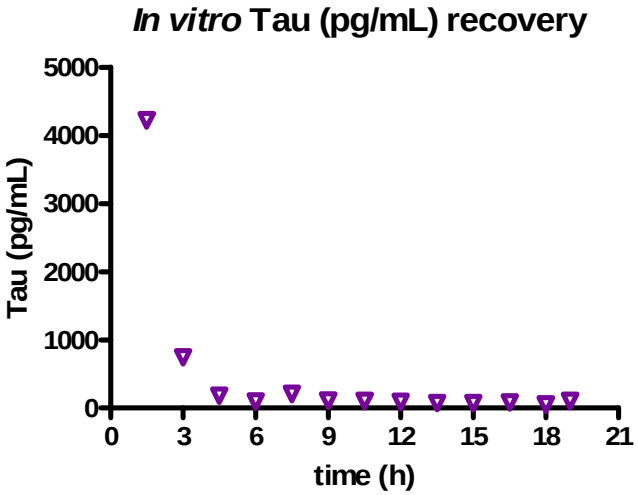

As with *in vivo* Aβ microdialysis, there is likely a period of equilibration. If we consider the first 3 hours (first 2 samples) to be a kind of equilibration period, and look at the tau dynamics beginning at 4.5 h, we can see they are still detectable (Fig. 23).

Figure 23. Tau recovery *in vitro* using the CMA12 probe perfused at 0.5 µL/min with 3% 150 kD dextrans. Probe was immersed in a 3X Tg mouse brain homogenate.

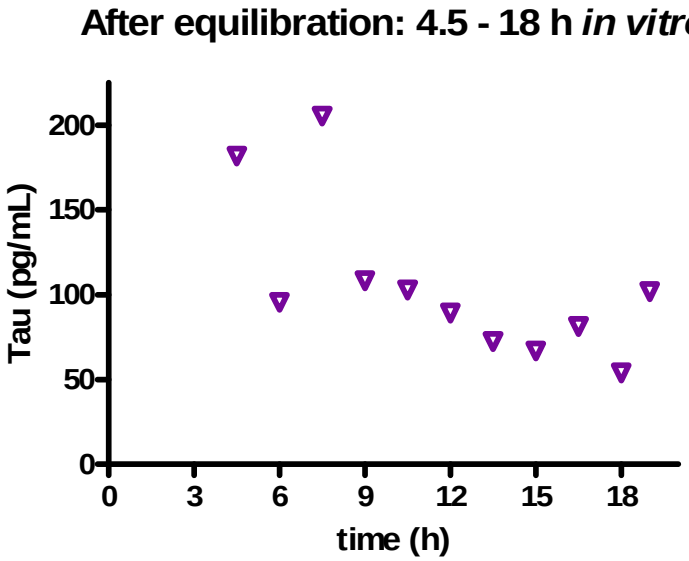

However, given that the volumes recovered were constantly changing, the meaning of these measurements is uncertain. Secondly, when the concentration of tau was measured for the *in vitro* solution, it was clear that the efficiency of recovery was quite low. Pre and post-experiment measurements of tau in the homogenate were 810 ng/mL and 897 ng/mL, respectively. Comparing the pre-experimental value with the concentration measured in the first sample of microdialysate, 4218 pg/mL, this is only a 0.52% recovery. The second sample had a tau concentration of 746 pg/mL, which is a 0.09% recovery. Clearly, the results of this experiment indicate that our methods are insufficient

for proper dialysis technique using the CMA 12 high molecular weight probe for recovery of larger proteins.

Very recently, as of the writing of this thesis, the Holtzman lab has reported the successful measurement of tau protein in mice using the CMA 12 probes, using push-pull perfusion technique and the addition of 4% human albumin to the perfusate. Previous experiments have shown push-pull perfusion to be a superior method for the recovery of IL-6 both *in vitro* and *in vivo* (Sjogren, et al., 2002). Future experiments using high molecular weight catheters such as the CMA 12 in this lab should test the push-pull strategy.

The following chapter will elaborate on development of the combined CCI-microdialysis model.

Chapter 4.

Development of the combined CCI-microdialysis model

Previous studies and specific requirements for site, study length, robustness

Experimental TBI combined with pre and post-injury microdialysis has been described in rat models. Most experiments combined microdialysis with Marmarou weight drop or fluid percussion injury (Alves, et al., 2005, Bramlett and Dietrich, 2001, Busto, et al., 1997, Chen, et al., 2000, Chen, et al., 2000, Globus, et al., 1995, Headrick, et al., 1994, Jiang, et al., 2004) or a weight drop model (Alessandri, et al., 2000, Koizumi, et al., 1997). Others combined CCI with microdialysis (Bell, et al., 1998, Krishnappa, et al., 1999, Marklund, et al., 2001, Marklund, et al., 2001, Marklund, et al., 1997, Palmer, et al., 1993, Rose, et al., 2002, Stover, et al., 2003). The successful combination of the techniques was encouraging for our project, and the geometry of a craniotomy in tandem with an implanted guide canula seemed feasible.

However, there were additional challenges to achieve this combination in our model. Firstly, all previous studies had been done in rats. The rat skull is significantly larger than the mouse cranium. Secondly, most of the previous work had measured acute timepoints, ranging from 3 hours to just 15 minutes before an injury to hours following an injury. Thirdly, rats are relatively robust animals and survive experimental TBI with minimal mortality. Transgenic mice can be remarkably sensitive to experimental TBI. Our task, therefore, was threefold. Firstly, the hippocampal microdialysis placement site would need to be ipsilateral to a CCI. The CCI impactor site also was required to be identical to the site used in standard EM-CCI experiments (Fig. 24). Secondly, we wanted to achieve longer periods of baseline and post-injury measurements, at least 12 hours of baseline measurement and 24 hours following an injury. Thirdly, we wanted an

injury that showed a robust effect compared to sham with minimal-to-no complications and mortality that could be used in fragile transgenic mice.

Figure 24. Standardized impact sites with and without microdialysis. A, EM-CCI impact at 2.0 mm depth with 5.0 mm craniotomy shown immediately after impact. Courtesy of C. Mac Donald. **B,** stereotactically-placed, 3.8 mm craniotomy to accommodate microdialysis guide canula.

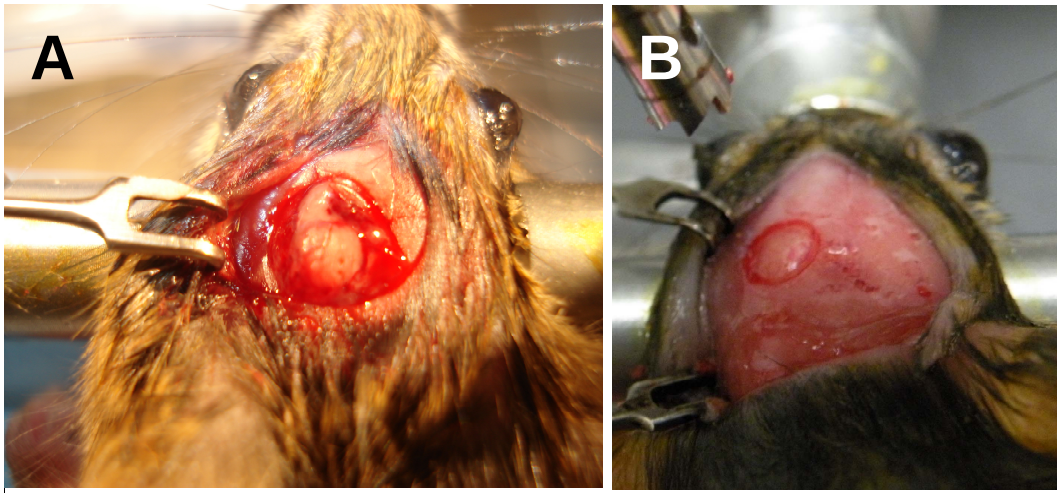

Geometrical requirements and implementation

First, using the Franklin and Paxinos atlas, we chose a site for probe placement that would best fit a 2-mm long, 35 kD BR-2 probe from Bioanalytical Systems (BAS, West Lafayette, IN). This probe had been extensively characterized by John Cirrito in his pioneering studies of Aβ microdialysis in transgenic mice (Cirrito, et al., 2008, Cirrito, et al., 2003, Cirrito, et al., 2005). The requirements for this placement were twofold: firstly, the guide canula could not block the trajectory of the impact; secondly, the probe needed to sample a region that was known to be damaged on histological and behavioral criteria. Additionally, this site must remain intact as a distinct tissue structure. For example, the

loss of architectural integrity and massive degeneration that occurs in the overlying cortex would not provide a representative tissue medium for microdialysis sampling.

Given ours and previous studies, the ipsilateral hippocampus was the best candidate. Other studies have established that CCI injury causes acute and subacute CA3 cell loss and hippocampal atrophy (Brody, et al., 2007, Nakagawa, et al., 1999, Nakagawa, et al., 2000, Saatman, et al., 2006, Smith, et al., 1998, Smith, et al., 1995). Additionally, injury severity is reflected by graded deficits in Morris water maze assessments (Brody, et al., 2007, Saatman, et al., 2006, Smith, et al., 1995). A guide canula placement that crossed midline was chosen so that the cement crown could attach to the contralateral skull, leaving the ipsilateral skull clear for craniotomy and impact. Again using the Franklin and Paxinos atlas, placement at -2.54 mm from bregma along the long axis of the hippocampus would serve our purposes (see Figure 25A). Coordinates were calculated for stereotaxic placement of the canula, and probe location was verified by T2 MRI and postmortem histology (Figure 25C, D). As in the original studies, mice are tethered in the electronic swivel cage (Rat Turn) with the affixed guide canula and microdialysis tubing, but are generally free to move about, eat, drink, and sleep (Figure 25B). The cement crown and guide canula did not appear to appreciably impair the animal's behavior in the RatTurn.

Figure 25. Microdialysis probe placement for combined studies with experimental traumatic brain injury. **A**, schematic of microdialysis probe placement and craniotomy for controlled cortical impact TBI. A rigid guide canula was inserted via a stereotaxically placed burr hole. Then, the microdialysis probe was placed through the guide canula into the left hippocampus. A 3.8 mm-diameter craniotomy was performed to allow controlled cortical impact TBI. Modified from Franklin and Paxinos (2001). **B**, photograph of awake, moving mouse with implanted canula and probe affixed with dental cement. The mice were tethered to an electronic swivel system to prevent tangling of the microdialysis tubing. **C**, a T2-weighted MR image of living mouse brain with implanted canula and probe. **D**, post-mortem staining of probe tract with Evans blue dye and counterstained with Neutral Red. Scale bar, 2.0 mm.

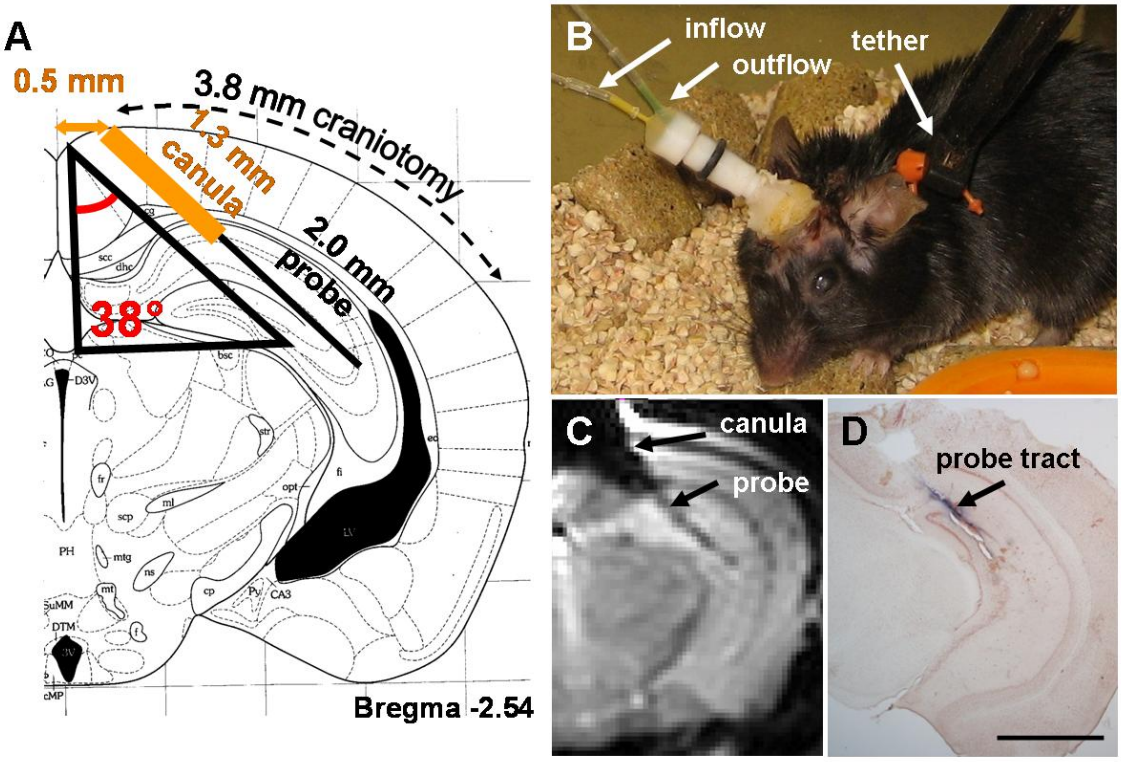

Refinement of the technique: craniotomy placement and sequence

As part of the model development, we needed to know whether necessary manipulations during the CCI injury would affect our measurements of Aβ. First, the craniotomy was assessed. Initially, we allowed the dental cement to cover the entire skull on the assumption that the trephine could drill through. This strategy was unsuccessful.

We then attempted to leave the ipsilateral skull clear by using a plastic ring to sequester the cement on the contralateral hemisphere. It soon became clear that a 5.0 mm-diameter trephine was inconvenient and difficult to use given the amount of glue necessary to create a stable structure. Because the 3.0 mm diameter impactor tip would still be used, we chose a smaller trephine of diameter 3.8 mm. This modification permitted a more consistent and clean craniotomy that is critical for a reliable and reproducible impact (Fig. 26).

Figure 26. Simultaneous craniotomy and guide canula placement. A, 3.8 mm craniotomy. **B,** craniotomy cap covers ipsilateral hemisphere only. **C,** guide canula, plastic ring to guide cement on contralateral hemisphere, and bone screws to anchor cement crown.

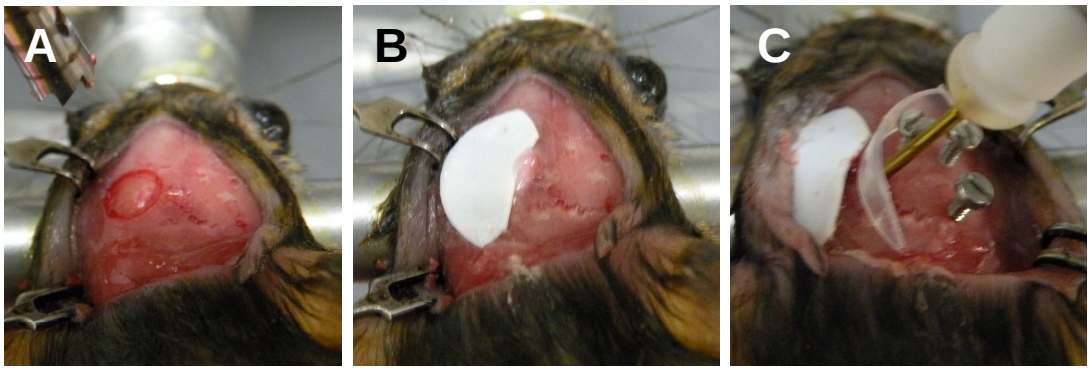

Controls for post-injury Aβ measurement: craniotomy and probe removal

Finally, we wanted to know whether or not the craniotomy and probe removal caused a change in Aβ levels as compared to no further manipulation after guide canula implantation and probe insertion. To assess the effect of a craniotomy, we implanted PDAPP$^{+/-}$ mice with guide canulas and microdialysis probes, allowed them to recover for approximately 12 hours, and collected baseline samples every 90 minutes for 9 hours. Then we reanesthetized the mice, opened the sutures, exposed the skull, removed the

microdialysis probe and placed it is a vial of perfusion fluid, and performed a craniotomy. The skull defect was sealed with a plastic cap as per usual, the skin was resutured around the glue cap, and microdialysis probe replaced. The entire procedure took 20-25 minutes. It was found that, for n = 4 mice, the craniotomy caused a modest but significant decrease in microdialysis levels of Aβ in the first 6 hours following the procedure (Fig. 27A). Therefore it was concluded that the craniotomy should be included in the initial implantation procedure, such that any changes it induced in microdialysis levels of Aβ were included in baseline measurements. A similar assessment with simple probe removal and replacement did not cause a significant change in levels (Fig. 27B). It was determined that this necessary manipulation during the CCI procedure would have no effect on post-injury measurements.

Figure 27. Effects of craniotomy and probe removal/reinsertion on ISF Aβ. **A**, effect of craniotomy on ISF Aβ. Young PDAPP $^{+/-}$ mice (n=4) were implanted with a microdialysis probe only and allowed to equilibrate. Then, baseline samples were collected for 7.5 hours. Mice were reanesthetized and a craniotomy was performed. The probe was removed just before the craniotomy was drilled, placed in a vial of perfusion fluid, and reinserted as soon as the plastic skull cap was secured. This procedure lasted approximately 20 minutes. Mice were returned to their swivel cages and samples were collected for an additional 6 hours. $A\beta_{1-x}$ in the pre and post-craniotomy samples was measured by ELISA. Although the difference between pre and post-craniotomy levels was not statistically significant (p=0.0556, Mann-Whitney U-test). **B**, effect of probe removal-reinsertion on ISF Aβ. Young PDAPP $^{+/-}$ mice (n=4) were implanted with a microdialysis probe and baseline samples were collected for 10.5 hours after equilibration. Mice were then briefly reanesthetized, the probe was removed for approximately 10 s, and immediately reinserted. Samples were collected for an additional 4.5 hours. $A\beta_{1-x}$ in pre and post-probe removal samples was measured by ELISA. There was no significant difference in $A\beta_{1-x}$ levels before vs. after probe removal (p=0.667, Mann-Whitney U-test).

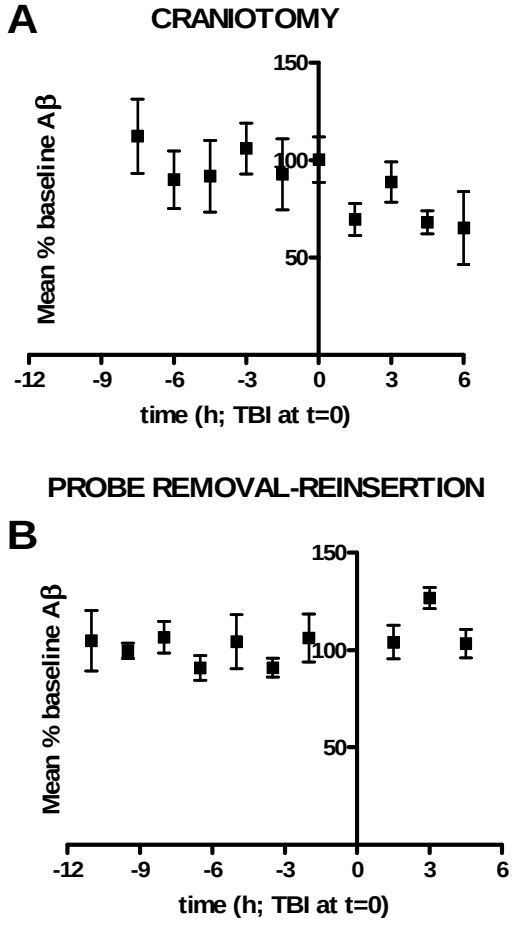

Preliminary experiments: measurement in Tg2576 / ApoEX mice

Having established these controls, we then attempted to measure pre- and post-TBI Aβ levels in the hippocampus. Preliminary experiments were conducted using transgenic mice that expressed the APPSw gene under the control of the prion promoter (Hsiao, et al., 1996) and that had human-sequence ApoE lipoprotein "knocked in" to the mouse ApoE locus (Xu, et al., 1996). These mice are referred to as "Tg2576 / ApoEX" where X stands for 2, 3, or 4 depending on the particular isoform. Typically, these mice were implanted and microdialysis sampling occurred over 24 hours prior to injury (baseline). Mice were then injured and sampling continued for the next 3-5 days.

Difficulties in survival and recovery after CCI: no effect of modified injury depth

A number of difficulties in recovery and survival of the mice after either implantation surgery or CCI injury were encountered during this time. The effects were seen in some mice during baseline sampling, in some only after injury, and in some, not at all. Our initial observations were that the mice appeared lethargic, failed to eat, drink, or move appropriately, lost weight, and became hypothermic. We measured temperatures as low as 24º or 25º C in some mice. These abnormalities strongly suggested a profound metabolic disturbance. Initially, we had been using an injury depth of 2.0 mm, which was characterized as mild-moderate in the wild-type B6SJL strain. We modified the depth to 1.5 mm. This did not significantly improve the morbidity and mortality.

Possible effect of age and / or particular transgenes

Since modification of the injury depth failed to improve morbidity, we considered the age and transgene expression in the mice independently of the TBI. Firstly, the mice were usually older. All were at least 6 months, usually 9-12 months, but some up to 15 months old. The Tg2576 (Swedish mutation in the amyloid precursor protein, APPSw) transgenic mouse model of AD develops parenchymal plaque pathology and prominent CAA beginning at 9 months of age (Hsiao, et al., 1996). Expression of human ApoEX under endogenous promoter control delays Aβ deposition by months, such that 12-month old mice have little or no plaques compared with animals expressing endogenous murine ApoE (Fryer, et al., 2005). Despite the relative lack of Aβ deposition in these mice compared with Tg2576 mice, we thought the Tg2576 / ApoEX animals might be fragile in other ways due to their age and multiple genetic manipulations. Additionally, because of their age, the older transgenic mice might have been more susceptible to anesthesia and injury. These mice also had a number of systemic health problems, including sores and bacterial infections. Rectal prolapse was common, especially in older animals. This condition indicates abnormal bacterial colonization of the gut. Their fur was often matted and patchy, suggesting underlying skin or connective tissue disorder.

Diagnosis of colonic perforation and peritonitis by autopsy

To fully evaluate the pathology of these sick mice, we sent a recently deceased exemplar to the Division of Comparative Medicine for veterinary autopsy. They found evidence of peritonitis resulting from colonic perforation, which likely accounted for the

behavioral and metabolic disturbances observed. As this had not occurred in other strains of mice, we hypothesized that it might be related to the particular combination of transgenes expressed by these animals. We confirmed our observations of sepsis with a former graduate student, John Fryer, who had previously characterized Tg2576 / ApoEX (Fryer, et al., 2005). Therefore, we concluded that the lethargy and sickness observed in some of our mice was not due to the implantation surgery or the CCI injury, but to the sepsis resulting from perforation by the rectal temperature probe.

Modified temperature control to avoid perforation

Temperature control in anesthetized mice is achieved using a feedback system in which a rectal probe monitors the animal's temperature, and a heating pad directly underneath the mouse's body warms until the probe reads the desired temperature. Previous use of the rectal probe in all earlier experiments with B6SJL (wildtype) mice had been successful in maintaining body temperature during anesthesia, without incident. We hypothesized that the probe caused colonic perforation and subsequent peritonitis, resulting in septic shock and death when it was used in these older Tg2576 / ApoEX transgenics. To avoid the risk of colonic perforation and peritonitis, we decided to use passive heating. The probe would be taped directly to the heating pad and would sense its temperature. The pad itself would be maintained at 37º C. Passive heating would ensure the mouse be kept warm during anesthesia.

Successful data collection: initial findings with Tg2576 / ApoE2 mice

After making this change to the protocol, we achieved better success with survival and microdialysis collection. In addition, we were able to collect data for 3-5 days post-TBI. The details of Aβ microdialysis sampling and ELISA detection are described in the next chapter. Our initial findings were shared with the Holtzman group during a lab meeting and with this Thesis Committee during the initial proposal in November 2007 (Fig. 28).

Figure 28. Pre and post-TBI levels of Aβ measured in Tg2576 / ApoE2 mice. A 1.5-mm CCI was given at t=0. Samples were normalized to individual baseline levels, and a group of 5 mice were averaged. Error bars, standard error of the mean.

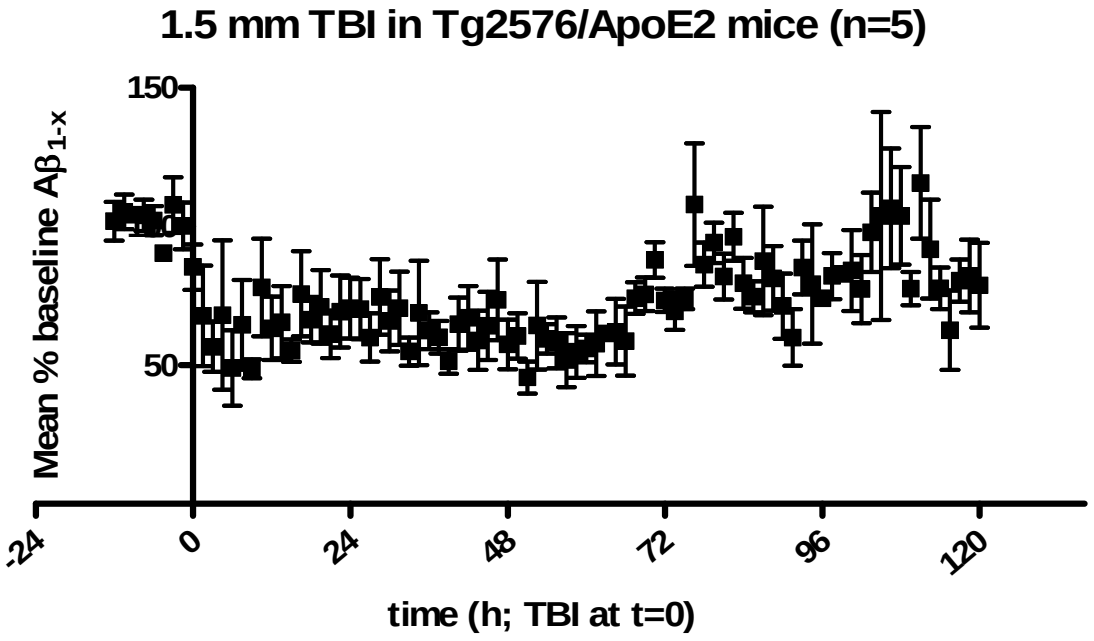

The chief observations from this experiment were that Aβ levels were essentially stable beginning 12 hours following implantation surgery before injury, the baseline period; that there was an immediate and persistent decrease in Aβ levels by the first timepoint, 90

minutes; and that possibly, levels began to rise again around 72 hours post-injury. These were consistent with previous, unpublished observations in the lab that when an animal was very sick, microdialysis levels of Aβ decreased and became undetectable near death. I had also measured a similar decline in Aβ levels as septic Tg2576 / ApoEX mice sickened and died.

Further controls necessary: switch from old Tg2576 / ApoEX to young PDAPP mice

There were several outstanding issues with this initial dataset, however. Firstly, there were no controls for injury and for probe function. We had focused on establishing whether or not there was a significant effect of TBI on ISF Aβ, and had encountered significant problems with the temperature control. By the time we had completed 5 successful experiments with Tg2576 / ApoE2 mice, the supply of this and the other ApoEX genotypes were nearly gone. There were not enough mice to complete a similar set of sham animals. In addition, we were concerned about the age of the mice. For these reasons, we decided to switch genotypes to the PDAPP mouse previously characterized by John Cirrito in his PhD thesis and described in his 2003 paper (Cirrito, et al., 2003). There was an ample supply of young, pre-plaque animals that were actively reproducing in the Washington University colony. Moreover, at younger ages the PDAPP mice showed none of the systemic health problems seen in the Tg2576 / ApoEX mice. It was therefore decided to switch to this transgenic line.

PDAPP mice

The PDAPP mouse possesses a transgene for human APP with a V717F mutation under the PDGF-β chain promoter (Games, et al., 1995). This promoter is specific for neuronal cell bodies, and a transgene under its control is expressed primarily in the cortex, hippocampus, and cerebellum (Sasahara, et al., 1991). The V717F mutation shifts the γ-site cleavage to longer isoforms, particularly the 42-amino acid length but some as long as 50-54 amino acids (Esh, et al., 2005).

Our mice were originally obtained from Eli Lilly and Company and bred at Washington University on a C57BL6 background. They were used for all initial experiments to establish the technique of Aβ microdialysis in transgenic mice. Given the previous experience with these mice and the abundance of young animals, we were confident that we could complete multiple experiments in different injury severities, including the critical sham controls.

Preliminary probe function control: use of urea in clinical microdialysis studies

The second outstanding issue was that of probe function. Others in the lab had seen unexplained increases in Aβ after a number of days; the meaning of its occurrence in the initial dataset was unclear. Were levels returning to baseline? This rise did not occur in all animals in contrast to the immediate decrease. Did this signify heterogeneity in recovery, or did it reflect variable permeability or changes in local tissue architecture and diffusion characteristics? It became obvious that an additional control was necessary.

Based on the clinical microdialysis literature, measurement of endogenous urea was chosen for the initial probe control (Ronne-Engstrom, et al., 2001).

Urea as endogenous, exchangeable marker of probe function

Urea is a small molecule naturally produced in the liver by the nitrogen cycle. It rapidly equilibrates throughout all tissues of the body and in all types of tissue spaces: intracellular, interstitial, and vascular. It is thought that if urea can exchange across the probe membrane, and if the levels are constant compared to other tissues, then the probe is permeable. There were definite instances of blockage by an air bubble or mechanical disruption in which we observed a sharp drop-off in urea levels. Similarly, we found that microdialysis urea was quite a sensitive marker for renal failure when we first began to use it in the Tg2576 / ApoEX mice. As the animals became septic and especially when death was imminent, urea levels might double or triple in the microdialysis samples, suggesting poor clearance by the kidneys.

Final modifications: preventing dural disruption on craniotomy cap removal

We began to use the PDAPP mice and to routinely measure urea in all samples. However, there were a few issues to be resolved before we designated the model "complete" and began to collect data in earnest. One issue had to do with the craniotomy cap. We were drilling the craniotomy as part of the initial implantation surgery. This necessitated a plastic cranitomoy cap to protect the underlying dura. In standard injury protocols, this cap is placed only after injury and is coated only with the VetBond

adhesive. It is not designed to be removed, although removal from the skull is not difficult. What was problematic was removal from the dura in preparation for the CCI injury. Often, the dura would be pulled off along with the plastic cap. This created a swollen, bleeding cortex to be impacted. A reference position from which to measure the depth of the injury was impossible to obtain with accuracy. To overcome this issue, we put PureLube petrolatum eye ointment on the middle region of the skull cap that was in contact with the dura, restricting the VetBond to just the outer edges of the cap. In this way, the cap did not stick to the dura when it was pulled off the skull before impact. The dura remained intact and reference positions could be determined as easily as in a simple CCI study (Fig. 24).

Final modification: probe removal technique

One final issue was that of probe removal. While it was clear from ours and previous studies that the probe needed to be removed prior to the impact to avoid shearing damage to the surrounding tissue, it was not clear exactly how to do this. We tried three ways: one, removal for the entire TBI procedure from anesthetic induction to recovery; two, "partial" removal whereby the stylet was pulled out just 2 mm, the length of the semi-permeable membrane resting in the guide canula shaft during impact; and finally, complete removal just before impact and immediate reinsertion following impact. In the cases of complete removal, the probe was always immersed in a vial of CMA CNS perfusion fluid and was never exposed to air longer than 60 seconds. We found that the brief but complete removal and reinsertion gave the best sham results, and decided to

conduct all experiments in this manner. Typically, the probe was immersed for no longer than 5 minutes at a time during a sham or injury procedure.

Model development complete

Once the geometry was designed and confirmed, and the exact details of the technique had been worked out to yield to most reproducible injury, we considered our combined CCI-microdialysis model complete. The written protocol we used on a routine basis for implantation surgery and CCI procedure is included along with a pictorial guide in Appendix 1. The written protocol for intraparenchymal EEG experiments is attached as Appendix 2

The main body of the proposed experiments is presented in the next section, which was submitted as a manuscript to Experimental Neurology in October 2009.

Chapter 5.

Submitted manuscript with main results

ABSTRACT

The amyloid-β peptide (Aβ) plays a central pathophysiological role in Alzheimer's disease, but little is known about its dynamics in the brain's extracellular space. A recent microdialysis-based study in human patients with severe brain injuries found that extracellular Aβ dynamics correlate with changes in neurological status. Because neurological status is generally diminished following injury, this correlation raises the possibility that extracellular Aβ is reduced relative to baseline. However, human studies cannot assess pre-injury Aβ levels, very early post-injury Aβ levels, nor the relationship between extracellular Aβ levels as measured by microdialysis and total tissue Aβ levels. Therefore, we developed a mouse model that combines experimental TBI with microdialysis to address these gaps. In this model Aβ levels were stable at baseline and after sham-injury. Following controlled cortical impact TBI, we found that Aβ levels as measured by microdialysis were immediately and persistently decreased in the ipsilateral hippocampus. These results were found in both wild-type mice and young pre-plaque PDAPP mice that produce human-sequence Aβ. Similar decreases were observed in PBS-soluble hippocampal extracts, but no changes were found in carbonate or guanidine extracts. Reductions in Aβ were not due to changes in microdialysis probe function, APP levels nor Aβ deposition. Hippocampal depth electrode recordings demonstrated that electroencephalographic activity was decreased over 24 hours following TBI. Thus, we propose that in mice and likely human patients with TBI, post-injury extracellular Aβ levels are acutely decreased relative to baseline. Reduced

neuronal activity may contribute, though the underlying mechanisms have not been definitively determined.

INTRODUCTION

Brain microdialysis is a minimally-invasive technique that permits longitudinal sampling of small molecules in the extracellular space of living, awake subjects. Previous experimental studies have demonstrated that it is possible to assess the dynamics of Aβ in the brain interstitial fluid (ISF) using intracerebral microdialysis in the brains of awake, behaving mice (Cirrito, et al., 2003). Additional studies uncovered a clear relationship between neuronal activity and ISF Aβ concentrations (Cirrito, et al., 2005, Kamenetz, et al., 2003). In a subsequent study, it was shown that ISF Aβ levels depend in large part on synaptically-coupled endocytosis (Cirrito, et al., 2008).

Physiological manipulations of neuronal activity also affect Aβ levels. Both acute and chronic stress can result in elevations of ISF Aβ levels (Kang, et al., 2007). Furthermore, ISF Aβ levels were found to correlate with cortical EEG measures of wakefulness (Kang, et al., 2009).

Recently, our group published a study in which we measured the concentration of amyloid-β peptide (Aβ) recovered by intracerebral microdialysis every 2 hours for at least 72 hours after catheter implantation in human patients who had suffered either an aneurysmal subarachoid hemorrhage or a traumatic brain injury (Brody, et al., 2008). We found a significant correlation between changes in microdialysis levels of ISF Aβ and changes in neurological status, as assessed by one or two-step changes in the GCS. Measures of impaired cerebral metabolism and physiological factors associated with

depressed functional status were significantly correlated with reduced Aβ levels. Marklund et al. presented results consistent with these findings; ISF Aβ levels were relatively high in a patient who did well and undetectable in a patient who died with severely abnormal brain metabolic parameters (Marklund, et al., 2009).

As is generally the case for clinical microdialysis studies, we could not measure pre-injury levels in our subjects. Intracerebral microdialysis is indicated only for severely injured patients under close supervision in a hospital ICU setting. Therefore, the question of the relationship of post-injury to pre-injury levels remained open to inquiry. Secondly, the relationship of Aβ concentrations in the ISF to levels in other tissue compartments could not be assessed in the human study. Finally, the dynamics of ISF Aβ immediately following an injury were not determined; most human patients did not begin monitoring until 12-24 hours or more after injury.

To address these gaps, we turned to an animal model that combined a standardized brain injury with standardized microdialysis catheter placement. We adapted methods successfully employed in rats (Alves, et al., 2005, Bell, et al., 1998, Krishnappa, et al., 1999, Palmer, et al., 1993, Rose, et al., 2002) to mice. Our group has previously published a well-characterized model of controlled cortical impact (CCI) using a precise, electromagnetically-driven device (Brody, et al., 2007). This combination of techniques permitted us to measure Aβ before and after an injury, and in sham-injured animals.

Given the findings in brain-injured human patients, we hypothesized that ISF Aβ would be reduced following experimental CCI-TBI compared to baseline. In agreement

with this hypothesis, we found that hippocampal levels of ISF Aβ were immediately decreased by approximately 30-50% after TBI. Similar changes were found in PBS-soluble tissue extracts, but not other tissue fractions. Furthermore, significant reductions in local electroencephalographic (EEG) activity after injury suggest a mechanistic relationship with reduced neuronal activity (Cirrito, et al., 2005, Kamenetz, et al., 2003).

MATERIALS and METHODS

Mice

Most experiments used male and female PDAPP$^{+/-}$ mice (Games, et al., 1995) on a C57Bl6 background at 3-6 months of age. These mice were originally obtained from Eli Lilly and Co., and have been bred at Washington University. Wild type mice used were C57Bl6 littermates of the PDAPP$^{+/-}$ mice. The mice were housed in standard cages at 3–5 mice per cage under standard laboratory conditions prior to the experiment. They were individually housed in Rat Turn electronic swivel cages (Bioanalytical Systems) during combined microdialysis-CCI experiments. All experiments were approved by the Animal Studies Committee at Washington University.

Combination microdialysis and controlled cortical impact (CCI) model of TBI

To allow for baseline Aβ microdialysis measurements, mice underwent an initial surgery for implantation of a microdialysis guide canula (MD-2250, Bioanalytical Systems) and craniotomy placement 24 hours prior to CCI. Isoflurane anesthesia was induced at 5% and maintained between 1.5 - 2% during the procedure. Following anesthesia, mice were placed on a stereotactic frame (David Kopf) on a thermoregulated

heating pad kept at 37º C for the duration of the 60-minute surgery. The scalp was shaved, 10% povidone-iodine applied to the skin and allowed to dry, and the skin opened to expose the skull. The mouse's head was fixed in place by cupped head holders (David Kopf) mounted on the stereotactic frame. The skull was leveled along the anterior-posterior and lateral axes to a tolerance of 0.10 mm with a digital stereotactic device (Benchmark Digital).

For microdialysis guide canula implantation, a 0.7-mm burr bit mounted an on an electric drill (Foredom) was used to create a groove beginning at 2.54 mm posterior to bregma suture, 0.0 mm midline through 1.0 mm left of midline, at a depth to visualize but not breach dura mater and the sagittal sinus. Three additional holes were placed for bone screw anchors at 1.0 mm right of midline, 0.75 mm posterior to bregma; 3.0 mm right, 0.75 mm posterior to bregma; and 3 mm right, 3.5 mm posterior to bregma. Finally, fiduciary markers for a 3.8 mm-diameter craniotomy were made at 3.6 mm left of midline, 1.1 mm anterior to lamboid suture and 1.7 mm left of midline, 3.0 mm anterior to lamboid suture.

The left craniotomy required for CCI-TBI was performed during the same surgical procedure as guide canula implantation. Our control experiments indicated that there was a small decrease in the microdialysis concentration of $A\beta_{1-x}$ after craniotomy (Fig. 11A, see above). Although this difference was not statistically significant at the 95% confidence level ($p=0.0556$, Mann-Whitney U-test), we included the craniotomy as part of the baseline procedure to separate its effect on levels of $A\beta_{1-x}$ from those due to the CCI-TBI. The craniotomy was created with a cylindrical, air-vent cooled, 3.8 mm-

diameter micro-trephine (Xemax Surgical) angled between 12-15º to create an even, circular groove through the skull. Once the skull bone under the trephine became translucent, the bone flap was carefully removed using a 1.0 mm cup rongeur and spatula. A plastic cap was immediately placed over the exposed dura. The central part of the cap touching the dura was coated with petrolatum-based veterinary ointment (Purelube) and the peripheral part was secured to the skull with veterinary adhesive (VetBond, 3M).

Bone screw anchors were inserted into the previously drilled holes at the minimum depth required for secure placement, typically between one-half and one full turn. The bone screw anchors provided necessary support for the dental cement crown to secure the guide canula to the skull.

The microdialysis guide canula was mounted on the right arm of the stereotactic frame, and the arm was positioned at 38º relative to the sagittal plane. The guide canula was introduced into the left cortex to a depth of 1.3 mm through the groove at 0.5 mm left of midline, 2.54 posterior to bregma (Ch. 4, Fig. 25A). The depth was measured from where the rightmost (bottom) edge of the guide canula contacted the dura. Then, the guide canula was secured using dental cement. A ½-circumference cap from a 1.7 mL microcentrifuge tube was placed just to the left of the canula to protect the craniotomy skull cap from the dental cement crown. Dental cement (DuraLay inlay pattern resin, Reliance) was carefully placed around the canula and bone screw anchors for maximum security and allowed to dry 10-15 minutes. Once dry, the head holders were released and skin sutured around the resultant cement crown using 4-0 interrupted nylon suture. Triple antibiotic ointment was applied to the entire area.

The guide canula stylet was removed and a primed, 2 mm microdialysis probe (MD2200 BR-2, Bioanalytical Systems) was carefully inserted by hand with visualization of the guide canula tract. The mouse was then removed from the stereotaxic frame, placed in the automatic swivel cage and allowed to wake from anesthesia. Most mice were alert and moving within 20 minutes. An adjustable plastic collar was loosely placed around the mouse's neck, and attached to the suspended tether of the automatic swivel arm. Microdialysis tubing was secured to the tether arm to prevent tangling. Standard cob bedding, mouse chow pellets, and fresh water were provided daily (Ch. 4, Fig. 25B).

Approximately 24 hours later, mice underwent a single, moderate left lateral controlled cortical impact with craniotomy, as described previously (Brody, et al., 2007). Briefly, mice were anesthetized with isoflurane, placed in the stereotaxic frame and maintained at 37°C as before. Head holders were used to secure the skull in a level position. The sutures were opened, plastic skull cap removed to expose underlying dura, and impactor tip aligned in the center of the craniotomy. Just prior to impact, the microdialysis probe was removed from the guide canula and immersed in a vial of CMA CNS perfusion fluid. Brief removal of the probe from the guide canula does not affect microdialysis levels of $A\beta_{1\text{-}x}$ (Ch. 4, Fig. 27B; p=0.667, Mann-Whitney U-test). Mice were subjected to controlled cortical impact (CCI) in which a 3 mm-diameter, flat metal tip impounder was driven by an electromagnetic device at a velocity of 5 m/s to various depths (1.0, 1.5, or 2.0 mm) into the cortex. In part because this electromagnetic device does not overshoot the way some pneumatic controlled cortical impact devices can, these impact depths produce less severe injuries than those produced by some pneumatic CCI

devices at the same nominal depth (Brody, et al., 2007). Sham-injured mice underwent identical procedures, except the impactor tip was discharged into the air and did not contact the dura. The microdialysis probe was re-inserted immediately after the impact such that entire duration of probe removal was 4-5 minutes. The wound was then cleaned by gentle irrigation with sterile-filtered phosphate-buffered saline (PBS), and a plastic skull cap replaced and again secured with VetBond. Skin was resutured around the cement crown using 4-0 interrupted nylon sutures and triple antibiotic ointment applied to the entire area. As before, mice were allowed to wake and recover in the electronic swivel cages where they were monitored by microdialysis for an additional 24 hours.

Microdialysis

Microdialysis parameters were based on previously published methods designed for the measurement of interstitial fluid (ISF) Aβ in PDAPP mice (Cirrito, et al., 2003). Microdialysis probes had a 2 mm-long, 320 μm outer diameter, 38 kDa molecular-weight cutoff membrane (MD2200 BR-2 probes; Bioanalytical Systems) and were connected to an infusion syringe pump (KDS 101, KD Scientific). The inlet tract of the probes were attached to the syringe pump via a 1.0 m-long, Teflon (FEP) tubing (inner diameter, 0.12 mm; SciPro) and primed for 1-2 hours with 0.15% sterile human albumin (diluted from 25% Human Albumin, Grifols) in sterile, isotonic saline solution (147 mM NaCl, 2.7 mM KCl, 1.2 mM $CaCl_2$, and 0.85 mM $MgCl_2$; CNS perfusion fluid, CMA, Sweden). During most experiments, flow rate was maintained at 0.3 μL/min for wild-type mice, and 1.5 μL/min for $PDAPP^{+/-}$ mice. Samples were collected every 90 minutes. The outlet tract

of the probe was connected to a second 1.0 m-long piece of FEP tubing. The outflow was collected in low-protein-binding polypropylene tubes housed in a 4ºC-refrigerated, automated fraction collector (Univentor 820 Microsampler, SciPro).

For the initial baseline sampling period, sampling was begun after the dead volume had cleared the outflow line. Similarly, microdialysis samples were collected as soon as the post-TBI dead volume had cleared the outflow lines. All samples were tightly capped and stored at 4ºC for 48 hours or less prior to analysis by ELISA.

MR imaging and histological verification of probe placement

To verify probe placement in the living animal, T2-weighted magnetic resonance (MR) images were acquired (Mac Donald, et al., 2007) (Ch. 4, Fig. 25C). Mice were implanted with a guide canula and probe as described above and allowed to wake and recover for 6-8 hours. Mice were re-anesthetized (induction, 5%; maintenance, 0.75-1%) and placed in an MR-compatible stereotaxic frame in a 4.7T scanner (Oxford Instruments 200/330). Scan duration was approximately 3.5-4 hours, after which the mice were allowed to wake and recover before sacrifice.

To verify probe placement post-mortem in a separate set of animals, 2 mg/mL Evans blue dye (Direct Blue 53, Sigma) in PBS was perfused through the microdialysis probe for a total volume of 50 µL. Mice were transcardially perfused with ice-cold PBS - 0.3% heparin, and the whole brain was extracted. After overnight fixation in 4% paraformaldehyde at 4°C, the brains were transferred to 30% sucrose for 72 hours of equilibration. Brain sections (50 µm) were cut in the coronal plane on a freezing

microtome and counterstained with Neutral Red. Sections were mounted, dried and coverslipped according to standard methods. Regions of interest demonstrating presence of Evans blue into tissue adjacent to the microdialysis probe were identified and photomicrographs acquired at 1× power with a light microscope (Nikon Eclipse E800; Ch. 4, Fig. 25D).

Aβ quantification

Microdialysis and tissue samples were analyzed for Aβ using a denaturing, sandwich ELISA specific for human $A\beta_{1-x}$ according to established methods (Cirrito, et al., 2003). The capture antibody is directed against amino acids 13-28 (m266, courtesy of Eli Lilly and Co.). The detection antibody is biotinylated and directed against N-terminal amino acids 1-5 (3D6, courtesy of Eli Lilly and Co.). The $PDAPP^{+/-}$ tissue samples and wild-type microdialysis samples were assayed for $A\beta_{x-40}$ using a capture antibody specific for amino acids 33-40 (HJ2, courtesy of Hong Jiang and David Holtzman). $PDAPP^{+/-}$ tissue samples were assayed for $A\beta_{1-42}$ using a capture antibody specific for amino acids 33-42 (21F12; see Cirrito, 2003). For the m266 and 21F12-based assay, we used biotinylated 3D6 as a detection antibody. For the HJ2-based assay, a biotinylated, middle-domain capture antibody directed against amino acids 13-28 (HJ5.1, courtesy of Hong Jiang and David Holtzman) was used. All secondary antibodies were followed by streptavidin-poly-horseradish peroxidase-20 (SA-HRP20, Research Diagnostics). Super Slow ELISA TMB (Sigma) was used for colorimetric detection and analyzed on a BioTek

Synergy 2 (BioTek) microtiter plate reader. $A\beta_{40}$ and $A\beta_{42}$ standard curves were generated from synthetic, human sequence Aβ peptide (American Peptide).

For analysis of microdialysis samples, PBS-soluble tissue extracts and carbonate-soluble tissue extracts, samples were diluted in a final buffer of 0.25% bovine serum albumin (BSA), 500 mM guanidine, 200 mM Tris-PBS, pH 7.4; for analysis of the guanidine-soluble tissue extracts, an equal volume of PBS substituted for the guanidine in the original sample buffer.

All microdialysis samples were loaded on 96-well plates in duplicate at a dilution factor of 2 for wild-type mice or in triplicate at a dilution factor of 3 for $PDAPP^{+/-}$ mice. Depending on the number of samples to be analyzed, samples were systematically dithered among two or three plates per experiment. We used strict inclusion criteria for the determination of acceptable ELISA values. Firstly, all raw concentration values were interpolated, rather than extrapolated, from the standard curve. Secondly, at most one of the three replicates was masked, and the values were only accepted if the coefficient of variation was less than 20%.

To quantify the differences in Aβ microdialysis levels between sham and TBI groups in $PDAPP^{+/-}$ mice over time, two approaches were taken. Firstly, raw concentration values were corrected for the dilution factor but not for fractional recovery. Then, these concentrations were averaged by group (TBI vs sham) at each 90-minute sampling period, and plotted as a function of time with standard error of the mean shown. Secondly, we compared normalized Aβ concentrations between groups. To perform this analysis, we first computed a mean baseline value for each experimental subject on each

96-well plate. The baseline was defined as the 12-hour period prior to the sham or TBI procedure, typically 6-12 hours after the initial implantation. Then, all baseline and post-TBI or post-sham measurements were normalized to their respective mean baseline values. Using our strict inclusion criteria, there were scattered missing data such that the most reliable analysis could be performed on 6-hour epochs. The normalized values from each experiment were binned into 6-hour epochs, and a group average for each epoch was computed. A repeated-measures ANOVA was used to test for differences between groups over time in these normalized data binned into 6 hour epochs.

For wild-type microdialysis, four 90-minute samples were pooled for $A\beta_{40}$ measurement over a 6-hour interval, and normalized to the mean of the three baseline values. Group mean data were plotted as a function of time for each 6-hour interval. All post-injury data were then averaged over time and a two-tailed Mann-Whitney U-test was used to compare sham and TBI groups.

Urea assay

After the volume required for Aβ quantification was removed from the microdialysis collection tubes, urea concentration was measured in the remaining volume using a commercially-available kit (Quanti-Chrom Urea Assay Kit, BioAssay Systems). If an experiment showed fluctuating or significantly decreased urea levels > 20%, it was excluded on the basis of probe malfunction. Approximately 1 in 15 experiments was excluded due to abnormal urea levels.

Zero-flow extrapolation

Flow rates were varied systematically and the concentration of Aβ was measured at each flow rate using the $A\beta_{1-x}$ ELISA. For each animal, a flow rate of 1.5 μl/min was used for the first 4.5 hours (3 samples) after probe insertion. An equilibration period of 4-5 hours has previously been described for microdialysis measurement of Aβ in the hippocampi of $PDAPP^{+/-}$ mice (Cirrito, et al., 2003). Then, the flow rates were changed in a systematic fashion to 0.1, 0.3 and 0.5 μl/min. These particular flow rates were used because they yielded the most efficient fit to an exponential curve among a set of 8 test flow rates in pilot experiments (not shown). After each flow rate change, the dead volume (12 μl) was allowed to clear the tubing before the sample was collected for analysis. This required 8 minutes at 1.5 μl/min and 120 minutes at 0.1 μl/min. Samples were collected for 90-540 minutes, and ELISA dilution factors were varied between 3-8. The same pattern of flow rate variation was followed in all animals. After TBI, an identical set of flow rate changes and ELISA dilutions were performed. Except for flow-rate variation, these experiments were conducted in an identical manner to other combined CCI-microdialysis experiments.

All Aβ concentrations were normalized to the 0.1 μL/min pre-TBI concentration for each mouse ([Aβ] / pre-TBI $[A\beta]_{0.1\ \mu L/min}$), and the resultant ratios were averaged to derive a group mean for each flow rate before and after TBI. The concentration as a function of flow rate was fit to a decaying exponential relationship (Jacobson, et al., 1985) using the Excel Solver tool:

$$C = C_0[1 - e^{-K0A/F}] \quad \text{(Equation 1)}$$

where C is the concentration at a given flow rate, C_0 is the zero-flow concentration, K_0 is the mass transfer coefficient, A is the microdialysis probe membrane surface area (160.85 μm^2) and F is the flow rate.

For comparison of pre- and post-TBI mass transfer coefficients, the natural logs of the mean ratios were plotted against their corresponding flow rates and a linear regression of the relationship was performed with a statistical analysis package (GraphPad Prism 5.0). The best-fit slope of this semi-log plot is equal to the $-K_0A$ term in Equation 1. The 95% confidence intervals of the best-fit slope were used to determine the significance of differences between pre- and post-TBI mass transfer coefficients.

Retrodialysis

An N-terminal-biotinylated, synthetic, human-sequence $A\beta_{1-40}$ peptide (rPeptide) was continually infused through the inlet port before and after CCI-TBI in $PDAPP^{-/-}$ wild-type littermates at a concentration of 3000 pg/mL in the standard 0.15% albumin-CMA CNS perfusion solution. To ensure that a loss of infused peptide could be reliably detected when comparing the infused and outflow concentrations, we used a slower flow rate of 1.0 μL/min. Microdialysis samples were analyzed by ELISA using m266 as the capture antibody and incubation with SA-HRP20 for detection of biotinylated $A\beta_{1-40}$. Percentage loss was calculated as the ratio of the concentration in each sample to the concentration in the infused substrate ($[A\beta] / [A\beta]_{IN}$). Both infused and outflow samples were measured on the same ELISA plates.

CA3 cell counts following TBI with and without microdialysis

Four groups of PDAPP$^{+/-}$ mice were assessed histologically for CA3 cell counts: sham with microdialysis, sham without microdialysis, 2.0 mm TBI with microdialysis, and 2.0 mm TBI without microdialysis. 4 mice per group were assessed in a blinded fashion. Brains were sacrificed at 24 hours after injury and prepared for histology. Every 6th section was mounted on a Fisher Superfrost slide, dried, and stained with Neutral Red.

Stereological methods were used to quantify the number of cells remaining in the inferior blade of the CA3 region. The inferior blade was defined within the region of CA3 in coronal sections approximately between the anterior-posterior dimension coordinates of Bregma -1.2 to -2.5 (Franklin and Paxinos, 2001), and extending from the midline to the most lateral edge (Fig. 29). The Optical Fractionator method was used to estimate the number of cells. First, the CA3 inferior blade was outlined at low power (4×). Individual cells were then visualized at high power (60×: oil immersion) within systematic, randomly sampled sites chosen by the StereoInvestigator 8.0 software (MicroBrightfield), and counted. Non-viable cells were excluded from counting as determined by the criteria of shrunken volume, abnormally dark staining, and irregular borders. To meet the prespecified criterion for the Gundersen coefficient of error (CE < 0.10, m=1), a 100 × 100 μm sampling grid and 40 × 40 μm counting frame was used, and a 15 μm dissector region was sampled.

Tissue homogenization and extractions

To compare microdialysis measurements of ISF Aβ with tissue levels after an acute TBI, we measured $A\beta_{1-x}$, $A\beta_{x-40}$ and $A\beta_{1-42}$ in serial homogenate extracts of hippocampus and cortex in separate animals that did not undergo microdialysis.

Two hours after the injury, deep anesthesia was induced with isoflurane, and mice were transcardially perfused with ice-cold PBS-0.3% heparin. The whole brain was quickly removed and divided along the sagittal plane into left (ipsilateral) and right (contralateral) halves. The cortex and hippocampus were dissected, immediately frozen, and stored at -80ºC. For the homogenization-extraction procedure, frozen tissues were weighed and 10 µl per mg of ice-cold PBS with protease inhibitors was added at a minimum volume of 200 µL. Tissues were then dounce-homogenized using a blunt-tip Teflon homogenizer in an ice-cold 1.7-mL microcentrifuge tube for a total of 75 up-and-down strokes. Tubes were spun at 14,000 rpm for 20 minutes at 4ºC in a refrigerated microcentrifuge. The supernatant (PBS-soluble extract) was carefully removed. This extract was stored at -80º C. The resultant pellet was resuspended in 200 uL of 0.1M carbonate buffer, pH 11.5 with protease inhibitors, and dounce-homogenized in the same manner as in the PBS extraction step. Tubes were spun at 14,000 rpm for 20 minutes at 4ºC. The supernatant (carbonate-soluble extract) was carefully removed and stored at -80ºC. Finally, the resultant pellet was extracted with 200 µL of 5M guanidine-HCl, pH 8.0 added to the tube, mixed 15-20 times with a P1000 pipettor, and rotated end-over-end at room temperature for three hours. The resultant extract ("guanidine-soluble") was stored at -80ºC. There was no visible tissue or particulate matter in this extract. Tissue

sample concentrations were normalized to protein concentration as measured by Micro BCA Assay (Pierce).

APP measurement by Western blot analysis

Two groups (n=3 sham and n=4 2.0 mm-injured) of PDAPP mice were sacrificed at 2 hours post-injury for biochemical analysis of APP levels. Brains were perfused and quickly removed. Ipsilateral and contralateral hippocampi and cortices were dissected on an ice-cold glass plate and immediately frozen at -80ºC. The following day, tissues were weighed and immersed in 200 μL of ice-cold, modified RIPA buffer optimized for Western blotting (50 mM Tris-HCl, pH 7.4; 1% NP-40 substitute, 0.25% sodium deoxycholate, 150 mM NaCl, 1 mM EDTA) with protease inhibitors (20 μg/mL aprotinin and 10 μg/mL leupeptin). Tissues were then dounce-homogenized with a small, Teflon-coated conical tip in a 1.7 mL-microcentrifuge tube for a total of 45 strokes (15 easy, 15 hard, 15 easy), with attention paid to minimize bubble formation of the detergent buffer. The homogenates were spun at 13,000 rpm at 4ºC for 20 minutes. The supernatant was removed and assayed for protein content using the Micro-BCA Assay (Pierce). Samples were diluted to 1 mg/mL of protein. 10 μg protein per well was loaded on a 4-12% Bis-Tris, 1 cm x 10 well mini-gel (Invitrogen). Following electrophoresis, gels were blotted onto nitrocellulose membranes, washed for 4-5 hours in TBS, blocked for 60 minutes at room temperature with 2.5% nonfat dry milk in TBS-0.125% Tween-20 (2.5% milk TBS-T), washed 3 times for 5 minutes each (same wash protocol hereafter), and incubated overnight at 4ºC with an anti-APP polyclonal rabbit antibody, Zymed 512700

(Invitrogen) at a concentration of 1:1000 in 2.5% milk in TBS-T. Blots were then washed and incubated with the Licor Odyssey infrared imaging system secondary antibody, goat anti-rabbit IR 680 at 1:10,000 (Licor). To probe the same membranes for β-tubulin as a loading control, membranes were exposed to Restore Western Blot Stripping Buffer (Thermo Scientific) for 10 minutes at room temperature, washed in PBS, blocked for 1 hour at room temperature with 4% milk-PBS, incubated for 3 hours with an anti-tubulin primary antibody at 1:5000 (Sigma-Aldrich T5168), washed, and incubated for 60 minutes with the Licor Odyssey infrared imaging system secondary antibody, goat anti-mouse IR 800 at 1:10,000 (Licor). Membranes were washed in PBS and imaged using the Licor Odyssey infrared imaging system. The average intensity of each band complex (APP) or single band (tubulin loading control) was quantified by the user-defined background subtraction tool in the Licor Odyssey V3.0 acquisition and analysis software. Identical rectangular area templates were used to calculate band intensity for each band complex or single band on the blot. The average band intensity for APP was normalized to that of the tubulin loading controls from the same sample to account for inhomogeneities between lanes.

Aβ immunohistochemistry

A randomly-selected subset of brains was chosen for Aβ immunohistochemistry. All mice were sacrificed at 24 hours after injury, and brains perfused, fixed and sliced coronally into 50 μm sections and placed immediately in TBS. Free-floating sections were treated with 0.3% H_2O_2 for 10 minutes at room temperature to inactivate

endogenous peroxidases and washed 3 times in TBS for 5 minutes each (hereafter, all washes are 3 times, 5 minutes each in TBS). Sections were then blocked at room temperature with 3% nonfat dry milk in TBS-0.125% Triton-X (3% milk in TBS-X) for 60 minutes, washed, then incubated overnight at 4ºC in 0.75 μg/mL of a biotinylated, monoclonal antibody directed against the N-terminus of human Aβ (HJ3.4, courtesy of Hong Jiang and David Holtzman) in 1% milk-TBS-X. Sections were washed, incubated for 60 minutes at room temperature with a 2.5% solution of the Vectastain Elite ABC kit (Vector Labs; 2.5% avidin-biotin complex in TBS), washed, and developed using 0.25% diaminobenzidine (DAB) chromagen substrate. The reaction was judged to be complete when Aβ deposits on the positive controls became visible at low power on a light microscope. Sections were then immediately washed and mounted on Fisher Superfrost slides, allowed to dry overnight in ambient conditions, dehydrated and coverslipped. Representative images were taken at 2× and 4× with a Nikon Eclipse E800 light microscope.

Intraparenchymal EEG recording

The EEG recording protocol was adapted from previous studies of combined EEG-microdialysis (Cirrito, et al., 2005). Two Teflon-coated platinum-iridium recording electrodes (Cat. No. 777000, 0.0055-inch diameter, A-M Systems; Fig. 6A) (Cirrito, et al., 2005, Kang, et al., 2007) were attached to either side of the cylindrical guide canula using an epoxy-cement (Elmer's Super-Fast Epoxy Cement). The electrodes extended to 2 mm past the end of the guide canula, the same distance as the probe, such that they

recorded potential differences in the vicinity of the probe membrane. They were cut on-end at a 45º angle such that the bare metal tip was exposed at the end of the 2 mm extension. These electrodes and a zero-reference to cerebellar dura were soldered to a three-pin prong. A custom-built head stage amplifier was used to eliminate external electrical noise (courtesy of the Washington University Electronics Shop). The signal was then amplified (P511 AC Amplifier, Grass Instruments) and digitized (MiniDigi 1A, Axon Instruments) for acquisition (Axoscope 9.2, Axon Instruments) and offline analysis (Clampfit 9.2, Axon Instruments) on a PC. The raw signal was filtered between 0.1 Hz and 0.1 kHz. The Clampfit 9.2 statistics package was used to quantitate RMS amplitude over 6 artifact-free, 1-2 min epochs per microdialysis sampling period. These amplitudes were averaged and data normalized to the mean baseline RMS amplitude.

Statistical methods

Statistica 6.0 was used for repeated-measures ANOVA testing for differences in microdialysis Aβ for sham vs. TBI by group and by time (Fig. 2B) (StatSoft, Tulsa, OK). Significance was determined at $p < 0.05$. Statistical analysis for other tests was performed using Prism version 5.00 for Windows (GraphPad, San Diego). Again, significance level was determined at $p < 0.05$. Two-tailed Mann-Whitney U-tests were used to test for differences in Aβ levels between sham and TBI groups. Mass transfer coefficients for pre and post-TBI exponential curves in the zero-flow control experiment were evaluated for statistical difference using overlap of the 95% confidence intervals, as calculated from a linear regression analysis of the natural log of group-mean normalized

concentrations at each flow rate. Two-tailed, paired t-tests were used to compare pre vs. post TBI levels of infused Aβ during retrodialysis and urea measurement control experiments. Comparison of EEG amplitude changes over the 24 hours following sham or TBI was also performed using the two-tailed Mann-Whitney U-test.

RESULTS

Intracerebral microdialysis combined with controlled cortical impact TBI

We initially established that experimental controlled cortical impact (CCI) TBI could be successfully combined with intracerebral microdialysis in mice (Ch.4, Fig. 25). This method was designed to allow microdialysis sampling from a large region of the hippocampus without hindering placement of the ipsilateral craniotomy required for CCI (Ch. 4, Fig. 25A). The microdialysis guide canula was affixed to the skulls of the mice with dental cement and they were tethered to an automatic swivel cage (Ch. 4, Fig. 25B). This allowed microdialysis to occur while the mice were freely moving before and after injury. To verify probe placement *in vivo*, three separate mice were anesthetized and imaged using magnetic resonance technology with a T2-weighted sequence (Ch. 4, Fig. 25C). This confirmed that the probe tract extended into the hippocampus, whereas the guide canula was restricted to the cortex. Additionally, we infused the probe with Evans blue dye just prior to sacrifice to again verify placement on histology. The blue tract of the probe was restricted to an area along the long axis of the hippocampus in the coronal plane (Ch. 4, Fig. 25D). These results established the accuracy of the placement of the microdialysis probe both *in vivo* and *post mortem*.

To evaluate the similarity of the CCI injury performed in conjunction with microdialysis and injury without microdialysis we made two comparisons. First, we consistently observed a 10-20% weight loss within the first 24 hours after CCI injury with or without microdialysis. Second, the CCI injury consistently results in neuronal cell loss in the CA3 region of the hippocampus in PDAPP mice. We found no significant difference in cell loss in the inferior blade of the CA3 region between injury with (24.5%) and without microdialysis (30.9%; p=0.572, unpaired, two-tailed t-test comparing cell counts; Figs. 29, 30). Importantly, there was no difference in inferior blade CA3 cell counts in sham mice with and without microdialysis (Fig. 29, 30; p=0.693, unpaired, two-tailed t-test). The CA3 cell loss in CCI-injured PDAPP mice was concordant with previous results (Hartman, et al., 2002, Smith, et al., 1998).

Figure 29. CA3 cell loss and cortical lesion at 24 hours post-injury in young, PDAPP$^{+/-}$ mice: injury with microdialysis vs. without microdialysis. Coronal sections from young PDAPP$^{+/-}$ mice sacrificed at 24h following TBI or sham injury were stained with Neutral Red. Representative images used to count CA3 cells are shown at 4× power (A-D) with the region of interest, CA3 inferior blade, bordered by arrows. A-D: scale bar, 500 μm. Corresponding views are shown at 2× power (E-H). E-H: scale bar, 1 mm. **A, E.** Sham with microdialysis. **B, F.** Sham, no microdialysis. **C, G.** 2.0 mm TBI, with microdialysis. **D, H.** 2.0 mm TBI, no microdialysis.

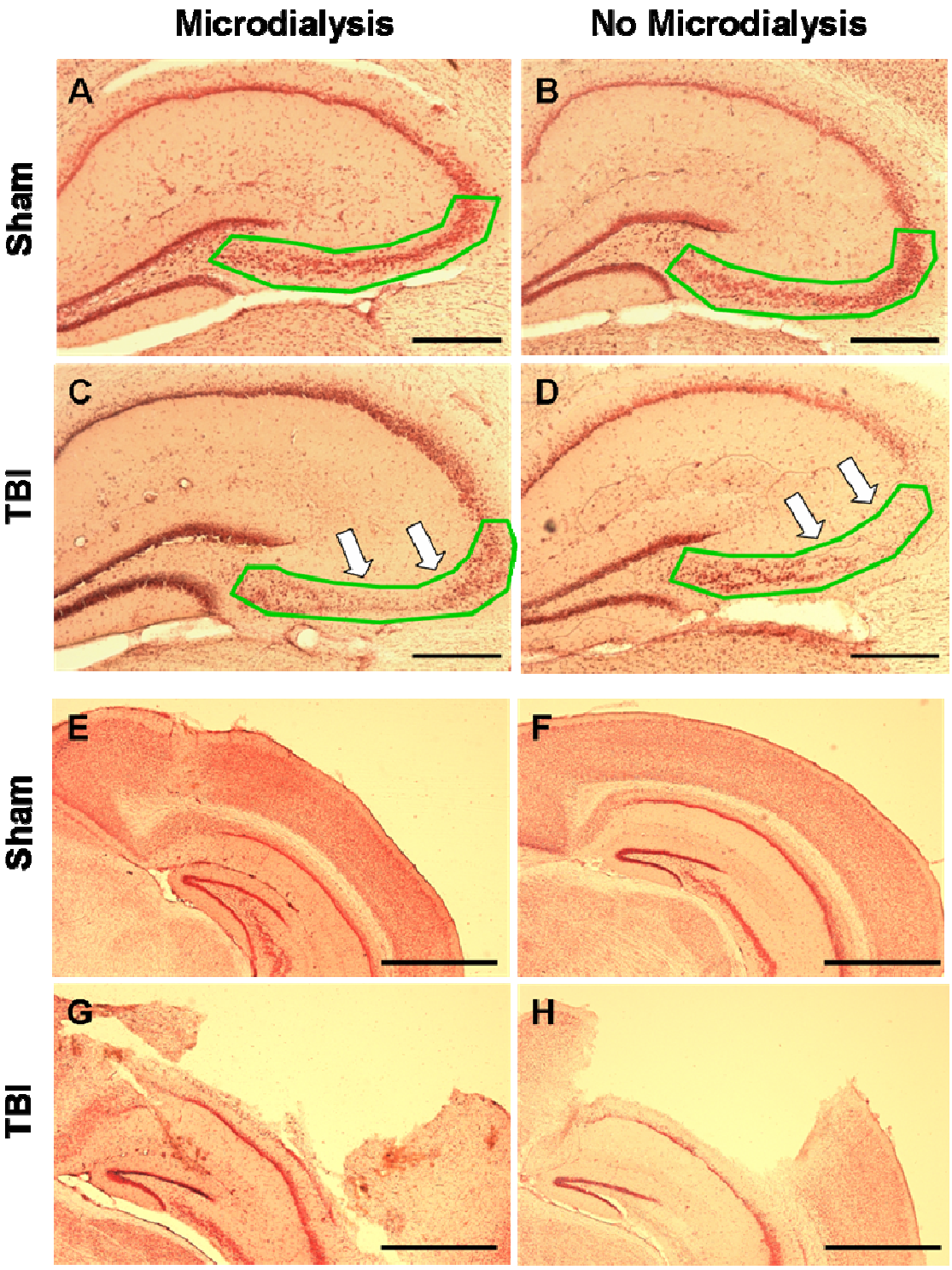
Microdialysis
No Microdialysis
Sham
TBI
Sham
TBI
A
B
C
D
E
F
G
H

Figure 30. CA3 cell loss at 24 hours post-injury in young, PDAPP$^{+/-}$ mice: injury with microdialysis vs without microdialysis. Mean cell counts with standard errors plotted for each group, n=4 per group: no significant differences between 2.0 mm-injured mice with and without microdialysis (p = 0.572, two-tailed t-test), nor between sham-injured animals with and without microdialysis (p=0.693, two-tailed t-test).

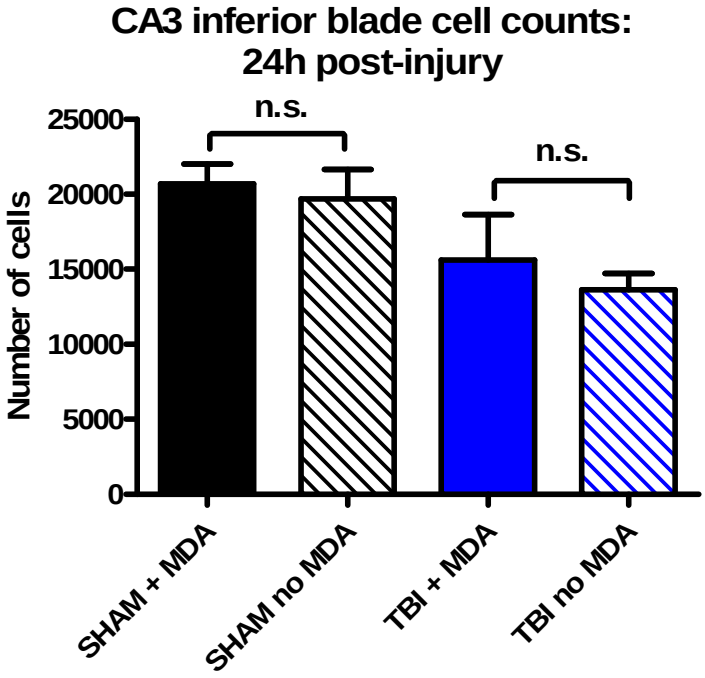

Microdialysis levels of Aβ decrease immediately following CCI

In 3-6 month old wild-type C57BL6 mice, we collected baseline microdialysis samples over 18-24 hours, then performed either sham (n=4) or 2.0 mm CCI TBI (n=4) (Fig. 31A, B). Measurements of endogenous $A\beta_{40}$ were made every 6 hours for 24 hours before and 42 h following an injury. Absolute levels during the baseline period were 68.0 ± 19.5 pg/mL. Levels of endogenous Aβ were low relative to the limits of detection, which averaged 28.6 pg/mL in this ELISA. Thus, time resolution better than 6 hours was not possible in wild-type mice.

There was a trend for Aβ levels to be decreased in the wild-type TBI group. They remained close to baseline in the wild-type sham group (Fig. 31A). Over the entire 42-hour post-TBI interval, $A\beta_{40}$ levels were 67.1% ± 4.6% of baseline in 2.0 mm-injured mice and 96.1% ± 5.0% of baseline in sham-injured mice (p=0.200, two-tailed Mann-Whitney U-test). It was not possible to measure $A\beta_{42}$ in microdialysates from wild-type mice.

In principle, human sequence Aβ could show dynamics in ways that differ from murine Aβ, i.e. due to aggregation or deposition. In order to address the dynamics of human sequence Aβ in the ISF after TBI, we turned to a transgenic mouse model, the $PDAPP^{+/-}$ mouse. Additionally, the ELISAs used to detect human Aβ is considerably more sensitive than the ELISA used to detect murine Aβ (typically 1.6-4.4 pg/ml). This permitted an improved time resolution from 6 hours to 90 minutes. We collected baseline microdialysis samples for $A\beta_{1-x}$ measurement over 18-24 hours, then performed either sham (n=6) or 2.0 mm CCI TBI (n=6) in 3-6 month old in $PDAPP^{+/-}$ mice (Fig. 31C). Baseline $A\beta_{1-x}$ values in sham and injured groups were relatively stable, showing little variation during the 12 hours preceding sham or TBI (Fig. 31C). For $PDAPP^{+/-}$ mice, baseline $A\beta_{1-x}$ values measured in microdialysates were 90 ± 53 pg/ml (mean ± SD) in the sham groups and 108 ± 57 pg/ml in the TBI group. These were not significantly different (p=0.6991, two-tailed Mann-Whitney U-test). Following injury the TBI group demonstrated an immediate and persistent decrease in $A\beta_{1-x}$ (Fig 31C). Taken in 6-hour epochs and normalized to baseline, levels fell to approximately 67 ± 23% of baseline during the first 6 hours, then 46 ± 13% over 6-12 hours, 37 ± 8% over 12-18 hours, and

34 ± 7% from 18-24 hours after injury (Fig 31D). $A\beta_{1-x}$ levels in the sham-injured group remained at or above baseline values. Overall, $A\beta_{1-x}$ levels were significantly different between TBI and sham groups (Fig. 31D) (repeated measures ANOVA $p < 0.00239$ for main effect of group).

Figure 31. Hippocampal Aβ dynamics before and after traumatic brain injury as measured by microdialysis. A, wild-type mice. $A\beta_{x\text{-}40}$ by ELISA beginning 18 hours before injury though 42 hours after injury in 3-6 month old C57BL6 mice. Sham-injured animals underwent the same procedures, except the impactor was discharged without contacting the cortical surface. Error bars represent the standard error of the mean for the group. **B,** data were normalized to each individual animal's baseline and averaged by group over the entire 42-hour, post-TBI interval. Error bars represent the standard error of the mean for the group. Injured animals showed a non-significant decrease in $A\beta_{x\text{-}40}$ compared to sham ($p = 0.200$, two-tailed Mann-Whitney U-test). **C**, PDAPP mice**.** $A\beta_{1\text{-}x}$ measured in 90-minute microdialysis samples by ELISA beginning 12 hours before injury though 24 hours after injury in 3-6 month old $PDAPP^{+/-}$ mice. Error bars represent the standard error of the mean for the group. **D**, data were normalized to each individual animal's baseline and binned into 6-hour epochs. Error bars represent the standard error of the mean for the group. Injured animals showed a statistically significant decrease in $A\beta_{1\text{-}x}$ compared to sham (**$p < 0.004$ for main effect of group, $p < 0.00004$ for group by time, repeated measures ANOVA).

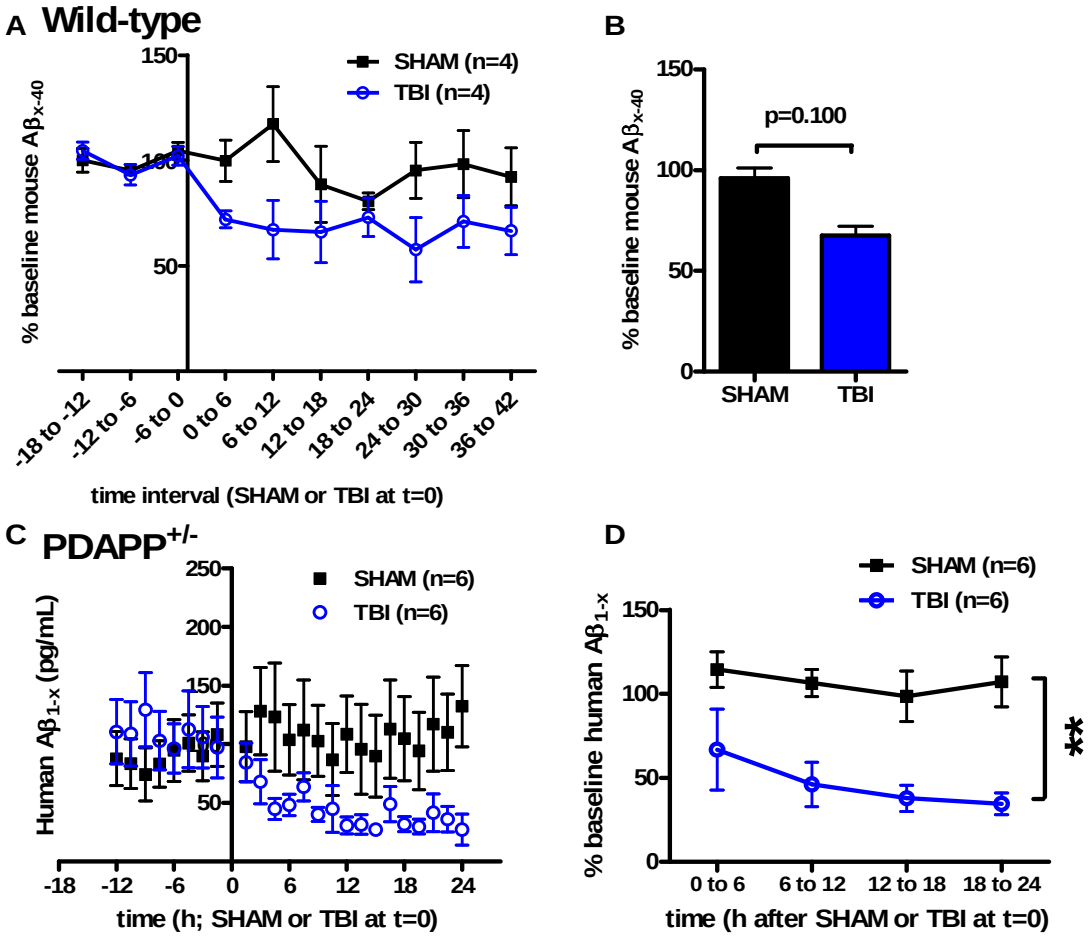

Decreases in $A\beta_{1-x}$ likely reflect physiological sequelae of TBI

A key assumption underlying the reliability of measurements made by microdialysis is that the probe is functioning normally throughout the experiment. For example, the probe should never be clogged or otherwise blocked from free exchange with the surrounding interstitial fluid (ISF). To address this concern, we used three approaches to test for consistent probe function: zero flow extrapolation, retrodialysis, and measurement of urea.

We performed zero-flow extrapolations during baseline periods and again during post-TBI periods in 4 $PDAPP^{+/-}$ mice undergoing 2.0 mm CCI injury (Fig. 32A). The zero-flow extrapolation method involves varying the flow rate over time and assumes that the underlying ISF concentration remains constant. Because the levels of post-TBI Aβ decreased by 4.5-6 hours after injury and remained relatively stable over the next 18 hours (Fig. 31C), we were able to vary the flow rate during the post-injury period. We plotted the Aβ levels before and after TBI as a function of flow rate, and fit this data to decaying exponential curves. The mass transfer coefficients for these exponential curves were not significantly different before and after TBI ($K_{0,\ pre\text{-}TBI} = 9.5 \pm 2.2$ $mL/(min*mm^2)$ and $K_{0,\ post\text{-}TBI} = 10.2 \pm 1.6$ $(mL/min*mm^2)$ as indicated by overlapping 95% confidence intervals. This result indicates that there was no significant change in the fractional recovery of Aβ before and after TBI. Normalized to the respective zero-flow concentrations, the mean fractional recoveries at 1.5 μL/min were 0.0527 ± 0.00129 (pre-TBI) and 0.0642 ± 0.00286 (post-TBI); these were not significantly different (two-tailed Mann-Whitney U-test, $p = 0.1333$).

Next, probe function was evaluated using retrodialysis of Aβ in the perfusion solution. For simple diffusion, Aβ diffusion rates from the microdialysis probe into the brain should be similar to diffusion rates from the brain into the microdialysis probe. Wild-type mice were subjected to the combined CCI-microdialysis procedure with perfusion of 3000 pg/ml of synthetic, biotinylated $A\beta_{1-40}$ through the inlet tubing. There was an average Aβ loss of approximately 20-25% both before and after a 2.0 mm CCI injury (Fig. 32B). Pre and post-injury levels were not significantly different ($p=0.1944$, paired t-test). This experiment further indicates that there were no changes in the diffusion of Aβ across the microdialysis probe after TBI.

Finally, the recovery of urea was used as a third control for probe function. Urea is a small molecule produced in the liver that rapidly equilibrates throughout all tissue compartments, and is frequently used as a control for probe function in human cerebral microdialysis (Ronne-Engstrom et al., 2001; Brody, Magnoni et al., 2008). Urea levels were comparable in all microdialysis samples (Fig. 32C). There were no significant differences between pre and post-TBI urea levels ($p=0.1747$, paired t-test).

Of note, in some animals in which microdialysis was performed for more than 24 hours after TBI, urea levels became inconsistent. Therefore, Aβ measurements were considered potentially unreliable after the first 24 hours. Thus, we restricted our analyses to measurements during the first 24 hours after of injury.

Figure 32. **Controls for changes in microdialysis probe function following TBI**. **A,** zero-flow extrapolation. Flow rates were changed systematically at baseline (left) and after 2.0 mm TBI (right) in 4 PDAPP$^{+/-}$ mice. Exponential fits to these data allow comparison of pre and post-TBI fractional recovery of Aβ. Statistically indistinguishable mass transfer coefficients ($K_{0\ pre\text{-}TBI}$, $K_{0\ post\text{-}TBI}$) suggest unchanged probe recovery before and after TBI. **B,** retrodialysis of biotinylated Aβ in wild-type mice did not differ before vs. after 2.0 mm TBI (n=4; p=0.1944, paired t-test); inset, averaged data for all samples pre and post-TBI. **C,** recovery of urea by microdialysis in PDAPP$^{+/-}$ mice was stable before and after TBI (p=0.1747, paired t-test).

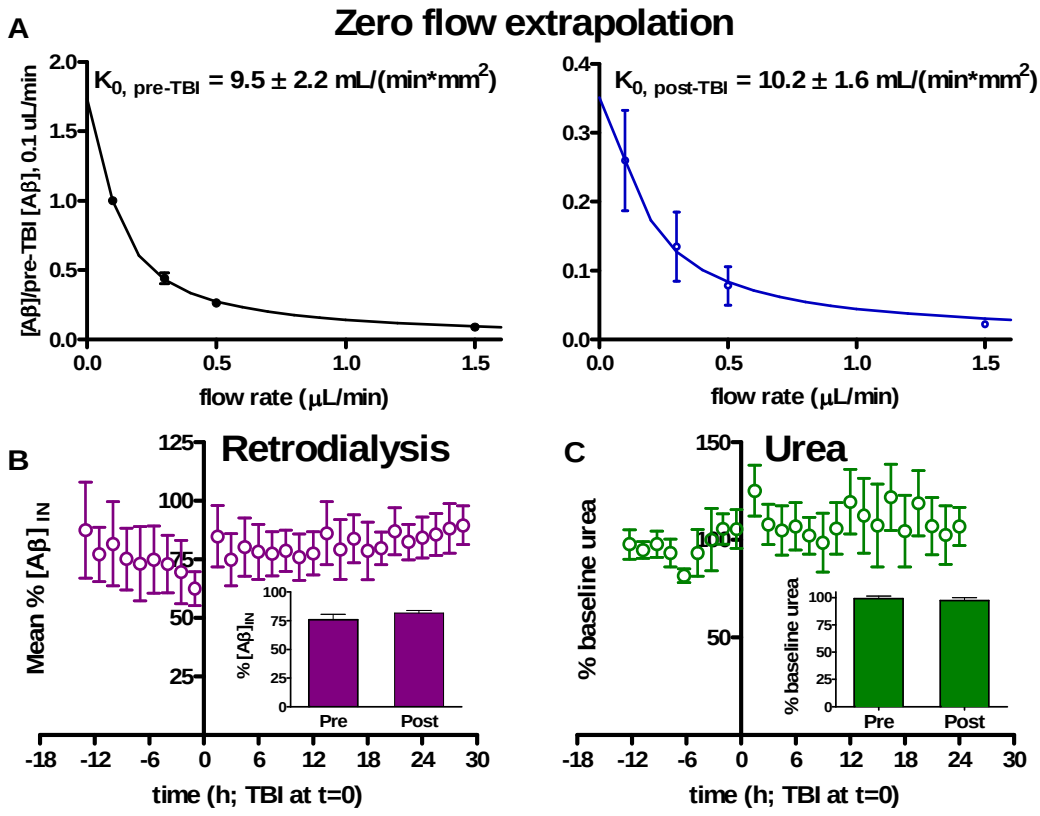

Decreases in microdialysate levels of $A\beta_{1\text{-}x}$ are reflected in tissue lysates

Post-TBI changes in microdialysate levels of Aβ might reflect changes in overall tissue levels or be specific to ISF Aβ. To assess these alternative hypotheses, we used a serial tissue extraction protocol in a separate set of PDAPP$^{+/-}$ mice sacrificed 2 hours after

TBI. Because the mice used for tissue homogenization did not undergo microdialysis, the similarity of injury with and without microdialysis was first assessed histologically (Fig. 29), including stereological quantification of cells in the inferior blade of the CA3 region of the hippocampus (Fig. 30). No significant differences were found between 2.0 mm injured mice with and without microdialysis qualitatively (Fig. 29) or stereologically (Fig. 30; p=0.572, unpaired, two-tailed t-test). This indicates that 2.0 mm impact depth injuries were similar in severity with and without microdialysis. Likewise, there were no differences between sham-injured mice with and without microdialysis (p=0.693, unpaired, two-tailed t-test; Fig. 30).

$A\beta_{1-x}$ levels in tissue lysates were reduced in both the hippocampus and cortex. For ipsilateral hippocampus, significant differences were measured in the PBS-soluble pool of $A\beta_{1-x}$ between sham and injured groups (Fig. 33A; p=0.0286, Mann-Whitney U-test). Specifically, after injury, tissue levels were reduced to approximately 50-60% of that found in sham-injured animals. This change is of the same magnitude as was measured by microdialysis (Fig. 31). Although $A\beta_{1-x}$ measurements in carbonate and guanidine-soluble extracts of ipsilateral hippocampus were not significantly different between sham and TBI, mean levels were decreased ~25-50% at the 2-hour timepoint (Fig. 33D, G).

Figure 33. Effects of experimental TBI on Aβ levels in ipsilateral hippocampal homogenates. PDAPP$^{+/-}$ mice underwent 2.0 mm injury or sham and were sacrificed after 2 hours (n=5 per group). Levels of Aβ isoforms were measured in serial extracts, and values were normalized to total protein in each homogenate. Data plotted for individual mice: $Aβ_{1-x}$ (**A, D, G**), $Aβ_{x-40}$ (**B, E, H**), $Aβ_{1-42}$ (**C, F, I**) levels in PBS (**A, B, C**), carbonate (**D, E, F**), and guanidine-soluble extracts (**G, H, I**). Significant differences were observed in the PBS-soluble pool of $Aβ_{1-x}$ between sham and TBI groups (p=0.0286, Mann-Whitney U-test); PBS-soluble levels of $Aβ_{x-40}$ also differed between sham and TBI groups (p=0.0159).

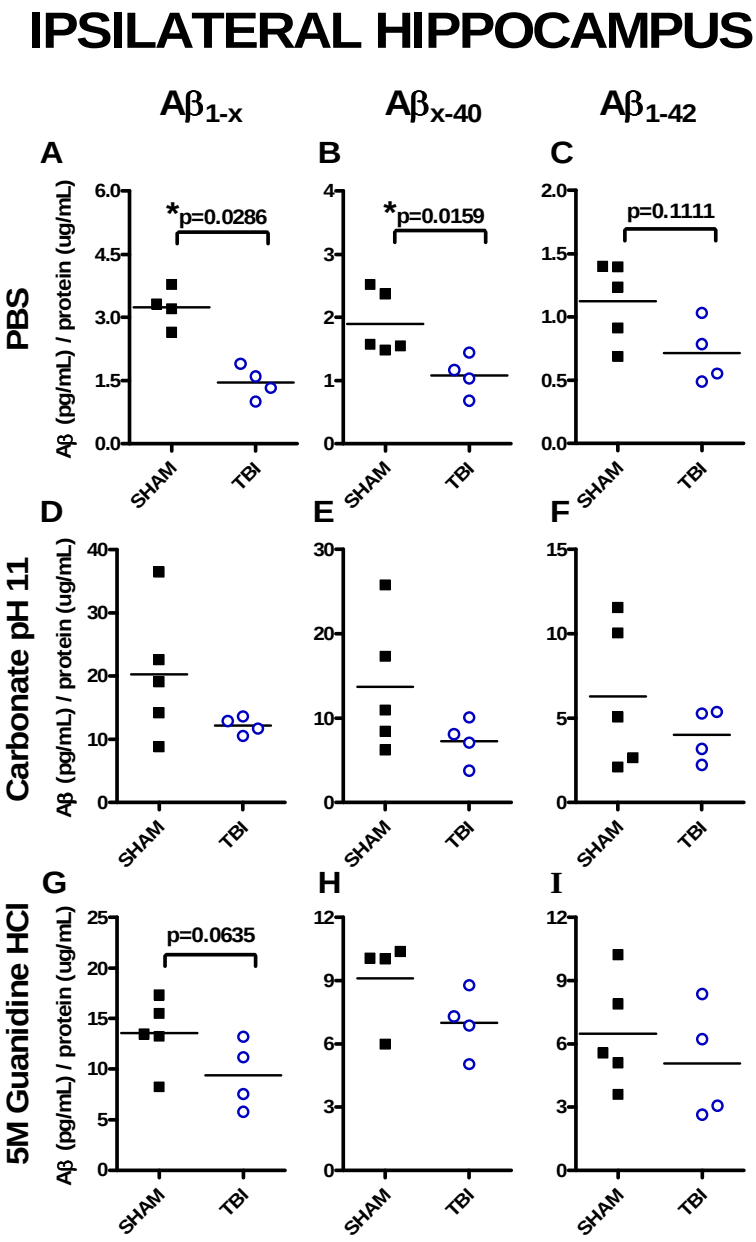

For ipsilateral cortex, there was a statistically significant difference of approximately 50% between sham and injured groups in $A\beta_{1-x}$ levels in all three homogenates: PBS-soluble extracts (Fig. 34A; p=0.0079), carbonate-soluble extracts (Fig. 34D; p=0.0159), and guanidine-soluble extracts (Fig. 34G; p=0.0079).

Figure 34. Effects of experimental TBI on Aβ levels in ipsilateral cortical homogenates. Cortical homogenates from the same mice as in Fig. 18. Values normalized to total protein in each homogenate plotted for individual mice: $A\beta_{1\text{-}x}$ (**A, D, G**), $A\beta_{x\text{-}40}$ (**B, E, H**), $A\beta_{1\text{-}42}$ (**C, F, I**) in PBS (**A, B, C**), carbonate (**D, E, F**) and guanidine-soluble extracts (**G, H, I**). Differences were detected in the PBS-soluble pool of $A\beta_{1\text{-}x}$ between the sham and TBI groups (p=0.0079, Mann-Whitney U-test), in the carbonate-soluble pool of $A\beta_{1\text{-}x}$ (p=0.0159), and the guanidine-soluble pools of both $A\beta_{1\text{-}x}$ (p=0.0079) and $A\beta_{1\text{-}42}$ (p=0.0159).

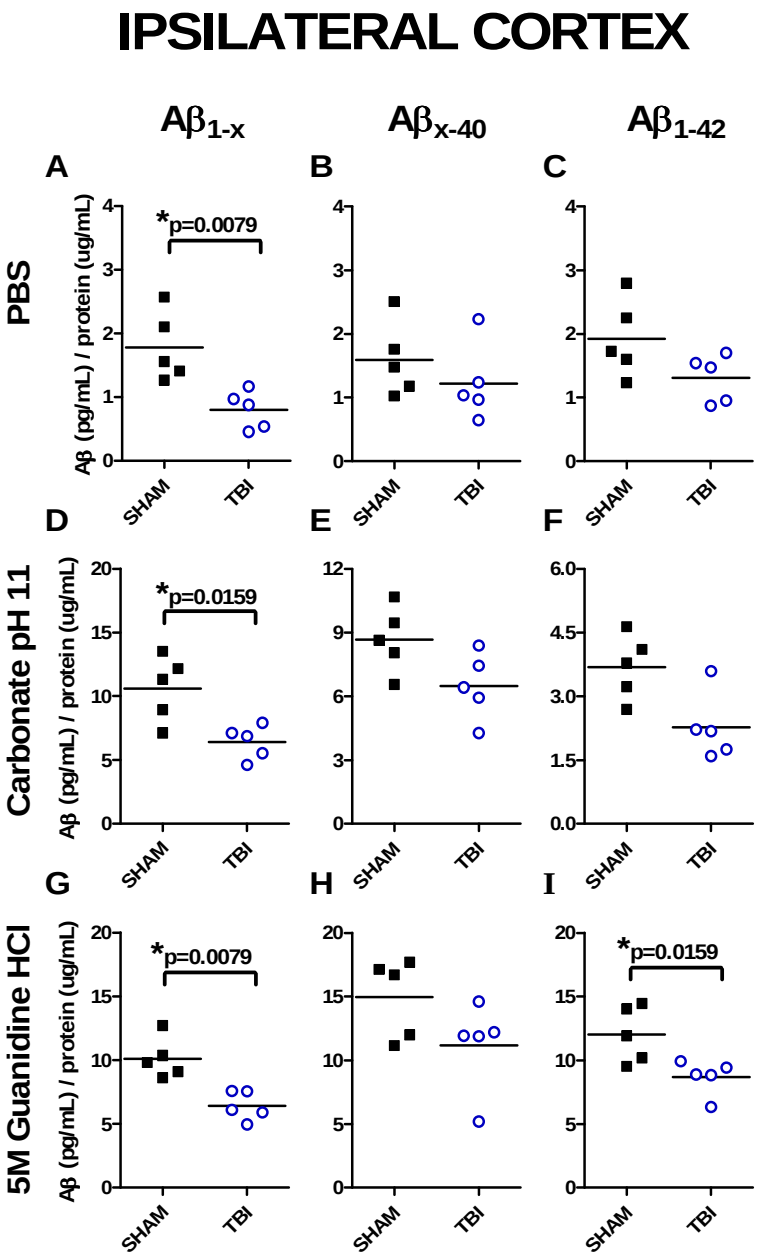

Decreases in $A\beta_{40}$ and $A\beta_{42}$

$A\beta_{x\text{-}40}$ and $A\beta_{1\text{-}42}$ were measured individually in tissue homogenates of ipsilateral hippocampus and cortex. Levels of PBS-soluble $A\beta_{x\text{-}40}$ in the ipsilateral hippocampus were significantly different between sham and TBI groups in (Fig. 33B; p=0.0159). There was also a significant difference in $A\beta_{1\text{-}42}$ levels in guanidine-soluble cortical extracts (Fig. 34I, p=0.0159). While changes in the levels of these specific isoforms in other PBS, carbonate and guanidine-soluble extracts did not reach statistical significance, levels of Aβ were decreased in injured tissues 25-50% compared to sham. No extracts showed evidence of increased Aβ.

We did not measure $A\beta_{x\text{-}40}$ and $A\beta_{1\text{-}42}$ separately in individual microdialysis samples due to the low sample volumes and lesser sensitivity of the isoform-specific Aβ ELISAs.

No changes in the amount of APP in the injured brain

Reductions in hippocampal $A\beta_{1\text{-}x}$ measured by microdialysis and in hippocampal and cortical homogenates could in principle be related to changes in the expression of the amyloid precursor protein (APP) in the brain after injury. To test the hypothesis that APP levels were affected in the acute post-injury period, we used Western blotting to quantify the amount of full-length APP in RIPA-extracted tissues from additional injured and sham $PDAPP^{+/-}$ mice. APP levels were found not to be significantly different between sham and TBI groups at 2 hours after injury in ipsilateral and contralateral hippocampi and cortices (Figs. 35, 36).

Figure 35. **Measurement of full-length APP at 2h post-injury.** Western blot probed for full-length APP in RIPA extracts of brain tissues at 2h post-injury. No differences in the RIPA-soluble pool of full-length APP were detected between sham and TBI groups as quantified by the average intensity per band, normalized to tubulin loading control. Tissues were loaded in the same order on each gel such that each lane corresponds with the same mouse on each blot (S=sham, T=TBI). **A.** Ipsilateral hippocampus. **B.** Contralateral hippocampus. **C.** Ipsilateral cortex. **D.** Contralateral cortex.

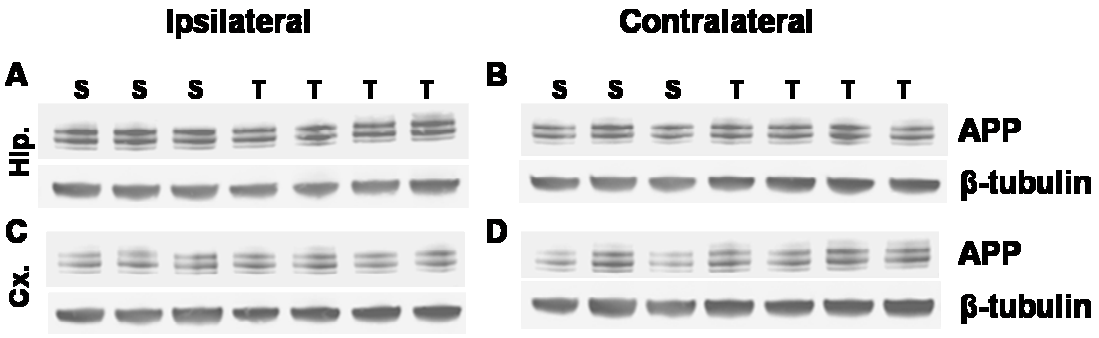

Figure 36. **Quantification of average band intensities, APP/tubulin loading control in RIPA-extracted tissues at 2 hours post-injury in young, PDAPP$^{+/-}$ mice.** Mean average band intensities of APP (normalized to tubulin), quantified by the user-defined background method on the Licor Odyssey imaging system, plotted for each group, n=5 each (see Fig. 35 for blot). No differences in APP levels were observed between sham and injured. Standard errors shown for group means. Unpaired, two-tailed t-tests used in all comparisons. **A.** Ipsilateral hippocampus (p = 0.419).**B.** Contralateral hippocampus (p=0.553). **C.** Ipsilateral cortex (p=0.382). **D.** Contralateral cortex (p=0.096).

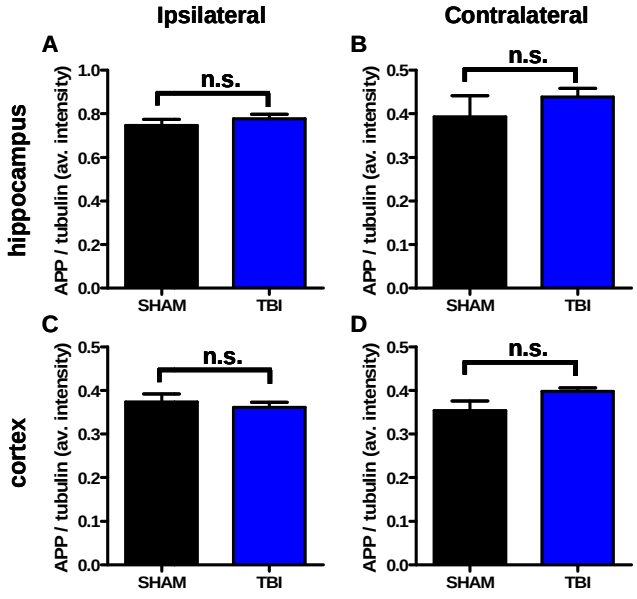

No Aβ deposits observed at 24 hours after injury in the young, injured mouse brain

Acute Aβ deposits have been observed as early as 2 hours in the brains of approximately 1/3 of adult human TBI patients not otherwise expected to have plaques (Fig. 1). We did not expect to see Aβ deposits after TBI in these animals based on previous results (Smith, et al., 1998) and our guanidine extract ELISA data (Figs. 33, 34). However, to explicitly test the hypothesis that Aβ deposition might underlie the decrease in the exchangeable pool of Aβ, we stained sections throughout the hippocampus, every 300 μm, from two groups of mice (n=5 2.0 mm TBI, n=5 sham) at 24 hours after injury or sham with a biotinylated anti-Aβ antibody (HJ3.4B, courtesy of Hong Jiang and David Holtzman). No deposition could be seen in any of the sections at this timepoint in young PDAPP$^{+/-}$ mice (Fig. 37, A-D). As positive controls, sections from 10 and 20-month old PDAPP$^{+/-}$ mice were stained with HJ3.4B. The 10-month old mouse showed nascent deposition in hippocampus and cortex (Fig. 37E), while the 20-month old mouse displayed widespread plaques throughout cortex and hippocampus (Fig. 37G). These patterns confirmed the sensitivity of the immunohistochemical methods.

Figure 37. **Aβ immunohistochemistry.** Coronal sections from animals sacrificed at 24h following 2.0 mm TBI or sham injury were stained with HJ3.4B, a monoclonal, biotinylated antibody directed against the N-terminus of human Aβ. Every sixth section was stained with HJ3.4B (**A, C, E, G, I**). The series adjacent to the stained series underwent the same processing, with omission of the primary antibody (**B, D, F, H, J**). Scale bar on all images, 2.5 mm. **A.** 4-5 month old PDAPP$^{+/-}$, 2.0 mm TBI with microdialysis. **B.** Same brain as (**A**), without primary antibody. **C.** 4-5 month old PDAPP$^{+/-}$, sham with microdialysis. **D.** Same as (**C**), without primary. **E.** 10 month old PDAPP$^{+/-}$ sham with microdialysis. **F**. Same as (**E**), without primary. **G**. 20 month old PDAPP$^{+/-}$, 2.0 mm TBI with microdialysis. **H**. Same as (**G**), without primary. **I**. 4-5 month old wild-type C57BL6 mouse underwent 2.0 mm TBI. **J**. Same as (**I**), without primary.

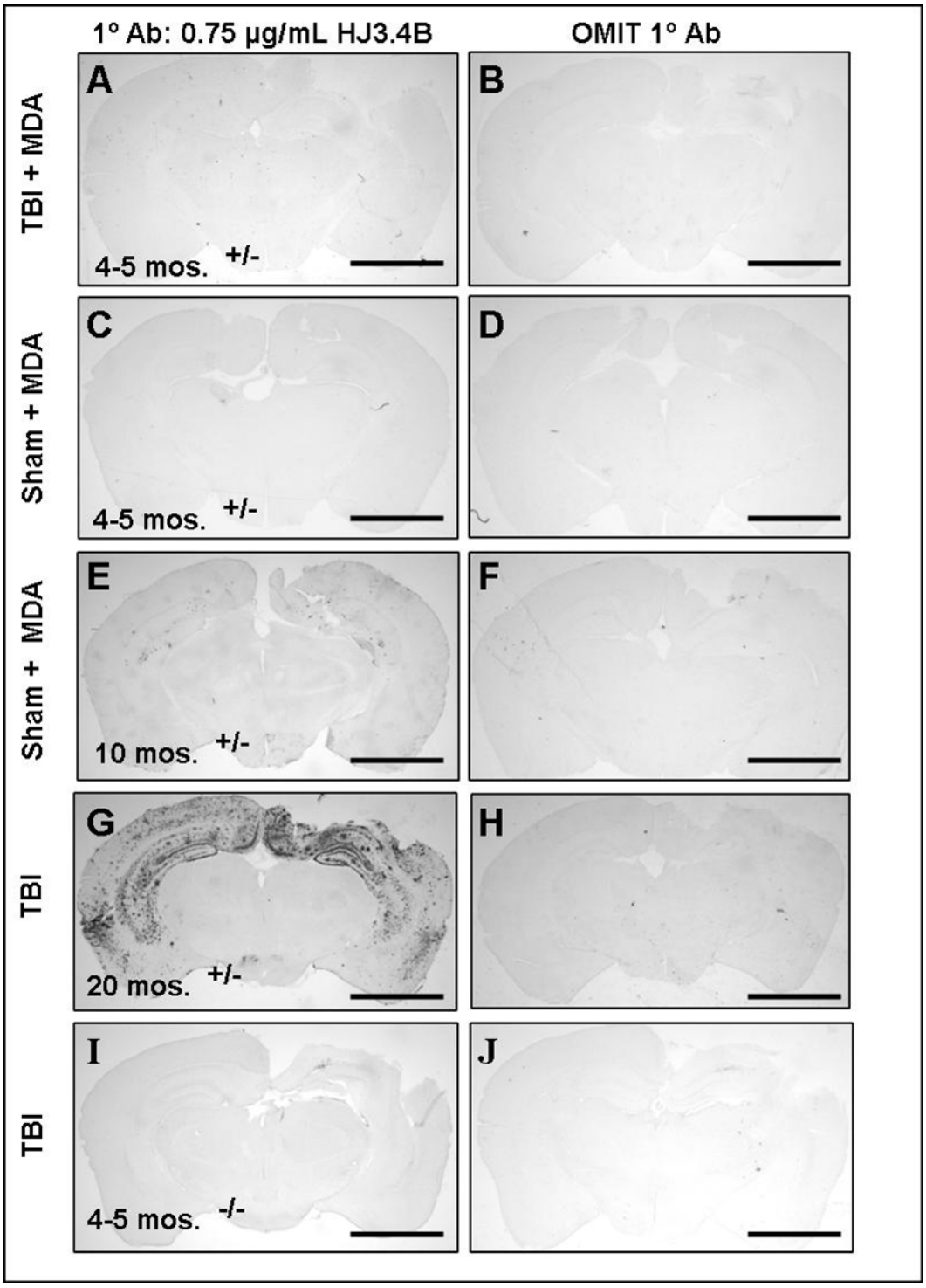
1° Ab: 0.75 µg/mL HJ3.4B
OMIT 1° Ab
TBI + MDA
Sham + MDA
Sham + MDA
TBI
TBI
A
B
C
D
E
F
G
H
I
J
4-5 mos. +/-
4-5 mos. +/-
10 mos. +/-
20 mos. +/-
4-5 mos. -/-

Reduced EEG activity in the injured hippocampus

Previous animal studies suggest that extracellular Aβ dynamics are highly correlated with neuronal activity (Cirrito, et al., 2008, Cirrito, et al., 2005, Kamenetz, et al., 2003). We asked whether the changes seen in microdialysis levels of Aβ in our model might be associated with changes in local neuronal activity using intra-parenchymal EEG. Using a modified guide canula with two affixed electrodes (Fig. 38A), EEG amplitude was continuously recorded during the baseline monitoring (Fig. 38B) and post-injury periods (Fig. 38C). Filtered tracings were sampled for statistical analysis of root-mean square (RMS) amplitude, and average baseline values corresponding to each microdialysis sampling period were plotted over time (Fig. 38D). EEG amplitude was stable during the baseline period. After TBI, the EEG amplitude was decreased compared to baseline (Fig. 38B, C; Fig. 38D). The extent of the reduction in EEG amplitude over the 24-hour period following sham or 2.0 mm injury was significantly different between groups (two-tailed Mann-Whitney U-test, $p = 0.0182$) (Fig. 38E). Taken together with the previous studies of extracellular Aβ dynamics and neuronal activity, our measurement of an overall reduction in EEG amplitude suggests a possible mechanism for the observed reduction in ISF Aβ in the injured hippocampus.

Figure 38. **Measurement of EEG changes following experimental TBI. A.** Photograph of modified guide canula with Teflon-coated platinum-iridium EEG leads attached. Scale bar, 5 mm. Inset demonstrates relationship of leads to probe membrane. Scale bar, 2 mm. **B.** Exemplar EEG tracing before injury. **C.** Exemplar EEG tracing 60 minutes after 2.0 mm TBI. **D**. Time course of EEG root mean square (RMS) amplitude changes following a 2.0 mm TBI in an individual mouse. **E**. Change in EEG amplitude over the 24-hour period following sham (n = 6) or 2.0 mm TBI (n = 11) (p = 0.0182, two-tailed Mann-Whitney U-test).

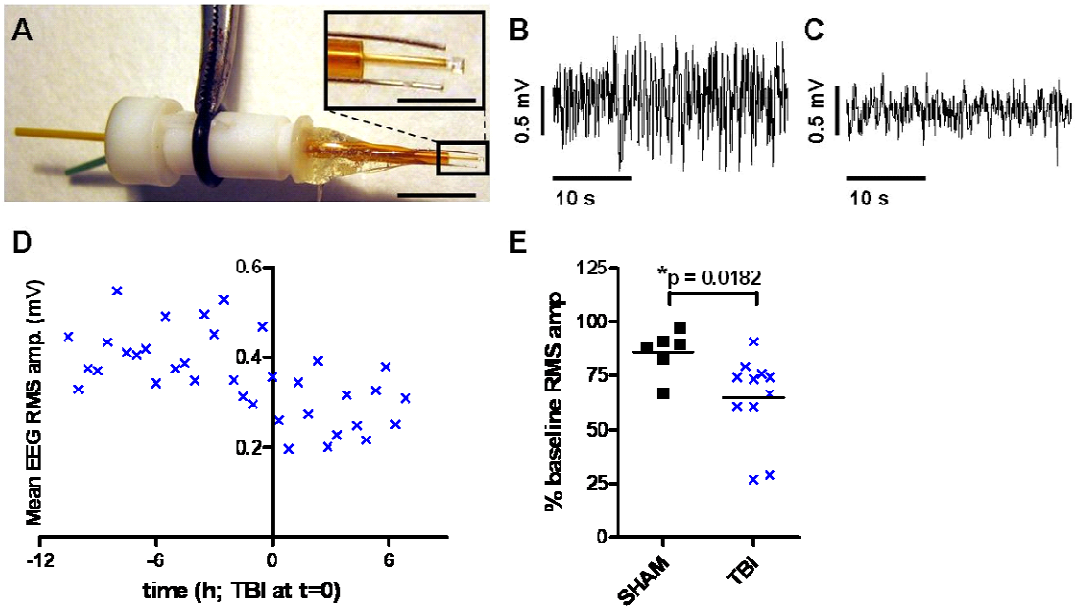

DISCUSSION

In both wild-type and young PDAPP$^{+/-}$ mice without Aβ plaque deposition, we found that ISF Aβ levels in the ipsilateral hippocampus were immediately reduced after experimental traumatic brain injury and remained low over the next 24 hours. Further, we measured a similar reduction of $A\beta_{1-x}$ and $A\beta_{40}$ in the PBS-soluble tissue extracts of ipsilateral hippocampus in injured PDAPP mice compared to sham-injured animals 2 hours after injury. We found no significant differences in APP levels in RIPA-soluble tissue extracts, indicating that changes in post-injury levels of $A\beta_{1-x}$ are not likely due to

acute reductions in APP. Immunohistochemistry revealed no intracellular or extracellular accumulations of Aβ. There were no significant changes in hippocampal carbonate or guanidine-soluble extract Aβ levels. This indicates that reductions in the hippocampal ISF and PBS-soluble tissue extract levels were not due to acute aggregation or deposition of Aβ. Finally, we measured a significant post-injury reduction in local EEG activity over 24 hours. Taken with our observed reductions in both ISF Aβ and Aβ in tissue extracts, our finding is consistent with earlier reports that extracellular Aβ levels are correlated with neuronal activity.

Previous studies that combined experimental TBI with pre- and post injury microdialysis have been performed in rats. Our study extends this approach to mice, broadening the scope of possible microdialysis assessments to include a wide variety of transgenic animals.

These experimental results complement the findings from recent clinical microdialysis studies of Aβ dynamics in human brain injury patients (Brody, Magnoni et al., 2008; Marklund et al., 2009) in three ways: first, pre-injury Aβ levels were measured prior to experimental TBI. This baseline measurement allowed us to clearly determine that ISF Aβ levels were reduced following injury. Second, Aβ levels were measured at very early times following injury, and these were also found to be immediately decreased within the first 90 minutes of TBI. In human patients, microdialysis catheters were typically placed 12-24 hours after injury, thus very early Aβ measurements were not possible. Third, Aβ levels in tissue compartments other than the ISF pool sampled by microdialysis were assessed in comparably injured animals. Levels of Aβ in

hippocampal PBS-soluble extracts were also found to be decreased at the 2-hour timepoint, but there were no changes in the hippocampal carbonate or guanidine-soluble extracts. Extrapolating these results to previous human studies, we suggest that post-injury extracellular Aβ levels are likely immediately decreased following TBI and then increase or decrease further in parallel with recovery or deterioration of neurological status in patients with acute brain injury.

What is the underlying cause for the trends in ISF Aβ dynamics described here? It has previously been demonstrated *in vitro* as well as *in vivo* that neuronal activity, and more specifically, synaptically coupled endocytic activity, is directly correlated with Aβ release (Cirrito, et al., 2008, Cirrito, et al., 2005, Kamenetz, et al., 2003). During the 24-hour period after 2.0 mm CCI-TBI, there was a significant reduction in EEG activity. However, this observation does not prove a causative link between neuronal activity and ISF Aβ in the setting of brain injury. The changes in the two measures might both be caused by a common post-insult factor, such as neuronal cell death. Future studies to test hypotheses regarding these mechanisms will be required to address the role of neuronal and synaptic activity as it relates to Aβ levels in the context of TBI.

Caveats associated with extrapolation from transgenic mouse models to human patients warrant consideration here. The mechanics of experimental TBI in rodents are different from those in human TBI patients. In contrast, some experimental TBI models in pigs are biomechanically more similar to human TBI (Smith, et al., 1999). Microdialysis measurements of other analytes have been performed in conjunction with TBI in pigs (Alessandri, et al., 2003), but Aβ has not yet been measured. Extension of

these methods to pigs could significantly advance current experimental understanding of Aβ dynamics following TBI.

The PDAPP mouse overexpresses a rare form of human APP, the V717F mutation, and this may affect Aβ dynamics. However, the similarity of post-injury Aβ dynamics in wild-type and transgenic mice indicates that the observed decrease is not unique to transcriptional control under the PDGF promoter used in the PDAPP mice, nor does it depend on absolute levels of the peptide or the specific assay used to measure Aβ.

Our experimental approach is not without limitations. First, the pool of Aβ in interstitial fluid is but one of many in the living brain. Our longitudinal microdialysis measurements were limited to the interstitial space. Second, levels of ISF Aβ are lower in PDAPP mice as compared to some other hAPP models, such as the Tg2576 mouse (Cirrito et al., 2005; Kang et al., 2007; Cirrito et al., 2008; Kang et al., 2009; and our unpublished results). Measurement of reduced ISF Aβ levels was bounded by the sensitivity of our ELISA assay. Future experiments using other lines of transgenic mice with higher ISF Aβ levels could increase time resolution and allow more detailed assessment of underlying mechanisms. Third, we were restricted to the first 24 hours after injury for microdialysis monitoring due to the apparent inconsistent probe function at later times.

Our findings fit well with a previous study that described a marked decrease in amyloid plaque burden in older PDAPP mice at 5 and 8 months after injury (Nakagawa, et al., 1999). We therefore suggest that reduced extracellular concentrations of Aβ after TBI resulted in diminished deposition at chronic timepoints in this mouse model.

However, our results differ from other descriptions of post-injury Aβ dynamics in tissue homogenates (Abrahamson, et al., 2006, Loane, et al., 2009, Smith, et al., 1998). Methodological differences preclude a direct comparison of our findings with these studies.

In conclusion, further studies of both experimental models and human TBI patients will be required to address these mechanisms underlying the observed Aβ dynamics. This mouse model demonstrates the potential experimental approaches to complement human microdialysis measurements.

Acknowledgements: This work was supported by grants from the NIH NS049237 (D.L.B.), AG13956 (D.M.H.), a Burroughs Wellcome Career Award in the Biomedical Sciences (D.L.B.), Thrasher Research Fund (D.L.B.), and Cure Alzheimer's Fund (D.M.H.). We are grateful to Eli Lilly and Co. for providing antibodies and the founders of our PDAPP mouse colony.

Chapter 6.

Synaptosomes to examine post-TBI localization of Aβ

Serial tissue extractions reveal decrease or trend to decrease at 2h

Based on the results from serial tissue extractions, hippocampal Aβ was significantly decreased in the PBS-soluble fraction, and trended towards decrease in the carbonate and guanidine fractions. Likewise, there was a significant decrease in ISF Aβ levels by microdialysis. It seemed to us that this selective decrease in extracellular and highly soluble compartments might be in part due to reduced synaptic activity, and subsequently, decreased release of the peptide into the extracellular space.

Other mechanisms: decreased production and/or increased clearance?

Because the carbonate and guanidine fractions trended towards decrease, suggesting an overall decrease in soluble and insoluble Aβ tissue content, it was also possible that decreased enzymatic production might contribute to our measurements. We did not detect a change in protein levels of APP at early timepoints, so we did not suspect decreased precursor proteins contributed to our measurements. However, failed APP transport to its sites of cleavage by β and γ-secretases, or impaired enzymatic activities themselves might lead to an overall decrease in Aβ tissue levels. We did not rule out increased clearance from the ISF as a contributing factor. Other experiments to address these possibilities were initiated and will be presented in the next chapter.

Disrupted synaptic homeostasis post-TBI

Previous studies had established a very early failure of synaptic homeostasis after CCI in rats (Sullivan, et al., 1998). To isolate the nerve terminals, the authors prepared

synaptosomes from ipsilateral and contralateral hemispheres of CCI-injured animals. As compared to the contralateral hemisphere, they measured reduced ATP levels within 30 minutes after injury with a significant increase in lipid peroxidation (Sullivan, et al., 1998). ATP is required for endocytosis at the synapse (Heidelberger, 2001), and lipid peroxidation impairs synaptic membrane functions (Braughler, 1985, Cohadon, 1984).

We hypothesized that disruption in homeostatic release and uptake of Aβ at the synapse might be one mechanism by which ISF Aβ levels are decreased in microdialysis measurements. In a complementary fashion, the synaptic compartment might have increased levels.

Previous studies of Aβ measurement in synaptosomes

It was unknown whether we would be able to measure Aβ in a synaptic location. Earlier studies had detected Aβ at the synapse in aged Tg2576 mice using gold-labeled immunogold electron microscopy (EM) (Takahashi, et al., 2008). This suggested that Aβ accumulates in a synaptic location and can be detected. Two recent reports describe a crude synaptosome preparation in conjunction with flow cytometry to quantify the Aβ, tau, and cholesterol content at the synapses of human brain tissue in AD and control cases (Fein, et al., 2008, Gylys, et al., 2007). These studies suggested to us that it was possible to detect Aβ in such a preparation if it were present. We wanted to explicitly test the notion that Aβ might be retained in a synaptic location after experimental TBI and chose a synaptosome preparation for our model system.

Synaptosomes: theory and technique

Synaptosome preparation was first described in the neuroscience literature by Hebb and Whittaker (Hebb and Whittaker, 1958) and employed in many studies, particularly involving neurotransmitter distribution and function, during the following decades (Whittaker, 1993). Essentially, these structures are detached, sealed presynaptic terminals. A portion of the target cell, such as a dendritic spine, can adhere to the synaptosome surface (Fig. 39).

Figure 39. Theoretical and actual structures of synaptosomes. Left, schematic from Gylys et al., 2004. Nerve terminals and axonal processes are sheared from axonal attachments and resealed. Right, a synaptosome imaged by transmission electron microscopy. Presynaptic terminal contains vesicles; closely apposed to the post-synaptic density. Electron micrograph by Marilyn Levy, Washington University Histology Core.

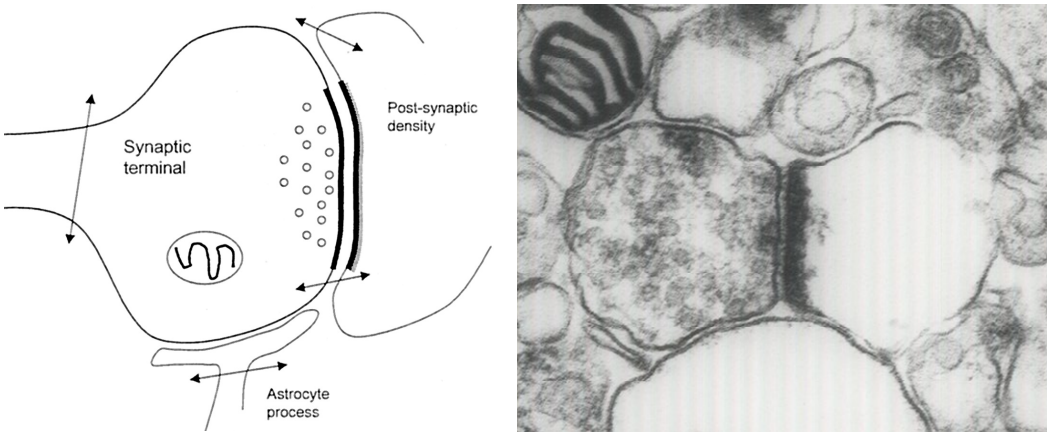

It has been shown that these structures can be prepared from a variety of neural tissues, including spinal cord, retina, sympathetic ganglia, myenteric plexus and electric organs (Whittaker, 1993). These structures have also been shown to respire, take up oxygen and glucose, release Na^+, take up K^+, maintain a normal membrane potential and, release neurotransmitter in a Ca^{2+}-dependent manner.

Crude preparation

In the first versions of the protocol, brains or brain regions are extracted immediately following decapitation. The tissue is coarsely chopped using a blade and placed in a glass vial. Using a strategy the originally termed "osmotic shock," a 0.32M hypertonic sucrose solution is added at various steps and washings to preserve cell membrane integrity. Then, a glass pestle, also called the dounce-homogenizer, is driven up and down to smear the tissue against the glass vial. This action shears nerve terminals from their axons. When these membranes reseal, synaptosomes are created. The remaining steps isolate and purify these structures from the rest of the tissue.

Ultracentrifugation across a sucrose gradient

Isolation of synaptosomes is achieved by gradient fractionation. The original versions utilize ultra-high speed centrifugation across a sucrose-based gradient. The main disadvantages of this technique are the amount of mechanical disruption during resuspension, and the fact that it often takes over 4-5 hours to complete all the steps. Traditional procedures often lead to a loss of functional integrity and low yields (De Robertis, et al., 1961, Fleming, et al., 1980, Gray and Whittaker, 1962). We were also concerned about the fundamental fragility of CCI-injured tissue. One way for reseachers to decrease the amount of time and manipulation is to simply use the crude mitochondrial fractions (P2) for their functional experiments, rather than to risk damage during the purification by fractionation of the pellet. In this way they can avoid hypertonic conditions and ultracentrifugation. The entire length of preparation is also reduced to 30-

40 minutes total. However, the P2 fraction is contaminated with myelin and extrasynaptosomal mitochondria, and these elements can interfere with biological assays (Dodd, et al., 1981).

High-speed centrifugation across a Percoll gradient

For these reasons, we chose an abbreviated procedure that eliminates the need for ultracentrifugation by substituting Percoll for sucrose in the discontinuous gradient. The methods were first described for isolation of white and red blood cells (Gutierrez, et al., 1979, Kurnick, et al., 1979, Rennie, et al., 1979, Ulmer and Flad, 1979). The use of Percoll gradients to isolate synaptosomes was first described in 1986 (Dunkley, et al., 1986), modified to an even shorter protocol in 1988 (Dunkley, et al., 1988, Harrison, et al., 1988) and published in full detail in 2008 (Dunkley, et al., 2008).

Percoll is a slurry of synthetic polyvinyl, pyrrolidone-coated silica particles of a uniform 17 nm diameter. A major advantage of Percoll over other gradients, such as sucrose and Ficoll, is its low viscosity. As a result, sedimentation occurs more rapidly at lower centrifugal forces using Percoll. In addition to blood elements, Percoll gradients have been used to isolate many other types of cells and subcellular organelles (Pertoft, 2000).

Dunkley et al. first applied this rapid Percoll gradient to isolate functional synaptosomes (Dunkley, et al., 1986). The crude P2 pellet was applied to a 4-layer discontinuous gradient and centrifuged for 5 minutes at 32,500 g, excluding acceleration and deceleration times. Fractions were collected at the interfaces between different

layers and were each resuspended to dilute Percoll contaminant, and concentrated by centrifugation at 15,000 g. Functional viability was tested by uptake assays for calcium, phosphate, and noradrenaline; and by the effects of depolarization on metabolism, calcium uptake, and protein phosphorylation. The purity of the synaptosomal content of each of the fractions was assessed by electron microscopy.

Soon after the first report, this same group modified the procedure slightly to apply the first supernatant, S1, directly to the Percoll gradient, instead of a second centrifugation step (Dunkley, et al., 1988, Harrison, et al., 1988). This both reduced the total time of the procedure and the possible mechanical damage resulting from resuspension. These methods were published in explicit detail in a more recent paper, which provided us the protocol for preparation of synaptosomes from CCI-injured brain (Dunkley, et al., 2008). The exact protocol used in the experiments described in this chapter is detailed in the Appendix 3 (Synaptosomes: materials and protocol).

Initial verification of the discontinuous Percoll gradient: colored layers

Upon the recommendation and instruction by a committee member, Dr. Timothy Miller, we first verified that our Percoll gradient was "clean" and that we could create separate layers by the use of food coloring. This was an important control. Without good technique to create separate layers, we would be unable to separate different fractions and therefore unable to isolate synaptosomes (Fig. 40).

Figure 40. Discontinuous Percoll gradient. Each layer, beginning with 23%, was carefully hand-poured using a 1-mL transfer pipette for 2 mL each in a 12 mL Sorvall polycarbonate centrifuge tube. Layer interfaces are marked with black Sharpie on the outside of the tube. Food coloring added prior to pouring indicates various concentrations of Percoll in each layer. With kind assistance from Tim Miller, MD, PhD.

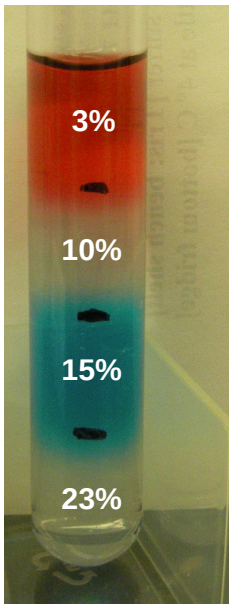

Once it was clear that we could prepare a consistent discontinuous gradient, we then attempted to separate fractions prepared from whole brain. Eventually, we would use isolated, ipsilateral hippocampi, one per gradient. Because an ipsilateral hippocampus was often less than 10% by weight of the total brain, we wanted to confirm our techniques with whole brain before moving on to a more challenging tissue.

Briefly, wild-type mice were deeply anesthetized and their brains were quickly perfused with 10 mL of homogenization buffer by transcardial perfusion using a large bore syringe (18-gauge needle). The skull was opened, brain removed and coarsely chopped into smaller pieces with a sharp #10 Exacto blade. Cerebellum and brain stem were not included in the homogenization. These pieces were suspended in 3 mL of homogenization buffer and dounce-homogenized in a 15 mL Teflon Wheaton

homogenization vial. We used a total of 10 up-and-down strokes, making sure that no gross particles of brain tissue remained. This solution was spun down briefly at a low speed (1000 g) to remove gross matter and large nuclei. The supernatant from this fraction, S1, contains synaptosomes, subcellular organelles and isolated membranes. This supernatant is fractionated by the Percoll gradient. Depending on the protein concentration, the supernatant was sometimes diluted for optimal centrifugation. A volume of 2 mL of the S1 supernatant was loaded on top of the gradient prior to the high-speed spin, shown on the left in Figure 41. The centrifuge tubes were spun down in a Sorvall SS34 rotor at 20,000 g, resulting in the fractionation of different sizes of subcellular organelles and membranes, as depicted in Figure 41 (right). The fractions enriched in synaptosomes are Fraction 4 (most pure) and Fraction 3 (less pure, but more abundant).

Figure 41. Discontinuous Percoll gradient before and after high-speed centrifugation. Left, loaded with 2 mL S1 supernatant just prior to 5 minute high-speed centrifugation at 20,000 g. Right, after high-speed centrifugation. Fractionation of S1 occurs at layer interfaces, marked here on the tube with black Sharpie. Fractions 2, 3, and 4 are indicated (F2, F3, F4, respectively).

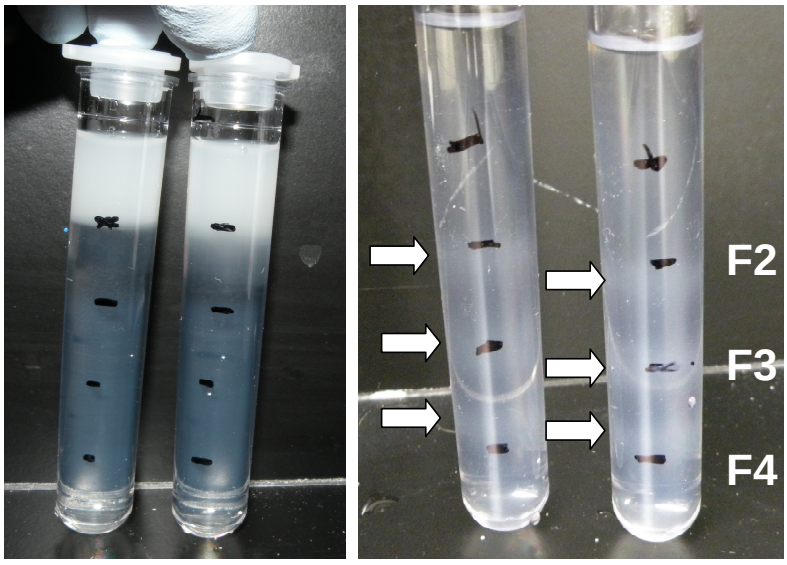

Finally, we removed each fraction by careful pipetting with a long-bore pipette tip, first removing Fraction 3, then Fraction 4 (Fig. 42).

Figure 42. Sequential removal of fraction 3 (left) and fraction 4 (right).

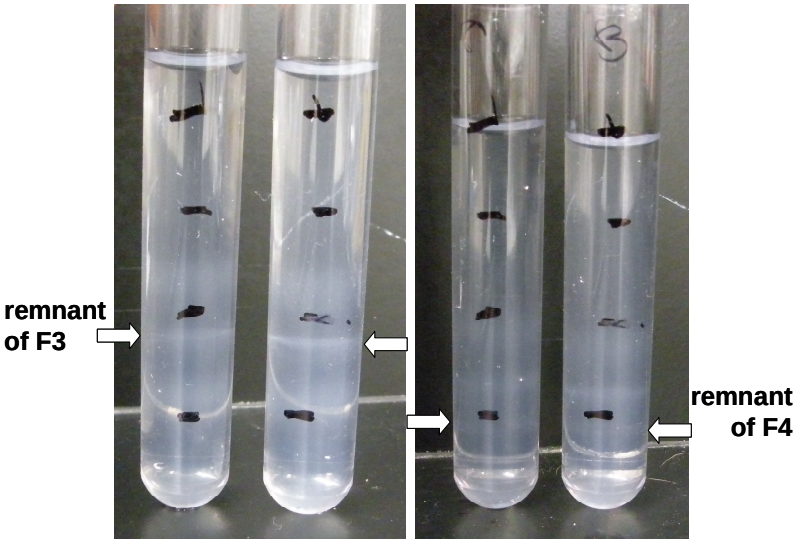

Synaptosomes prepared from mouse brain: verification by electron microscopy

Because the previous protocols used transmission electron microscopy (TEM) to verify the morphology and concentration of synaptosomes in each of the resultant fractions, along with any contamination, we wanted to compare our fractions to validate the similarity of our technique (Dunkley, et al., 1988, Dunkley, et al., 1986, Dunkley, et al., 2008, Harrison, et al., 1988). To do this, we enlisted the help of Marilyn Levy at the Washington University Histology Core. As a specialist in the technique of TEM, she was able to recommend the best method for preparing and fixing our fractions. Briefly, we spun down the fractions at low speed into a pellet, gently washed the pellet with 0.9% NaCl, and resuspended the pellet in ice-cold, 2.5% gluteraldehyde in PBS. These fixed pellets were then embedded in plastic, sliced, and stained with osmium tetroxide. We examined these slices using the electron microscope, and were able to validate our technique against published results in a qualitative fashion. Below are images we took of fractions 3 and 4, separately, at different magnifications (Figs. 43-45).

Figure 43. Fractions 3 (left) and 4 (right) at 7X power. Scale bars as marked.

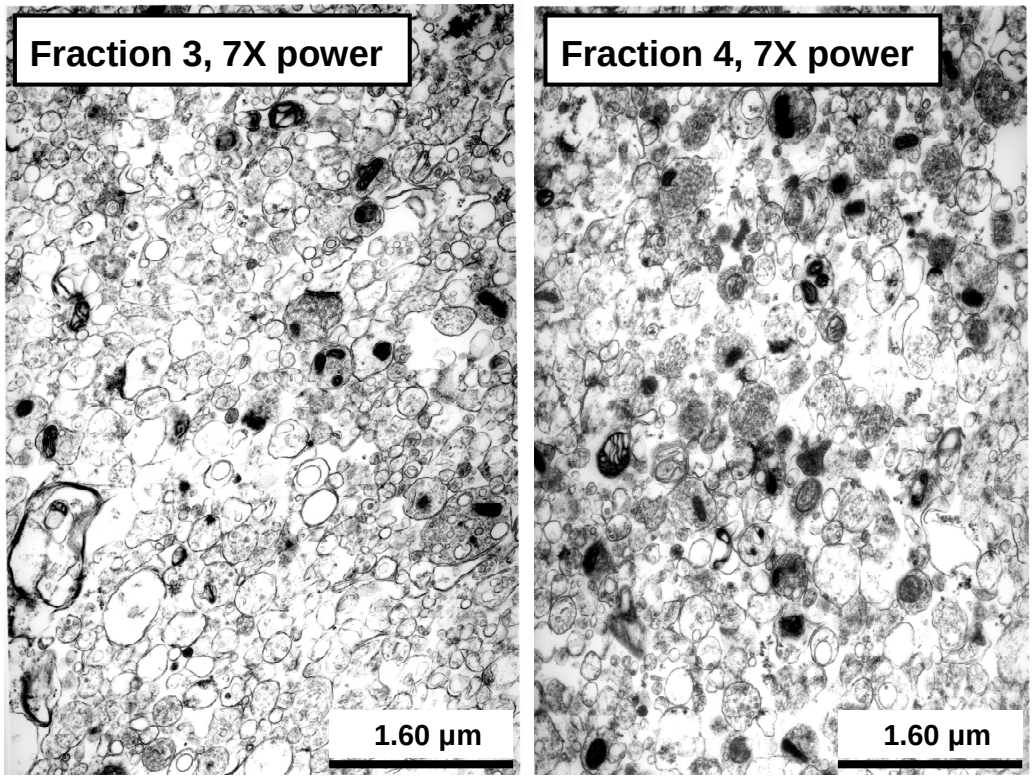

Figure 44. Fraction 3 at 12X (left) and 20X power. Scale bars as marked.

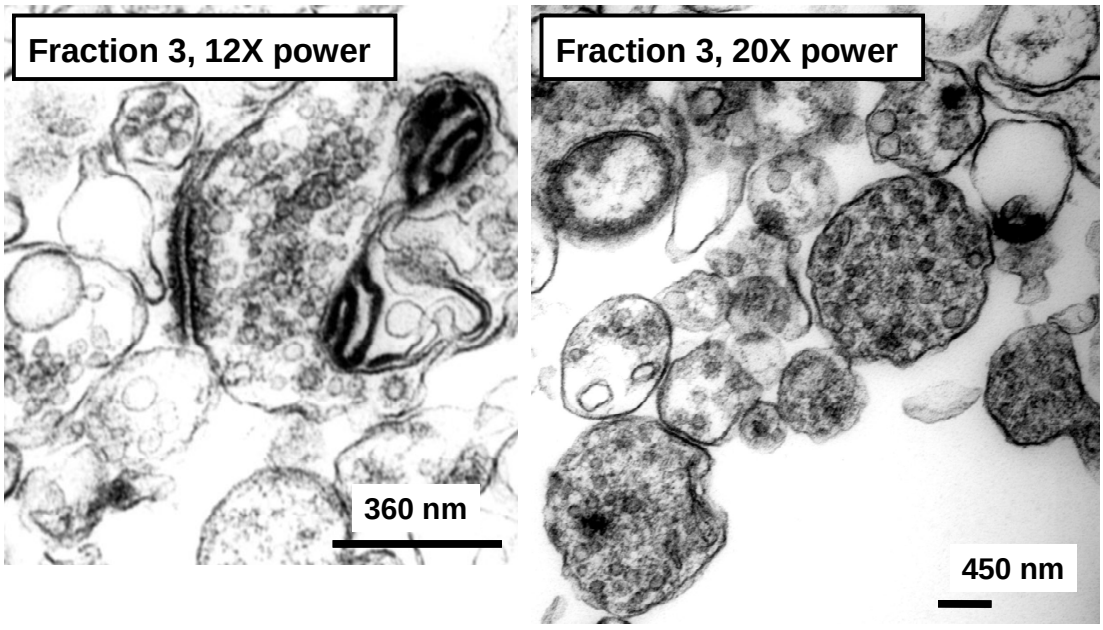

Figure 45. Fraction 3 at 20X power. Scale bars as marked.

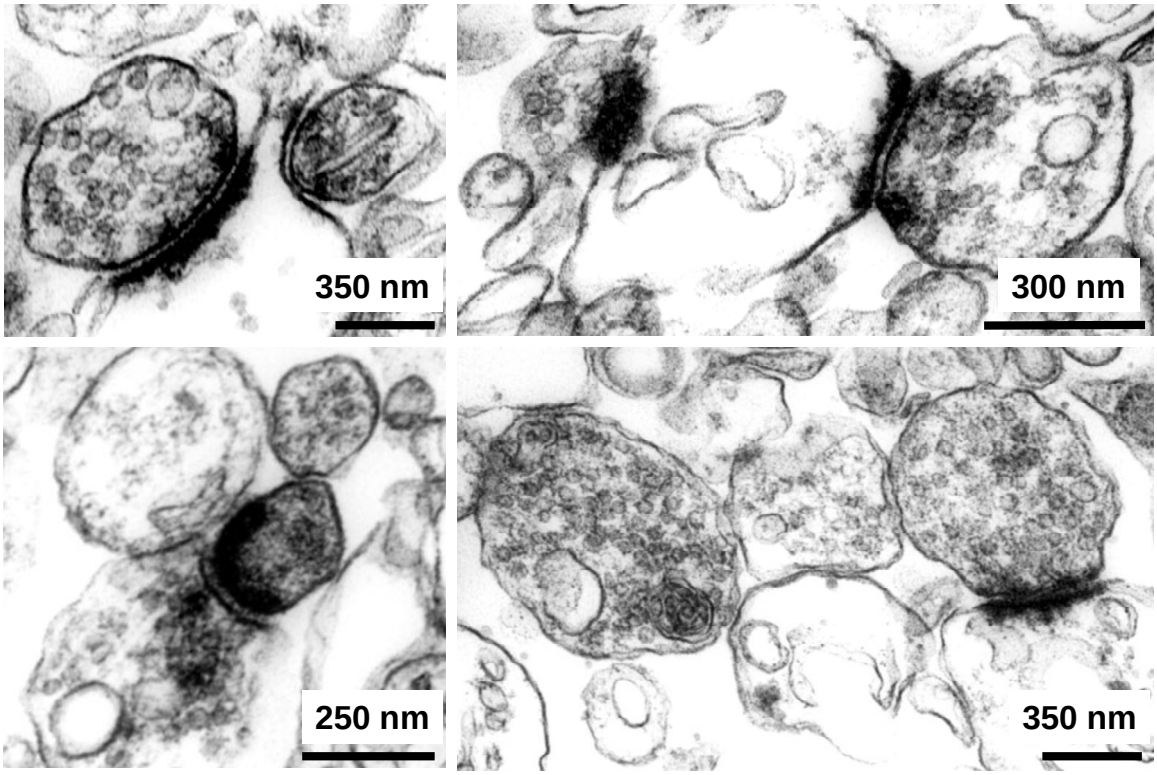

By a qualitative assessment, we determined that our homogenization, fractionation, and purification protocol yielded morphological synaptosomes, with the greatest proportion in Fraction 3. Because we were ultimately going to measure Aβ content in a single, ipsilateral hippocampus, we decided to combine Fractions 3 and 4 for the greatest possible yield based on these electron micrographs.

Preparation of synaptosomes from single hippocampus

Having shown that we could prepare synaptosomes from whole brain, we now wanted to know whether we could prepare them from a single ipsilateral hippocampus (both sham and injured). In this experiment, we perfused mice and extracted the brains

as before, except we dissected and isolated each side (left and right) of the hippocampus. Notably, these tissues were much smaller than the whole brain. The coarse chopping step became very brief as there was little tissue to parse. We also substituted a smaller dounce-homogenizer (5 mL) for the 15 mL vial used to homogenize the whole brain. After spinning the crude homogenate at 1000 g, we were able to pellet out gross matter and derive an S1 supernatant for fractionation (Fig. 46).

Figure 46. S1 supernatant prepared from single hippocampus, left and right. Pellet is seen at the base of the each tube.

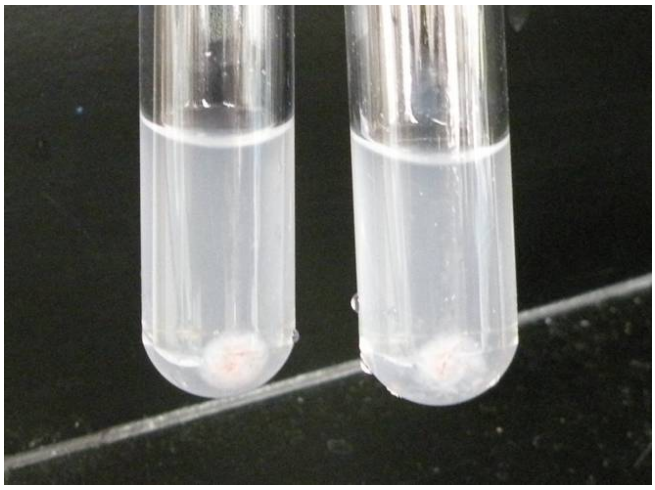

Fractionation with this supernatant was possible, albeit at low yield.

Next, we wanted to demonstrate that Fractions 3 and 4 were enriched for synaptosomes. To do this, we chose a highly conserved presynaptic marker, SV2 (Bindra, et al., 1993, Feany, et al., 1992). Using a Western blot, we compared SV2 content in S1, the original supernatant, with combined fractions 3 and 4 for each single hippocampus. For a positive control, we used a RIPA-extract whole brain homogenate (Fig. 47). In the same blot, using a strip-reprobe method, we looked at the APP content (Fig. 48).

Figure 47. SV2 protein in S1 as compared to combined fractions 3 and 4. "A" and "B" represent left and right sides of a hippocampus. Enrichment of SV2 in fractions 3 and 4 suggests the enrichment for presynaptic terminals, as compared with crude homogenate. Positive control, RIPA-extract from whole brain of a PDAPP mouse. All lanes were loaded with 10 ug of total protein.

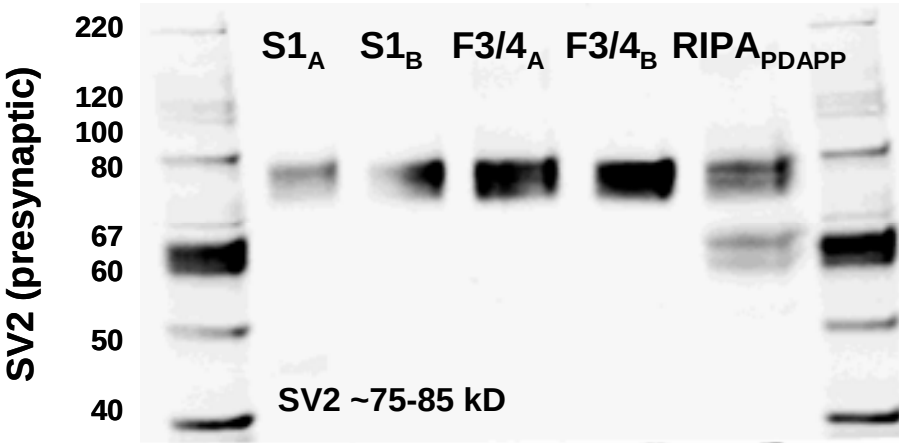

Figure 48. APP in S1 as compared to combined fractions 3 and 4. APP is present in both crude homogenate supernatant S1 and in the synaptosome-enriched fractions. Positive control, RIPA-extract of whole brain from a PDAPP mouse. All lanes were loaded with 10 ug of total protein.

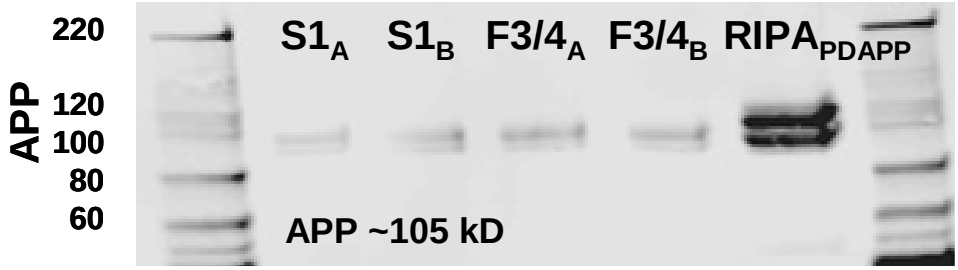

Having shown now that our fractions were enriched for synaptic structures, we wanted to test the hypothesis that Aβ might be retained within a synaptic terminal in injured tissue rather than be released into the extracellular space. Again, this was a proposed mechanism for the observed reduction in the ISF Aβ levels in the ipsilateral hippocampus immediately after a 2.0 mm CCI injury.

To test this hypothesis, we performed either a sham or 2.0 mm CCI injury on young, pre-plaque PDAPP mice. Mice were allowed to recover for 2 hours, then quickly perfused. Synaptosomes were prepared as described in Appendix 3 from ipsilateral and contralateral sides of the hippocampus. The purified suspensions were subject to either of two conditions. In the first, synaptosomes were simply diluted in standard Aβ ELISA buffer, without guanidine, as described in Chapter 5 and loaded onto ELISA plates for measurement of $A\beta_{x\text{-}40}$ and $A\beta_{1\text{-}42}$. Secondly, we hypothesized that if indeed Aβ were retained within a membrane-bound presynaptic terminal such as a synaptosome, the lysis of such a structure might liberate total intra-synaptic content. To do this, we treated synaptosomes for 10 minutes in the same carbonate buffer at pH 11 that was used in the serial extractions as described in Chapter 5. We chose a volume that was approximately half that of the total volume required for triplicate measurement on the ELISA. After the short incubation, we completed the volume with standard Aβ ELISA buffer and loaded the samples onto coated plates for measurement of $A\beta_{x\text{-}40}$ and $A\beta_{1\text{-}42}$. Finally, we measured the protein content of each sample prior to loading on the ELISA plates so all values could be normalized to protein content.

The results of those measurements are reported below for synaptosomes diluted in ELISA buffer only (Fig. 49) and in carbonate buffer pH 11 first, then ELISA buffer (Fig. 50). Firstly, there were no significant differences for either condition between the levels of $A\beta_{x\text{-}40}$ and $A\beta_{1\text{-}42}$ in synaptosomes prepared from sham and injured animals, either in the ipsilateral or the contralateral sides of the hippocampus. However, the carbonate buffer-treated synaptosomes yielded Aβ levels that were approximately tenfold increased

as compared to the ELISA buffer-only preparation, suggesting that indeed most of the Aβ is inside these structures and requires the lysis of membranes for detection of Aβ from the presynaptic terminal.

Figure 49. Aβ content, normalized to total protein levels, in synaptosomes resuspended in ELISA buffer only. $A\beta_{x\text{-}40}$ and $A\beta_{1\text{-}42}$ measured separately for each animal, for ipsilateral and contralateral sides of the hippocampus (top two panels) and added for an estimate of total Aβ (bottom panel). No significant differences between sham and TBI animals in either isoform, nor when added together.

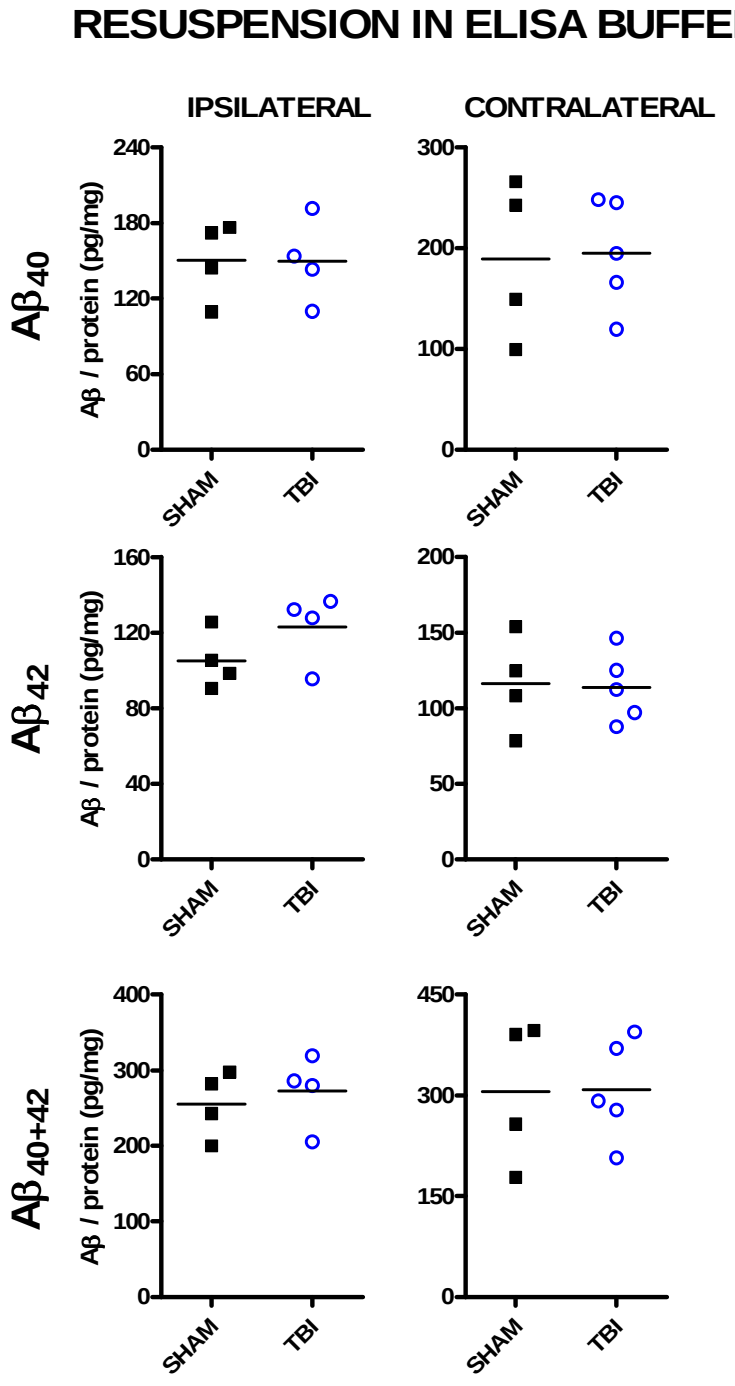

Figure 50. Aβ content, normalized to total protein levels, in synaptosomes incubated in ½ volume of carbonate buffer pH 11 before completing with ½ volume of ELISA buffer. $A\beta_{x\text{-}40}$ and $A\beta_{1\text{-}42}$ measured separately for each animal, for ipsilateral and contralateral sides of the hippocampus (top two panels) and added for an estimate of total Aβ (bottom panel). No significant differences between sham and TBI animals in either isoform, nor when added together.

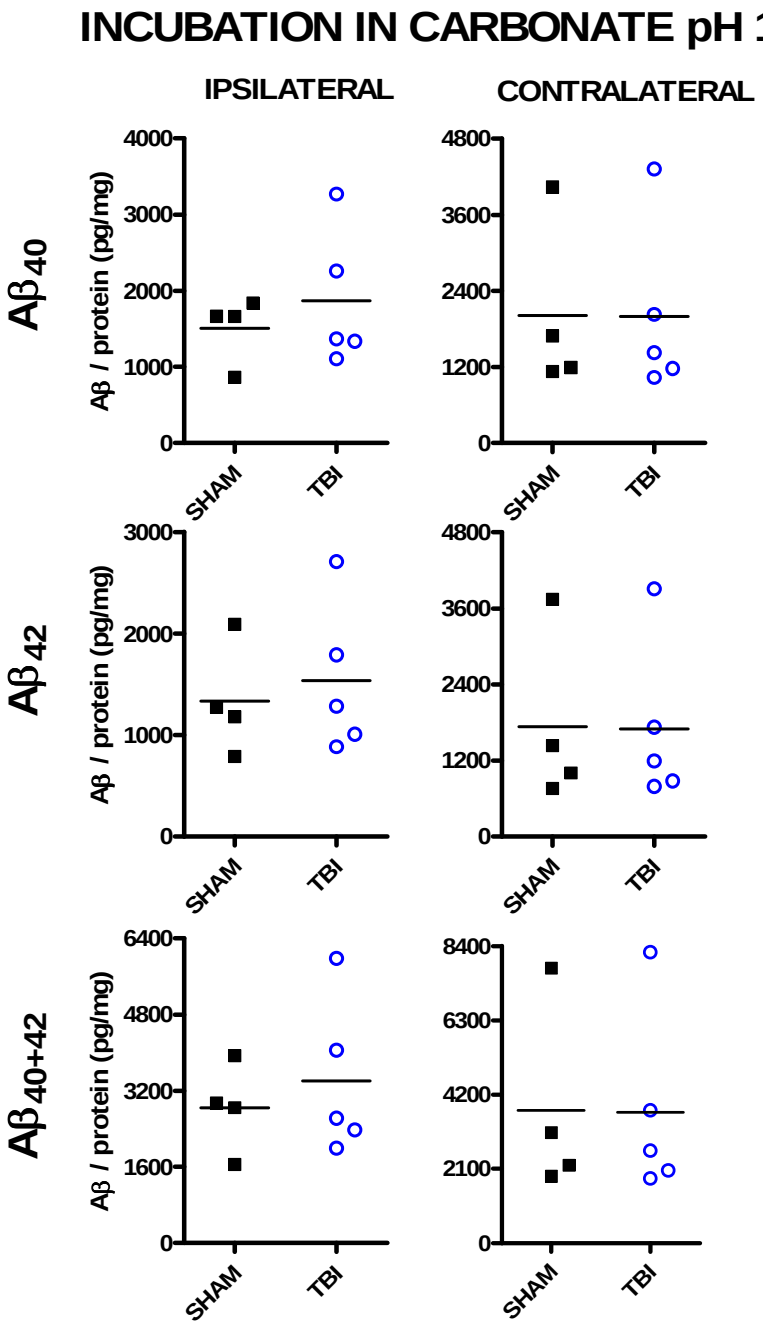

Finally, we repeated this experiment in a separate group of mice and pooled the results of the first and second experiments. Shown in Figure 51 are the results for $A\beta_{40}$ in carbonate-treated synaptosomes from ipsilateral and contralateral sides of the hippocampus. Again, no significant differences were seen, although there might be a trend towards increased $A\beta_{40}$ in synaptosomes prepared from the injured hippocampus.

Figure 51. Aβ content, normalized to total protein levels, in synaptosomes incubated in ½ volume of carbonate buffer pH 11 before completing with ½ volume of ELISA buffer. $A\beta_{x\text{-}40}$ measured in ipsilateral and contralateral sides of the hippocampus of each animal. Results of two experiments have been pooled here, one performed in April and one in June 2009. No significant differences between sham and TBI groups, although a possible trend towards increased $A\beta_{x\text{-}40}$ in the injured ipsilateral hippocampus.

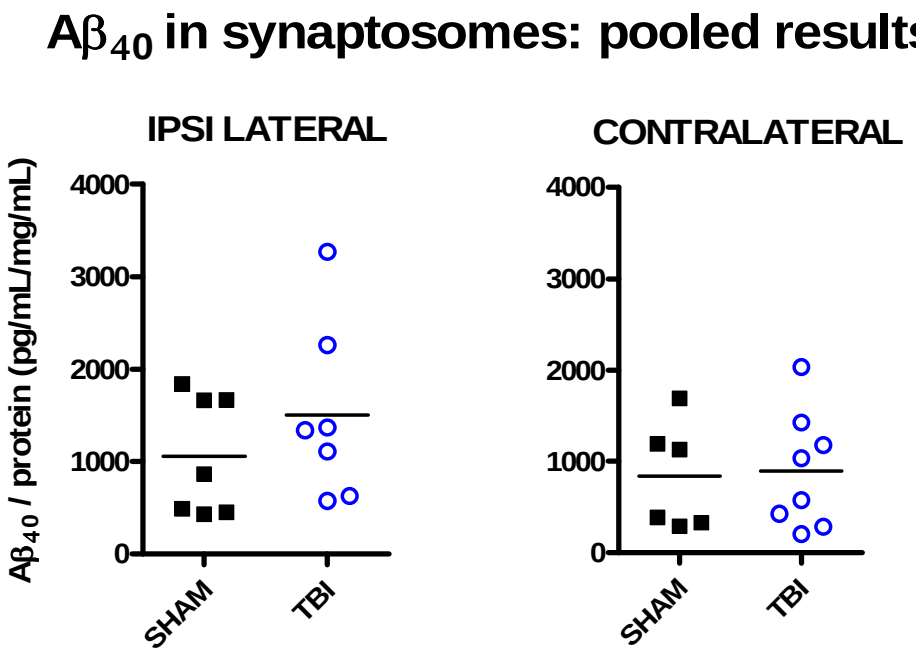

We also attempted to measure APP in the fractions by ELISA, guided by the hypothesis that if Aβ were increased in this compartment, it might be due to a proportional increase

in APP. An ELISA kit from R & D Systems allowed quantification of APP. We began by comparing the S1 supernatant with combined fractions 3-4 (Fig. 52):

Figure 52. APP content in synaptosomes incubated in RIPA-extracted synaptosomes and diluted in standard Aβ ELISA buffer. APP measured in S1 supernatant and synaptosomal F3-F4 fractions from naïve hippocampi. A trend towards enrichment for APP in F3-F4 as compared to S1, but levels are not significantly different.

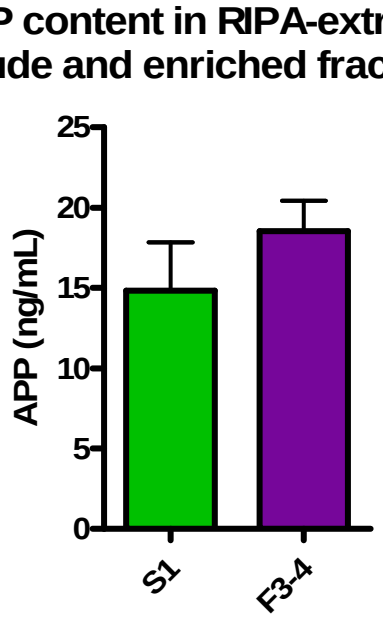

In conclusion, while our efforts to prepare synaptosomes from single hippocampi were successful, the results of this experiment suggest that there are no significant differences in synaptosomal Aβ levels at the 2h timepoint between sham and TBI groups. The conclusions that can be drawn from this result are less clear. Because the synaptosome is an artificial, prepared structure, it may not be representative of synaptic terminals *in vivo*. Membranous compartments abound in fractions 3 and 4, and it is possible that soluble Aβ may have been artificially trapped or redistributed during the homogenization procedure. To further test the hypothesis that Aβ might be retained at

the synaptic terminal, an immunogold technique might be considered as demonstrated in previous studies of aged Tg2576 mice (Takahashi, et al., 2008).

If a 2.0 mm injury was sufficient to reduce Aβ levels by ~50% and average RMS amplitude ~30% in the 24 hours following TBI, what might a less severe injury do? Others have demonstrated that 2.5 and 2.0 mm injuries produce deficits in the Morris water maze visible and hidden tasks in a B6SJL (wild-type) mouse, but 1.5 mm injury does not. We wanted to know if there was an effect on ISF Aβ dynamics and local electrical activity in less-severe injuries, and if so, was there a correlation between these two variables across different injury severities? The following chapter will address the elaboration of the original findings using a graded response approach.

Chapter 7.

Effect of injury severity on ISF Aβ, tissue levels, and activity

One way to determine how injury affects both ISF Aβ levels and neuronal activity is to compare the effects of different severities of injury (graded response). Previous studies of CCI-injured mice have used a graded-response approach for histological and behavioral measures (Brody, et al., 2007, Saatman, et al., 2006). We applied this method for the microdialysis measurement of ISF Aβ and quantification of local neuronal activity. First, we chose two lesser injury severities (1.5 and 1.0 mm) and measured ISF Aβ dynamics for each, beginning approximately 12 hours after initial implantation, and measuring the baseline period for 12 hours before injury through 24 hours following injury (Fig. 53).

The 1.0 mm impact did not produce a replicable injury in this model. Grossly, the dura was broken in some cases, but sometimes remained intact. This variable tissue response likely resulted in variable ISF Aβ levels. Because of the inhomogeneity of the 1.0 mm injury, it was excluded from further analysis of ISF Aβ dynamics.

Post-TBI dynamics of sham, 1.5 mm and 2.0 mm groups were significantly different ($p = 0.0142$, repeated measures ANOVA, group × time interaction). The means for post-TBI timepoints of injuries vs sham were significantly different ($p < 0.05$ for both sham vs. 1.5 mm and sham vs. 2.0 mm; Kruskal-Wallis test followed by Dunn's multiple comparisons test). Howevere, the dynamics of the 1.5 mm injury were not significantly different from the 2.0 mm injury ($p = 0.893$, repeated measures ANOVA) (Fig. 53).

Figure 53. Effect of different injury severities on ISF Aβ dynamics after TBI. Microdialysis measurements of ISF Aβ beginning approximately 12 hours after implantation, from 12 hours prior to injury through 24 hours post-TBI. Data shown for 4 groups: sham (n=6), 1.0 mm (n=5), 1.5 mm (n=6), and 2.0 mm (n=6).

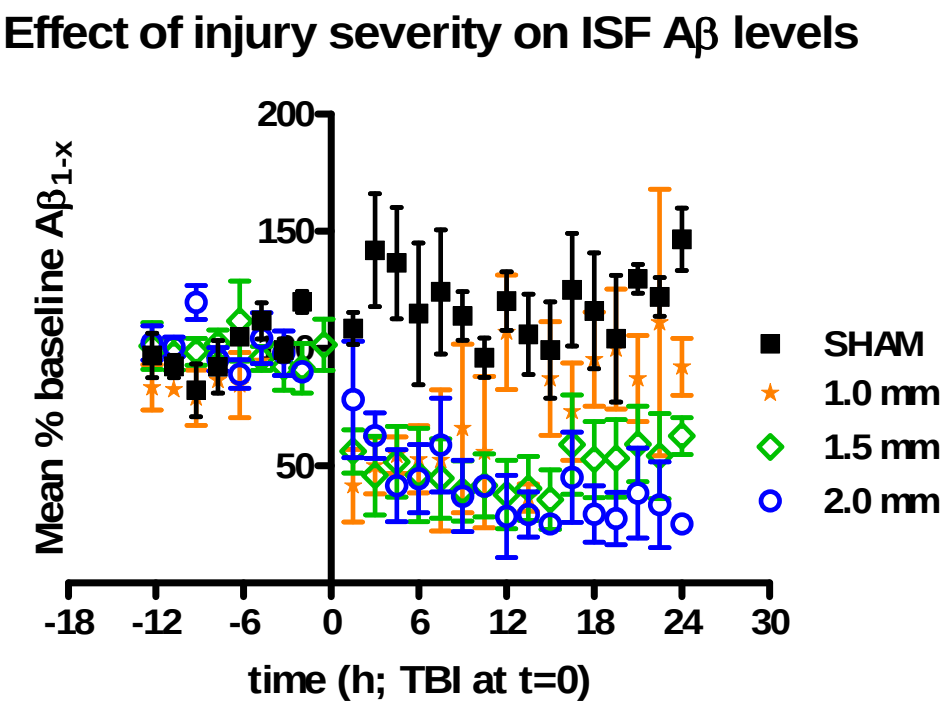

We also measured local EEG and quantified the average RMS amplitudes for each 90-minute period corresponding to a single microdialysis sample. Below are the group-averaged results for sham, 1.0, 1.5 and 2.0 mm injury severities (Fig. 54). Post-TBI dynamics of all four injury severities were significantly different ($p = 0.0272$, repeated measures ANOVA, group × time interaction).

Figure 54. Effect of different injury severities on neuronal activity after TBI. Local EEG activity as quantified by RMS amplitude, beginning approximately 12 hours after implantation, from 12 hours prior to injury through 24 hours post-TBI. Data shown for 4 groups: sham (n=5), 1.0 mm (n=5), 1.5 mm (n=5), and 2.0 mm (n=5).

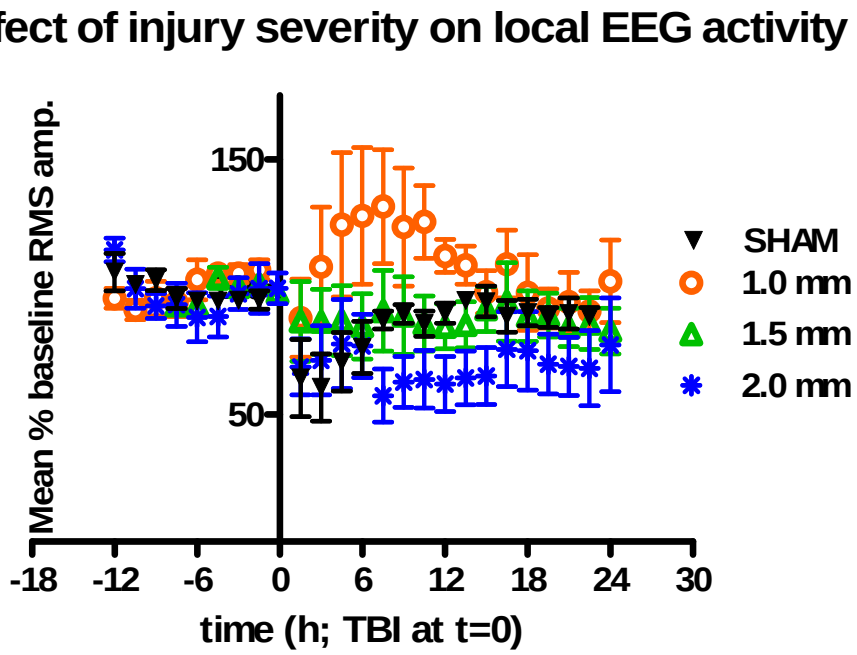

Among mice in the 1.0 mm group, the local EEG signals were highly variable. Similar to the dynamics of ISF Aβ after TBI, this variability was likely due to the variable effect of the 1.0 mm impact on the dura. Some mice demonstrated epileptiform activity in the first 6-12 hours after injury, contributing to the apparent increase in amplitude. However, after 12 hours post-TBI the EEG amplitude in this group was no different than baseline. By contrast, the 1.5 and 2.0 mm-injured groups showed significant decreases in neuronal activity by repeated measures-ANOVA that were not significantly different from one another ($p = 0.826$, group × time interaction).

To determine the relationship between these decreases in neuronal activity with ISF Aβ dynamics in the 1.5 and 2.0 mm injury groups, we plotted paired coordinates of the group means for each 90-minute sampling period. If it is generally true that reduced Aβ is associated with reduced RMS amplitude following a 1.5 or 2.0 mm impact, then we can test the strength of the hypothesized relationship by a non-parametric test, the Spearman's rank order correlation (Fig. 55). Because previous work has shown that epileptiform activity induced by high-frequency stimulation can increase ISF Aβ in the hippocampus (Cirrito, et al., 2005), it was also possible that increased activity in the 1.0 mm group in the first 12 hours post-TBI could be associated with the increased ISF Aβ levels observed in the 12-24 hour period. Based on this hypothesis, a Spearman correlation was also tested for data pooled from all four severities: sham, 1.0, 1.5, and 2.0 mm (Fig. 55A) and for non-sham injured groups only (Fig. 55B). However, due to the variable tissue response to the 1.0 mm impact, a separate analysis was performed on data from just the 1.5 and 2.0 mm injuries (Fig. 55C). Finally, because we used the 2.0 mm injury as the standard TBI in our manuscript, we computed a Spearman correlation for data from only this group as well (Fig. 55D). The timepoints began at 6 hours prior to TBI (baseline) through 24 hours post-injury, for a total of 20 coordinate pairs per injury severity.

There were significant correlations using all injury severities including sham (Fig. 55A, Spearman r = 0.3190, 95% C.I., 0.1061-0.5073; p=0.0037) and the three non-sham injuries (Fig. 55B, Spearman r = 0.4117, 95% C.I., 0.1731-0.6046; p=0.009). However, the strength of the correlation further increased when we included data from just the 1.5

and 2.0 mm injuries (Fig. 55C, Spearman r = 0.4388, 95% C.I., 0.1465-0.6606; p = 0.0037) and was the strongest for the most severe injury alone: 2.0 mm (Fig. 55D, Spearman r = 0.6506, 95% C.I., 0.2919-0.8489; p = 0.0037). Because the pooling of multiple, lesser severities yielded weaker correlations, it might be hypothesized that milder injuries including sham tend to produce more variable results, and that ISF Aβ is not well-correlated with neuronal activity in milder injury and sham. However, the correlation within just the 2.0 mm group yielded a Spearman r = 0.6506. Although this is not significantly stronger than correlations computed for pooled data due to overlap of the 95% confidence intervals, this anaylsis suggests that there may not be a linear response across injuries in terms of the relationship between ISF Aβ and local EEG activity. Specifically, more severe injuries (1.5 and 2.0 mm impacts) tended to show a better correlation of these two measures, while less severe injuries (1.0 mm and sham) did not show significant correlations between these measures. Perhaps this is because the more severe injuries have a larger range of coordinates, from baseline (100% on average) to post-TBI, which could be as low as ~40% for ISF Aβ and 60% for RMS amplitude. Figure 56 compares correlation strengths between different pools of data analyzed.

Figure 55. Correlation between change in ISF Aβ with change in RMS amplitude after TBI for different injury severities. Each point represents paired measurements of mean % baseline Aβ and mean % baseline RMS amplitude. The baseline coordinates are included, beginning 6 hours prior to injury. Data are plotted for all 90-minute periods, from -6 h to 24 h after injury for a total of 20 pairs per group. **A**, Spearman correlation for sham, 1.0, 1.5, and 2.0 mm. (r = 0.3190; two-tailed p = 0.0037). **B,** Spearman correlation for 1.0, 1.5, and 2.0 mm. (r = 0.4117; two-tailed p = 0.0009). **C,** Spearman correlation for 1.5 and 2.0 mm. (r = 0.4388; two-tailed p = 0.0037). **D,** Spearman correlation for 2.0 mm (r = 0.6506, two-tailed p = 0.0014).

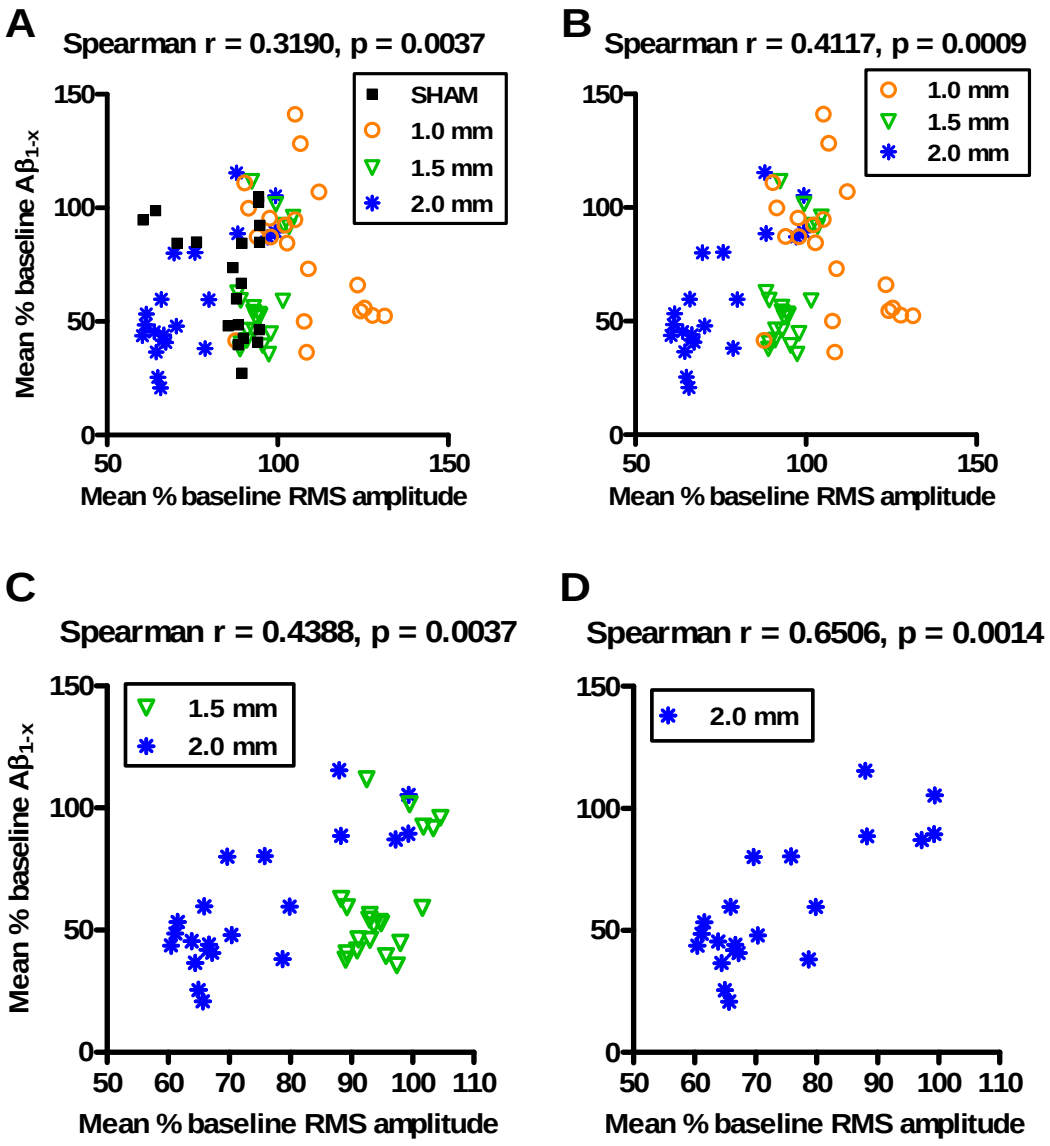

Figure 56. Correlation between change in ISF Aβ and change in RMS amplitude after TBI for different injury severities. Plot of Spearman r (correlation strength) for each pool of data analyzed in Figure 55; 95% confidence intervals are shown.

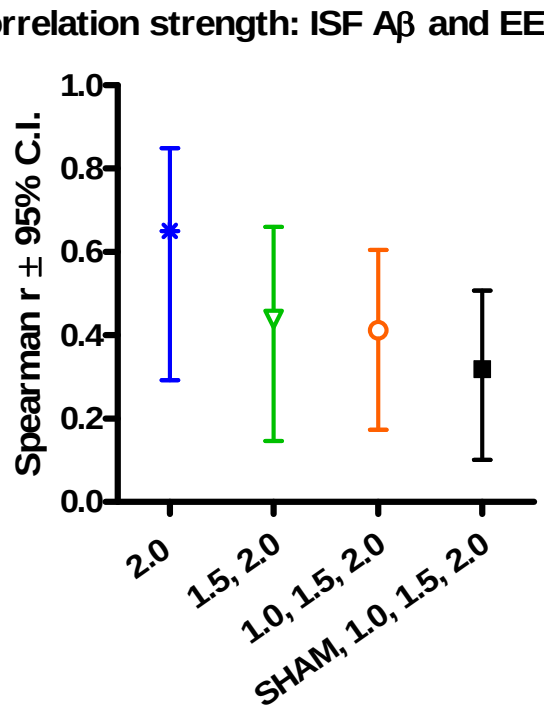

Finally, given that the 1.5 and 2.0 mm injuries yielded similar results in terms of post-TBI decreases in ISF Aβ and local EEG activity, we asked whether there were any tissue changes in the 1.5 mm group, and again whether 1.5 and 2.0 mm groups were similar. Below is a scatterplot of $A\beta_{1\text{-}x}$ levels for sham, 1.5, and 2.0 mm groups at 2h after injury in serial tissue extracts (PBS, carbonate, and guanidine) from ipsilateral hippocampus and cortex (Fig. 57). Again, data from the 1.5 mm-injured group looked much like the 2.0 mm-injured group in that there was a significant decrease in PBS-soluble hippocampus (Fig. 57A). There were no significant changes in carbonate and guanidine-soluble

hippocampal extracts, and no changes in any extracts from cortical tissues (Fig. 57B-F). In addition, $A\beta_{x-40}$ and $A\beta_{1-42}$ were also measured in all extracts (data not shown). Except for a significant decrease in $A\beta_{x-40}$ in the PBS-soluble hippocampal extract for both 1.5 mm and 2.0 mm groups, no changes were seen in individual 40 and 42 isoforms.

In summary, the 1.5 mm injury produced similar results to a 2.0 mm severity in terms of decreased ISF Aβ levels, decreased PBS-soluble hippocampal levels, and decreased neuronal activity. By contrast, the 1.0 mm injury yielded highly variable and unpredictable dynamics based on the variable tissue response to impact. There was not a clear "graded response," then, among these three severities. Future studies might use a different range, for example, a 1.25 mm and 2.5 or 2.75 mm injury, to determine whether a relationship exists between response to injury as measured by ISF Aβ dynamics, acute tissue levels, and neuronal activity.

Figure 57. Effects of 1.5 and 2.0 mm injury severities on Aβ levels in ipsilateral hippocampal and cortical homogenates. PDAPP$^{+/-}$ mice underwent sham, 1.5 mm, or 2.0 mm injury and were sacrificed after 2 hours (n=5 per group). $A\beta_{1-x}$ was measured in serial extracts, and values were normalized to total protein in each homogenate. Data plotted for individual mice in PBS (**A, D**), carbonate (**B, E**), and guanidine-soluble extracts (**C, F**). Significant differences were observed in the PBS-soluble hippocampal extract between sham and both TBI groups (p=0.0493, Kruskal-Wallis test).

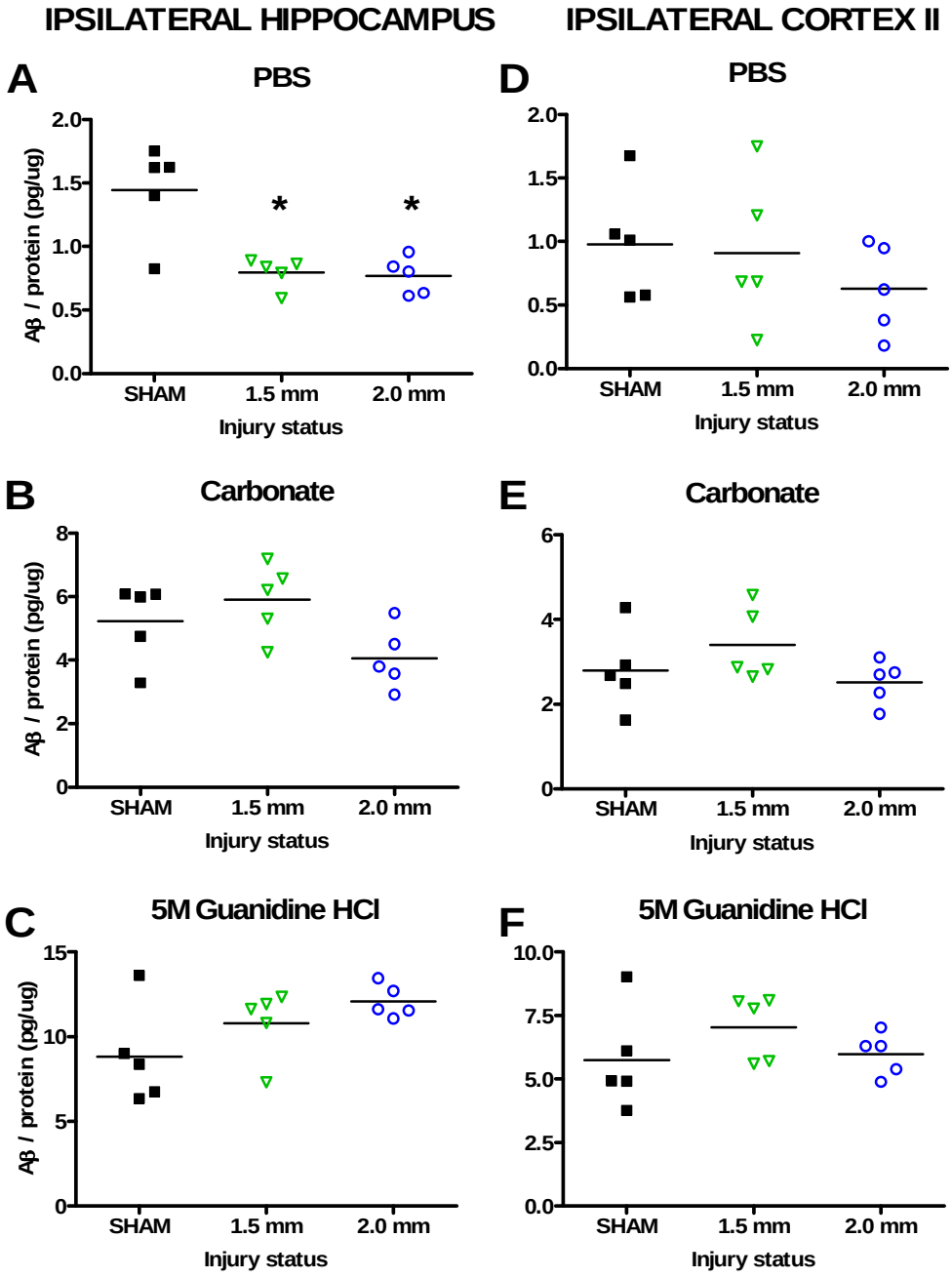

Chapter 8.

Proposed studies of mechanism: production vs. clearance

The question of mechanism is raised by our main finding, that hippocampal Aβ was immediately reduced by approximately 50% of baseline levels in the ISF as measured by microdialysis and in PBS-soluble tissue extracts at 2h post-injury. What underlies the observed decreases? Based on the concept that ISF Aβ levels result from the balance between production and clearance rates, we can divide subsequent tests of mechanism into production and clearance. Two mechanisms resulting in changes of production of Aβ: changes in full-length APP protein levels and changes in local neuronal activity, as well as a clearance mechanism, acute Aβ deposition, have already been tested (Ch. 5).

Firstly, on the production side, if amyloid precursor protein (APP) were downregulated, there would be less available substrate for the Aβ-cleaving enzymes, β- and γ-secretases, leading to reduced Aβ levels. Our RIPA-extracted homogenates did not reveal any differences in APP content between sham and injured hippocampi at the 2 h timepoint. This result is consistent with our finding that carbonate and guanidine-extracted tissues contained equal amounts of Aβ in injured and sham tissues.

Also on the production side, we drew an analogy between ours and previous experiments reported by Cirrito et al. in his 2005 paper that established a role for neuronal activity in the regulation of ISF Aβ (Cirrito, et al., 2005). Briefly, if neuronal activity was increased, ISF Aβ was increased, and if neuronal activity was decreased, so was ISF Aβ. Our local measurements of electrical activity in the vicinity of the microdialysis probe demonstrated an acute decrease in neuronal activity that lasted over 24 hours following injury. This result strongly suggests that decreased neuronal activity

may play a role in the decreased levels of ISF Aβ. However, it remains unknown whether neuronal activity is causal, coincident, or parametrically related to ISF Aβ following injury.

On the clearance side, we examined the possibility that Aβ was acutely deposited into extracellular plaques or intra-axonal aggregations, thereby leading to reduced ISF levels and a lesser amount in the PBS-soluble tissues. When brains were examined at the 24 h timepoint, no deposition or aggregation was seen using a middle-domain antibody that detects Aβ deposition in PDAPP mice at 10 and 20 months of age (Ch. 5, Fig. 37).

In summary, APP levels were unchanged at the 2h timepoint and no Aβ deposition or aggregation was observed at the 24 h timepoint. Therefore, these mechanisms likely play no direct role in ISF Aβ dynamics. By contrast, neuronal activity was acutely decreased after injury. As compared to baseline, changes in neuronal activity correlated with changes in ISF Aβ levels. However, the correlation was not strong enough to suggest that neuronal activity is solely responsible for observed changes (Spearman r = 0.6506, 95% C.I. 0.2919-0.8489 for n=5, 2.0 mm-injured PDAPP mice; Ch. 6, Fig. 55D). A general approach to mechanisms of production vs. clearance is addressed in this chapter. Two experiments are proposed to test the hypotheses that either one of these could lead to the observed post-injury ISF Aβ dynamics.

Tests of clearance

Generally, differences in clearance can be quantified using a very simple method in which production of Aβ is shut off using a γ-secretase inhibitor, and Aβ is measured as

it clears from the ISF. The kinetics of clearance can be modeled using an exponential decay function. We chose the highly potent γ-secretase inhibitor LY411,575, whose effects on Aβ production in Tg2576 mice have been described (Lanz, et al., 2004). This compound was also previously used to determine ISF Aβ half-life in PDAPP mice using *in vivo* microdialysis (Cirrito, et al., 2003).

In some preliminary experiments using young Tg2576 / hApoE3 mice, we measured clearance rates in terms of half life in uninjured animals. Briefly, mice were implanted with microdialysis probes in the standard location and allowed to equilibrate for at least 4-5 hours. Baseline samples were collected for at least 4 hours prior to administration of LY411,575. We increased the sampling rate from every 90 to every 20 minutes, 80 minutes prior to drug administration. Mice were then subcutaneously injected with 3 mg/kg of LY411,575 suspended in corn oil. In these mice, the half-life of ISF Aβ was approximately 55 minutes. The results of those experiments are shown in Figure 58 (plot of mean % baseline Aβ) and Figure 59 (semi-log plot of data in Fig. 58).

Figure 58. Effect of γ-secretase inhibitor on ISF Aβ. Mean % baseline Aβ as measured by microdialysis every 20-min in uninjured Tg2576 / hApoE3 (n=4) at baseline and after injection of 3 mg/kg LY411,575 at t=0. Error bars, standard error of the mean.

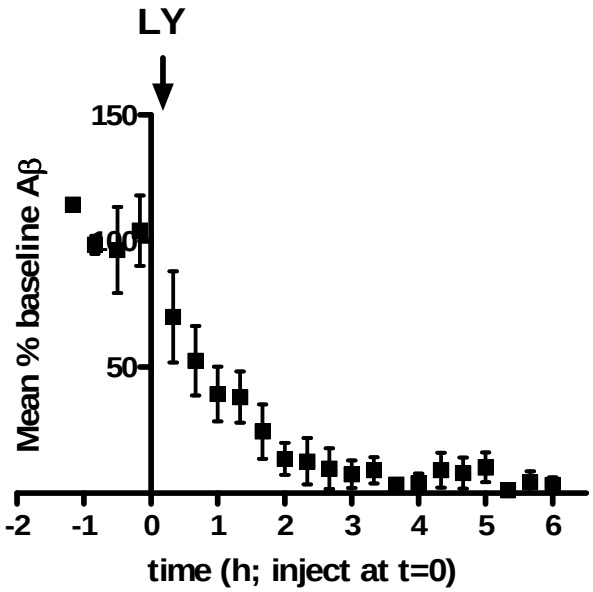

Figure 59. Determination of half-life of ISF Aβ using exponential decay model. Natural log of mean % baseline Aβ plotted against time. Slope value gives decay constant then used to calculate half-life (~55 min).

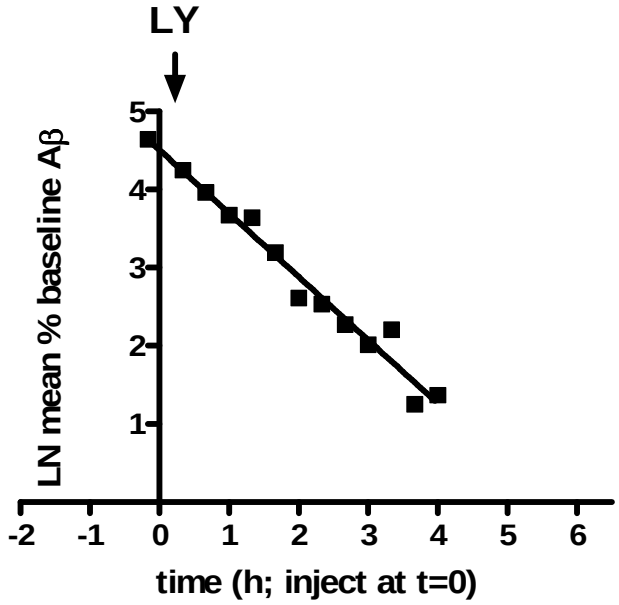

As shown in our preliminary experiments and other published results (Cirrito, et al., 2003), clearance of ISF Aβ occurs according to first-order kinetics. Figure 60 depicts idealized data for two outcomes of a clearance experiment in sham and TBI groups (Fig. 60A, B). In Figure 60A, SHAM and TBI curves display predicted dynamics of mean % baseline Aβ if clearance is unchanged within the first ~2-8 h after injury. After administration of LY411,575 and inhibition of γ-secretase, the kinetics of Aβ clearance would be identical in the sham and injured groups. Alternatively, Figure 60B displays predicted dynamics of SHAM and TBI groups if clearance is increased in the TBI group after injury.

To compare the clearance rates of two groups, sham and TBI, the natural log values of the mean % baseline Aβ values would be plotted against time. Figure 60C-F displays semi-log plots of the hypothetical data in Figure 60A and B. If clearance is unchanged, then post-LY slopes should not be significantly different (Fig. 60C). If clearance is increased after TBI, then the slope of the TBI group should be significantly more negative (Fig. 60D).

Using a program such as GraphPad or Statistica, a linear regression analysis would be performed on this data to compare slope values and the 95% confidence intervals around each slope (Fig. 60E-F). If the 95% confidence intervals of the TBI and SHAM slopes overlap, then the clearance rates would be considered not significantly different (Fig. 60E). If they do not overlap, then TBI would have a significantly increased clearance rate (Fig. 60F).

Figure 60. Alternative results of a hypothetical experiment to test for differences in clearance rate of ISF Aβ. Two groups of mice would receive either a 2.0 mm or sham injury. After 2h, when levels have reached a new equilibrium (100% for sham, or reduced to 50% for TBI), LY411,575 would be injected at 3 mg/kg. **A,** expected results if clearance is unchanged after injury. **B,** expected results if clearance is increased after injury. To compare clearance rates, natural log values for mean % baseline Aβ would be calculated and plotted vs. time (**C**-**F**). **C,** expected results for unchanged clearance after injury. Model shown for baseline, post-TBI, and post-LY periods. **D,** expected results for increased clearance after injury. Model shown for baseline, post-TBI, and post-LY periods. **E,** expected results for unchanged clearance after injury. Model shown for post-LY period only, 95% C.I. of regression line. **F,** expected results for increased clearance after injury. Model shown for post-LY period only, 95% C.I. of regression line.

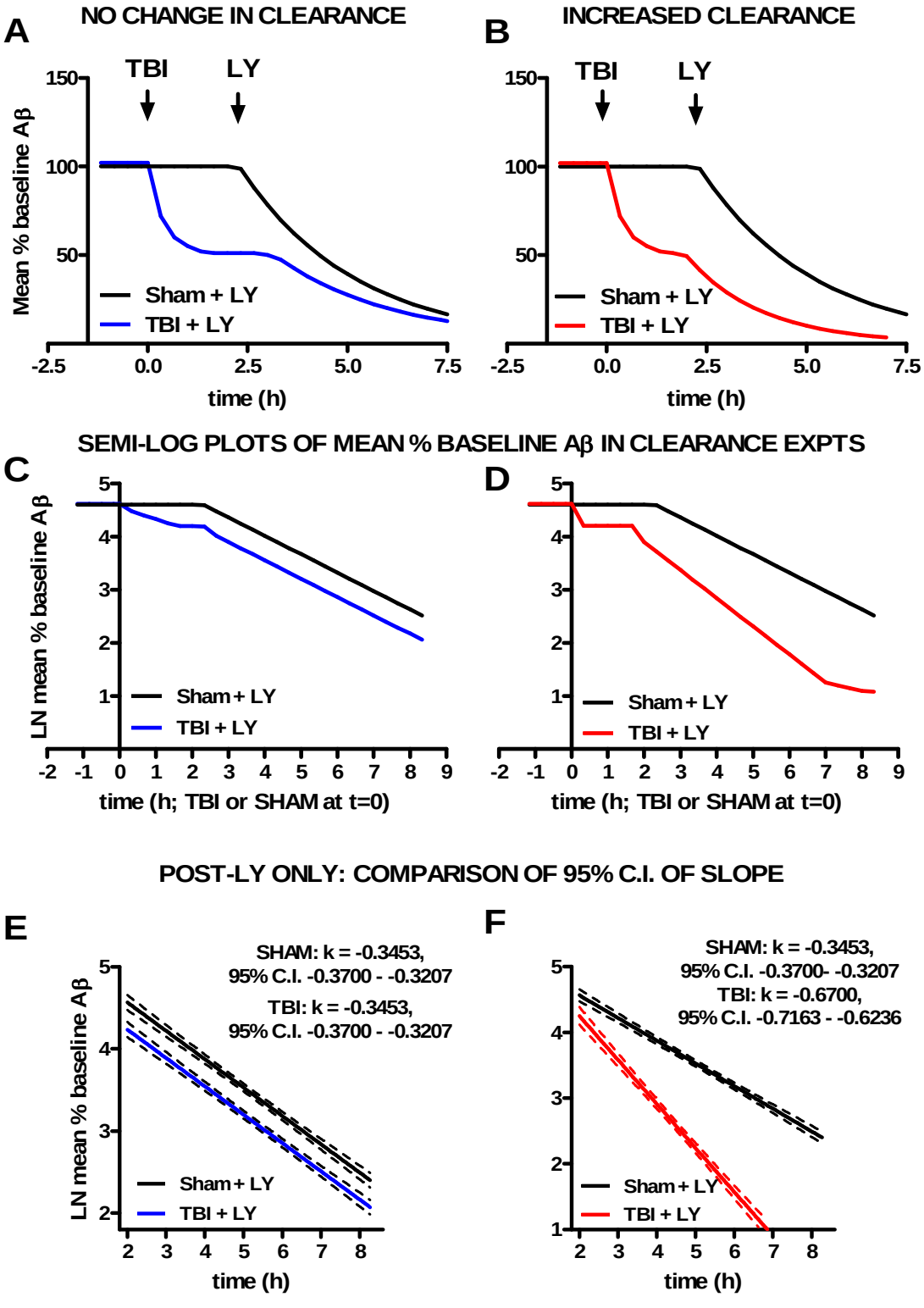
A
NO CHANGE IN CLEARANCE
TBI
LY
Mean % baseline Aβ
150
100
50
Sham + LY
TBI + LY
-2.5
0.0
2.5
5.0
7.5
time (h)
B
INCREASED CLEARANCE
TBI
LY
150
100
50
Sham + LY
TBI + LY
-2.5
0.0
2.5
5.0
7.5
time (h)
SEMI-LOG PLOTS OF MEAN % BASELINE Aβ IN CLEARANCE EXPTS
C
LN mean % baseline Aβ
5
4
3
2
1
Sham + LY
TBI + LY
-2 -1 0 1 2 3 4 5 6 7 8 9
time (h; TBI or SHAM at t=0)
D
5
4
3
2
1
Sham + LY
TBI + LY
-2 -1 0 1 2 3 4 5 6 7 8 9
time (h; TBI or SHAM at t=0)
POST-LY ONLY: COMPARISON OF 95% C.I. OF SLOPE
E
SHAM: k = -0.3453,
95% C.I. -0.3700 - -0.3207
TBI: k = -0.3453,
95% C.I. -0.3700 - -0.3207
LN mean % baseline Aβ
5
4
3
2
Sham + LY
TBI + LY
2 3 4 5 6 7 8
time (h)
F
SHAM: k = -0.3453,
95% C.I. -0.3700- -0.3207
TBI: k = -0.6700,
95% C.I. -0.7163 - -0.6236
5
4
3
2
1
Sham + LY
TBI + LY
2 3 4 5 6 7 8
time (h)

If experimental data indicate an increase in clearance rate following TBI, further experiments would be needed to evaluate specific clearance mechanisms, such as the degradation of Aβ by insulin-degrading enzyme (IDE) and neprilysin. Inhibition of these enzymes or use of an IDE or neprilysin knockout mouse would resolve their potential roles in post-TBI ISF Aβ dynamics.

Statistical power calculations for tests of clearance

How do we determine the number of mice needed in each group to reliably detect a difference in clearance rates? The G*Power 3.1.0 program (written by Franz Faul, Universitat Kiel, Germany; available for free download) was used to estimate sample sizes for different levels of power. The linear bivariate regression test was chosen. Assuming equal numbers of animals in each group, and statistical measures based on the preliminary experiment: standard deviation of the residuals = 0.18 (see Fig. 59), and a standard deviation of 1 for log-transformed y values, a plot of sample size as a function of power was generated (Fig. 61). For power = 0.80, 4 mice per group are required to see an effect of 50% difference between slopes of the semi-log plot.

Figure 61. Plot of power vs. sample size for an effect of 0.5 (50% difference in rates). Generated by the G*Power 3.1.0 program.

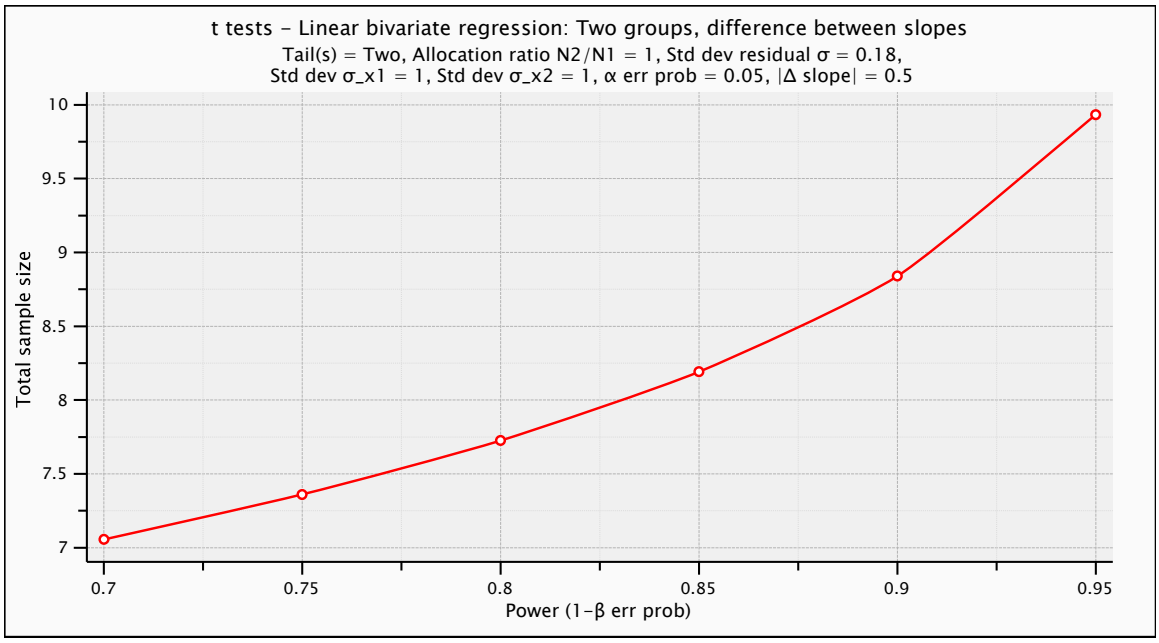

If clearance were only one of several contributing factors to the observed decreases in Aβ levels such that clearance was increased less than 50%, then we would need larger sample sizes. Table 1 gives the sample sizes necessary to detect different clearance rates at different levels of power.

Table 1: sample sizes to detect differences in clearance at different levels of power*

Power level	Δ slope	Sample size (per group)
0.80	50%	4
	40%	5
	30%	7
	20%	13
	15%	24
0.90	50%	5
	40%	6
	30%	9
	20%	18
	15%	32
0.95	50%	5
	40%	7
	30%	11
	20%	22
	15%	36

*model assumptions: standard deviation of the residuals = 0.18;
standard deviation = 1 for transformed y-values in each group

In addition, controls are necessary for the injection of LY411,575. A vehicle-injected group would be included. To determine differences in clearance for the 2.0 mm-injured group, a total of four groups would be required. Assuming a statistical power level of 0.80 to detect either a 50%, 30%, or 20% difference in clearance rates (Table 1), the following numbers of mice would be needed (Table 2):

Table 2: Number of mice needed for clearance experiment

Group	Purpose	n (Δ = 50%)	N (Δ = 30%)	n (Δ = 20%)
TBI + LY	Experimental	4	7	13
TBI + vehicle	Control: injection	4	7	13
SHAM + LY	Control: injury	4	7	13
SHAM + vehicle	Control: both	4	7	13
TOTAL		16	28	52

Pilot experiments should be done with n = 4 mice per group to approximate the size of the effect and to determine whether the residuals are of the expected magnitude based on data collected in naïve animals.

Tests of production

Since EEG recordings suggest a positive correlation between decreases in neuronal activity and ISF Aβ following TBI, further experiments could be performed to determine whether this relationship is causal. The contribution of neuronal activity to post-TBI levels of ISF Aβ will be assessed using textrodotoxin (TTX), a voltage-gated sodium channel blocker which strongly inhibits neuronal activity. A continuous infusion of 5 uM TTX can be administered by reverse microdialysis beginning 6 h prior to TBI and ISF Aβ can be measured for further changes. This dose has been used in previous experiments not involving TBI (Fig. 62). A dose-response approach could be used to achieve at least a 30% decrease in EEG activity, based on the observed (average) decreases during the post-TBI period in 2.0 mm-injured mice.

Figure 62. Inhibition of neuronal activity with TTX occludes the effect of restraint stress on ISF Aβ. Reverse microdialysis delivery of 5 μM TTX immediately decreased Aβ levels; three hours of restraint stress at 8 h after TTX treatment did not result in significant change in Aβ levels compared with controls treated with TTX alone controls (n = 5). Modified from Kang et al., PNAS 2007.

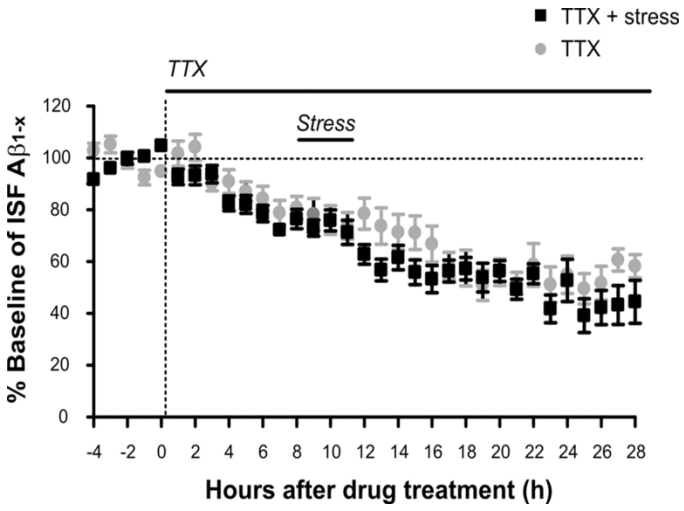

To test the hypothesis that the changes in post-TBI ISF Aβ levels depend on neuronal activity, 5 μM TTX can be infused by reverse microdialysis during the baseline period, approximately 6 hours before TBI. Two possible results of the alternative hypotheses are shown in Figure 64. If the effects of TBI on ISF Aβ depend on TTX-insensitive mechanisms, an additive effect of TTX would be expected; TBI would further decrease ISF Aβ in the presence of TTX (Fig. 63A). However, if the effect of TBI on ISF Aβ is mediated by TTX-sensitive mechanisms, the rate of decease after TBI should be identical in injured mice pretreated with TTX compared to uninjured sham controls. In other words, TTX would occlude the effects of TBI if the effects of TBI are exclusively mediated decreased TTX-sensitive neuronal activity (Fig. 63B).

Figure 63. Hypothetical results for effect of TTX on ISF Aβ after TBI. **A,** most of the pool of ISF Aβ is regulated in the post-TBI period by TTX-insensitive mechanisms, so TTX will not occlude decreases in ISF Aβ due to TBI. **B,** ISF Aβ is regulated in the post-TBI period by TTX-sensitive mechanisms, since TTX will occlude decreases in ISF Aβ due to TBI.

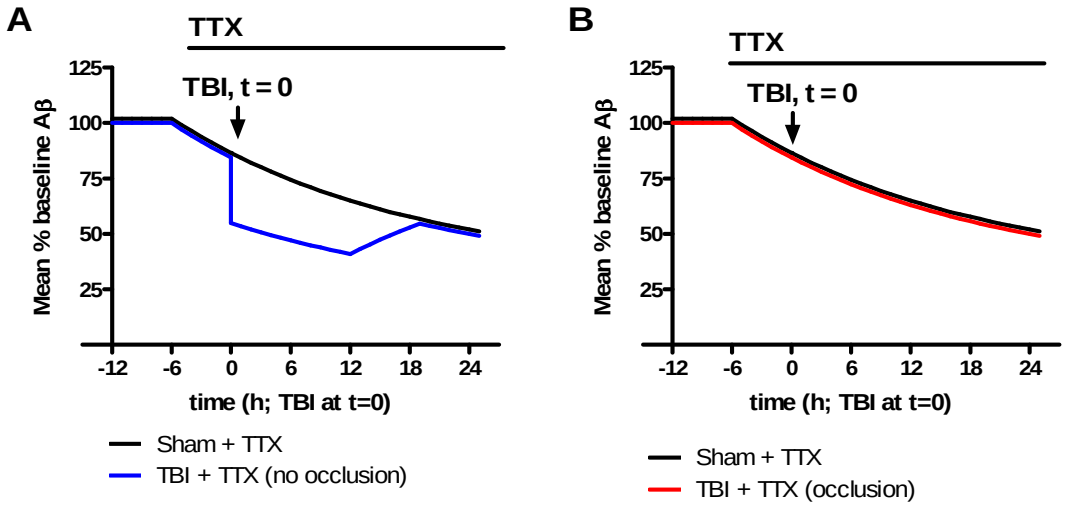

It has been suggested that even a reverse-microdialysis delivery approach might be lethal in CCI-injured animals. Due to the breach of the blood-brain barrier, TTX could enter the bloodstream and reach the lungs and heart, where it could inhibit respiration and cardiac muscle signaling (J. Cirrito, unpublished observations). If TTX is in fact lethal at the dosages required to achieve a significant decrease in the remaining neuronal activity following TBI, then another, non-lethal way to inhibit neuronal activity would be required. Two strategies would be to increase inhibitory firing using a GABAergic agonist and to inhibit excitatory firing using either an antagonist of the metabotropic glutamate receptors 2/3 (mGluR2/3), or inhibitors of ionotropic glutamate channels, such as MK-801 for NMDA receptors. Like TTX, the optimal dosing would be empirically determined based on the decrease in EEG RMS amplitude.

In summary, the proposed clearance and production experiments could be used to test hypothesized factors that contribute to the balance of ISF Aβ levels. It is possible that mechanisms other than those specified here are involved. On the production side, recent data suggest a role for endocytic-independent mechanisms in the regulation of ~30% of total ISF Aβ levels (Cirrito, et al., 2008). Tests involving the molecular mechanisms involved in this system would help elucidate the sources of hypothesized decreases in neuronal activity-dependent production following injury.

Chapter 9.

Conclusions and future directions

Summary of main findings

In conclusion, we present here the development of a mouse model of combined microdialysis-experimental traumatic brain injury. Using this model, we measured the dynamics of ISF Aβ levels in PDAPP and wildtype mice, both before and after a 2.0 mm electromagnetic-controlled cortical impact injury (EM-CCI). In PDAPP mice, we were able to achieve a time resolution of 90-minute samples for a baseline period of approximately 12 hours and a post-injury period of 24 hours in n=6 mice per group. It was found that post-injury ISF levels were immediately decreased to approximately 50% of baseline levels, and remained low over the post-injury sampling period. Probe function was controlled for in 3 different experiments: zero-flow extrapolation, measurement of endogenous urea, and retrodialysis of infused Aβ. Probe function was unchanged before and after TBI as indicated by zero-flow and retrodialysis experiments. Based on the low frequency of abnormal probe function as indicated in routine urea measurements, we concluded that decreases in ISF Aβ reflected physiological phenomena rather than technical difficulty.

One potential mechanism for the observed dynamics, the role of neuronal activity in the regulation of ISF Aβ, was suggested by the work of Cirrito, Kang and others. We used intraparenchymal EEG recordings to measure local neuronal activity in the vicinity of the microdialysis probe. We found the strongest positive correlation for group-averaged coordinates from 2.0 mm-injured mice, from 6 hours before injury through 24 hours post-injury (Spearman r = 0.6506, 95% C.I. 0.2919-0.8489; p = 0.0014). This

correlation is consistent with a role for neuronal activity in the observed decreases in post-TBI ISF Aβ levels.

To determine the relationship of Aβ levels in interstitial fluid to tissue levels, we also measured total $A\beta_{1-x}$, $A\beta_{x-40}$, and $A\beta_{1-42}$ in serial extracts of PBS, carbonate, and guanidine-soluble homogenates from ipsilateral hippocampal and cortical tissues in mice sacrificed 2h after sham or 2.0 mm injury. PBS-soluble levels of $A\beta_{1-x}$ and $A\beta_{x-40}$ were significantly decreased to approximately 50% of sham levels in the hippocampus, consistent with the magnitude of decrease in ISF levels. PBS and guanidine-soluble cortical extracts were also reduced in $A\beta_{1-x}$, as were guanidine-soluble cortical extracts for $A\beta_{1-42}$.

We tested the hypothesis that Aβ might be retained within a pre-synaptic compartment, consistent with our measurements of reduced ISF and PBS-soluble tissue levels as well as reduced neuronal activity. To do this, we prepared synaptosomes at the 2h timepoint in sham and 2.0 mm injured mice and measured $A\beta_{x-40}$ and $A\beta_{1-42}$ in individual hippocampi from ipsilateral and contralateral sides. There were no significant differences between sham and TBI groups in either isoform, suggesting that retention within this compartment is not likely a mechanism of reduced ISF and extracellular Aβ levels.

We used a range of severities to determine whether there was a graded response to injury in terms of ISF Aβ, neuronal activity, and tissue levels. We compared sham, 1.0 mm, 1.5 mm, and 2.0 mm groups. The 1.0 mm group demonstrated variable responses to the impact, possibly contributing to the variable ISF Aβ dynamics and EEG patterns.

The 1.5 mm group showed similar ISF Aβ dynamics to the 2.0 mm group. These dynamics were not significantly different between 1.5 and 2.0 mm-injured groups by repeated measures ANOVA. The 1.5 mm-injured group also showed reduced neuronal activity that was not significantly different than the 2.0 mm group, on average, for the post-injury period. Likewise, tissue levels of $A\beta_{1-x}$ in the 1.5 mm group were similar to the 2.0 mm group in all serial extracts of hippocampal and cortical homogenates.

We proposed an approach to testing hypothesized mechanisms based on the concept of a balance between ISF Aβ production and clearance. Two mechanisms of decreased Aβ production were tested: decreased full-length APP protein levels, and decreased neuronal activity. One theoretical clearance mechanism, acute Aβ deposition, was also tested. While there appeared to be no acute changes in APP levels and no observed Aβ deposition, neuronal activity was reduced. We proposed two main experiments to further test clearance vs. production mechanisms. First, we can measure the rate of clearance from the ISF by inhibition of the Aβ-cleaving enzyme, γ-secretase. An enhanced, or increased, clearance rate might contribute to the acute deceases seen in the ISF. On the production side, we have already determined that neuronal activity is locally decreased after a 2.0 mm injury. To test whether this decrease causes or actively contributes to the decreases in ISF Aβ, we can inhibit neuronal activity using TTX prior to injury. Any further decreases in ISF Aβ as a result of TBI would be attributed to TTX-insensitive mechanisms, suggesting a role for activity-independent production of Aβ.

Finally, we have used the results of these experiments to help interpret the post-injury dynamics in human clinical microdialysis studies, in which baseline measurements

cannot be taken. In turn, the clinical study demonstrated that changes in neurological status were correlated with ISF Aβ dynamics, suggesting that neuronal activity might be worth investigating as a mechanism in the animal model. Thus, our studies exemplify the complementary relationship of clinical and animal microdialysis research. Table 3 compares study parameters between the human and mouse studies.

Table 3. Comparison of clinical and research microdialysis studies of Aβ dynamics.

	Human clinical study	**Mouse research study**
Injury	variable	consistent (CCI)
Time of initial measurement	12-24 h after injury	18-24 h before injury
Duration of measurements	72 h post-implantation	24 h pre, 24 h post-injury
Catheter or probe location	most in right, prefrontal subcortical white matter	ipsilateral hippocampus
Catheter or probe type	CMA 71, 100 kD MWCO	BAS BR-2, 38 kD MWCO
Aβ assay	m266/3D6 sandwich ELISA	m266/3D6 sandwich ELISA
Time resolution	2 h	90 min

Future translational studies should be designed to measure pre and post-TBI dynamics of different small molecules and peptides, and to explore the potential mechanisms underlying these dynamics. Others in the lab have applied and adapted this combined microdialysis-TBI mouse model to measure the neuropeptide orexin in the hypothalamus and other brain regions (J. Willie, unpublished results). Plans are underway to measure this peptide in human CSF and microdialysates, and to test a hypothesized correlation with measures of activity and arousal in human clinical studies.

Given these findings, what can be said about the relationship of this project to outstanding questions in the fields of clinical microdialysis, Aβ deposition, TBI-related dementia, and future directions?

What does this project contribute to our understanding of clinical studies in human patients?

A main goal of this project was to measure pre and post-injury ISF Aβ dynamics in the same animal, avoiding the potential errors of cross-sectional, timepoint studies of post-TBI tissue levels of Aβ. We hypothesized these results would contextualize the findings of the clinical study, in which only *post*-injury levels and dynamics could be measured. In human patients, it was unknown whether the levels at some time after injury were low, equal, or higher than before injury. Furthermore, it was not clear whether levels remained below baseline, normalized within the typical 3-6 day measurement period, or were rising beyond baseline. Using a 2.0 mm CCI injury, the mouse experiments suggested that ISF Aβ levels dropped below baseline within the first 90-minute sample, decreased to ~50% and remained low throughout the 24 hour period of measurement. Using a 1.5 mm injury, the ISF Aβ levels dropped to nearly the same levels as with a 2.0 mm injury (mean ± standard deviation: 51 ± 35% for 1.5 mm, 51± 37% for 2.0 mm). Local, intrahippocampal EEG activity as quantified by RMS amplitude was also decreased after an injury. Although neuronal activity was not as depressed in the 1.5 mm group (87 ± 24%) as the 2.0 mm group (69 ± 26%), this difference was not statistically significant. Using a mild injury at an impact depth of 1.0 mm, the variable tissue responses precluded inclusion of these data in subsequent analyses.

The relatively stable dynamics of both post-TBI ISF Aβ and neuronal activity over 24 h in this experimental model were non-identical to most of the human patient

data, for which levels tended to fluctuate over at least 72 hours. One important difference between the model and the clinical study was the homogeneity of subjects, especially with respect to injury type and severity. All mice were similarly injured and were of similar age. By contrast, the clinical data were collected from a variety of acute brain injuries, including both TBI and aneurysmal subarachnoid hemorrhage. Additionally, patient ages ranged from early 20s to late 60s. Finally, microdialysis catheter placement within the brain was not always standardized. One way to better match the animal model to the clinical data would be to have a variety of injuries besides CCI, including a model of subarachnoid hemorrhage, performed across different ages.

However, despite the potential discrepancies, the results of the experimental studies are fundamentally concordant with the findings of the clinical study, in which changes in the Glasgow Coma Score (GCS) correlated with changed in ISF Aβ levels. What does it mean that correlations were found in both the experimental and clinical studies? One criticism is that comparing GCS with local EEG activity is an invalid analogy. The GCS is an ordinal assessment of voluntary and involuntary behavioral responses to stimuli, in contrast to the relatively continuous EEG data representing intrinsic field-potentials. Even if there is a direct relationship between neuronal activity and behavioral output, intrahippocampal EEG measurement is localized, whereas the GCS depends largely on the integration of central and peripheral nervous system functions. Nonetheless, the correlation between ISF Aβ dynamics and changes in either local EEG activity in the mouse experiments, or GCS in the clinical patients, suggest that future experiments be done in both mouse and human patients to determine the

relationship between local neuronal activity and global measures such as the GCS. To address this criticism, the mouse study could be better matched to the original clinical study by using a mouse behavioral scale, such as the NeuroScore. Alternatively, future clinical studies might plan to measure electrical signals as captured by 5-lead EEG or the BIS monitoring system to see if the correlation holds for intrinsic neuronal activity.

What does this project contribute to our understanding of acute deposition after TBI in mice and in human patients?

This study offers no additional insight into mechanisms responsible for the acute deposition of Aβ observed in 30% of severely injured or deceased human patients. Our findings are consistent with the experimental literature, in which there are no reports of positive findings of acute deposition after CCI injury in PDAPP mice. By contrast, there are reports of a *reduced* total burden of Aβ plaque 5-8 months after TBI (Nakagawa, et al., 1999) and a regression of established plaques in aged mice 16 weeks after injury (Nakagawa, et al., 2000). In summary, the lack of positive findings in the literature is consistent with our observations, that there is no acute Aβ deposition in either PDAPP or Tg2576 mice acutely after CCI injury.

By contrast, some models of experimental TBI in swine recapitulate key elements of human neuropathology: accumulations of APP, neurofilament, and Aβ in axonal bulbs; axonal bulbs near regions of foamy macrophage infiltration; and plaque-like extracellular Aβ deposits (Chen, et al., 2004, Smith, et al., 1999). These features were seen both at 7 days and 6 months post-injury. Swine models might better model acute Aβ deposition

and accumulation in the setting of axonal injury. However, certain transgenic mouse strains also show post-TBI deposition (see "Future work to expand repertoire of injury types and animal models").

What does this project contribute to our understanding of chronic deposition after TBI in mice and in human patients?

As with acute deposition, this study does not explicitly test the hypothesis that TBI might lead to increased deposition during the chronic phase. We examined PDAPP mice from 24-120 hours after injury. Other studies have looked 4-8 months later, and have found persistent behavioral deficits as well as histological evidence of damaged tissue, such as atrophy, reductions of Aβ plaque burden, and even regression of established plaques (Nakagawa, et al., 1999, Nakagawa, et al., 2000). Based on these findings, future experiments should be designed to compare ISF Aβ levels at baseline with chronic stages. Given the atrophy and cell loss, it would be worthwhile to determine if or how levels change over time. A multiple regression model would be most appropriate for this type of analysis given the effect of age on ISF Aβ levels in PDAPP mice (Cirrito, et al., 2003).

One recent study examined autopsy samples from TBI patients who died in chronic stages of injury for evidence of Aβ deposition (Chen, et al., 2009). Interestingly, within a few years of injury, it appears the majority of immunohistochemical staining is intra-axonal with a paucity of extracellular plaques. This finding is not inconsistent with other reports of extracellular plaques and tangles in brains with known TBI residuals in

patients who died at least 7 years after their injuries (Jellinger, et al., 2001). One hypothesis is that, given the increased incidence of abnormal intra-axonal accumulations, there might be increased neuronal dysfunction, leading to or coincident with an earlier occurrence of plaque deposition. These elements of accelerated neuropathology are consistent with the notion that TBI might hasten the onset of dementia. Again, future studies should be designed to examine a large cross section of autopsied brains from TBI patients who died over a broad range of time from injury to determine the natural history of Aβ accumulation and deposition associated with brain injury.

What does this project contribute to our understanding of the link between remote TBI and the development of dementia later in life?

This project does not suggest any definite role for acute ISF Aβ dynamics in the later development of dementia. The Alzheimer's literature contains many studies that test hypotheses concerning the pathological link between Aβ and dementia, and whether plaque load corresponds directly to the degree of clinical impairment (Nelson, et al., 2009). Similarly, both animal studies and recent clinical data in which anti-Aβ antibodies were shown to clear plaques suggest that even when plaques are reduced or eliminated, cognitive deficits may persist. Hence, Aβ plaque load is certainly not solely responsible for cognitive dysfunction and deficits. There are several alternative possibilities: plaques contribute to neuronal dysfunction; plaques are a sign of neuronal dysfunction, but neither exacerbate nor ameliorate it; or, plaques are actually neuroprotective. Further

work is required to determine this peptide's relative contribution to acute and chronic deficits.

Future work to characterize other proteins implicated in TBI-related neurodegeneration

Besides Aβ deposition, many other proteins and peptides have been linked to both genetic (familial) and sporadic neurodegenerative dementias. Chief among these is tau, a microtubule-stabilizing protein that exists in abundance in neurons. In its hyperphosphorylated, paired-helical-filament (PHF) form, tau is widely known as the other pathological hallmark of Alzheimer's disease. This protein is important in axonal transport, and disruption of its function has profound implications for neuronal viability. Tau is also increased in the CSF of both clinical patients and in rodent studies of TBI in the setting of acute injury, and is detectable by high molecular weight catheters in humans and most recently, mice. Due to its myriad known functions, and evidence for its aberrant dynamics in TBI, tau is of great interest for its potential role in the association between remote TBI and dementia. Future experiments should be designed to characterize the pre and post-injury dynamics of tau and the immunohistochemical patterns of its various isoforms.

Future work to expand repertoire of injury types and animal models

One limitation of these findings is the injury model in which they were made. The controlled cortical impact has been a reliable model for many investigations over the

past two decades. However, the majority of clinical patients have very different injuries than a focal contusion. Other mixed models should be explored, particularly those incorporating diffuse axonal injury (DAI) and repeated concussive injuries.

Different transgenic mice demonstrate different responses to injury. Other transgenic models might yield additional insights into the dynamics of both Aβ and other proteins, such as tau. One example is the 3X Tg mouse, which expresses mutant human isoforms of PS1, APP, and tau shown to be associated with familial AD (Oddo, et al., 2003). However, while mice are a convenient species for genetic manipulation, the mouse brain has less-than-ideal biomechanics to model human brain injury.

Swine models bear a closer resemblance to the human brain in terms of size, presence of gyri and sulci, and distribution of gray and white matter. Moreover, previous studies have demonstrated the similarities between brain injuries in swine and humans in multiple aspects. For example, experimental TBI in swine often necessitates multimodal monitoring, including intubation, sedation, controlled ventilation, and control of intracranial pressure and cerebral perfusion (Manley, et al., 2006). The protocol is similar to that used for severely-injured human patients in an intensive-care setting, but very unlike in rodents who generally recover without external assistance. Another experimental TBI model, inertial brain injury, uses a rapid rotational acceleration of the head (Smith, et al., 1997). Axial rotation alone induces coma, whereas axial and coronal rotations yield a robust model of DAI (Chen, et al., 2004, Smith, et al., 1999, Smith, et al., 1997, Smith, et al., 2000). The ability to model DAI is a unique advantage of the swine model, since the biomechanics of the rodent brain preclude such an injury (Smith,

et al., 1997). Finally, it has been shown that microdialysis monitoring can be combined with experimental CCI in a swine model (Alessandri, et al., 2003). This combined model further expands the possibilities for improved translational research into the physiology of interstitial species, potential biomarkers, and pharmocodynamics (Hillered, et al., 2005). Swine can also better model pediatric TBI (Duhaime, 2006). Although TBI research in large-animal models is far more costly in terms of capital expenses and time spent per animal, well-designed studies may reveal more about human injury and in the end save resources otherwise spent on limited mouse models. However, a major advantage of mouse models is that genetic manipulations of the mice can be readily performed.

Because certain genetic risk factors are unique to humans, they can be modeled only by transgenic manipulation in mice. For example, the ApoE4 allele is a strong risk factor for sporadic and late-onset Alzhemier's disease (Strittmatter, et al., 1993). One mechanism by which ApoE4 increases the risk for AD was described by Holtzman et. al (Holtzman, et al., 2000). Using PDAPP mice that co-expressed human ApoE isoforms, this study found that Aβ tends to aggregate into fibrillar plaques more readily in ApoE4+ animals than other ApoE genotypes (Holtzman, et al., 2000). Epidemiological studies have strongly suggested that ApoE4 acts synergistically with TBI to increase the risk of dementia (Mayeux, et al., 1995). Taken together, these findings suggest that the effects of ApoE4 to increase the risk of TBI-related dementia may be mediated through Aβ pathology. Evidence to support this hypothesis was shown in a study by Hartman et al. (Hartman, et al., 2002). PDAPP mice co-expressing human isoforms of ApoE3 or

ApoE4, or that expressed no ApoE (mouse or human), were subjected to CCI injury at 9-10 months of age and were examined 3 months later for neuropathology. In the absence of TBI, these genotypes do not have Aβ deposits at the ages studied. By contrast, in the CCI-injured mice, the PDAPP/ApoE4 animals were found to have thioflavin-S positive amyloid, and all genotypes showed positive staining for diffuse Aβ plaque deposition. Other measures of neurodegeneration did not differ among the genotypes. The results of this study provide evidence that human isoforms of ApoE may be required for any sort of Aβ deposition after TBI, diffuse and fibrillar, and that ApoE4 in particular is required for fibrillar deposition. This study could not have been done in a large-animal model, such as swine, due to the complicated nature of transgenic manipulations.

In conclusion, both rodent studies and large-animal models are necessary and valuable in TBI research. Mice are currently the best model for important transgenic investigations, while swine are better suited for recapitulating the biomechanics and diffuse axonal injury of human TBI.

Future directions for translational models involving microdialysis and experimental TBI

In conclusion, this project presents a combined mouse model of microdialysis and experimental TBI. Using pre and post-TBI measurements of ISF Aβ, we may be able to infer a relationship between baseline and post-injury levels in clinical data. The correlations between changes in either GCS or local EEG activity with changes in ISF Aβ found in both the clinical data and the mouse model are consistent with the notion that a

similar underlying mechanism gives rise to the observed phenomena. Future mouse and swine models should be designed to further test hypothesized mechanisms. Better matching of clinical and experimental designs will improve the accuracy and predictions gleaned from such translational research.

Works cited

1. Abrahamson, E. E., Ikonomovic, M. D., Ciallella, J. R., Hope, C. E., Paljug, W. R., Isanski, B. A., Flood, D. G., Clark, R. S., and DeKosky, S. T., 2006. Caspase inhibition therapy abolishes brain trauma-induced increases in Abeta peptide: implications for clinical outcome. Exp Neurol 197**,** 437-450.
2. Alessandri, B., al-Samsam, R., Corwin, F., Fatouros, P., Young, H. F., and Bullock, R. M., 2000. Acute and late changes in N-acetyl-aspartate following diffuse axonal injury in rats: an MRI spectroscopy and microdialysis study. Neurol Res 22**,** 705-712.
3. Alessandri, B., Heimann, A., Filippi, R., Kopacz, L., and Kempski, O., 2003. Moderate controlled cortical contusion in pigs: effects on multi-parametric neuromonitoring and clinical relevance. J Neurotrauma 20**,** 1293-1305.
4. Alves, O. L., Bullock, R., Clausen, T., Reinert, M., and Reeves, T. M., 2005. Concurrent monitoring of cerebral electrophysiology and metabolism after traumatic brain injury: an experimental and clinical study. J Neurotrauma 22**,** 733-749.
5. Bell, M. J., Kochanek, P. M., Carcillo, J. A., Mi, Z., Schiding, J. K., Wisniewski, S. R., Clark, R. S., Dixon, C. E., Marion, D. W., and Jackson, E., 1998. Interstitial adenosine, inosine, and hypoxanthine are increased after experimental traumatic brain injury in the rat. J Neurotrauma 15**,** 163-170.
6. Benveniste, H., and Huttemeier, P. C., 1990. Microdialysis--theory and application. Prog Neurobiol 35**,** 195-215.
7. Bindra, P. S., Knowles, R., and Buckley, K. M., 1993. Conservation of the amino acid sequence of SV2, a transmembrane transporter in synaptic vesicles and endocrine cells. Gene 137**,** 299-302.
8. Bito, L., Davson, H., Levin, E., Murray, M., and Snider, N., 1966. The concentrations of free amino acids and other electrolytes in cerebrospinal fluid, in vivo dialysate of brain, and blood plasma of the dog. J Neurochem 13**,** 1057-1067.
9. Borjigin, J., and Liu, T., 2008. Application of long-term microdialysis in circadian rhythm research. Pharmacol Biochem Behav 90**,** 148-155.
10. Bramlett, H. M., and Dietrich, W. D., 2001. Neuropathological protection after traumatic brain injury in intact female rats versus males or ovariectomized females. J Neurotrauma 18**,** 891-900.
11. Braughler, J. M., 1985. Lipid peroxidation-induced inhibition of gamma-aminobutyric acid uptake in rat brain synaptosomes: protection by glucocorticoids. J Neurochem 44**,** 1282-1288.
12. Brody, D. L., and Holtzman, D. M., 2006. Morris water maze search strategy analysis in PDAPP mice before and after experimental traumatic brain injury. Exp Neurol 197**,** 330-340.
13. Brody, D. L., Mac Donald, C., Kessens, C. C., Yuede, C., Parsadanian, M., Spinner, M., Kim, E., Schwetye, K. E., Holtzman, D. M., and Bayly, P. V., 2007. Electromagnetic controlled cortical impact device for precise, graded experimental traumatic brain injury. J Neurotrauma 24**,** 657-673.

14. Brody, D. L., Magnoni, S., Schwetye, K. E., Spinner, M. L., Esparza, T. J., Stocchetti, N., Zipfel, G. J., and Holtzman, D. M., 2008. Amyloid-beta dynamics correlate with neurological status in the injured human brain. Science 321**,** 1221-1224.
15. Busto, R., Dietrich, W. D., Globus, M. Y., Alonso, O., and Ginsberg, M. D., 1997. Extracellular release of serotonin following fluid-percussion brain injury in rats. J Neurotrauma 14**,** 35-42.
16. Cernak, I., and Noble-Haeusslein, L. J., 2009. Traumatic brain injury: an overview of pathobiology with emphasis on military populations. J Cereb Blood Flow Metab.
17. Chen, T., Qian, Y. Z., Di, X., Rice, A., Zhu, J. P., and Bullock, R., 2000. Lactate/glucose dynamics after rat fluid percussion brain injury. J Neurotrauma 17**,** 135-142.
18. Chen, T., Qian, Y. Z., Di, X., Zhu, J. P., and Bullock, R., 2000. Evidence for lactate uptake after rat fluid percussion brain injury. Acta Neurochir Suppl 76**,** 359-364.
19. Chen, X. H., Johnson, V. E., Uryu, K., Trojanowski, J. Q., and Smith, D. H., 2009. A lack of amyloid beta plaques despite persistent accumulation of amyloid beta in axons of long-term survivors of traumatic brain injury. Brain Pathol 19**,** 214-223.
20. Chen, X. H., Siman, R., Iwata, A., Meaney, D. F., Trojanowski, J. Q., and Smith, D. H., 2004. Long-term accumulation of amyloid-beta, beta-secretase, presenilin-1, and caspase-3 in damaged axons following brain trauma. Am J Pathol 165**,** 357-371.
21. Cirrito, J. R., Kang, J. E., Lee, J., Stewart, F. R., Verges, D. K., Silverio, L. M., Bu, G., Mennerick, S., and Holtzman, D. M., 2008. Endocytosis is required for synaptic activity-dependent release of amyloid-beta in vivo. Neuron 58**,** 42-51.
22. Cirrito, J. R., May, P. C., O'Dell, M. A., Taylor, J. W., Parsadanian, M., Cramer, J. W., Audia, J. E., Nissen, J. S., Bales, K. R., Paul, S. M., DeMattos, R. B., and Holtzman, D. M., 2003. In vivo assessment of brain interstitial fluid with microdialysis reveals plaque-associated changes in amyloid-beta metabolism and half-life. J Neurosci 23**,** 8844-8853.
23. Cirrito, J. R., Yamada, K. A., Finn, M. B., Sloviter, R. S., Bales, K. R., May, P. C., Schoepp, D. D., Paul, S. M., Mennerick, S., and Holtzman, D. M., 2005. Synaptic activity regulates interstitial fluid amyloid-beta levels in vivo. Neuron 48**,** 913-922.
24. Clausen, H., McCrory, P., and Anderson, V., 2005. The risk of chronic traumatic brain injury in professional boxing: change in exposure variables over the past century. Br J Sports Med 39**,** 661-664; discussion 664.
25. Clinton, J., Ambler, M. W., and Roberts, G. W., 1991. Post-traumatic Alzheimer's disease: preponderance of a single plaque type. Neuropathol Appl Neurobiol 17**,** 69-74.
26. Clough, G. F., 2005. Microdialysis of large molecules. Aaps J 7**,** E686-692.

27. Cohadon, F., 1984. [Cell membrane alterations during situations of acute stress to the cerebral parenchyma. Mechanisms, consequences and therapeutic perspectives]. Neurochirurgie 30**,** 69-83.
28. Corsellis, J. A., and Brierley, J. B., 1959. Observations on the pathology of insidious dementia following head injury. J Ment Sci 105**,** 714-720.
29. Crawley, J. N., 2000. What's Wrong with My Mouse? Wiley-Liss, New York.
30. de Lange, E. C., Danhof, M., de Boer, A. G., and Breimer, D. D., 1997. Methodological considerations of intracerebral microdialysis in pharmacokinetic studies on drug transport across the blood-brain barrier. Brain Res Brain Res Rev 25**,** 27-49.
31. De Robertis, E., Pellegrino De Iraldi, A., Rodriguez, G., and Gomez, C. J., 1961. On the isolation of nerve endings and synaptic vesicles. J Biophys Biochem Cytol 9**,** 229-235.
32. Delgado, J. M., DeFeudis, F. V., Roth, R. H., Ryugo, D. K., and Mitruka, B. M., 1972. Dialytrode for long term intracerebral perfusion in awake monkeys. Arch Int Pharmacodyn Ther 198**,** 9-21.
33. Delgado, J. M., Lerma, J., Martin del Rio, R., and Solis, J. M., 1984. Dialytrode technology and local profiles of amino acids in the awake cat brain. J Neurochem 42**,** 1218-1228.
34. Delgado, J. M., and Rubinstein, L., 1964. Intracerebral Release of Neurohumors in Unanesthetized Monkeys. Arch Int Pharmacodyn Ther 150**,** 530-546.
35. Dodd, P. R., Hardy, J. A., Oakley, A. E., Edwardson, J. A., Perry, E. K., and Delaunoy, J. P., 1981. A rapid method for preparing synaptosomes: comparison, with alternative procedures. Brain Res 226**,** 107-118.
36. Drucker-Colin, R. R., 1973. Crossed perfusion of a sleep inducing brain tissue substance in conscious cats. Brain Res 56**,** 123-134.
37. Duhaime, A. C., 2006. Large animal models of traumatic injury to the immature brain. Dev Neurosci 28**,** 380-387.
38. Dunkley, P. R., Heath, J. W., Harrison, S. M., Jarvie, P. E., Glenfield, P. J., and Rostas, J. A., 1988. A rapid Percoll gradient procedure for isolation of synaptosomes directly from an S1 fraction: homogeneity and morphology of subcellular fractions. Brain Res 441**,** 59-71.
39. Dunkley, P. R., Jarvie, P. E., Heath, J. W., Kidd, G. J., and Rostas, J. A., 1986. A rapid method for isolation of synaptosomes on Percoll gradients. Brain Res 372**,** 115-129.
40. Dunkley, P. R., Jarvie, P. E., and Robinson, P. J., 2008. A rapid Percoll gradient procedure for preparation of synaptosomes. Nat Protoc 3**,** 1718-1728.
41. Esh, C., Patton, L., Kalback, W., Kokjohn, T. A., Lopez, J., Brune, D., Newell, A. J., Beach, T., Schenk, D., Games, D., Paul, S., Bales, K., Ghetti, B., Castano, E. M., and Roher, A. E., 2005. Altered APP processing in PDAPP (Val717 --> Phe) transgenic mice yields extended-length Abeta peptides. Biochemistry 44**,** 13807-13819.

42. Feany, M. B., Lee, S., Edwards, R. H., and Buckley, K. M., 1992. The synaptic vesicle protein SV2 is a novel type of transmembrane transporter. Cell 70**,** 861-867.
43. Fein, J. A., Sokolow, S., Miller, C. A., Vinters, H. V., Yang, F., Cole, G. M., and Gylys, K. H., 2008. Co-localization of amyloid beta and tau pathology in Alzheimer's disease synaptosomes. Am J Pathol 172**,** 1683-1692.
44. Fleming, L. H., Hodach, A. E., and Reynolds, N. C., 1980. Effects of isolation and incubation on the biochemical and morphological integrity of synaptosomes. Brain Res 202**,** 469-473.
45. Fleminger, S., Oliver, D. L., Lovestone, S., Rabe-Hesketh, S., and Giora, A., 2003. Head injury as a risk factor for Alzheimer's disease: the evidence 10 years on; a partial replication. J Neurol Neurosurg Psychiatry 74**,** 857-862.
46. Fox, G. B., LeVasseur, R. A., and Faden, A. I., 1999. Behavioral responses of C57BL/6, FVB/N, and 129/SvEMS mouse strains to traumatic brain injury: implications for gene targeting approaches to neurotrauma. J Neurotrauma 16**,** 377-389.
47. Fox, R. H., and Hilton, S. M., 1958. Bradykinin formation in human skin as a factor in heat vasodilatation. J Physiol 142**,** 219-232.
48. Franklin, K. B. J., and Paxinos, G., 2001. The mouse brain in stereotaxic coordinates. Elsevier/Academic Press, San Diego; London.
49. French, L. R., Schuman, L. M., Mortimer, J. A., Hutton, J. T., Boatman, R. A., and Christians, B., 1985. A case-control study of dementia of the Alzheimer type. Am J Epidemiol 121**,** 414-421.
50. Fryer, J. D., Simmons, K., Parsadanian, M., Bales, K. R., Paul, S. M., Sullivan, P. M., and Holtzman, D. M., 2005. Human apolipoprotein E4 alters the amyloid-beta 40:42 ratio and promotes the formation of cerebral amyloid angiopathy in an amyloid precursor protein transgenic model. J Neurosci 25**,** 2803-2810.
51. Fujimoto, S. T., Longhi, L., Saatman, K. E., Conte, V., Stocchetti, N., and McIntosh, T. K., 2004. Motor and cognitive function evaluation following experimental traumatic brain injury. Neurosci Biobehav Rev 28**,** 365-378.
52. Gabrieli, J. D., 1998. Cognitive neuroscience of human memory. Annu Rev Psychol 49**,** 87-115.
53. Games, D., Adams, D., Alessandrini, R., Barbour, R., Berthelette, P., Blackwell, C., Carr, T., Clemens, J., Donaldson, T., Gillespie, F., and et al., 1995. Alzheimer-type neuropathology in transgenic mice overexpressing V717F beta-amyloid precursor protein. Nature 373**,** 523-527.
54. Gedye, A., Beattie, B. L., Tuokko, H., Horton, A., and Korsarek, E., 1989. Severe head injury hastens age of onset of Alzheimer's disease. J Am Geriatr Soc 37**,** 970-973.
55. Globus, M. Y., Alonso, O., Dietrich, W. D., Busto, R., and Ginsberg, M. D., 1995. Glutamate release and free radical production following brain injury: effects of posttraumatic hypothermia. J Neurochem 65**,** 1704-1711.

56. Graves, A. B., White, E., Koepsell, T. D., Reifler, B. V., van Belle, G., Larson, E. B., and Raskind, M., 1990. The association between head trauma and Alzheimer's disease. Am J Epidemiol 131**,** 491-501.
57. Gray, E. G., and Whittaker, V. P., 1962. The isolation of nerve endings from brain: an electron-microscopic study of cell fragments derived by homogenization and centrifugation. J Anat 96**,** 79-88.
58. Guo, Z., Cupples, L. A., Kurz, A., Auerbach, S. H., Volicer, L., Chui, H., Green, R. C., Sadovnick, A. D., Duara, R., DeCarli, C., Johnson, K., Go, R. C., Growdon, J. H., Haines, J. L., Kukull, W. A., and Farrer, L. A., 2000. Head injury and the risk of AD in the MIRAGE study. Neurology 54**,** 1316-1323.
59. Gutierrez, C., Bernabe, R. R., Vega, J., and Kreisler, M., 1979. Purification of human T and B cells by a discontinuous density gradient of percoll. J Immunol Methods 29**,** 57-63.
60. Gylys, K. H., Fein, J. A., Yang, F., Miller, C. A., and Cole, G. M., 2007. Increased cholesterol in Abeta-positive nerve terminals from Alzheimer's disease cortex. Neurobiol Aging 28**,** 8-17.
61. Hanrieder, J., Wetterhall, M., Enblad, P., Hillered, L., and Bergquist, J., 2009. Temporally resolved differential proteomic analysis of human ventricular CSF for monitoring traumatic brain injury biomarker candidates. J Neurosci Methods 177**,** 469-478.
62. Harrison, S. M., Jarvie, P. E., and Dunkley, P. R., 1988. A rapid Percoll gradient procedure for isolation of synaptosomes directly from an S1 fraction: viability of subcellular fractions. Brain Res 441**,** 72-80.
63. Hartman, R. E., Laurer, H., Longhi, L., Bales, K. R., Paul, S. M., McIntosh, T. K., and Holtzman, D. M., 2002. Apolipoprotein E4 influences amyloid deposition but not cell loss after traumatic brain injury in a mouse model of Alzheimer's disease. J Neurosci 22**,** 10083-10087.
64. Hartman, R. E., Shah, A., Fagan, A. M., Schwetye, K. E., Parsadanian, M., Schulman, R. N., Finn, M. B., and Holtzman, D. M., 2006. Pomegranate juice decreases amyloid load and improves behavior in a mouse model of Alzheimer's disease. Neurobiol Dis 24**,** 506-515.
65. Headrick, J. P., Bendall, M. R., Faden, A. I., and Vink, R., 1994. Dissociation of adenosine levels from bioenergetic state in experimental brain trauma: potential role in secondary injury. J Cereb Blood Flow Metab 14**,** 853-861.
66. Hebb, C. O., and Whittaker, V. P., 1958. Intracellular distributions of acetylcholine and choline acetylase. J Physiol 142**,** 187-196.
67. Heidelberger, R., 2001. ATP is required at an early step in compensatory endocytosis in synaptic terminals. J Neurosci 21**,** 6467-6474.
68. Helmy, A., Carpenter, K. L., Skepper, J. N., Kirkpatrick, P. J., Pickard, J. D., and Hutchinson, P. J., 2009. Microdialysis of cytokines: methodological considerations, scanning electron microscopy, and determination of relative recovery. J Neurotrauma 26**,** 549-561.

69. Hillered, L., Vespa, P. M., and Hovda, D. A., 2005. Translational neurochemical research in acute human brain injury: the current status and potential future for cerebral microdialysis. J Neurotrauma 22**,** 3-41.
70. Hillman, J., Aneman, O., Anderson, C., Sjogren, F., Saberg, C., and Mellergard, P., 2005. A microdialysis technique for routine measurement of macromolecules in the injured human brain. Neurosurgery 56**,** 1264-1268; discussion 1268-1270.
71. Hillman, J., Aneman, O., Persson, M., Andersson, C., Dabrosin, C., and Mellergard, P., 2007. Variations in the response of interleukins in neurosurgical intensive care patients monitored using intracerebral microdialysis. J Neurosurg 106**,** 820-825.
72. Himanen, L., Portin, R., Isoniemi, H., Helenius, H., Kurki, T., and Tenovuo, O., 2006. Longitudinal cognitive changes in traumatic brain injury: a 30-year follow-up study. Neurology 66**,** 187-192.
73. Holtzman, D. M., Bales, K. R., Tenkova, T., Fagan, A. M., Parsadanian, M., Sartorius, L. J., Mackey, B., Olney, J., McKeel, D., Wozniak, D., and Paul, S. M., 2000. Apolipoprotein E isoform-dependent amyloid deposition and neuritic degeneration in a mouse model of Alzheimer's disease. Proc Natl Acad Sci U S A 97**,** 2892-2897.
74. Hsiao, K., Chapman, P., Nilsen, S., Eckman, C., Harigaya, Y., Younkin, S., Yang, F., and Cole, G., 1996. Correlative memory deficits, Abeta elevation, and amyloid plaques in transgenic mice. Science 274**,** 99-102.
75. Hunt, R. F., Scheff, S. W., and Smith, B. N., 2009. Posttraumatic epilepsy after controlled cortical impact injury in mice. Exp Neurol 215**,** 243-252.
76. Hutchinson, P. J., O'Connell, M. T., Rothwell, N. J., Hopkins, S. J., Nortje, J., Carpenter, K. L., Timofeev, I., Al-Rawi, P. G., Menon, D. K., and Pickard, J. D., 2007. Inflammation in human brain injury: intracerebral concentrations of IL-1alpha, IL-1beta, and their endogenous inhibitor IL-1ra. J Neurotrauma 24**,** 1545-1557.
77. Ikonomovic, M. D., Uryu, K., Abrahamson, E. E., Ciallella, J. R., Trojanowski, J. Q., Lee, V. M., Clark, R. S., Marion, D. W., Wisniewski, S. R., and DeKosky, S. T., 2004. Alzheimer's pathology in human temporal cortex surgically excised after severe brain injury. Exp Neurol 190**,** 192-203.
78. Jacobson, I., Sandberg, M., and Hamberger, A., 1985. Mass transfer in brain dialysis devices--a new method for the estimation of extracellular amino acids concentration. J Neurosci Methods 15**,** 263-268.
79. Janus, C., 2004. Search strategies used by APP transgenic mice during navigation in the Morris water maze. Learn Mem 11**,** 337-346.
80. Jellinger, K. A., 2004. Head injury and dementia. Curr Opin Neurol 17**,** 719-723.
81. Jellinger, K. A., Paulus, W., Wrocklage, C., and Litvan, I., 2001. Traumatic brain injury as a risk factor for Alzheimer disease. Comparison of two retrospective autopsy cohorts with evaluation of ApoE genotype. BMC Neurol 1**,** 3.
82. Jiang, J. Y., Liang, Y. M., Luo, Q. Z., and Zhu, C., 2004. Effect of mild hypothermia on brain dialysate lactate after fluid percussion brain injury in rodents. Neurosurgery 54**,** 713-717; discussion 717-718.

83. Johnson, R. D., and Justice, J. B., 1983. Model studies for brain dialysis. Brain Res Bull 10**,** 567-571.
84. Johnson, V. E., Stewart, W., Stewart, J. E., Graham, D. I., Praestgaard, A. H., and Smith, D. H., 2009. A Neprilysin Polymorphism and Amyloid-beta Plaques Following Traumatic Brain Injury. J Neurotrauma.
85. Kamenetz, F., Tomita, T., Hsieh, H., Seabrook, G., Borchelt, D., Iwatsubo, T., Sisodia, S., and Malinow, R., 2003. APP processing and synaptic function. Neuron 37**,** 925-937.
86. Kang, J. E., Cirrito, J. R., Dong, H., Csernansky, J. G., and Holtzman, D. M., 2007. Acute stress increases interstitial fluid amyloid-beta via corticotropin-releasing factor and neuronal activity. Proc Natl Acad Sci U S A 104**,** 10673-10678.
87. Kang, J. E., Lim, M. M., Bateman, R. J., Lee, J. J., Smyth, L. P., Cirrito, J. R., Fujiki, N., Nishino, S., and Holtzman, D. M., 2009. Amyloid-{beta} Dynamics Are Regulated by Orexin and the Sleep-Wake Cycle. Science.
88. Kesler, S. R., Adams, H. F., Blasey, C. M., and Bigler, E. D., 2003. Premorbid intellectual functioning, education, and brain size in traumatic brain injury: an investigation of the cognitive reserve hypothesis. Appl Neuropsychol 10**,** 153-162.
89. Koizumi, H., Fujisawa, H., Ito, H., Maekawa, T., Di, X., and Bullock, R., 1997. Effects of mild hypothermia on cerebral blood flow-independent changes in cortical extracellular levels of amino acids following contusion trauma in the rat. Brain Res 747**,** 304-312.
90. Krishnappa, I. K., Contant, C. F., and Robertson, C. S., 1999. Regional changes in cerebral extracellular glucose and lactate concentrations following severe cortical impact injury and secondary ischemia in rats. J Neurotrauma 16**,** 213-224.
91. Kurnick, J. T., Ostberg, L., Stegagno, M., Kimura, A. K., Orn, A., and Sjoberg, O., 1979. A rapid method for the separation of functional lymphoid cell populations of human and animal origin on PVP-silica (Percoll) density gradients. Scand J Immunol 10**,** 563-573.
92. Lanz, T. A., Hosley, J. D., Adams, W. J., and Merchant, K. M., 2004. Studies of Abeta pharmacodynamics in the brain, cerebrospinal fluid, and plasma in young (plaque-free) Tg2576 mice using the gamma-secretase inhibitor N2-[(2S)-2-(3,5-difluorophenyl)-2-hydroxyethanoyl]-N1-[(7S)-5-methyl-6-oxo -6,7-dihydro-5H-dibenzo[b,d]azepin-7-yl]-L-alaninamide (LY-411575). J Pharmacol Exp Ther 309**,** 49-55.
93. Launer, L. J., Andersen, K., Dewey, M. E., Letenneur, L., Ott, A., Amaducci, L. A., Brayne, C., Copeland, J. R., Dartigues, J. F., Kragh-Sorensen, P., Lobo, A., Martinez-Lage, J. M., Stijnen, T., and Hofman, A., 1999. Rates and risk factors for dementia and Alzheimer's disease: results from EURODEM pooled analyses. EURODEM Incidence Research Group and Work Groups. European Studies of Dementia. Neurology 52**,** 78-84.
94. Leon-Carrion, J., 2002. Dementia Due to Head Trauma: An obscure name for a clear neurocognitive syndrome. NeuroRehabilitation 17**,** 115-122.

95. Lewin, W., Marshall, T. F., and Roberts, A. H., 1979. Long-term outcome after severe head injury. Br Med J 2**,** 1533-1538.
96. Loane, D. J., Pocivavsek, A., Moussa, C. E., Thompson, R., Matsuoka, Y., Faden, A. I., Rebeck, G. W., and Burns, M. P., 2009. Amyloid precursor protein secretases as therapeutic targets for traumatic brain injury. Nat Med.
97. Loosemore, M., Knowles, C. H., and Whyte, G. P., 2007. Amateur boxing and risk of chronic traumatic brain injury: systematic review of observational studies. Bmj 335**,** 809.
98. Luukinen, H., Viramo, P., Herala, M., Kervinen, K., Kesaniemi, Y. A., Savola, O., Winqvist, S., Jokelainen, J., and Hillbom, M., 2005. Fall-related brain injuries and the risk of dementia in elderly people: a population-based study. Eur J Neurol 12**,** 86-92.
99. Lye, T. C., and Shores, E. A., 2000. Traumatic brain injury as a risk factor for Alzheimer's disease: a review. Neuropsychol Rev 10**,** 115-129.
100. Mac Donald, C. L., Dikranian, K., Song, S. K., Bayly, P. V., Holtzman, D. M., and Brody, D. L., 2007. Detection of traumatic axonal injury with diffusion tensor imaging in a mouse model of traumatic brain injury. Exp Neurol 205**,** 116-131.
101. Magnoni, S., Carbonara, M., Guenzani, S., Paternò, R., Carrabba, G., Esparza, T.J., Spinner, M.L., Holtzman, D.M., Stocchetti, N., Brody, D.L., 2009. Inverse relationship between Aβ and tau in the extracellular space of the injured human brain. High tau levels may reflect injury, whereas Aβ dynamics correlates with neurological status, Second Joint Symposium of the International and National Neurotrauma Societies. Mary Ann Liebert, Santa Barbara, CA, US.
102. Manley, G. T., Rosenthal, G., Lam, M., Morabito, D., Yan, D., Derugin, N., Bollen, A., Knudson, M. M., and Panter, S. S., 2006. Controlled cortical impact in swine: pathophysiology and biomechanics. J Neurotrauma 23**,** 128-139.
103. Marklund, N., Blennow, K., Zetterberg, H., Ronne-Engstrom, E., Enblad, P., and Hillered, L., 2009. Monitoring of brain interstitial total tau and beta amyloid proteins by microdialysis in patients with traumatic brain injury. J Neurosurg.
104. Marklund, N., Clausen, F., Lewander, T., and Hillered, L., 2001. Monitoring of reactive oxygen species production after traumatic brain injury in rats with microdialysis and the 4-hydroxybenzoic acid trapping method. J Neurotrauma 18**,** 1217-1227.
105. Marklund, N., Lewander, T., Clausen, F., and Hillered, L., 2001. Effects of the nitrone radical scavengers PBN and S-PBN on in vivo trapping of reactive oxygen species after traumatic brain injury in rats. J Cereb Blood Flow Metab 21**,** 1259-1267.
106. Marklund, N., Salci, K., Lewen, A., and Hillered, L., 1997. Glycerol as a marker for post-traumatic membrane phospholipid degradation in rat brain. Neuroreport 8**,** 1457-1461.
107. Mayeux, R., Ottman, R., Maestre, G., Ngai, C., Tang, M. X., Ginsberg, H., Chun, M., Tycko, B., and Shelanski, M., 1995. Synergistic effects of traumatic head injury and apolipoprotein-epsilon 4 in patients with Alzheimer's disease. Neurology 45**,** 555-557.

108. Mayeux, R., Ottman, R., Tang, M. X., Noboa-Bauza, L., Marder, K., Gurland, B., and Stern, Y., 1993. Genetic susceptibility and head injury as risk factors for Alzheimer's disease among community-dwelling elderly persons and their first-degree relatives. Ann Neurol 33**,** 494-501.
109. McLennan, H., 1964. The Release of Acetylcholine and of 3-Hydroxytyramine from the Caudate Nucleus. J Physiol 174**,** 152-156.
110. McMurtray, A., Clark, D. G., Christine, D., and Mendez, M. F., 2006. Early-onset dementia: frequency and causes compared to late-onset dementia. Dement Geriatr Cogn Disord 21**,** 59-64.
111. Mehta, K. M., Ott, A., Kalmijn, S., Slooter, A. J., van Duijn, C. M., Hofman, A., and Breteler, M. M., 1999. Head trauma and risk of dementia and Alzheimer's disease: The Rotterdam Study. Neurology 53**,** 1959-1962.
112. Mellergard, P., Aneman, O., Sjogren, F., Pettersson, P., and Hillman, J., 2008. Changes in extracellular concentrations of some cytokines, chemokines, and neurotrophic factors after insertion of intracerebral microdialysis catheters in neurosurgical patients. Neurosurgery 62**,** 151-157; discussion 157-158.
113. Menacherry, S., Hubert, W., and Justice, J. B., Jr., 1992. In vivo calibration of microdialysis probes for exogenous compounds. Anal Chem 64**,** 577-583.
114. Mizumori, S. J., Yeshenko, O., Gill, K. M., and Davis, D. M., 2004. Parallel processing across neural systems: implications for a multiple memory system hypothesis. Neurobiol Learn Mem 82**,** 278-298.
115. Morales, D. M., Marklund, N., Lebold, D., Thompson, H. J., Pitkanen, A., Maxwell, W. L., Longhi, L., Laurer, H., Maegele, M., Neugebauer, E., Graham, D. I., Stocchetti, N., and McIntosh, T. K., 2005. Experimental models of traumatic brain injury: do we really need to build a better mousetrap? Neuroscience 136**,** 971-989.
116. Morris, R. G., Garrud, P., Rawlins, J. N., and O'Keefe, J., 1982. Place navigation impaired in rats with hippocampal lesions. Nature 297**,** 681-683.
117. Mortimer, J. A., French, L. R., Hutton, J. T., and Schuman, L. M., 1985. Head injury as a risk factor for Alzheimer's disease. Neurology 35**,** 264-267.
118. Mortimer, J. A., van Duijn, C. M., Chandra, V., Fratiglioni, L., Graves, A. B., Heyman, A., Jorm, A. F., Kokmen, E., Kondo, K., Rocca, W. A., and et al., 1991. Head trauma as a risk factor for Alzheimer's disease: a collaborative re-analysis of case-control studies. EURODEM Risk Factors Research Group. Int J Epidemiol 20 Suppl 2**,** S28-35.
119. Myers, R. D., 1986. Development of push-pull systems for perfusion of anatomically distinct regions of the brain of the awake animal. Ann N Y Acad Sci 473**,** 21-41.
120. Myers, R. D., Adell, A., and Lankford, M. F., 1998. Simultaneous comparison of cerebral dialysis and push-pull perfusion in the brain of rats: a critical review. Neurosci Biobehav Rev 22**,** 371-387.
121. Nakagawa, Y., Nakamura, M., McIntosh, T. K., Rodriguez, A., Berlin, J. A., Smith, D. H., Saatman, K. E., Raghupathi, R., Clemens, J., Saido, T. C., Schmidt, M. L., Lee, V. M., and Trojanowski, J. Q., 1999. Traumatic brain injury in young,

amyloid-beta peptide overexpressing transgenic mice induces marked ipsilateral hippocampal atrophy and diminished Abeta deposition during aging. J Comp Neurol 411**,** 390-398.

122. Nakagawa, Y., Reed, L., Nakamura, M., McIntosh, T. K., Smith, D. H., Saatman, K. E., Raghupathi, R., Clemens, J., Saido, T. C., Lee, V. M., and Trojanowski, J. Q., 2000. Brain trauma in aged transgenic mice induces regression of established abeta deposits. Exp Neurol 163**,** 244-252.
123. Nakamura, M., Saatman, K. E., Galvin, J. E., Scherbel, U., Raghupathi, R., Trojanowski, J. Q., and McIntosh, T. K., 1999. Increased vulnerability of NFH-LacZ transgenic mouse to traumatic brain injury-induced behavioral deficits and cortical damage. J Cereb Blood Flow Metab 19**,** 762-770.
124. Nelson, P. T., Braak, H., and Markesbery, W. R., 2009. Neuropathology and cognitive impairment in Alzheimer disease: a complex but coherent relationship. J Neuropathol Exp Neurol 68**,** 1-14.
125. Nemetz, P. N., Leibson, C., Naessens, J. M., Beard, M., Kokmen, E., Annegers, J. F., and Kurland, L. T., 1999. Traumatic brain injury and time to onset of Alzheimer's disease: a population-based study. Am J Epidemiol 149**,** 32-40.
126. Nilsson, P., Ronne-Engstrom, E., Flink, R., Ungerstedt, U., Carlson, H., and Hillered, L., 1994. Epileptic seizure activity in the acute phase following cortical impact trauma in rat. Brain Res 637**,** 227-232.
127. O'Keefe, J., and Dostrovsky, J., 1971. The hippocampus as a spatial map. Preliminary evidence from unit activity in the freely-moving rat. Brain Res 34**,** 171-175.
128. Oddo, S., Caccamo, A., Shepherd, J. D., Murphy, M. P., Golde, T. E., Kayed, R., Metherate, R., Mattson, M. P., Akbari, Y., and LaFerla, F. M., 2003. Triple-transgenic model of Alzheimer's disease with plaques and tangles: intracellular Abeta and synaptic dysfunction. Neuron 39**,** 409-421.
129. Ost, M., Nylen, K., Csajbok, L., Ohrfelt, A. O., Tullberg, M., Wikkelso, C., Nellgard, P., Rosengren, L., Blennow, K., and Nellgard, B., 2006. Initial CSF total tau correlates with 1-year outcome in patients with traumatic brain injury. Neurology 67**,** 1600-1604.
130. Ottens, A. K., Kobeissy, F. H., Fuller, B. F., Liu, M. C., Oli, M. W., Hayes, R. L., and Wang, K. K., 2007. Novel neuroproteomic approaches to studying traumatic brain injury. Prog Brain Res 161**,** 401-418.
131. Ouseph, R., Hutchison, C. A., and Ward, R. A., 2008. Differences in solute removal by two high-flux membranes of nominally similar synthetic polymers. Nephrol Dial Transplant 23**,** 1704-1712.
132. Palmer, A. M., Marion, D. W., Botscheller, M. L., Swedlow, P. E., Styren, S. D., and DeKosky, S. T., 1993. Traumatic brain injury-induced excitotoxicity assessed in a controlled cortical impact model. J Neurochem 61**,** 2015-2024.
133. Paul, C. M., Magda, G., and Abel, S., 2009. Spatial memory: Theoretical basis and comparative review on experimental methods in rodents. Behav Brain Res 203**,** 151-164.

134. Pertoft, H., 2000. Fractionation of cells and subcellular particles with Percoll. J Biochem Biophys Methods 44**,** 1-30.
135. Plassman, B. L., Havlik, R. J., Steffens, D. C., Helms, M. J., Newman, T. N., Drosdick, D., Phillips, C., Gau, B. A., Welsh-Bohmer, K. A., Burke, J. R., Guralnik, J. M., and Breitner, J. C., 2000. Documented head injury in early adulthood and risk of Alzheimer's disease and other dementias. Neurology 55**,** 1158-1166.
136. Prieto, D. A., Ye, X., and Veenstra, T. D., 2008. Proteomic analysis of traumatic brain injury: the search for biomarkers. Expert Rev Proteomics 5**,** 283-291.
137. Rasmusson, D. X., Brandt, J., Martin, D. B., and Folstein, M. F., 1995. Head injury as a risk factor in Alzheimer's disease. Brain Inj 9**,** 213-219.
138. Rennie, C. M., Thompson, S., Parker, A. C., and Maddy, A., 1979. Human erythrocyte fraction in "Percoll" density gradients. Clin Chim Acta 98**,** 119-125.
139. Roberts, G. W., Gentleman, S. M., Lynch, A., Murray, L., Landon, M., and Graham, D. I., 1994. Beta amyloid protein deposition in the brain after severe head injury: implications for the pathogenesis of Alzheimer's disease. J Neurol Neurosurg Psychiatry 57**,** 419-425.
140. Ronne-Engstrom, E., Cesarini, K. G., Enblad, P., Hesselager, G., Marklund, N., Nilsson, P., Salci, K., Persson, L., and Hillered, L., 2001. Intracerebral microdialysis in neurointensive care: the use of urea as an endogenous reference compound. J Neurosurg 94**,** 397-402.
141. Rose, M. E., Huerbin, M. B., Melick, J., Marion, D. W., Palmer, A. M., Schiding, J. K., Kochanek, P. M., and Graham, S. H., 2002. Regulation of interstitial excitatory amino acid concentrations after cortical contusion injury. Brain Res 943**,** 15-22.
142. Rosenbloom, A. J., Sipe, D. M., and Weedn, V. W., 2005. Microdialysis of proteins: performance of the CMA/20 probe. J Neurosci Methods 148**,** 147-153.
143. Saatman, K. E., Feeko, K. J., Pape, R. L., and Raghupathi, R., 2006. Differential behavioral and histopathological responses to graded cortical impact injury in mice. J Neurotrauma 23**,** 1241-1253.
144. Salib, E., and Hillier, V., 1997. Head injury and the risk of Alzheimer's disease: a case control study. Int J Geriatr Psychiatry 12**,** 363-368.
145. Sasahara, M., Fries, J. W., Raines, E. W., Gown, A. M., Westrum, L. E., Frosch, M. P., Bonthron, D. T., Ross, R., and Collins, T., 1991. PDGF B-chain in neurons of the central nervous system, posterior pituitary, and in a transgenic model. Cell 64**,** 217-227.
146. Scherbel, U., Raghupathi, R., Nakamura, M., Saatman, K. E., Trojanowski, J. Q., Neugebauer, E., Marino, M. W., and McIntosh, T. K., 1999. Differential acute and chronic responses of tumor necrosis factor-deficient mice to experimental brain injury. Proc Natl Acad Sci U S A 96**,** 8721-8726.
147. Schofield, P. W., Tang, M., Marder, K., Bell, K., Dooneief, G., Chun, M., Sano, M., Stern, Y., and Mayeux, R., 1997. Alzheimer's disease after remote head injury: an incidence study. J Neurol Neurosurg Psychiatry 62**,** 119-124.

148. Siman, R., Toraskar, N., Dang, A., McNeil, E., McGarvey, M., Plaum, J., Maloney, E., and Grady, M. S., 2009. A Panel of Neuron-Enriched Proteins as Markers for Traumatic Brain Injury in Humans. J Neurotrauma.
149. Sinz, E. H., Kochanek, P. M., Dixon, C. E., Clark, R. S., Carcillo, J. A., Schiding, J. K., Chen, M., Wisniewski, S. R., Carlos, T. M., Williams, D., DeKosky, S. T., Watkins, S. C., Marion, D. W., and Billiar, T. R., 1999. Inducible nitric oxide synthase is an endogenous neuroprotectant after traumatic brain injury in rats and mice. J Clin Invest 104**,** 647-656.
150. Sjogren, F., Svensson, C., and Anderson, C., 2002. Technical prerequisites for in vivo microdialysis determination of interleukin-6 in human dermis. Br J Dermatol 146**,** 375-382.
151. Smith, D. H., Chen, X. H., Iwata, A., and Graham, D. I., 2003. Amyloid beta accumulation in axons after traumatic brain injury in humans. J Neurosurg 98**,** 1072-1077.
152. Smith, D. H., Chen, X. H., Nonaka, M., Trojanowski, J. Q., Lee, V. M., Saatman, K. E., Leoni, M. J., Xu, B. N., Wolf, J. A., and Meaney, D. F., 1999. Accumulation of amyloid beta and tau and the formation of neurofilament inclusions following diffuse brain injury in the pig. J Neuropathol Exp Neurol 58**,** 982-992.
153. Smith, D. H., Chen, X. H., Xu, B. N., McIntosh, T. K., Gennarelli, T. A., and Meaney, D. F., 1997. Characterization of diffuse axonal pathology and selective hippocampal damage following inertial brain trauma in the pig. J Neuropathol Exp Neurol 56**,** 822-834.
154. Smith, D. H., Nakamura, M., McIntosh, T. K., Wang, J., Rodriguez, A., Chen, X. H., Raghupathi, R., Saatman, K. E., Clemens, J., Schmidt, M. L., Lee, V. M., and Trojanowski, J. Q., 1998. Brain trauma induces massive hippocampal neuron death linked to a surge in beta-amyloid levels in mice overexpressing mutant amyloid precursor protein. Am J Pathol 153**,** 1005-1010.
155. Smith, D. H., Nonaka, M., Miller, R., Leoni, M., Chen, X. H., Alsop, D., and Meaney, D. F., 2000. Immediate coma following inertial brain injury dependent on axonal damage in the brainstem. J Neurosurg 93**,** 315-322.
156. Smith, D. H., Soares, H. D., Pierce, J. S., Perlman, K. G., Saatman, K. E., Meaney, D. F., Dixon, C. E., and McIntosh, T. K., 1995. A model of parasagittal controlled cortical impact in the mouse: cognitive and histopathologic effects. J Neurotrauma 12**,** 169-178.
157. Stern, Y., 2009. Cognitive reserve. Neuropsychologia 47**,** 2015-2028.
158. Stover, J. F., Sakowitz, O. W., Beyer, T. F., Dohse, N. K., Kroppenstedt, S. N., Thomale, U. W., Schaser, K. D., and Unterberg, A. W., 2003. Effects of LY379268, a selective group II metabotropic glutamate receptor agonist on EEG activity, cortical perfusion, tissue damage, and cortical glutamate, glucose, and lactate levels in brain-injured rats. J Neurotrauma 20**,** 315-326.
159. Strittmatter, W. J., Saunders, A. M., Schmechel, D., Pericak-Vance, M., Enghild, J., Salvesen, G. S., and Roses, A. D., 1993. Apolipoprotein E: high-avidity

binding to beta-amyloid and increased frequency of type 4 allele in late-onset familial Alzheimer disease. Proc Natl Acad Sci U S A 90**,** 1977-1981.
160. Sullivan, P. G., Keller, J. N., Mattson, M. P., and Scheff, S. W., 1998. Traumatic brain injury alters synaptic homeostasis: implications for impaired mitochondrial and transport function. J Neurotrauma 15**,** 789-798.
161. Takahashi, R. H., Capetillo-Zarate, E., Lin, M. T., Milner, T. A., and Gouras, G. K., 2008. Co-occurrence of Alzheimer's disease beta-amyloid and tau pathologies at synapses. Neurobiol Aging.
162. Ulmer, A. J., and Flad, H. D., 1979. Discontinuous density gradient separation of human mononuclear leucocytes using Percoll as gradient medium. J Immunol Methods 30**,** 1-10.
163. Ungerstedt, U., and Pycock, C., 1974. Functional correlates of dopamine neurotransmission. Bull Schweiz Akad Med Wiss 30**,** 44-55.
164. Uryu, K., Laurer, H., McIntosh, T., Pratico, D., Martinez, D., Leight, S., Lee, V. M., and Trojanowski, J. Q., 2002. Repetitive mild brain trauma accelerates Abeta deposition, lipid peroxidation, and cognitive impairment in a transgenic mouse model of Alzheimer amyloidosis. J Neurosci 22**,** 446-454.
165. Vakil, E., 2005. The effect of moderate to severe traumatic brain injury (TBI) on different aspects of memory: a selective review. J Clin Exp Neuropsychol 27**,** 977-1021.
166. Van Den Heuvel, C., Thornton, E., and Vink, R., 2007. Traumatic brain injury and Alzheimer's disease: a review. Prog Brain Res 161**,** 303-316.
167. Whittaker, V. P., 1993. Thirty years of synaptosome research. J Neurocytol 22**,** 735-742.
168. Williams, D. B., Annegers, J. F., Kokmen, E., O'Brien, P. C., and Kurland, L. T., 1991. Brain injury and neurologic sequelae: a cohort study of dementia, parkinsonism, and amyotrophic lateral sclerosis. Neurology 41**,** 1554-1557.
169. Winter, C. D., Iannotti, F., Pringle, A. K., Trikkas, C., Clough, G. F., and Church, M. K., 2002. A microdialysis method for the recovery of IL-1beta, IL-6 and nerve growth factor from human brain in vivo. J Neurosci Methods 119**,** 45-50.
170. Winter, C. D., Pringle, A. K., Clough, G. F., and Church, M. K., 2004. Raised parenchymal interleukin-6 levels correlate with improved outcome after traumatic brain injury. Brain 127**,** 315-320.
171. Xu, P. T., Schmechel, D., Rothrock-Christian, T., Burkhart, D. S., Qiu, H. L., Popko, B., Sullivan, P., Maeda, N., Saunders, A. M., Roses, A. D., and Gilbert, J. R., 1996. Human apolipoprotein E2, E3, and E4 isoform-specific transgenic mice: human-like pattern of glial and neuronal immunoreactivity in central nervous system not observed in wild-type mice. Neurobiol Dis 3**,** 229-245.
172. Yaksh, T. L., and Myers, R. D., 1972. Neurohumoral substances released from hypothalamus of the monkey during hunger and satiety. Am J Physiol 222**,** 503-515.
173. Yaksh, T. L., and Yamamura, H. I., 1974. Factors affecting performance of the push-pull cannula in brain. J Appl Physiol 37**,** 428-434.

174. Yoshiyama, Y., Uryu, K., Higuchi, M., Longhi, L., Hoover, R., Fujimoto, S., McIntosh, T., Lee, V. M., and Trojanowski, J. Q., 2005. Enhanced neurofibrillary tangle formation, cerebral atrophy, and cognitive deficits induced by repetitive mild brain injury in a transgenic tauopathy mouse model. J Neurotrauma 22**,** 1134-1141.

APPENDIX 1.

Combined microdialysis-controlled cortical impact protocol

TBI + Microdialysis protocol sheet From the RIGHT, impact on the LEFT
Investigator _____ Date _____Experiment _____
Mouse strain ___ _ Genotype: _____ Sex ____ Weight (g)____ **Toe clip # _____**
Retrieve mouse from animal facility 6-24 hours before to acclimate to surgery room.

SET-UP Day 1:
Make **0.15% human albumin**-CMA perfusion fluid (30 uL 25% hAlb in 5 mL CMA)
Tubing connectors in 100% EtOH, 5-10 min
Syringe pump settings: 51.7 mm length for 3 cc Luer-slip syringe.
Wash 0.12 mm FEP tubing + BR-2 probe in **CMA + 0.15% hAlb** @ 3 µl/min x 10'
Put **BR-2** on holder, *flush* with hAlb/CMA according to instructions.
Put guide cannula on holder on 23 cm arm, tighten.
Right arm: drill w/burr bit, 0° switch to 23 cm arm for guide canula insertion at **37.6°**
Cut ring off top of 1.5 mL test tube, cut out ~150-180° to slip around screws
Assemble: 2 large weigh boats for DuraLay, bone screws, suture, extra plastic rings, etc.
Bead-sterilize tools. Turn on stereotactic, lights, temp.

CRANIOTOMY and GUIDE CANULA PLACEMENT: Day 1
Induce Anesthesia: isoflurane 5%: time _____ (**valve open to induction ONLY**)
Shake to assess depth of anesthesia: if no response, **turn to 2%, valve open to nosecone**
Clear tongue, position on tooth bar
Insert temperature probe ____ record time _____
Shave head gently, protect airway, align earbars *(head adjuster on left)*, tighten; clean
Level skull: Bregma ___ Lambda ___bregma -2.54 mm: 2.2 mm L ____, 2.2 mm R_____
Mark 3.8 mm crani: (**1.1 Ant of lamba, 3.6 L); (3 Ant of lamba, 1.7 L**).
Drill groove at Bregma -2.54 mm: 0.0 mm, 0.5 mm L, 0.3 above/below at 0.5 mm L of groove, 1.0 mm L (0.2 mm above/below 1.0 mm L also helps)
**Shiny tissue MUST be visible for clean probe insertion.*
Drill 3 holes for bone screws: (-0.75 Ant, 1 R); (-0.75 Ant, 3 R); (-3.75 Ant, 3 R).
Insert small bone anchor screws – flat (BAS)
Using 3.8 mm trephine: crani drill at 15-20° or greater; drill skull.
Check depth frequently. Use curette and rongeur to remove flap.
Remove arm with drill to improve visualization of landmarks & guide canula.
Vet-Bond modified skull cap. Leave groove fully open!
Remove drill, replace with clamp on 23 cm arm.
Insert guide canula at **37.6°** (38°) into Left hippocampus at bregma -2.54 mm:
Right edge at ***0.5 mm left of midline***, touch to brain tissue
Zero D-V, lower **to -1.3 mm** slowly.
*Watch for slipping/grinding of the canula on skull edges. DRY SKULL well.
Position plastic ring around screws; clear skin away, drape on ring edge.
Mix DuraLay powder/solvent: very liquid at first so that it pours, "soupy"
Hold ring flush against screws as needed; allow cement to harden, ~10-15 min.
Out of earbars, loosen nosecone to allow ***free head rotation***
Unscrew canula holder, take off arm.

Suture posterior skin, take out of frame, suture anterior skin, antibiotic ointment.
Secure canula w/ needle drivers, stabilize lateral wrist on small white box:
Pull stylet out (NO twisting!); look for hole, carefully insert probe.
Attach orange collar and black RatTurn "leash;" **drape mouse gently in Rat Turn**
Pump at 1.5 µl/min, wait for dead volume to clear (12µl/m – measure tube length)
Start baseline: ____ min fractions at _____ µl/min. Time started ____
Check 1st, 2nd fractions to ensure equal volumes; **2x/day, refresh H_2O, sharp pellets**

SET-UP 2: allow t ≥ 30 min
Equip stereotactic arms: Left: EM CCI, 20°
Assemble: suture, skull cap trimmed to indent for DuraLay.
Check that all tools are clean and ready. Turn on stereotactic, lights, temp. probe.
Turn on computer, EM CCI power, then Cntl-Alt-Del: pass = Qwer1234;
Matlab: "main," "3," **Velocity: 7 V for 5 m/s,** dwell 100 ms. Test impact.
Return to "main," "3," STOP at "position impact at reference depth."
Cut a plastic disk to make a modified skull cap (tongue-and-groove to fit with glue).

TBI: Day 2
Reanesthetize isoflurane 5%, lines still attached. Time _____
Record Baseline Temp _____ and record time _____
Eye protectant, cut sutures, in earbars.
Position head: use eyes to align in ear bars. Top of ear bar = lower canthus. Raise incisor bar as needed.
Position impactor tip in dead center of 3.8 mm crani.
Dry impactor tip, dry brain, clip touch detector to impactor tip, pad under paw, turn on touch detector
Lower Z-axis to touch brain (singing detector); remove alligator clip, paw pad.
Press "enter" to pull the EM impactor up to ready position
SET INJURY SEVERITY: lower Z axis to -____ mm or SHAM____
Stabilize wrist on small white box, grip guide w/ needle driver, pull probe STRAIGHT out 2 mm
Hold probe poised in hand, drop needle driver, reach over, press "enter" to deliver impact: time _____
Note breathing – remove isoflurane, loosen from earbars if necessary.
Stabilize wrist on small white box, grip guide w/ needle driver, look for hole, replace probe carefully.
Raise Z-axis up to clear field. Irrigate with PBS if bleeding; dry with swabs, hemostasis with swabs.
Vet-Bond modified skull cap, suture, turn off isoflurane & thermo controller. Antibiotic, eye protectant.
Weigh mouse _____ g
Return to Raturn. Wait _8-10_min for dead volume to clear, advance fraction collector.
Restart dialysis: ____ minute fractions. Fraction #s _____ Time started _____

APPENDIX 2.

Manufacture of guide canula with EEG leads, EEG monitoring, and analysis

Instructions and troubleshooting guide: intraparenchymal EEG and microdialysis

Manufacture equipment:

a. MD-2250 guide canula (or other appropriate canula)
b. Teflon-coated, platinum-iridium wire (A-M Systems, #777000)
    - Outer diameter 0.0055" (coated), inner diameter 0.003" (bare)
c. Exacto scalpel + #10 blade
d. Elmer's Super-Fast Epoxy & Resin, 200 uL tip, weigh boats to mix
e. 1 bone screw (Bioanalytical Systems MD-1310)
f. 3-pin strip header (Newark-In-One, Mfr. #929647-01-36-I)
    - 0.1" pit spacing
    - Copper alloy contact material
    - Gold plated
g. Solder
    - Radioshack #64-002E, Standard Rosin Core Solder, 0.062" diam.
h. Soldering iron
    - Radioshack #64-2802B, ***30 Watt****, 120 V, 60 Hz
i. Stay Clean tinning flux
h. fine, flat-tipped FST forceps (2 pair), small Roboz RS7107 hemostat

*** 30W is key to getting a fast "melt" on your solder for good contact; irons with less power than 30W do not melt solder very well and harder to get good contact**

I. Manufacture
    a. Preparation of electrodes
        i. Cut off 3 strands of Teflon-coated platinum-iridium wire from roll with Exacto knife on black lab bench
        ii. 2 for recording (~4 cm long), 1 for ground (~6 cm long)
        iii. <u>Recording leads:</u> using Exacto knife, scrape off layer of Teflon such that > 0.5 mm of bare metal is exposed from ONE end
        iv. These ends will be soldered to the prongs on 3-prong plug
        v. You might see "sheaths" of plastic-appearing Teflon peel back from bare wire; cut these scraps off
        vi. Bare metal is shiny, and skinnier than dull-appearing coated wire
        vii. Other end: leave blunt for now; these are inserted and will be cut on diagonal just before implantation
        viii. <u>Ground:</u> scrape off Teflon from both ends; one end is soldered to ground screw, the other end to a prong on 3-prong plug
    b. Adhesion of recording leads to guide canula
        i. Using flat forceps, bend recording leads at a 90º angle so scraped/soldered end is ~1.5 cm, inserted/blunt end is ~2.5 cm

ii. Mix Elmer's epoxy-cement in 1:1 ratio (enough just to cover guide canula shaft) just before ready to attach wires
iii. Epoxy tends to begin drying immediately, use within 2-3 min. of mixing together
iv. Grip guide canula with small hemostat; balance hemostat handle off end of tip box so canula shaft extends parallel to, over bench
v. Attach the longer (2.5 cm), blunt-tip end to guide canula shaft; leave AT LEAST 2 mm end free to allow insertion through skull groove into parenchyma, and to prevent epoxy from clogging shaft
vi. **NOTE**: epoxy tends to run or drip off canula if too wet or too much; be sparing in application.
vii. **VERY IMPORTANT:** leads must be parallel to and at 180º around shaft circumference from one another, ~0.5 mm apart
viii. Allow 1st epoxy application to dry ~15 min, and reinforce with 2nd application.

c. Soldering ground electrode to bone screw and 3-prong plug
i. While 2nd application of epoxy on guide canula-recording leads dries, prepare ground screw for soldering (MD-1310, BAS Inc.)
ii. Grip flat screw head with spring-loaded clamp, place on tip box so threaded end extends over bench
iii. **IMPORTANT:** apply tinning flux to threaded end to clean before attempting to solder; only enough tinning flux to coat, remove excess by pulling back on syringe
iv. Curl one, bare-stripped end of ground electrode in half-circumference to fit around top thread of bone screw
v. Drape curled end on thread so electrode hangs off; apply small pearl of tin solder
vi. Make sure to avoid getting tin a) in groove on head; b) along bottom threads.
vii. **VERY IMPORTANT**: when screwing the ground screw into bone, the electrode sometimes breaks off at junction of tin solder; make sure this is well adhered and that most of the bared end is covered by solder. If not, insulate and strengthen with epoxy.
viii. Solder other bared end to 1 (outside) prong on 3-prong plug; grip black plastic of plug with spring-loaded clamp, lay flat on tip box, extend plug over benchtop
ix. Mark long side of prong with Black Sharpie: designates GROUND
x. Clean short prong with tinning flux, curl or bend other (bared) end of ground electrode around short prong; apply pearl of tin solder
xi. Again – make sure most of bared end is covered by solder; if not, insulate with epoxy.

d. Soldering recording leads to 3 prong plug

i. Once 2nd application of epoxy is dry, secure guide canula stylet head in hemostat, balance handles on tip box with canula extending out over bench
ii. Rotate canula such that bared ends of leads face 3-prong plug (also extending out over bench, gripped with spring-loaded device
iii. Clean short prongs with tinning flux just before application of tin solder
iv. Curl bared ends or allow them to "grip" prongs before attempting to apply pearl of solder
v. Ensure bare wire is covered in solder, or apply epoxy for insulation after solder hardens
vi. **IMPORTANT NOTES**: solder can be applied once or twice, but multiple applications and removals compromise electrical contact between metal prong and bare wire. Avoid this. If wire appears compromised, dirty, oxidized, etc., cut off, scrape off more Teflon, and start over. **ALWAYS apply tinning flux** just before every solder attempt.
vii. **Finally, cut off recording leads** at the blunt or "insertion end" **at 45º angle** to increase surface area. They should **extend 2 mm past end of guide canula shaft**. This will place recording electrodes at end of microdialysis probe. Do not make too short (records from cortex rather than hippocampus) or too long (could puncture lateral ventricle). Do not bend – must remain as straight as possible. Cirrito et al. attempted to use stainless steel wire, but was too flexible so switched to a stiffer platinum-iridium wire.

II. Surgery
a. Drilling groove for canula insertion; dural puncture
i. SAME as normal 38º microdialysis-CCI procedure: after leveling skull, drill groove at 3 locations medial-lateral (0, 0.5, 1 mm left-lateral at -2.54 Bregma along A-P axis); use 0.70 mm burr bit
ii. Additionally, allow for increased width of canula + electrodes: drill anterior and posterior ~0.4 mm (for example, -2.14 mm Bregma and 2.98 mm Bregma) at 0.5 and 1.0 mm lateral to midline
iii. Clear groove of bone chip debris, irrigate with sterile-filtered PBS, ensure dura is visualized
b. Placement of ground (occipital/cerebellar bone screw anchor)
i. Drill an additional hole on RIGHT lateral occipital bone above cerebellum. This bone screw is larger than anchors, so increase circumference by slightly shifting burr bit ("mini-groove"). This bone is deep at this angle.
ii. **VERY IMPORTANT**: ***a secure ground screw is the KEY to a good signal. Drill deep so the bone screw is well-anchored!***

iii. Next, drill craniotomy, place skull cap, screw in 3 cortical bone anchors as usual for simple microdialysis-CCI procedure
iv. Align canula+electrodes on stereotactic arm at 38º; lower enough so that ground screw is within reach of occipital groove.
v. Screw in ground screw until secure (1-2 rotations). Take care not to break off electrode wire. It will twist around the ground screw, this is normal.
vi. **NOTE**: I have done "spot repair" to solder a ground lead back in pace during surgery; this sometimes works but is not optimal.

c. Insertion of canula-electrodes into groove
    i. Once ground screw is secure, carefully lower canual+electrodes through left-lateral groove. **Electrodes should enter dura & parenchyma easily, without resistance, and straight!** No bending allowed. Some bleeding may occur more than with canula alone. This is normal. Dab and allow clotting to occur, it will subside once canula is inserted to full depth (1.3 mm).
d. Dental cement as insulator
    i. Building a dental cement crown is more challenging in this procedure, as you must **wrap the excess wire** around the crown and **"bury" it within the dental cement**. Take care to ***cover the ground-screw area very well,*** to both secure the screw and **insulate any bare wire** that might be exposed.
    ii. The long prongs on the 3-prong plug should sit at a 50-60º angle relative to the plane of the skull, the more vertical the better. Wipe any excess cement off the prongs for good electrical contact.
    iii. Allow dental cement to dry ~15 min. Make sure it has hardened before suturing.
e. Skin closure
    i. Close skin well, the crown is larger and somewhat irregular compared to a crown without EEG leads.

III. Monitoring during microdialysis
a. Equipment: head stage amplifier, Grass amplifier, Mini-Digitizer, PC
    i. ***PLUG IN YOUR MOUSE***: be **very gentle when plugging in the 3-prong strip into its small black receptacle**. This is easiest when **mouse is still anesthetized**. If the mouse is fighting or tossing its head, especially when just awakening from anesthesia, you risk breaking off the crown. Make sure mouse is still KO'd.
    ii. Electrical noise in the room can vary. Sometimes the signal can pick up noise (ex., 60 Hz signal) from the surroundings and then appear more physiological; it is hard to predict when this is the case. Sometimes there is an equilibration period, up to ~60 minutes, for the signal to reach a steady state***. If the signal has not***

"settled down" after 90 minutes, it is more likely that your grounding or insulation is faulty, and you will not be able to use EEG recordings from that experiment.

b. Axoscope program (Axoscope 9.2)
    i. Turn on head stage amplifier, Grass amplifier, and PC. Make sure the green LED on the Mini-Digi is lit when the circuit is on. The usual settings on the Grass amplifier are:
        1. Low-pass filter, 0.1 Hz; high pass filter, 0.1 kHz
        2. Calibrator = 200 μV; x 1000 or 10? x 1000
        3. Input = Use
        4. Amplification = 10
        5. Line filter = In
c. Attaching 3-prong plug to head stage amplifier
    i. **NOTE**: **head stage amplifier** can run off a **9V battery** or via an **AC adaptor**. The **AC house supply** can introduce **noise**. You must **change the 9V battery every 24 hours**; although the amplifier has a battery power "check" (lights a green LED; bright = more power, dim / off = less or dead) the battery can be depleted to 7.5 or 8V and still appear to "check" as good. Use a Voltmeter (bottom drawer, red tool cabinet) to verify battery voltage.
    ii. The receptacle for the 3 prong plug is a fixed input into the head stage amplifier (custom designed by WU Electronics Shop)
    iii. The receptacle has a large black mass on one side; this is the GROUND side. Make sure your GROUND prong (marked with black Sharpie) is plugged in on this side.
    iv. From head stage amplifier, an OUTPUT coaxial cable splits into 3 lines: ground (black); EEG reference (white); and EEG active (red). These three lines are plugged into the gray 3 pin receptacle, marked with colored dots: YELLOW for ground, BLUE for EEG reference, and GREEN for EEG active. This gray 3 pin receptacle re-winds into one cable, is INPUT into the Grass amplifier (front).
    v. The output for the Grass amplifier goes directly to the MiniDigi (note which Channel, 0 or 1, so you can enter this information in the Axoscope program. Default is Channel 0).
    vi. MiniDigi output is a USB ending, plug into PC laptop. Make sure laptop "recognizes" the New Device. Has not been a problem yet.
d. Securing lines to reduce electrical noise
    i. **Tape all electrical cables securely** to **bench, wall, shelf**, or whatever fixed surface is available. Pay special attention to securing the 3 wires from head-stage amplifier output as they go into the gray 3 pin receptacle. Tape each side of this connection firmly to the shelf, tape the junction as well.
e. Display on Axoscope

i. Open the Axoscope 9.2 program (oscilloscope icon on Desktop). A blank grid should pop up immediately.
ii. The recording program we use should be the default. Look for "Gap-free" at the top. If not, specify the recording parameters:
1. Under "Configure" menu, choose "Acquire"
2. Under "Acquire → Digitizer → MiniDigi → OK."
3. Next, go back to "Configure" → "Acquire."
4. Under "Acquire → Edit Protocol → Mode/Rate."
5. Choose "Gap-free" mode; "Trial Length = Disk Space"
6. Choose "Sample rate = 1 kHz."

f. Now, "Gap-free" should be displayed at the top of the grid.
g. Click the black arrow to "Play," black dot to "Stop," and red dot to "Record."
i. If **no trace appears** at all when you click on "Play," **try closing the program and/or restarting the computer.**
ii. You can modify the timescale on the X-axis (200-500 ms is generally useful) and the voltage scale on the Y-axis (5-10 V is what we use, but for smaller amplitudes $\leq$ 2V may be necessary)
h. When you are finished recording:
i. Click the black dot to "Stop."
ii. Under "File," click on "***Last recording****"
iii. The entire trace should appear on the grid. It may take a minute or so to display. Be patient.
iv. Save your file on the PC before transferrng it to your USB.
v. **NOTE:** ***if you record another file before saving the last***, you have ***lost the previous record***! Make sure to save last recorded file before recording again. Saving can also take a minute or two.
vi. The PC in the Surgery Room is not hooked up to the network. You must transfer files by USB. An >8 GB USB device is optimal. Files tend to be quite large (100,000 KB for 24h)
vii. Files are saved as "Axon Binary File" or .abf.

IV. Analysis of RMS amplitude signal by Clampfit 9.2
a. Opening files
i. Open Clampfit 9.2 (white X-Y plot icon on Desktop)
ii. A blank data spreadsheet should appear named "Results 1."
iii. Go to "File → Open data → (choose USB port) → your file"
iv. Your trace should appear exactly as you saved it in Axoscope
b. Selecting a window for analysis
i. There are 4 cursors that should appear on your tracing: use cursors 1 and 2 to select a window
ii. Go to "View → Zoom → Between cursors"
iii. The portion of the record between Cursors 1 and 2 should appear

iv. Absolute time (from beginning of record) is displayed on Cursor 1, and the difference between 1 and 2 is displayed on Cursor 2
v. Zoom in until you have about ~40-60 min. displayed
vi. Then use Cursors 1 and 2 to find your selected epochs

c. Using Clampfit 9.2 to calculate
i. Place Cursors 1-2 at 1-1.5 min. distance at your desired epoch
ii. Choose "Analyze → Power Spectrum → Hamming window"
iii. "Exclude 1st "1" spectral bins"
iv. "Trace selection" should be "Active signal, one continuous trace"
v. "Region to analyze: Cursors 1…2; "click "OK"
vi. A new window appears: a "Power Spectrum" graph, and in the "Results" spreadsheet you should see your data
vii. Look at "RMS incl., RMS excl., and RMS all bins" in Results
viii. If data is uniform over the 1-1.5 min epoch, then "RMS excl." should be "0" or very small. This is good quality data. If not, then perhaps choose another epoch or look at the quality of your signal.
ix. You can copy this spreadsheet into Excel for further analysis.

APPENDIX 3

Synaptosomes: materials and protocol

Materials:
47 mm diameter filtration apparatus
Millipore AP15 “prefilter” (ordered; to be used with Hirsch-type filter, also ordered)

12 mL polycarbonate centrifuges tubes, 16 x 100 mm
50 mL polycarbonate centrifuge tubes (transparent)
- Wheaton cat. # 358009

Beckmann JA-20/Sorvall SS-34: fixed angle rotor

Percoll – received as slurry. Filter through Millipore AP15 prefilters to remove aggregated incompletely coated particles.
Store filtered solution at 4º C if required in next few days; otherwise, store at -20º C in 200 mL lots; repeat filtration every 2 weeks.

CRITICAL: use double distilled or double deionized water throughout.

Solutions:

1. 100 mM HCl
    a. 10 mL of 1M into glass beaker w/ 90 mL water; store at RT
2. 0.2 M EDTA
    a. Add 7.445 g EDTA to 75 mL water; adjust to pH 7.4 with saturated solution of Tris base while stirring on magnetic stirrer
    b. Then, dilute to 100 mL and store in 100 mL bottle at 4º C
3. 4X gradient buffer
    a. Dissolve 109.54 g sucrose and 606 *mg* Tris in ~ 200 mL water
    b. Add 5 mL 0.2M EDTA stock
    c. Dilute to 240 mL
    d. Check pH, adjust if necessary.
    e. Dilute to final volume of 250 mL; store as 50 mL aliquots in capped 50 mL plastic tubes at -20º C
4. Sucrose/EDTA buffer
    a. Dilute 50 mL 4X gradient buffer to 200 mL total with water; store on ice.
5. 50 mM DTT
    a. Dissolve 154 mg DTT in 10 mL water
    b. Store as 1 mL aliquots in 1.5 mL-capped tubes at -20º C **[in lab, -20 box]**
6. Percoll gradient solutions
    a. Thaw 1 tube 4X gradient buffer + 1 tube 50 mM DTT stock, on ice.
    b. Filter Percoll, insert stir bar, adjust to pH 7.4 with 100 mM HCl.
    c. To 50 mL capped tubes, add specified amount of Percoll, 4X gradient buffer, 50 mM DTT, and water according to TABLE 1 (see below) to make a total volume of 25 mL.

d. NOTE: Addition of salts to Percoll/gradient buffer leads to aggregation of membranes, disruption of normal subcellular fractions. It is essential to minimize addition of extra salts in gradient solutions.

Reagent	**Percoll (mL)**	**4X Gradient buffer (mL)**	**50 mM DTT (uL)**	**Water (mL)**
Homogenizing buffer	0	6.25	125	18.625
3% Percoll (v/v)	0.75	6.25	125	17.875
10% Percoll (v/v)	2.50	6.25	125	16.125
15% Percoll (v/v)	3.75	6.25	125	14.875
23% Percoll (v/v)	5.75	6.25	125	12.875

What is Percoll?

- Polyvinyl, pyrrolidone-coated silica particles
- 17 nm diameter (uniform)
- Developed for cell & subcellular fractionation
- Advantages?
    - Low viscosity = more rapid sedimentation than Ficoll
    - Can be prepared in isotonic solution (isotonic sucrose)

Two labs independently developed Percoll gradient procedures for synaptosome prep, beginning with P2 fraction → applying P2 to discontinuous Percoll gradient

This procedure took less centrifugation time, but Dunkley et al. is in widespread use.

Also, further reduced time by applying S1 directly to gradient; avoided need to prepare P2 fraction and eliminated the mechanically-damaging step of P2 resuspension.

Briefly:

1. S1 fraction prepared by homogenization of fresh brain tissue in isotonic sucrose
2. S1 then directly applied to discontinuous Percoll gradient: 3, 10, 15, 23% (v/v)
3. Centrifuge gradient in medium-speed centrifuge x 5 min (exclude acc/decel time)
4. Five (5) major fractions then collected from INTERFACES of Percoll layers
    a. Fraction 1: small, unidentified membranous material (0-3%)
    b. Fraction 2: myelin, membranes and membrane vesicles (3-10%)
    c. Fraction 3: synaptosomes and membrane vesicles (10-15%)
    d. *Fraction 4: synaptosomes (15-23%)
    e. Fraction 5: extrasynaptosomal mitochondria (below 23%, bottom)
5. Fractions are diluted, centrifuged to remove Percoll, and resuspended in physiological buffer for analysis

6. *Authors recommend using ***Fraction 4*** for most highly purified and maximally viable synaptosomes are required; however, yield is low.
7. If maximal yield is required and membrane contamination is NOT a concern, some labs pool Fractions 3 + 4 either AFTER purification or by omitting 15% Percoll layer during purification; then, collect in single fraction atop 23% layer.
8. Fraction 3 vs Fraction 4: Fraction 4 synaptosomes are larger and denser (for cortex, 0.64 um vs 0.55 um). Fraction 4 contains more mitochrondria.

Notes from 2.2.09 Tim Miller training session

1. Go very slowly, circling the inner diameter of centrifuge tube with pipette tip
2. Stay close to meniscus
3. Mark after each layer so interfaces may be detected after spin to best approximate location of desired fraction (Fraction 4)

Prepare Percoll gradient

1. Filtered Percoll may be kept up several days at 4º C
2. Percoll gradients may be used up to ***24h*** after manufacture (kept on ice or refrigerated)

Preparation of S1 fraction from brain tissue (~30 min)

1. Extract required tissue from brain
    a. Rinse several times in excess volumes of ice-cold homogenizing buffer to reduce blood levels
    b. Remove as much liquid as possible using filter paper
    c. Add 9 mL of ice-cold homogenizing buffer to 1 g of fresh brain tissue in small glass beaker
    d. NOTE: although synaptosomes have been prepared from frozen tissue using Percoll, it is preferable that tissue never be frozen or fixed before use because no studies exist on homogeneity, yield or viability of these synaptosomes
    e. Complete sacrifice as quickly as possible; remove all bone, blood and meninges by washing in ice-cold homogenizing buffer; cool tissue to 4º C as quickly as possible
    f. AVOID saline (PBS-heparin) ,as salts will disrupt distribution of subcellular tissues in the gradient***
    g. If anesthesia is used before killing animals, it will still be present in resulting synaptosomes; consider effect on synaptic transmission / functional experiments
    h. CRITICAL: all equipment should be kept at 4º C
    i. Ratio of homogenization buffer : tissue weight is critical is critical to subsequent fractionization of synaptosomes; must carefully control
    j. If 2X amount of tissue is used, Fraction 2 becomes overloaded during centrifugation and it is difficult to separate from Fraction 3 synaptosomes, and recovery of Fraction 4 synaptosomes is decreased

2. Homogenization (30 min)
    a. Rapidly cut brain tissue into small pieces, using scissors (step not required if smaller amounts of tissue or slices are to be used that can be readily homogenized
    b. Wheaton tissue grinder (358009 15 mL, 19 x 84, $158.92 from Wheaton) 1501 North 10th Street, Millville, NJ 08332-2038, USA
    Tel: 800-225-1437 Fax: 856-825-1368
    c. Pour chopped tissue into 15 mL Teflon-glass tissue grinder; homogenize with 10 even strokes (1^{st} stroke = 5 s, subsequent strokes = 3-4 s) using motor driven pestle @ 500-800 rpm (?) ask!
    d. Pre-chill in beaker of ice before homogenization
    e. ***Time between sacrifice and homogenization is critical; try for 1-2 min
    f. Clearance of Teflon-glass tissue grinder, speed of pestle rotation, and and rate of up and down strokes all contribute to eventual SIZE of synaptosomes and contaminating membrane vesicles formed during homogenization; strokes may vary 6-10, rpm may vary 500-800 rpm
3. Centrifugation (30 min)
    a. STEP 1: centrifuge at **3600 rpm** (1000g @ average radius of centrifuge tube) x 10 min @ 4º C in 12 mL polycarbonate tube using JA-20 rotor (equivalent, Sorvall SS34) in high-speed centrifuge
    b. Collect supernatant ("S1"), transfer to 50 mL plastic tube on ice, and CAP
    c. Discard pellet
    d. Original paper call for S1 to be centrifuged again @ 15,000g x 30 min → P2; P2 was then resuspended and treated as per S1 in current protocol
    e. S1 procedure as good as P2; synaptosomes as pure, viable, homogenous
4. Percoll gradient fractionation procedure (30 min)
    a. Dilute S1 supernatant (9 mL) to 10-14 mL with homogenizing buffer; keep on ice, measure protein content with BCA → essential that final protein content of S1 = 4-5 mg/mL; if protein content too high, add more buffer; if too low, then adjust ratio of tissue to homogenizing buffer in Step 2 (increase tissue/buffer)
    b. Slowly and carefully pipette 2 mL of diluted S1 fraction over top 3% layer in each tube containing Percoll gradient from step 1; pipette @ 1 mL/min,, should be slow and smooth
    c. Centrifuge tubes @ **20,000 rpm** (31,000g) @ 4º C x 5 min (AT SPEED)
    d. Brake should be set to full for most of deceleration, but very slow for last 500 rpm
    e. ***Must be timed precisely so time @ max speed = 5 min exactly
    f. Remove centrifuge tubes from rotor, place on ice; careful not to disturb the gradient; collect all fractions individually OR specific fractions
5. Collection of fractions

a. If only synaptosomes are required, attach a thin metal tube (extremely wide bore 18-20 gauge, 9-10 cm long needle) via 2 cm silicon tubing @ end of 10 mL pipette
b. Using pipette-aid, carefully insert tube into gradient down to required fraction; withdraw and dispense in pre-chilled tube on ice

6. Transfer from sucrose to isotonic solution (45 min)
    a. Dilute Fraction 4 (or other fraction of interest) to 80 mL with ice-cold sucrose-EDTA buffer in beaker, or other suitable container
    b. Divide over 2 50-mL polycarbonate centrifuge tubes
    c. Centrifuge at **16,000 rpm** (20,000g) in SS34 rotor @ 4º C x 30 min
    d. If Fractions 3 + 4 are combined, ensure that Percoll is diluted 3-4X before centrifugation
    e. If material is NOT properly pelleted, apply less brake to avoid disturbing the pellet when centrifuge reaches a sudden stop
    f. Combine pellets and carefully resuspend in the required amount of isotonic physiological buffer of choice (CHECK)
    g. Synaptosomes can be used at this point → saves time and potentially damaging, resuspension step
    h. If presence of sucrose or EDTA might interfere with subsequent assays, synaptosomes can be washed free of sucrose/EDTA by centrifuging resuspended synaptosomes x 10 min @ **15,000 rpm** (18,000g), 4º C
    i. Resulting pellet should be gently resuspended in isotonic physiological buffer to required concentration for subsequent experiments
    j. Measure amount of protein to standardize $[X]_{protein}$ (expect 5 mg/mL when all of Fraction 4 is fully resuspended in 600 uL of isotonic buffer (without extra wash step), assuming 1 g cortex was used as starting material

Sucrose/EDTA buffer

- 0.32M sucrose, 1 mM EDTA, 5 mM Tris pH 7.4)
- Dilute 50 mL of 4X gradient buffer to 200 mL with MQ water; add 5 mL 0.2M EDTA stock and keep on ice.

Isotonic buffer

- Freshly prepare a batch of isotonic physiological buffer
- Buffer depends on particular experiments planned for synaptosomes, etc.
- Examples given in refs. 39, 40, 49, 60

Notes:

- Sacrifice: deep anesthesia with isoflurane, open chest, cut R.A., infuse 5 mL ice-cold homogenizing buffer; put into cold preweighed histology vial and weighed
- Homogenized 0.5 g whole brain in 5 mL buffer (add to vial, cut w/ Exacto 1st)
- 10 strokes, slowly with half-twists, 5 s down and up
- Spin down (S1 fraction; pour off supernatant, discard pellet)

- Ended up saving S1 fraction; frozen in centrifuge tubes at -80º C
- Poured 2 mL each on two gradients (saved two gradients for Thurs if needed)
- Spun down, collected both Fractions 3 and 4 and pooled immediately
    - Diluted fractions to ***8 mL*** with ice-cold sucrose-EDTA buffer in beaker, or other suitable container
- Did not resuspend, but protein content 3-4.5 mg/mL (expected)